NOAA Project
Report

Development of two tsunami inundation maps in the GOM and inclusion of the USGS' Yucatan landslide tsunami sources

Final Report to the
National Tsunami Hazard Mitigation Program (NTHMP)
in Completion of Project Awards
NA17NWS4670015

Authors

Juan J Horrillo	Texas A&M University at Galveston
Wei Cheng	
Jens Figlus	
Rozita Kian	

Collaborators:

Brad Baker	Santa Rosa County Emergency Management Director
Daniel Hahn	Santa Rosa County Emergency Management Plans Chief

Under the guidance of
NTHMP Mapping and Modeling Subcommittee

National Tsunami Hazard Mitigation Program

National Oceanic and Atmospheric Administration

OCEAN ENGINEERING
TEXAS A&M UNIVERSITY

Ocean Engineering
Texas A&M University at Galveston
Galveston, Texas, 77553

November 2018

Contents

1 Executive Summary 1
2 Introduction 2
2.1 Background 2
2.2 Regional and Historical Context 6
3 Tsunami Inundation Modeling 9
3.1 Landslide Tsunami Sources 9
3.2 Numerical Models 47
4 Tsunami Maps 48
4.1 Osprey-Venice-Englewood, FL 48
4.2 Sanibel Island-Naples, FL 89
5 Tsunami and Hurricane Storm Surge Inundation 130
5.1 Osprey-Venice-Englewood, FL 131
5.2 Sanibel Island-Naples, FL 137
6 Tsunami Maritime Products 142
6.1 Osprey-Venice-Englewood, FL 145
6.2 Sanibel Island-Naples, FL 152
7 Conclusions 159

List of Figures

1 Selected communities or geography regions along the US GOM coastline where tsunami maps have been developed. Red rectangles denote 3 arcsecond (∼90m) domains of coastal communities where tsunami inundation has been modeled; red hatched areas are historical landslide sources; blue hatched areas are Probabilistic Submarine Landslide (PSL) sources; yellow dots are locations of numerical wave gauges. The zero-meter elevation contour is drawn to show the GOM coastline. 4
2 EastBreaks submarine landslide location, excavation limits, and surrounding bathymetry (in meters). 11
3 Tsunami arrival time for the East Breaks Submarine Landslide scenario. . . 13
4 Maximum tsunami wave amplitude (one arcminute resolution) for the East Breaks Submarine Landslide scenario. 14
5 Probabilistic Submarine Landslide -A- location, excavation limits, and surrounding bathymetry (in meters). 15
6 Tsunami arrival time for the Probabilistic Submarine Landslide -A- (PSL-A) scenario. 17
7 Maximum tsunami wave amplitude (one arcminute resolution) for the Probabilistic Submarine Landslide -A- (PSL-A) scenario. 18
8 Probabilistic Submarine Landslide -B1- location, excavation limits, and surrounding bathymetry (in meters). 19
9 Tsunami arrival time for the Probabilistic Submarine Landslide -B1- (PSL-B1) scenario. 21
10 Maximum tsunami wave amplitude (one arcminute resolution) for the Probabilistic Submarine Landslide -B1- (PSL-B1) scenario. 22
11 Probabilistic Submarine Landslide -B2- location, excavation limits, and surrounding bathymetry (in meters). 23
12 Tsunami arrival time for the Probabilistic Submarine Landslide -B2- (PSL-B2) scenario. 25
13 Maximum tsunami wave amplitude (one arcminute resolution) for the Probabilistic Submarine Landslide -B2- (PSL-B2) scenario. 26
14 Mississippi Canyon submarine landslide location, excavation limits and surrounding bathymetry (in meters). 27
15 Tsunami arrival time for the Mississippi Canyon Submarine Landslide scenario. 29

16 Maximum tsunami wave amplitude (one arcminute resolution) for the Mississippi Canyon Submarine Landslide scenario. 30
17 Probabilistic Submarine Landslide -C- location, excavation limits, and surrounding bathymetry (in meters). 31
18 Tsunami arrival time for the Probabilistic Submarine Landslide -C- (PSL-C) scenario. 33
19 Maximum tsunami wave amplitude (one arcminute resolution) for the Probabilistic Submarine Landslide -C- (PSL-C) scenario. 34
20 West Florida submarine landslide location, excavation limits and surrounding bathymetry (in meters). 35
21 Tsunami arrival time for the West Florida Submarine Landslide scenario. . 37
22 Maximum tsunami wave amplitude (one arcminute resolution) for the West Florida Submarine Landslide scenario. 38
23 Yucatan #3 submarine landslide location, excavation limits and surrounding bathymetry (in meters). 39
24 Tsunami arrival time for the Yucatan #3 Submarine Landslide scenario. . . 41
25 Maximum tsunami wave amplitude (one arcminute resolution) for the Yucatan #3 Submarine Landslide scenario. 42
26 Yucatan #5 submarine landslide location, excavation limits and surrounding bathymetry (in meters). 43
27 Tsunami arrival time for the Yucatan #5 Submarine Landslide scenario. . . 45
28 Maximum tsunami wave amplitude (one arcminute resolution) for the Yucatan #5 Submarine Landslide scenario. 46
29 Maximum momentum flux (m^3/s^2) caused by the East Breaks submarine landslide in Osprey-Venice, FL. Arrows represent direction of maximum momentum flux. Contour drawn is the zero-meter contour for land elevation. . . . 49
30 Maximum momentum flux (m^3/s^2) caused by the East Breaks submarine landslide in Englewood, FL. Arrows represent direction of maximum momentum flux. Contour drawn is the zero-meter contour for land elevation. 50
31 Maximum inundation depth (m) caused by the East Breaks submarine landslide in Osprey-Venice, FL. Contour drawn is the zero-meter contour for land elevation. 51
32 Maximum inundation depth (m) caused by the East Breaks submarine landslide in Englewood, FL. Contour drawn is the zero-meter contour for land elevation. 52
33 Maximum momentum flux (m^3/s^2) caused by the Probabilistic Submarine Landslide A in Osprey-Venice, FL. Arrows represent direction of maximum momentum flux. Contour drawn is the zero-meter contour for land elevation. 53
34 Maximum momentum flux (m^3/s^2) caused by the Probabilistic Submarine Landslide A in Englewood, FL. Arrows represent direction of maximum momentum flux. Contour drawn is the zero-meter contour for land elevation. 54

35 Maximum inundation depth (m) caused by the Probabilistic Submarine Landslide A in Osprey-Venice, FL. Contour drawn is the zero-meter contour for land elevation. 55
36 Maximum inundation depth (m) caused by the Probabilistic Submarine Landslide A in Englewood, FL. Contour drawn is the zero-meter contour for land elevation. 56
37 Maximum momentum flux (m^3/s^2) caused by the Probabilistic Submarine Landslide B1 in Osprey-Venice, FL. Arrows represent direction of maximum momentum flux. Contour drawn is the zero-meter contour for land elevation. 57
38 Maximum momentum flux (m^3/s^2) caused by the Probabilistic Submarine Landslide B1 in Englewood, FL. Arrows represent direction of maximum momentum flux. Contour drawn is the zero-meter contour for land elevation. 58
39 Maximum inundation depth (m) caused by the Probabilistic Submarine Landslide B1 in Osprey-Venice, FL. Contour drawn is the zero-meter contour for land elevation. 59
40 Maximum inundation depth (m) caused by the Probabilistic Submarine Landslide B1 in Englewood, FL. Contour drawn is the zero-meter contour for land elevation. 60
41 Maximum momentum flux (m^3/s^2) caused by the Probabilistic Submarine Landslide B2 in Osprey-Venice, FL. Arrows represent direction of maximum momentum flux. Contour drawn is the zero-meter contour for land elevation. 61
42 Maximum momentum flux (m^3/s^2) caused by the Probabilistic Submarine Landslide B2 in Englewood, FL. Arrows represent direction of maximum momentum flux. Contour drawn is the zero-meter contour for land elevation. 62
43 Maximum inundation depth (m) caused by the Probabilistic Submarine Landslide B2 in Osprey-Venice, FL. Contour drawn is the zero-meter contour for land elevation. 63
44 Maximum inundation depth (m) caused by the Probabilistic Submarine Landslide B2 in Englewood, FL. Contour drawn is the zero-meter contour for land elevation. 64
45 Maximum momentum flux (m^3/s^2) caused by the Mississippi Canyon submarine landslide in Osprey-Venice, FL. Arrows represent direction of maximum momentum flux. Contour drawn is the zero-meter contour for land elevation. 65
46 Maximum momentum flux (m^3/s^2) caused by the Mississippi Canyon submarine landslide in Englewood, FL. Arrows represent direction of maximum momentum flux. Contour drawn is the zero-meter contour for land elevation. 66
47 Maximum inundation depth (m) caused by the Mississippi Canyon submarine landslide in Osprey-Venice, FL. Contour drawn is the zero-meter contour for land elevation. 67
48 Maximum inundation depth (m) caused by the Mississippi Canyon submarine landslide in Englewood, FL. Contour drawn is the zero-meter contour for land elevation. 68

49 Maximum momentum flux (m^3/s^2) caused by the Probabilistic Submarine Landslide C in Osprey-Venice, FL. Arrows represent direction of maximum momentum flux. Contour drawn is the zero-meter contour for land elevation. 69
50 Maximum momentum flux (m^3/s^2) caused by the Probabilistic Submarine Landslide C in Englewood, FL. Arrows represent direction of maximum momentum flux. Contour drawn is the zero-meter contour for land elevation. 70
51 Maximum inundation depth (m) caused by the Probabilistic Submarine Landslide C in Osprey-Venice, FL. Contour drawn is the zero-meter contour for land elevation. 71
52 Maximum inundation depth (m) caused by the Probabilistic Submarine Landslide C in Englewood, FL. Contour drawn is the zero-meter contour for land elevation. 72
53 Maximum momentum flux (m^3/s^2) caused by the West Florida submarine landslide in Osprey-Venice, FL. Arrows represent direction of maximum momentum flux. Contour drawn is the zero-meter contour for land elevation. 73
54 Maximum momentum flux (m^3/s^2) caused by the West Florida submarine landslide in Englewood, FL. Arrows represent direction of maximum momentum flux. Contour drawn is the zero-meter contour for land elevation. . . . 74
55 Maximum inundation depth (m) caused by the West Florida submarine landslide in Osprey-Venice, FL. Contour drawn is the zero-meter contour for land elevation. 75
56 Maximum inundation depth (m) caused by the West Florida submarine landslide in Englewood, FL. Contour drawn is the zero-meter contour for land elevation. 76
57 Maximum momentum flux (m^3/s^2) caused by the Yucatan #3 submarine landslide in Osprey-Venice, FL. Arrows represent direction of maximum momentum flux. Contour drawn is the zero-meter contour for land elevation. . . . 77
58 Maximum momentum flux (m^3/s^2) caused by the Yucatan #3 submarine landslide in Englewood, FL. Arrows represent direction of maximum momentum flux. Contour drawn is the zero-meter contour for land elevation. 78
59 Maximum inundation depth (m) caused by the Yucatan #3 submarine landslide in Osprey-Venice, FL. Contour drawn is the zero-meter contour for land elevation. 79
60 Maximum inundation depth (m) caused by the Yucatan #3 submarine landslide in Englewood, FL. Contour drawn is the zero-meter contour for land elevation. 80
61 Maximum momentum flux (m^3/s^2) caused by the Yucatan #5 submarine landslide in Osprey-Venice, FL. Arrows represent direction of maximum momentum flux. Contour drawn is the zero-meter contour for land elevation. . . . 81
62 Maximum momentum flux (m^3/s^2) caused by the Yucatan #5 submarine landslide in Englewood, FL. Arrows represent direction of maximum momentum flux. Contour drawn is the zero-meter contour for land elevation. 82

63 Maximum inundation depth (m) caused by the Yucatan #5 submarine landslide in Osprey-Venice, FL. Contour drawn is the zero-meter contour for land elevation. 83
64 Maximum inundation depth (m) caused by the Yucatan #5 submarine landslide in Englewood, FL. Contour drawn is the zero-meter contour for land elevation. 84
65 Maximum of maximums inundation depth (m) in Osprey-Venice, FL, calculated as the maximum inundation depth in each grid cell from an ensemble of all tsunami sources considered. Contour drawn is the zero-meter contour for land elevation. 85
66 Maximum of maximums inundation depth (m) in Englewood, FL, calculated as the maximum inundation depth in each grid cell from an ensemble of all tsunami sources considered. Contour drawn is the zero-meter contour for land elevation. 86
67 Indication of the tsunami source which causes the maximum of maximums inundation depth (m) in each grid cell from an ensemble of all tsunami sources in Osprey-Venice, FL. Contour drawn is the zero-meter contour for land elevation. 87
68 Indication of the tsunami source which causes the maximum of maximums inundation depth (m) in each grid cell from an ensemble of all tsunami sources in Englewood, FL. Contour drawn is the zero-meter contour for land elevation. 88
69 Maximum momentum flux (m^3/s^2) caused by the East Breaks submarine landslide in Sanibel Island, FL. Arrows represent direction of maximum momentum flux. Contour drawn is the zero-meter contour for land elevation. . . . 90
70 Maximum momentum flux (m^3/s^2) caused by the East Breaks submarine landslide in Naples, FL. Arrows represent direction of maximum momentum flux. Contour drawn is the zero-meter contour for land elevation. 91
71 Maximum inundation depth (m) caused by the East Breaks submarine landslide in Sanibel Island, FL. Contour drawn is the zero-meter contour for land elevation. 92
72 Maximum inundation depth (m) caused by the East Breaks submarine landslide in Naples, FL. Contour drawn is the zero-meter contour for land elevation. 93
73 Maximum momentum flux (m^3/s^2) caused by the Probabilistic Submarine Landslide A in Sanibel Island, FL. Arrows represent direction of maximum momentum flux. Contour drawn is the zero-meter contour for land elevation. 94
74 Maximum momentum flux (m^3/s^2) caused by the Probabilistic Submarine Landslide A in Naples, FL. Arrows represent direction of maximum momentum flux. Contour drawn is the zero-meter contour for land elevation. . . . 95
75 Maximum inundation depth (m) caused by the Probabilistic Submarine Landslide A in Sanibel Island, FL. Contour drawn is the zero-meter contour for land elevation. 96
76 Maximum inundation depth (m) caused by the Probabilistic Submarine Landslide A in Naples, FL. Contour drawn is the zero-meter contour for land elevation. 97

77 Maximum momentum flux (m^3/s^2) caused by the Probabilistic Submarine Landslide B1 in Sanibel Island, FL. Arrows represent direction of maximum momentum flux. Contour drawn is the zero-meter contour for land elevation. 98
78 Maximum momentum flux (m^3/s^2) caused by the Probabilistic Submarine Landslide B1 in Naples, FL. Arrows represent direction of maximum momentum flux. Contour drawn is the zero-meter contour for land elevation. . . . 99
79 Maximum inundation depth (m) caused by the Probabilistic Submarine Landslide B1 in Sanibel Island, FL. Contour drawn is the zero-meter contour for land elevation. 100
80 Maximum inundation depth (m) caused by the Probabilistic Submarine Landslide B1 in Naples, FL. Contour drawn is the zero-meter contour for land elevation. 101
81 Maximum momentum flux (m^3/s^2) caused by the Probabilistic Submarine Landslide B2 in Sanibel Island, FL. Arrows represent direction of maximum momentum flux. Contour drawn is the zero-meter contour for land elevation. 102
82 Maximum momentum flux (m^3/s^2) caused by the Probabilistic Submarine Landslide B2 in Naples, FL. Arrows represent direction of maximum momentum flux. Contour drawn is the zero-meter contour for land elevation. . . . 103
83 Maximum inundation depth (m) caused by the Probabilistic Submarine Landslide B2 in Sanibel Island, FL. Contour drawn is the zero-meter contour for land elevation. 104
84 Maximum inundation depth (m) caused by the Probabilistic Submarine Landslide B2 in Naples, FL. Contour drawn is the zero-meter contour for land elevation. 105
85 Maximum momentum flux (m^3/s^2) caused by the Mississippi Canyon submarine landslide in Sanibel Island, FL. Arrows represent direction of maximum momentum flux. Contour drawn is the zero-meter contour for land elevation. 106
86 Maximum momentum flux (m^3/s^2) caused by the Mississippi Canyon submarine landslide in Naples, FL. Arrows represent direction of maximum momentum flux. Contour drawn is the zero-meter contour for land elevation. 107
87 Maximum inundation depth (m) caused by the Mississippi Canyon submarine landslide in Sanibel Island, FL. Contour drawn is the zero-meter contour for land elevation. 108
88 Maximum inundation depth (m) caused by the Mississippi Canyon submarine landslide in Naples, FL. Contour drawn is the zero-meter contour for land elevation. 109
89 Maximum momentum flux (m^3/s^2) caused by the Probabilistic Submarine Landslide C in Sanibel Island, FL. Arrows represent direction of maximum momentum flux. Contour drawn is the zero-meter contour for land elevation. 110
90 Maximum momentum flux (m^3/s^2) caused by the Probabilistic Submarine Landslide C in Naples, FL. Arrows represent direction of maximum momentum flux. Contour drawn is the zero-meter contour for land elevation. . . . 111

91 Maximum inundation depth (m) caused by the Probabilistic Submarine Landslide C in Sanibel Island, FL. Contour drawn is the zero-meter contour for land elevation. 112
92 Maximum inundation depth (m) caused by the Probabilistic Submarine Landslide C in Naples, FL. Contour drawn is the zero-meter contour for land elevation. 113
93 Maximum momentum flux (m^3/s^2) caused by the West Florida submarine landslide in Sanibel Island, FL. Arrows represent direction of maximum momentum flux. Contour drawn is the zero-meter contour for land elevation. 114
94 Maximum momentum flux (m^3/s^2) caused by the West Florida submarine landslide in Naples, FL. Arrows represent direction of maximum momentum flux. Contour drawn is the zero-meter contour for land elevation. 115
95 Maximum inundation depth (m) caused by the West Florida submarine landslide in Sanibel Island, FL. Contour drawn is the zero-meter contour for land elevation. 116
96 Maximum inundation depth (m) caused by the West Florida submarine landslide in Naples, FL. Contour drawn is the zero-meter contour for land elevation. 117
97 Maximum momentum flux (m^3/s^2) caused by the Yucatan #3 submarine landslide in Sanibel Island, FL. Arrows represent direction of maximum momentum flux. Contour drawn is the zero-meter contour for land elevation. . . . 118
98 Maximum momentum flux (m^3/s^2) caused by the Yucatan #3 submarine landslide in Naples, FL. Arrows represent direction of maximum momentum flux. Contour drawn is the zero-meter contour for land elevation. 119
99 Maximum inundation depth (m) caused by the Yucatan #3 submarine landslide in Sanibel Island, FL. Contour drawn is the zero-meter contour for land elevation. 120
100 Maximum inundation depth (m) caused by the Yucatan #3 submarine landslide in Naples, FL. Contour drawn is the zero-meter contour for land elevation. 121
101 Maximum momentum flux (m^3/s^2) caused by the Yucatan #5 submarine landslide in Sanibel Island, FL. Arrows represent direction of maximum momentum flux. Contour drawn is the zero-meter contour for land elevation. . . . 122
102 Maximum momentum flux (m^3/s^2) caused by the Yucatan #5 submarine landslide in Naples, FL. Arrows represent direction of maximum momentum flux. Contour drawn is the zero-meter contour for land elevation. 123
103 Maximum inundation depth (m) caused by the Yucatan #5 submarine landslide in Sanibel Island, FL. Contour drawn is the zero-meter contour for land elevation. 124
104 Maximum inundation depth (m) caused by the Yucatan #5 submarine landslide in Naples, FL. Contour drawn is the zero-meter contour for land elevation. 125
105 Maximum of maximums inundation depth (m) in Sanibel Island, FL, calculated as the maximum inundation depth in each grid cell from an ensemble of all tsunami sources considered. Contour drawn is the zero-meter contour for land elevation. 126

106 Maximum of maximums inundation depth (m) in Naples, FL, calculated as the maximum inundation depth in each grid cell from an ensemble of all tsunami sources considered. Contour drawn is the zero-meter contour for land elevation. 127
107 Indication of the tsunami source which causes the maximum of maximums inundation depth (m) in each grid cell from an ensemble of all tsunami sources in Sanibel Island, FL. Contour drawn is the zero-meter contour for land elevation. 128
108 Indication of the tsunami source which causes the maximum of maximums inundation depth (m) in each grid cell from an ensemble of all tsunami sources in Naples, FL. Contour drawn is the zero-meter contour for land elevation. . 129
109 Hurricane category which produces inundation at high tide that best matches the MOM tsunami inundation shown in Figure 110 for Osprey-Venice, FL. The contours drawn and labeled are at -5 m, -10 m, and -15 m levels. 133
110 Actual difference $\Delta\zeta$ (in meters) between SLOSH MOM storm surge inundation and MOM tsunami inundation for the best-match hurricane category shown in Figure 109 for Osprey-Venice, FL. Note that negative values indicate where tsunami inundation is higher than hurricane inundation, and pale colors indicate relatively good agreement between tsunami and storm surge inundation, i.e. $|\Delta\zeta| \leq 0.5$ m. The contours drawn and labeled are at -5 m, -10 m, and -15 m levels. 134
111 Hurricane category which produces inundation at high tide that best matches the MOM tsunami inundation shown in Figure 112 for Englewood, FL. The contours drawn and labeled are at -5 m, -10 m, and -15 m levels. 135
112 Actual difference $\Delta\zeta$ (in meters) between SLOSH MOM storm surge inundation and MOM tsunami inundation for the best-match hurricane category shown in Figure 111 for Englewood, FL. Note that negative values indicate where tsunami inundation is higher than hurricane inundation, and pale colors indicate relatively good agreement between tsunami and storm surge inundation, i.e. $|\Delta\zeta| \leq 0.5$ m. The contours drawn and labeled are at -5 m, -10 m, and -15 m levels. 136
113 Hurricane category which produces inundation at high tide that best matches the MOM tsunami inundation shown in Figure 114 for Sanibel Island, FL. The contours drawn and labeled are at -5 m, -10 m, and -15 m levels. 138
114 Actual difference $\Delta\zeta$ (in meters) between SLOSH MOM storm surge inundation and MOM tsunami inundation for the best-match hurricane category shown in Figure 115 for Sanibel Island, FL. Note that negative values indicate where tsunami inundation is higher than hurricane inundation, and pale colors indicate relatively good agreement between tsunami and storm surge inundation, i.e. $|\Delta\zeta| \leq 0.5$ m. The contours drawn and labeled are at -5 m, -10 m, and -15 m levels. 139
115 Hurricane category which produces inundation at high tide that best matches the MOM tsunami inundation shown in Figure 116 for Naples, FL. The contours drawn and labeled are at -5 m, -10 m, and -15 m levels. 140

116 Actual difference $\Delta\zeta$ (in meters) between SLOSH MOM storm surge inundation and MOM tsunami inundation for the best-match hurricane category shown in Figure 115 for Naples, FL. Note that negative values indicate where tsunami inundation is higher than hurricane inundation, and pale colors indicate relatively good agreement between tsunami and storm surge inundation, i.e. $|\Delta\zeta| \leq 0.5$ m. The contours drawn and labeled are at -5 m, -10 m, and -15 m levels. 141
117 Maximum of maximum velocity magnitude contour in GOM for all landslide scenarios and all locations. 143
118 Maximum of maximum velocity magnitude contour in Osprey-Venice-Englewood, FL (Grid 2 - 3 arcsecond) for all landslide scenarios. 145
119 Maximum of maximum velocity magnitude contour in Osprey-Venice-Englewood, FL (Grid 3 - 1 arcsecond) for all landslide scenarios. 146
120 Maximum of maximum velocity magnitude contour in Osprey-Venice, FL (Grid 4 - 1/3 arcsecond) for all landslide scenarios. 147
121 Maximum of maximum velocity magnitude contour in Englewood, FL (Grid 5 - 1/3 arcsecond) for all landslide scenarios. 148
122 Maximum of maximum vorticity magnitude contour in Osprey-Venice-Englewood, FL Grid 3 (1 arcsecond) for all landslide scenarios. 149
123 Maximum of maximum vorticity magnitude contour in Osprey-Venice, FL Grid 4 (1/3 arcsecond) for all landslide scenarios. 150
124 Maximum of maximum vorticity magnitude contour in Englewood, FL Grid 5 (1/3 arcsecond) for all landslide scenarios. 151
125 Maximum of maximum velocity magnitude contour in Sanibel Island-Naples, FL (Grid 2 - 3 arcsecond) for all landslide scenarios. 152
126 Maximum of maximum velocity magnitude contour in Sanibel Island-Naples, FL (Grid 3 - 1 arcsecond) for all landslide scenarios. 153
127 Maximum of maximum velocity magnitude contour in Sanibel Island, FL (Grid 4 - 1/3 arcsecond) for all landslide scenarios. 154
128 Maximum of maximum velocity magnitude contour in Naples, FL (Grid 5 - 1/3 arcsecond) for all landslide scenarios. 155
129 Maximum of maximum vorticity magnitude contour in Sanibel Island-Naples, FL Grid 3 (1 arcsecond) for all landslide scenarios. 156
130 Maximum of maximum vorticity magnitude contour in Sanibel Island, FL Grid 4 (1/3 arcsecond) for all landslide scenarios. 157
131 Maximum of maximum vorticity magnitude contour in Naples, FL Grid 5 (1/3 arcsecond) for all landslide scenarios. 158

List of Tables

1 Submarine Landslide general information. 10
2 Eastbreaks Submarine Landslide general information 11
3 Coordinate limits for the EastBreaks Submarine Landslide Domain to obtain initial dynamic tsunami wave source 12
4 Probabilistic Submarine Landslide A 15
5 Coordinate limits for the PSL-A Submarine Landslide Domain to obtain initial dynamic tsunami wave source 16
6 Probabilistic Submarine Landslide B1 19
7 Coordinate limits for the PSL-B1 Submarine Landslide Domain to obtain initial dynamic tsunami wave source 20
8 Probabilistic Submarine Landslide B2 23
9 Coordinate limits for the PSL-B2 Submarine Landslide Domain to obtain initial dynamic tsunami wave source 24
10 Mississippi Canyon Submarine Landslide 27
11 Coordinate limits for the Mississippi Canyon Submarine Landslide Domain to obtain initial dynamic tsunami wave source 28
12 Probabilistic Submarine Landslide C 31
13 Coordinate limits for the PSL-C Submarine Landslide Domain to obtain initial dynamic tsunami wave source 32
14 West Florida Submarine Landslide 35
15 Coordinate limits for the West Florida Submarine Landslide Domain to obtain initial dynamic tsunami wave source 36
16 Yucatan #3 Submarine Landslide 39
17 Coordinate limits for the Yucatan #3 Submarine Landslide Domain to obtain initial dynamic tsunami wave source 40
18 Yucatan #5 Submarine Landslide 43
19 Coordinate limits for the Yucatan #5 Submarine Landslide Domain to obtain initial dynamic tsunami wave source 44
20 Maximum tsunami wave amplitude and corresponding arrival time after landslide failure at Osprey-Venice-Englewood, FL numerical wave gauge: 26°56'19.22"N, 82°39'34.28"W (Fig. 1), approximate water depth 20 m. 48
21 Maximum tsunami wave amplitude and corresponding arrival time after landslide failure at Sanibel Island-Naples, FL numerical wave gauge: 26°14'34.61"N, 82°25'32.45"W, approximate water depth 20 m. 89

1 Executive Summary

Potential tsunami sources for the GOM are local submarine landslides, which have been examined in the past by the Atlantic and Gulf of Mexico Tsunami Hazard Assessment Group [ten Brink et al., 2009b]. In their findings, they stated that submarine landslides in the GOM are considered a potential tsunami hazard. However, the probability of such an event (tsunamis generated by large landslides) is low. The probability of occurrence is related to ancient (historical) massive landslides which were probably active prior to 7,000 years ago when large quantities of sediments were emptied into the Gulf of Mexico. Nowadays, sediment continues to empty into the Gulf of Mexico mainly from the Mississippi River. This sediment supply contributes to the slope steepening and the increase of fluid pore pressure in sediments, which may lead to further landslide activities and hence, the reason for this study in determining the potential tsunami hazard and its effects in the Gulf of Mexico.

For the triggering mechanism (tsunami generation) we use 5 historical sources, i.e., the Eastbreaks, Mississippi Canyon, West Florida landslides, and 2 new Yucatan landslides introduced in this work. A probabilistic approach was implemented in our previous study, see [Horrillo et al., 2015], to fill gaps along the continental shelf between the historical landslide sources by adding synthetic landslide sources (4 in total) to cover the entire northern part of the GOM. Our probabilistic approach confirmed a recurrence period of major landslide events of around 8000 years, consistent with findings by [Geist et al., 2013].

These historical and probabilistic tsunami sources (9 in total) are used as the maximum credible events that could happen in the region according to the local bathymetry, seafloor slope, and sediment information. These credible events are then used to determine the inundation impact on selected communities along the GOM. The extent and magnitude of the tsunami inundation in those selected locations are achieved by using a combination of 3D and 2D coupled-numerical models. For instance, the 3D model, TSUNAMI3D, is used for tsunami generation to determine the initial dynamic wave or initial source and results are passed as an input to the 2D non-hydrostatic model, NEOWAVE, to determine the tsunami wave propagation and the detailed runup and inundation extent in each of the communities. Tsunami flooding inland-extent, maximum inundation water depth, momentum flux and direction, current velocity and vorticity can then be determined within the inundation-prone areas of the selected communities. Also, tsunami inundation and hurricane category flooding can be compared to access tsunami hazard in unmapped locations.

This project focused on the implementation of recent developments in the tsunami science recommended by the National Tsunami Hazard Mitigation Program - Modeling Mapping Subcommittee - Strategic Plan (NTHMP-MMS-SP) into our current Gulf of Mexico (GOM) tsunami mitigation products. Three main developments for tsunami mitigation have been created under this project for communities in the GOM that will provide guidance to state emergency managers for tsunami hazard mitigation and warning purposes.

The first is the development of tsunami inundation maps in Osprey-Venice-Englewood, FL and Sanibel Island-Naples, FL. Maximum tsunami inundation extent, water height, and momentum flux magnitude and direction are determined from each landslide sources, as well as the maximum of maximum inundation maps from all 9 landslide sources. The two new tsunami inundation map products add to the existing ten mapped locations, which provide

so far good coverage of the most populous coastal areas along the GOM.

The second is a continuing study of the comparison between existing SLOSH hurricane flooding data and our tsunami inundation result, in order to provide temporal-low-order estimate for tsunami hazard areas (community) where inundation studies have not yet been assigned/executed or where little bathymetric and elevation data exists. The adopted approach to define a quick estimate of tsunami vulnerability areas in the GOM has been taken from the existing hurricane storm surge flooding results along coastal areas, in which storm flooding map products are based on hurricane category. The existing storm surge flooding maps cover almost the entire GOM coastal regions and thus they are very well known among GOM regional emergency managers and other parties. This study was first carried out in Horrillo et al. [2016] (award number NA14NWS4670049) where five locations were studied, namely South Padre Island, TX, Galveston, TX, Mobile, AL, Panama City, FL, and Tampa, FL; then in Horrillo et al. [2017] (award number NA15NWS4670031 and NA16NWS4670039), where the comparison was performed in Pensacola, FL, Key West, FL, Okaloosa County, FL, Santa Rosa County, FL and Mustang Island, TX.

The third is to produce the velocity and vorticity magnitude maps for all the landslide scenarios, for Osprey-Venice-Englewood, FL and Sanibel Island-Naples, FL. Based on these maritime maps, location of strong currents and their damaging levels are identified. The tsunami hazard maritime products such as tsunami current magnitude, vorticity, safe/hazard zones would be central for future developments of maritime hazard maps, maritime emergency response and as well as infrastructure planning. We hope that the results herein may assist the maritime communities, port managers and other NTHMP's interested parties.

Although the recurrence of destructive tsunami events have been verified to be quite low in the GOM, our work has confirmed that submarine landslide events with similar characteristics to those used here, have indeed the potential to cause severe damage to GOM coastal communities. Therefore, this work is intended to provide guidance to local emergency managers to help managing urban growth, evacuation planning, and public education with final objective to mitigate potential tsunami hazards in the GOM.

2 Introduction

2.1 Background

The U.S. Tsunami Warning System has included Gulf of Mexico (GOM) coasts since 2005 in order to enable local emergency management to act in response to tsunami warnings. To plan for the warning response, emergency managers must understand what specific areas within their jurisdictions are threatened by tsunamis. Coastal hazard areas susceptible to tsunami inundation can be determined by historical events, by modeling potential tsunami events (worst-case scenarios), or by using a probabilistic approach to determine the rate of recurrence or likelihood of exceeding a certain threshold. As the GOM coastal regions have no significant recent historical tsunami records, numerical modeling and probabilistic methodologies for source identification must be used to determine coastal hazard zones.

Potential tsunami sources for the GOM are local submarine landslides [ten Brink et al.,

2009b]; sources outside the GOM are considered a very low threat and may not significantly impact GOM coastal communities or infrastructure [Knight, 2006]. Although a massive tsunamigenic underwater landslide in the GOM is considered a potential hazard, the frequency of such events (though not well-constrained) is probably quite low based on historical evidence [Dunbar and Weaver, 2008] and available data on ages of failures which suggest they were probably active prior to 7,000 years ago when large quantities of sediments were emptied into the GOM [ten Brink et al., 2009b]. However, sediments continue to empty into the GOM, mainly from the Mississippi River, contributing to slope steepening and the increase of fluid pore pressure in sediments which may lead to unstable slopes that can be subsequently triggered to failure by seismic loading [Masson et al., 2006, ten Brink et al., 2009a, Dugan and Stigall, 2010, Harbitz et al., 2014]. In addition, the unique geometry of the GOM basin makes even unlikely tsunami events potentially hazardous to the entire Gulf Coast. Waves tend to refract along continental slopes; thus, given the curved geomorphology of the GOM shelf and the concave shape of the coastline, any outgoing tsunami wave could potentially affect the opposite coast in addition to the coast close to the landslide source.

Five large-scale historical (ancient) submarine landslides with tsunamigenic potential have been identified within the GOM [ten Brink et al., 2009b, Chaytor et al., 2016], representing possible worst-case tsunami scenarios affecting GOM coasts in the past. In order to generate a more complete picture of landslide tsunami potential in the GOM, a probabilistic approach has been implemented to develop four additional synthetic landslide sources which fill gaps along the continental shelf between the historical landslide sources [Pampell-Manis et al., 2016]. These probabilistic tsunami sources are considered to be the maximum credible events that could happen in a particular region of the GOM according to the local bathymetry, seafloor slope, sediment information, and seismic loading. The probabilistic maximum credible events together with the historical sources form a suite of tsunami sources that have been used within coupled 3D and 2D numerical models to model tsunami generation and propagation throughout the GOM and to develop high-resolution inundation maps for the inundation-prone areas of two new communities along the Gulf Coast: Osprey-Venice-Englewood, FL and Sanibel Island-Naples, FL. These inundation studies showed that tsunamis triggered by massive submarine landslides have the potential to cause widespread and significant inundation of coastal cities. All of the twelve communities from both previous and current work and nine landslide sources are shown in Fig. 1.

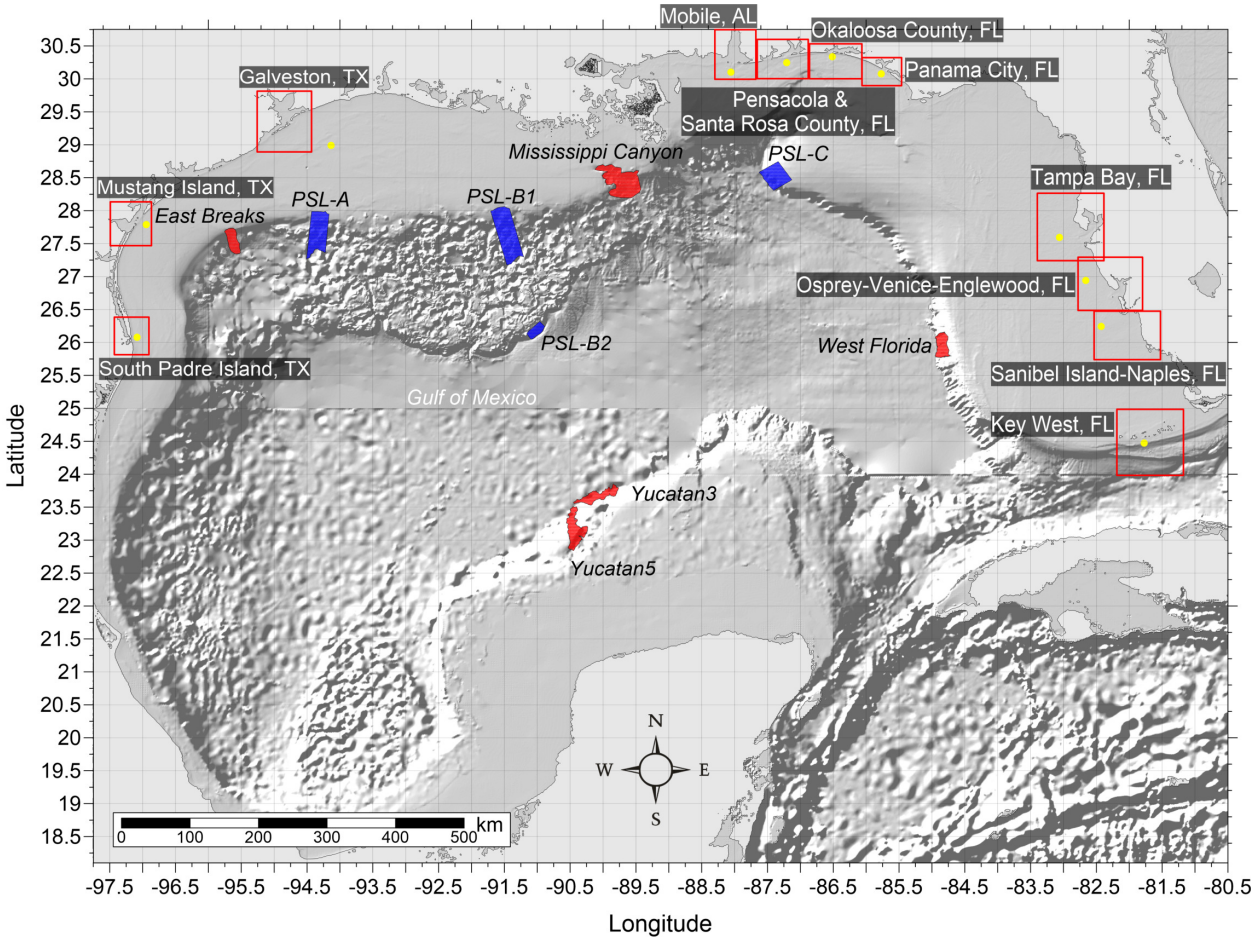

Figure 1: Selected communities or geography regions along the US GOM coastline where tsunami maps have been developed. Red rectangles denote 3 arcsecond (∼90m) domains of coastal communities where tsunami inundation has been modeled; red hatched areas are historical landslide sources; blue hatched areas are Probabilistic Submarine Landslide (PSL) sources; yellow dots are locations of numerical wave gauges. The zero-meter elevation contour is drawn to show the GOM coastline.

While high-resolution tsunami inundation studies have been completed for these twelve communities and are planned for additional locations, vulnerability assessments are still essential for coastal locations where inundation studies have not yet been performed or planned, or where there is a lack of high-resolution bathymetric and/or elevation data. Therefore, we aim to extend the results of the completed mapping studies in order to provide estimates of tsunami inundation zones for hazard mitigation efforts in un-mapped locations. Inundation maps with even low resolution are useful to emergency managers to create first-order evacuation maps, and some methods currently exist to provide low-resolution estimates of hazard zones for regions which do not currently have or warrant high-resolution maps. For example, guidance given by the National Tsunami Hazard Mitigation Program (NTHMP) Mapping and Modeling Subcommittee in "Guidelines and Best Practices to Establish Areas of Tsunami Inundation for Non-modeled or Low-hazard Regions" (available from `https://nws.weather.gov/nthmp/documents/3nonmodeledregionguidelines.pdf`) recommends that coastal areas and areas along ocean-connected waterways that are below 10 m (33 ft) elevation are at risk for most tsunamis, and rare and large tsunamis may inundate above this elevation. However, in low-lying coastal regions such as along the Gulf Coast, the 10 m (33 ft) elevation contour is too far inland to be reasonably applicable for estimating potential tsunami inundation zones. The guidance additionally suggests that low-lying areas are prone to inundation within 3 km (1.9 mi) inland for locally-generated tsunamis and within 2 km (1.3 mi) inland for distant sources. While these distances may be reasonable for some regions of the Gulf Coast, prevalent bathymetric and topographic features such as barrier islands/peninsulas complicate the method of delineating inundation-prone areas based on distance from the shoreline. As a result, the purpose of the current work is to improve the methodology which compares modeled tsunami inundation to modeled/predicted hurricane storm surge. Specifically, we aim to identify the hurricane category which produces modeled maximum storm surge that best approximates the maximum tsunami inundation in the two new locations modeled in this project. Even though many physical aspects of storm surge inundation are completely different from those of tsunamis (time scale, triggering mechanism, inundation process, etc.), good agreement or clear trends between tsunami and storm surge flooding on a regional scale can be used to provide first-order estimates of potential tsunami inundation in communities where detailed inundation maps have not yet been developed or are not possible due to unavailability of high-resolution bathymetry/elevation data. Additionally, since tsunamis are not well-understood as a threat along the Gulf Coast, while hurricane hazards are well-known, this method of predicting tsunami inundation from storm surge provides a way for GOM emergency managers to better prepare for potential tsunami events based on more understandable and accessible information.

Recent tsunamis have shown that the maritime community requires additional information and guidance about tsunami hazards and post-tsunami recovery [Wilson et al., 2012, 2013]. To accomplish mapping and modeling activities to meet NTHMP's planning/response purposes for the maritime community and port emergency management and other customer requirements, it is necessary to continue the process to include maritime products in our current inundation map development. These activities will include tsunami hazard maritime products generated by GOM's tsunami sources (submarine landslides) that may impact specifically ship channels, bay inlets, harbors, marinas, and oil infrastructures (e.g., des-

ignated lightering and oil tanker waiting zones), which has already been applied in other tsunami risk regions, e.g., California, Oregon and Washington. It is worth noting that Galveston was the first city where we implemented the maritime products [Horrillo et al., 2016]. The other nine locations, South Padre Island, TX, Mobile, AL, Panama City, FL, and Tampa, FL, mapped during project NA13NWS4670018 [Horrillo et al., 2015], and Pensacola, FL, Key West, FL, Okaloosa County, FL, Santa Rosa County, FL and Mustang Island, TX, were implemented in project NA15NWS4670031 and NA16NWS4670039 [Horrillo et al., 2017], and Osprey-Venice-Englewood, FL and Sanibel Island-Naples, FL, are added to the maritime portfolio in this project.

2.2 Regional and Historical Context

Osprey-Venice, FL

In this study, the Osprey-Venice, FL computational domain also includes the more inland cities like Vamo, Laurel and Nokomis, FL. This area lies in the Sarasota County, adjoined by the Manatee County to the north, DeSoto County to the east, and Charlotte County to the south. A long barrier island extends from the northwest Siesta Key to the southeast Venice Inlet. The Venice Island lies to the south of the inlet. Several bays east of the barrier island connect with each other, including the Little Sarasota Bay, Dryman Bay, Blackburn Bay, Lyons Bay, and Roberts Bay, from north to south. Toward the east of Venice Island, the Roberts bay is connected to a man-made channel, the Venetian Waterway, which is part of the Gulf Intracoastal Waterway. The barrier island and the Venice Island are linked to the mainland by several bridges; the historic one-lane swing bridge, Black Point Bridge, connects Cassey Key with mainland Osprey; the Albee Rd W, connects Nokomis Beach with mainland Nokomis; and Venice Island is connected to the mainland via N Tamiami Trail, E Venice Ave, and S Tamiami Trail, from north to south. U.S. 41 is the major highway going through the area, and the closest interstate highway is I-75 further to the east.

Englewood, FL

About 2/3 of the northern portion of Englewood belongs to the Sarasota County, while the southern portion belongs to the Charlotte County. Similar to Osprey-Venice, FL, this study area is protected by a long and thin barrier island, called Manasota Key, extending from South Venice to Stump Pass inlet. East of the barrier island, the Lemon Bay thins gradually toward the north where it meets the Venetian Waterway. By road, the Manasota Key is accessible from the mainland only via the Manasota Beach Rd and the Beach Rd, both joining Florida State Road 776, which eventually connects to U.S. 41 to the north.

The beautiful beaches in Osprey-Venice-Englewood, FL attract hundreds of thousands of tourists each year, and the barrier island is mostly occupied by hotels and residential areas. According to the 2010 census, the population of individual cities and towns are, Vamo 4727, Osprey 6100, Laurel 8171, Nokomis 3167, Venice 20746, and Englewood 14863.

Sanibel Island, FL

In this study, the Sanibel Island area includes Sanibel Island and Estero Island, located in Lee County. Unlike Osprey-Venice-Englewood, FL, these two islands are more detached from the mainland, featuring wide and more open bays like the San Carlos Bay. Sanibel Island is a spoon-shaped island off the southwest coast of Cape Coral and Fort Myers, FL. Most of the residents live on the south coast of Sanibel Island and the JN Ding Darling National Wildlife Refuge takes over half of the island. Sanibel-Captiva Road runs across west-east on Sanibel Island, separating the refuge from the southern residential region. By land, Sanibel Island is only accessible via the Sanibel Causeway to the east. Separated by San Carlos Bay from the Sanibel Island, Estero Island is also included in the inundation study grid because it is densely populated. Estero Island is connected to the mainland via FL-865, which runs through San Carlos Island. To the south, Estero Island is separated from Black Island by the Big Carlos Pass, which links the GOM to the Estero Bay Aquatic Preserve.

Naples, FL

The Naples, FL area includes the southeastern Bonita Springs, west North Naples, and Naples, FL, which are all within the Collier County. From north to south, the barrier island chain comprises Big Hickory Island, Little Hickory Island, Wiggins Island, Vanderbilt Beach, and most of Naples west of the bays. As the barrier island widens toward the south, the bays (Estero Bay, Little Hickory Bay, Inner Clam Bay, Outer Clam Bay, Venetian Bay, Moorings Bay, Naples Bay) becomes thinner. According to the 2010 census, the population of individual cities and towns are, Sanibel Island 6469, Fort Myers Beach (Estero Island) 6277, Bonita Springs 43914, Naples park 5967, Pelican Bay 6346, Pine Ridge 1918, and Naples 19537.

Recent Hurricane History

Florida is frequented by hurricanes due to its unique location and long coastlines. Our study location in southwestern Florida is no exception. This area has been visited by many major hurricanes, and recent ones are briefly summarized as follows. Hurricane Irma became category 4 when it landed Florida in 2017, down from category 5 when it first hit Cuba, which greatly reduced the damage. Nonetheless, Irma still remains as one of the costliest storms in the history of Florida. Wind from Hurricane Irma damaged many homes and uprooted and knocked over trees, and caused power outage to Collier County, Lee County, Charlotte County, and Sarasota County. The last major hurricane that hit Florida before Irma was Hurricane Wilma which made landfall in Collier County, FL on October 24, 2005. Mandatory evacuations were ordered for Collier County residents southwest of US 41. The peak of storm surge occurred in the Naples area, and the Naples Airport was damaged significantly. Charlotte and Manatee only suffered minor damage from Wilma. Hurricane Charley, a category 4 hurricane, made landfall in southwest Florida in mid-August, 2004, and caused ten deaths and severe damage to buildings and crops, making it the second costliest hurricane at the time. Southwestern Florida, including Sarasota and Charlotte County, has seen the most severe damage. Other major hurricanes that have made landfall in Florida

but did not make much impact in southwestern Florida include Hurricane Ivan in 2004, Hurricane Dennis in 2005.

Although the probability of a large-scale tsunami event in the GOM is low, this and previous studies have indicated that tsunami events with characteristics similar to those detailed in Horrillo et al. [2015] have the potential to cause severe flooding and damage to GOM coastal communities that is similar to or even greater than that seen from major hurricanes, particularly in open beach and barrier island regions. Tsunami hazard maritime products such as tsunami current magnitude, vorticity, safe/hazard zones would be central for future developments of maritime hazard maps, maritime emergency response as well as infrastructure planning. The results of this work are intended to provide guidance to local emergency managers to help with managing urban growth, evacuation planning, and public education with the vision to mitigate potential GOM tsunami hazards.

This report is organized as follows. Section 3 briefly describes all 9 landslide sources, including the 2 new Yucatan sources, used for tsunami modeling (3.1) and the numerical models used for simulations (3.2). Section 4 covers the inundation and momentum flux maps for Osprey-Venice-Englewood, FL and Sanibel Island-Naples, FL. The comparison between tsunami inundation and hurricane storm surge inundation is given in Section 5 for the two new Gulf Coast communities. Current velocity and vorticity maps are described in Section 6 for the two new communiteis. Concluding remarks on general trends seen among the communities and practical applications for other regions are given in Section 7.

3 Tsunami Inundation Modeling

3.1 Landslide Tsunami Sources

Nine large-scale landslide configurations were created assuming an unstable (gravity-driven) sediment deposit condition. Five of these landslide configurations are historical events identified by ten Brink et al. [2009b]: the Eastbreaks, Mississippi Canyon, and West Florida submarine landslides; and Chaytor et al. [2016]: the Yucatan #3 and Yucatan #5 landslides, which are shown as red hatched regions in Fig. 1. The Yucatan Shelf/Campeche Escarpment was the last remaining area of the GOM that had not been evaluated for landslide tsunami hazards, until high-resolution mapping data collected in 2013 [Paull et al., 2014] shows that the Yucatan Shelf/Campeche Escarpment margin has been subjected to intense modifications by Cenozoic mass wasting processes. Although no known tsunami events have been linked to these Yucatan sources, numerical modeling result shows that they are capable of generating tsunamis that could propagate throughout the GOM Basin [Chaytor et al., 2016]. Our simulation results show that the two new Yucatan sources can generate some impact on South Padre Island, TX and Panama City, FL regions, with maximum wave amplitude of 1 - 3 m (Fig. 25 and Fig. 28). The other four were obtained using a probabilistic methodology based on work by Maretzki et al. [2007] and Grilli et al. [2009] and extended for the GOM by Pampell-Manis et al. [2016]. The probabilistic landslide configurations were determined based on distributions of previous GOM submarine landslide dimensions through a Monte Carlo Simulation (MCS) approach. The MCS methodology incorporates a statistical correlation method for capturing trends seen in observational data for landslide size parameters while still allowing for randomness in the generated landslide dimensions. Slope stability analyses are performed for the MCS-generated trial landslide configurations using landslide and sediment properties and regional seismic loading (Peak Horizontal ground Acceleration, PHA) to determine landslide configurations which fail and produce a tsunami. The probability of each tsunamigenic failure is calculated based on the joint probability of the earthquake PHA and the probability that the trial landslide fails and produces a tsunami wave above a certain threshold. Those failures which produce the largest tsunami amplitude and have the highest probability of occurrence are deemed the most extreme probabilistic events, and the dimensions of these events are averaged to determine maximum credible probabilistic sources. The four maximum credible Probabilistic Submarine Landslides (PSLs) used as tsunami sources for this study are termed PSL-A, PSL-B1, PSL-B2, and PSL-C and are shown as blue hatched regions in Fig. 1. Table 1 summarizes general information (location, age/recurrence, area, volume, excavation depth and modeled volume) of submarine landslide sources listed in Table 2 through Table 19. Two values for volume are given for the landslides in Table 1: Maximum Credible Volume/Probabilistic Average Volume and Modeled Volume; this is because landslide configurations are carved out from the actual bathymetry to obtain the 3D numerical model volumes. The volumes are different in some places due to the amount of seafloor irregularity present in that region. For a more complete discussion of GOM submarine landslide sources, the reader can consult Horrillo et al. [2015], Pampell-Manis et al. [2016].

Odd-numbered Tables from 3 to 19 summarize coordinate limits of the 3D domain for

Table 1: Submarine Landslide general information.

Submarine Landslide	Location (Lon, Lat)	Age/Recurrence (Years)	Area (km^2)	Volume (km^3)	Excavation Depth (m)	Modeled Volume (km^3)
East Breaks	-95.68, 27.70	$\sim 10000 - 25000$	~ 519.52	~ 21.95	~ 160	26.7
Mississippi	-90.00, 28.60	$\sim 7500 - 11000$	~ 3687.26	~ 425.54	~ 300	425
West Florida	-84.75, 25.95	> 10000	~ 647.57	~ 16.2	~ 150	18.4
Yucatan #3	-90.07, 23.00	–	~ 578	~ 38	~ 278	39.3
Yucatan #5	-89.80, 23.54	–	~ 1094	~ 70.2	~ 385	69.5
PSL-A	-94.30, 27.98	$\sim 7700 - 7800$	~ 1686	~ 57	~ 67	58
PSL-B1	-91.56, 28.05	$\sim 5400 - 5500$	~ 3118	~ 69	~ 44	57.3
PSL-B2	-91.01, 26.17	$\sim 4700 - 4800$	~ 282	~ 45	~ 323	68
PSL-C	-87.20, 28.62	$\sim 550 - 650$	~ 1529	~ 315	~ 404	357

each landslide event and other important information including: spatial resolution, time step size, domain maximum water depth, number of computational cells, and the elapsed time of landslide deformation from the onset of sediment failure to the time of maximum potential energy transferred from the landslide to the water. The elapsed time of the landslide deformation is determined by the 3D domain size and the total energy of the water induced by the submarine landslide to obtain the initial dynamic tsunami surface deformation.

Figures 2, 5, 8, 11, 14, 17, 20, 23 and 26 together with even-numbered Tables from 2 to 18, depict some important characteristics of the submarine landslides used in this work. The figures portray the 3D model domain limits for each of the submarine landslides and indicate the location and the pre-failure landslide configuration. The tables present general information on the submarine landslides and important characteristics required for the numerical calculations of the initial dynamic surface deformation.

Eastbreaks Submarine Landslide General Information

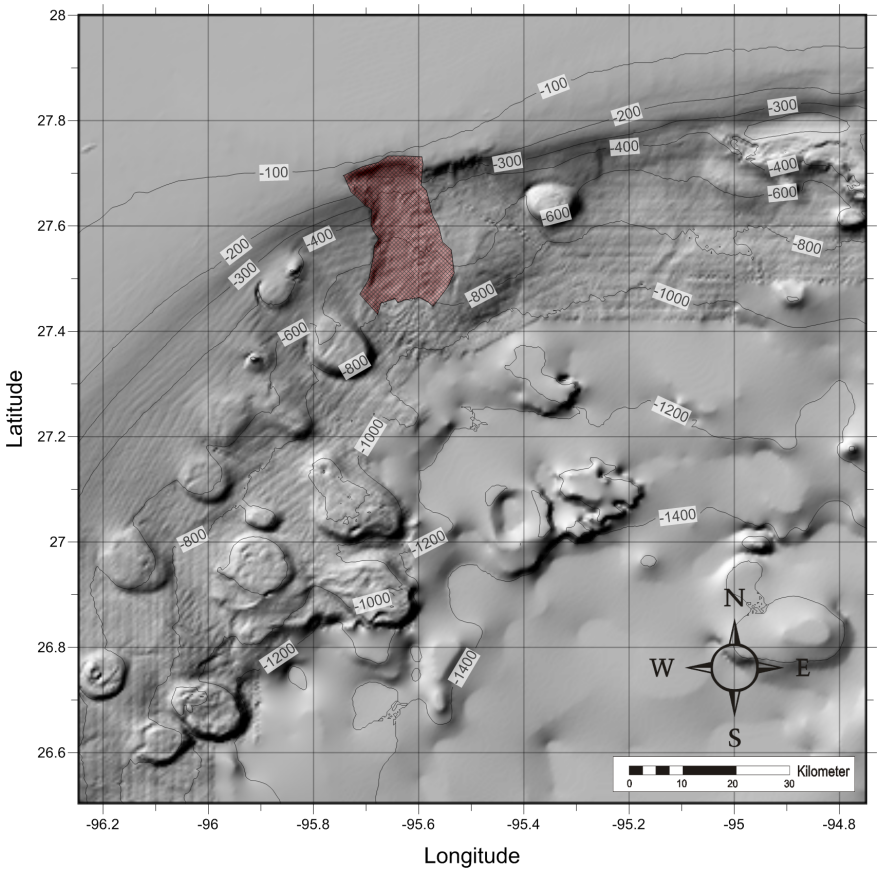

Figure 2: EastBreaks submarine landslide location, excavation limits, and surrounding bathymetry (in meters).

Table 2: Eastbreaks Submarine Landslide general information

Geologic Setting	Shelf break edge
Post Failure Sedimentation:	Canyon appears to be partially filled (predominantly failure deposits with some post-failure sedimentation)
Age:	10000 - 25000 years
Maximum Credible Single Event:	Maximum: Volume: 21.95 km^3 Area: 519.52 km^2
Other Reported Volumes:	50 - 60 km^3
Excavation Depth:	$\sim$ 160 m (shelf to base of headwall scarp)
Run-out Distance:	91 km from end of the excavation and 130 km from headwall based on GLORIA mapping effort
Other Reported Run-out Distance:	160 km
3D Numerical Model volume	26.7 km^3

Figure 3 depicts tsunami arrival time of the East Breaks Submarine Landslide scenario for the entire GOM (one arcminute resolution). Figure 4 shows maximum tsunami wave amplitude using the same lower spatial resolution (one arcminute) to obtain on a global scale the energy focusing mechanisms along the continental shelf and the effect of predominant bathymetric features of the GOM like shelf break slopes, submarine escarpments, and submarine canyons.

Table 3: Coordinate limits for the EastBreaks Submarine Landslide Domain to obtain initial dynamic tsunami wave source

EastBreaks Submarine Landslide 3D Domain (Resolution 15 arcseconds)	
Longitude	$96.25°W$ - $94.75°W$
Latitude	$26.50°N$ - $28.00°N$
$dx = dy$ and dz	15 arcsec and variable 1 - 10 m
Max. Water Depth	$1,703$ m
dt (variable)	≤ 0.50 sec
# of Cells in the x, y, z-direction	$360 \times 360 \times 350$
Total # of Cells	$45,360,000$
Elapsed time of landslide deformation	960 sec (16 min)

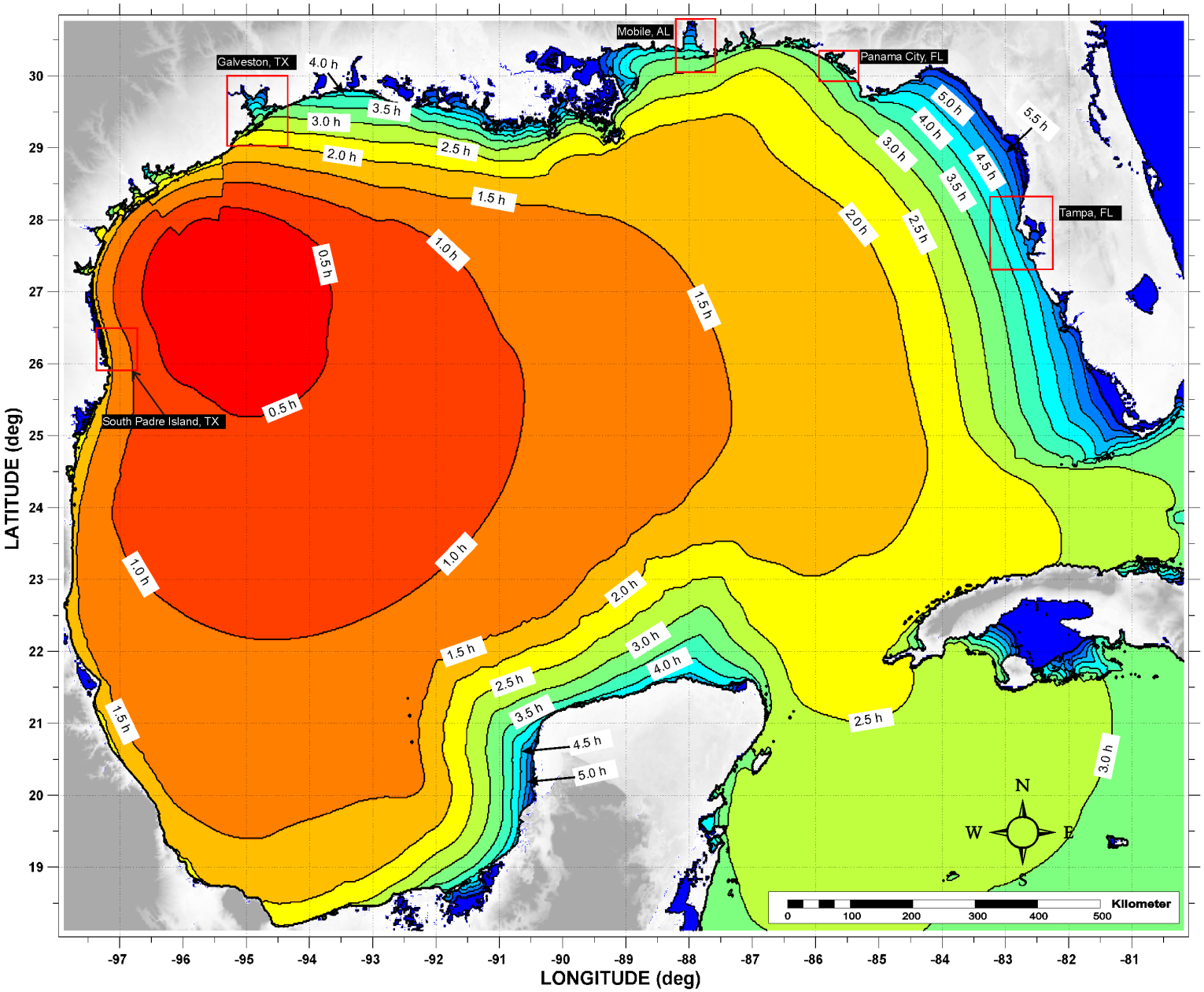

Figure 3: Tsunami arrival time for the East Breaks Submarine Landslide scenario.

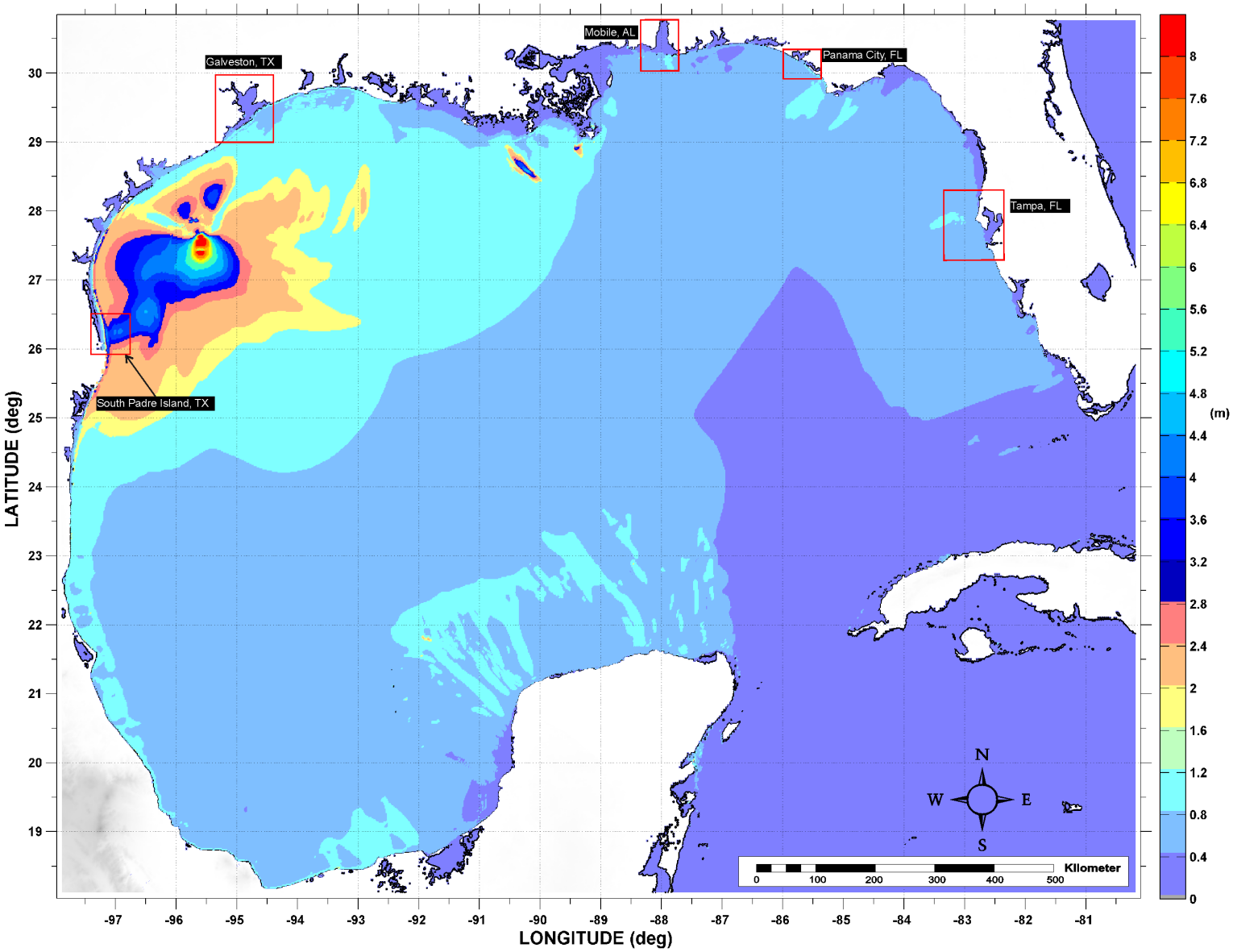

Figure 4: Maximum tsunami wave amplitude (one arcminute resolution) for the East Breaks Submarine Landslide scenario.

Probabilistic Submarine Landslide A (PSL-A) General Information

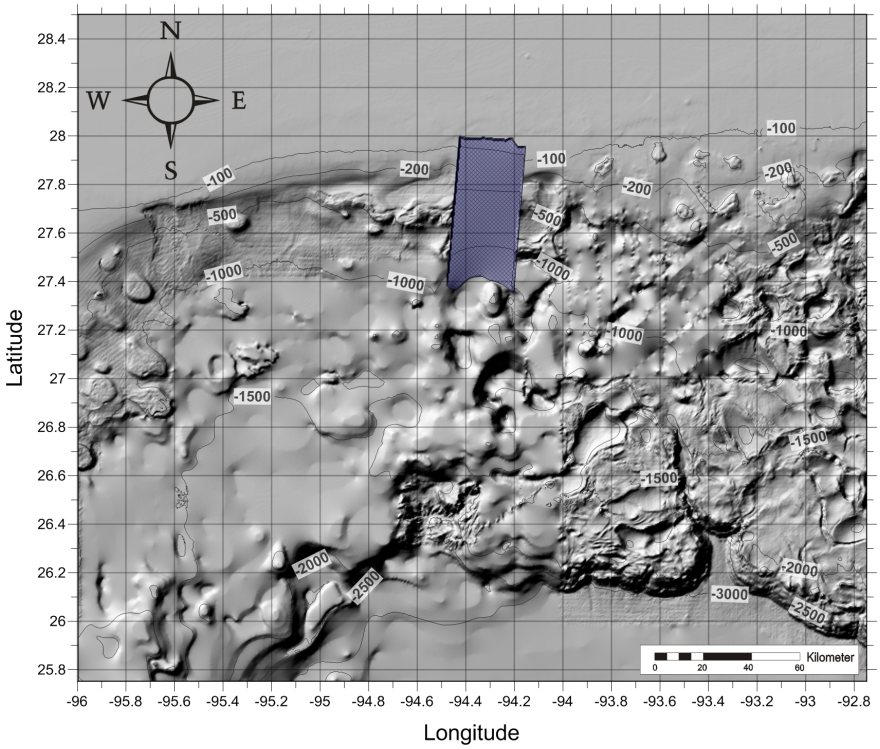

Figure 5: Probabilistic Submarine Landslide -A- location, excavation limits, and surrounding bathymetry (in meters).

Table 4: Probabilistic Submarine Landslide A

Geologic Setting	Shelf break edge
Predominant Sediment	Clay
Trigger Mechanism / Recurrence	Earthquake / $3,940 - 4,570$ years
Type of Sediment Failure	Translational
Probabilistic Tsunami Recurrence	$7,700 - 7,800$ years
Probabilistic Avg: Volume	~ 57 km^3
Area	$\sim 1,686$ km^2
Excavation: Headscarp Thickness	~ 67 m
Length	~ 68 km
Width	~ 25 km
3D Model Volume	58 km^3

Figure 6 depicts tsunami arrival time of the Probabilistic Submarine Landslide A (PSL-A) scenario (one arcminute resolution) for the entire GOM. Figure 7 shows maximum tsunami wave amplitude using the same lower spatial resolution (one arcminute) to obtain on a global scale the energy focusing mechanisms along the continental shelf and the effect of predominant bathymetric features of the GOM like shelf break slopes, submarine escarpments, and submarine canyons.

Table 5: Coordinate limits for the PSL-A Submarine Landslide Domain to obtain initial dynamic tsunami wave source

PSL-A Submarine Landslide 3D Domain (Resolution 15 arcseconds)	
Longitude	$96.00°W$ - $92.75°W$
Latitude	$25.75°N$ - $28.50°N$
$dx = dy$ and dz	15 arcsec and 1 - 34 m
Max. Water Depth	$3,340$ m
dt (variable)	≤ 0.75 sec
# of Cells in the x, y, z-direction	$780 \times 660 \times 200$
Total # of Cells	$102,960,000$
Elapsed time of landslide deformation	1500 sec (25 min)

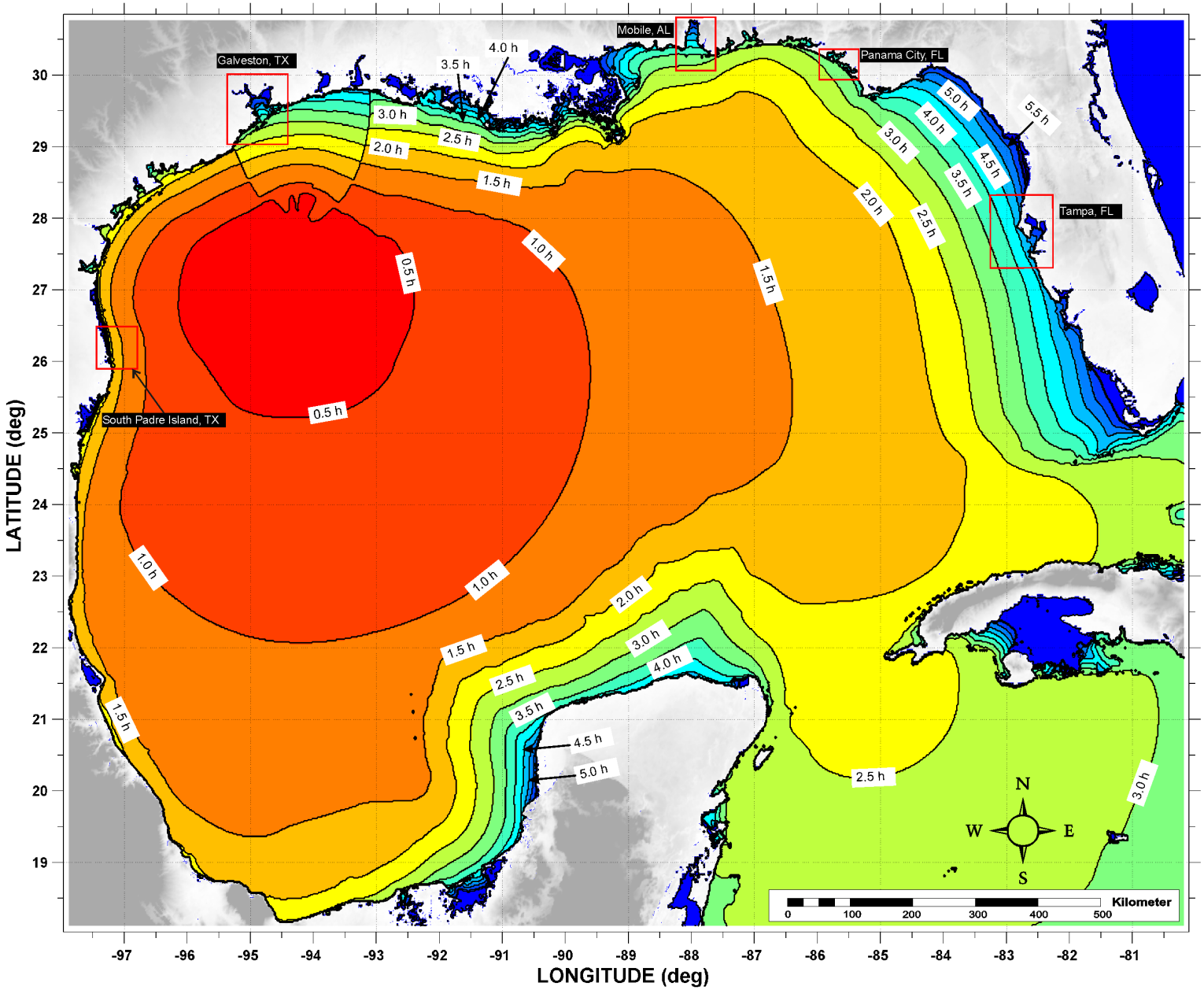

Figure 6: Tsunami arrival time for the Probabilistic Submarine Landslide -A- (PSL-A) scenario.

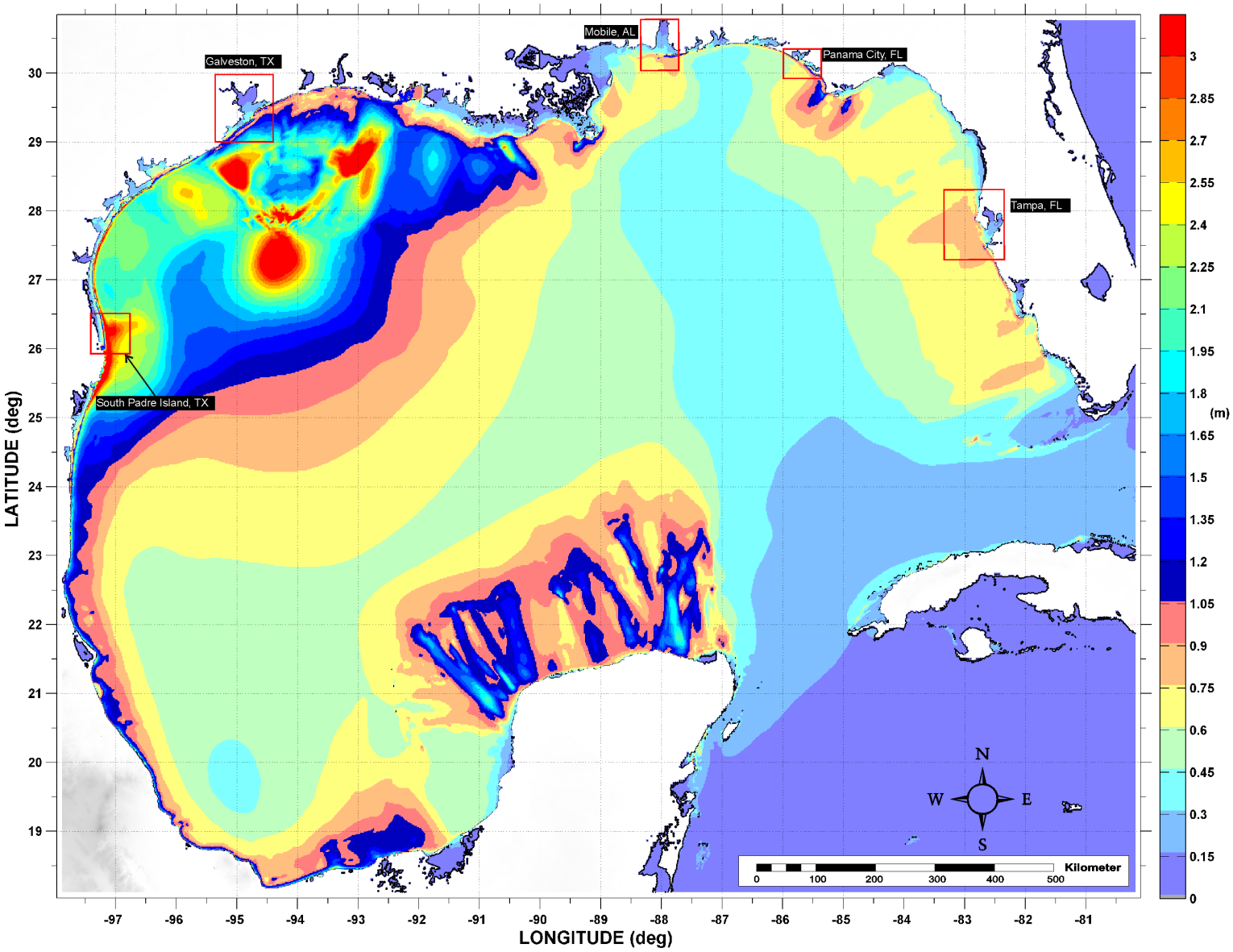

Figure 7: Maximum tsunami wave amplitude (one arcminute resolution) for the Probabilistic Submarine Landslide -A- (PSL-A) scenario.

Probabilistic Submarine Landslide B1 (PSL-B1) General Information

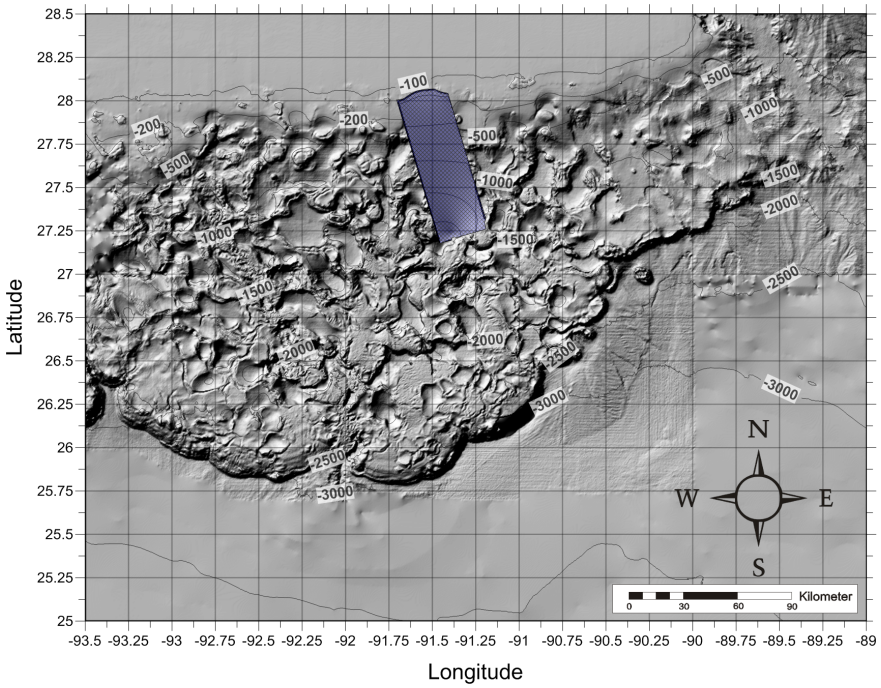

Figure 8: Probabilistic Submarine Landslide -B1- location, excavation limits, and surrounding bathymetry (in meters).

Table 6: Probabilistic Submarine Landslide B1

Geologic Setting	Shelf break edge
Predominant Sediment	Clay
Trigger Mechanism / Recurrence	Earthquake / $3,460 - 3,790$ years
Type of Sediment Failure	Translational
Probabilistic Tsunami Recurrence	$5,400 - 5,500$ years
Probabilistic Avg: Volume	69 km^3
Area	3118 km^2
Excavation: Headscarp Thickness	$\sim$ 44 m
Length	$\sim$ 96 km
Width	$\sim$ 32 km
3D Model Volume	57.3 km^3

Figure 9 depicts tsunami arrival time of the Probabilistic Submarine Landslide B1 (PSL-B1) scenario (one arcminute resolution) for the entire GOM. Figure 10 shows maximum tsunami wave amplitude using the same lower spatial resolution (one arcminute) to obtain on a global scale the energy focusing mechanisms along the continental shelf and the effect of predominant bathymetric features of the GOM like shelf break slopes, submarine escarpments, and submarine canyons.

Table 7: Coordinate limits for the PSL-B1 Submarine Landslide Domain to obtain initial dynamic tsunami wave source

PSL-B1 Submarine Landslide 3D Domain (Resolution 15 arcseconds)	
Longitude	$93.50°W$ - $89.00°W$
Latitude	$25.00°N$ - $28.50°N$
$dx = dy$ and dz	15 arcsec and 1 - 37 m
Max. Water Depth	$3,658$ m
dt (variable)	≤ 0.72 sec
# of Cells in the x, y, z-direction	$1,080 \times 840 \times 200$
Total # of Cells	$181,440,000$
Elapsed time of landslide deformation	1800 sec (30 min)

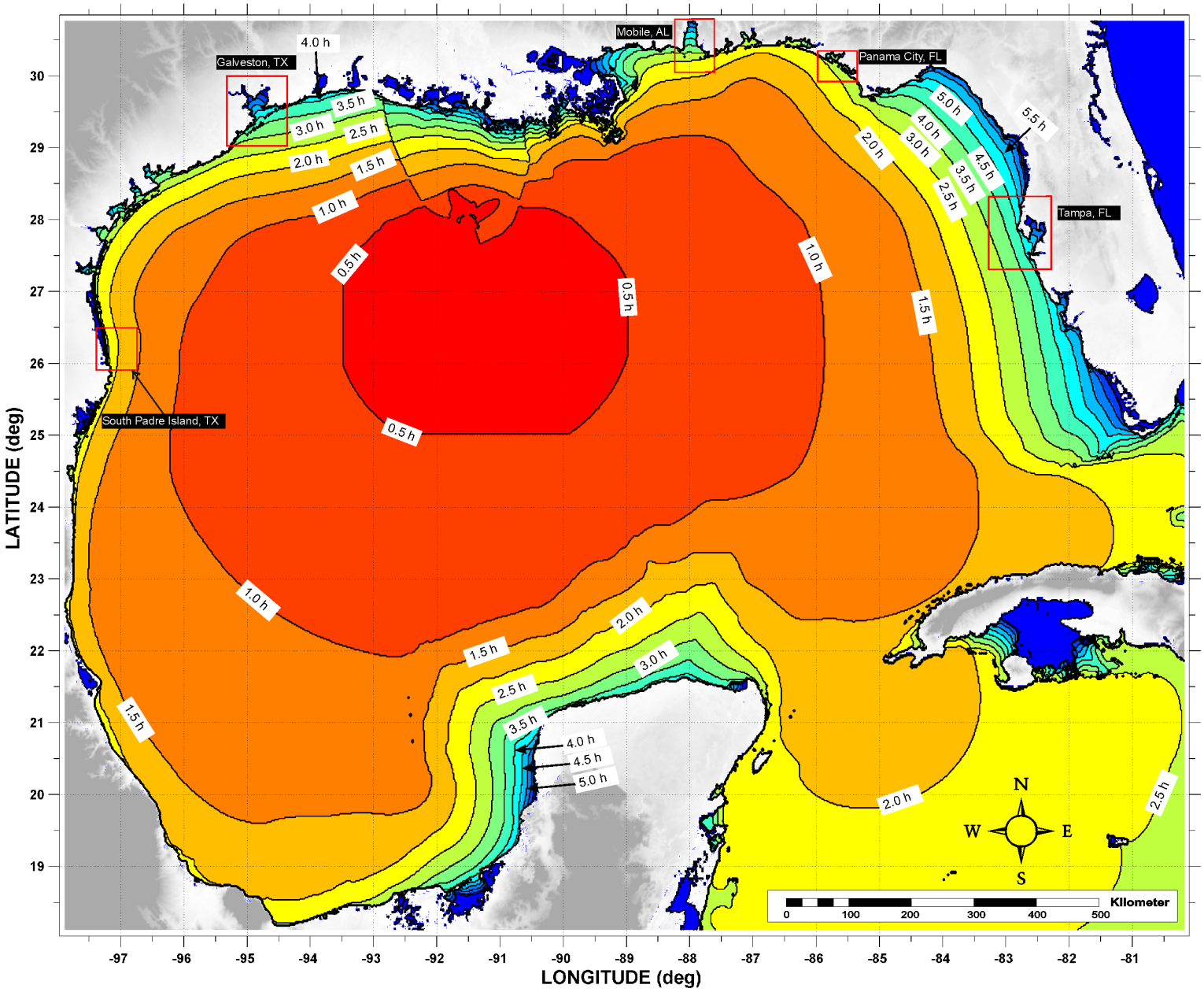

Figure 9: Tsunami arrival time for the Probabilistic Submarine Landslide -B1- (PSL-B1) scenario.

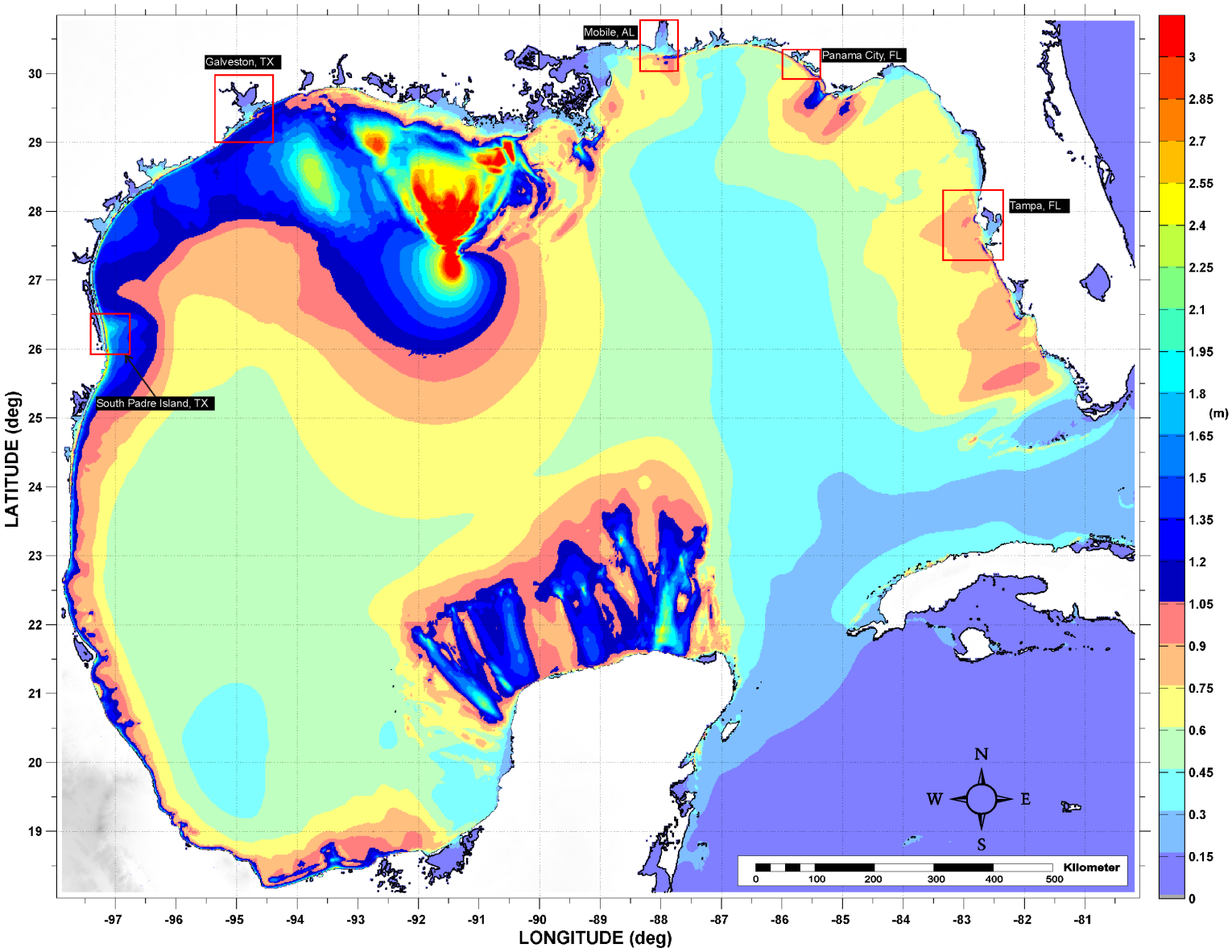

Figure 10: Maximum tsunami wave amplitude (one arcminute resolution) for the Probabilistic Submarine Landslide -B1- (PSL-B1) scenario.

Probabilistic Submarine Landslide B2 (PSL-B2) General Information

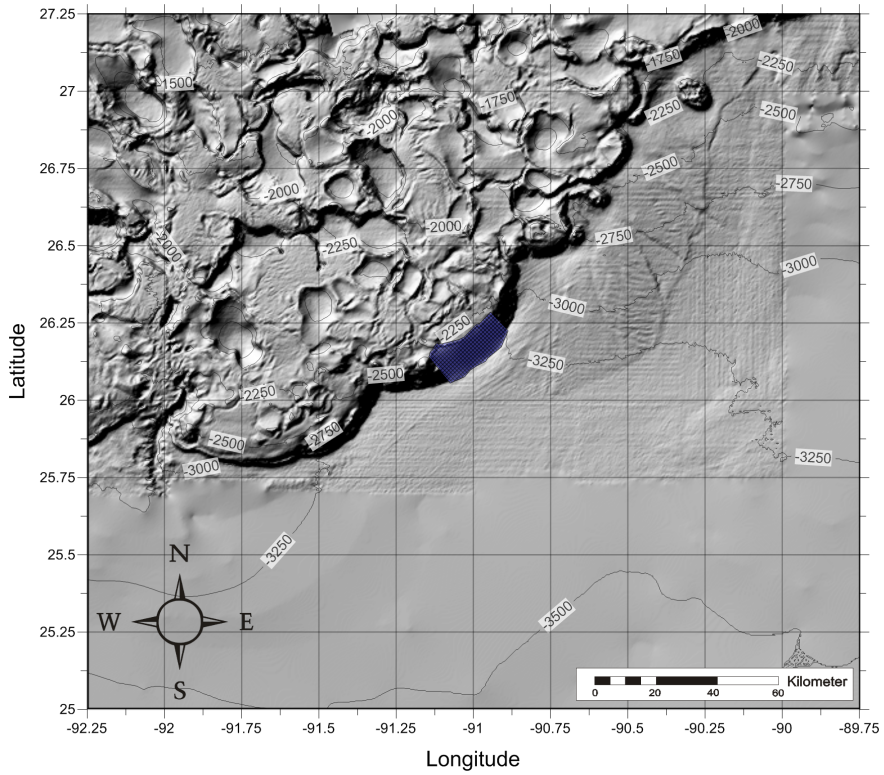

Figure 11: Probabilistic Submarine Landslide -B2- location, excavation limits, and surrounding bathymetry (in meters).

Table 8: Probabilistic Submarine Landslide B2

Geologic Setting	Escarpment-edge
Predominant Sediment	Clay
Trigger Mechanism / Recurrence	Earthquake /$340 - 350$ years
Type of Sediment Failure	Translational
Probabilistic Tsunami Recurrence:	$4,700 - 4,800$ years
Probabilistic Avg: Volume	45 km^3
Area	282 km^2
Excavation: Headscarp Thickness	$\sim$ 323 m
Length	$\sim$ 13 km
Width	$\sim$ 22 km
3D Model Volume	68 km^3

Figure 12 depicts tsunami arrival time of the Probabilistic Submarine Landslide B2 (PSL-B2) scenario (one arcminute resolution) for the entire GOM. Figure 13 shows maximum tsunami wave amplitude using the same lower spatial resolution (one arcminute) to obtain on a global scale the energy focusing mechanisms along the continental shelf and the effect of predominant bathymetric features of the GOM like shelf break slopes, submarine escarpments, and submarine canyons.

Table 9: Coordinate limits for the PSL-B2 Submarine Landslide Domain to obtain initial dynamic tsunami wave source

PSL-B2 Submarine Landslide 3D Domain (Resolution 15 arcseconds)	
Longitude	$92.25°W$ - $89.75°W$
Latitude	$25.00°N$ - $27.25°N$
$dx = dy$ and dz	15 arcsec and 1 - 37 m
Max. Water Depth	$3,607$ m
dt (variable)	≤ 0.8 sec
# of Cells in the x, y, z-direction	$600 \times 540 \times 200$
Total # of Cells	$64,800,000$
Elapsed time of landslide deformation	480 sec (8 min)

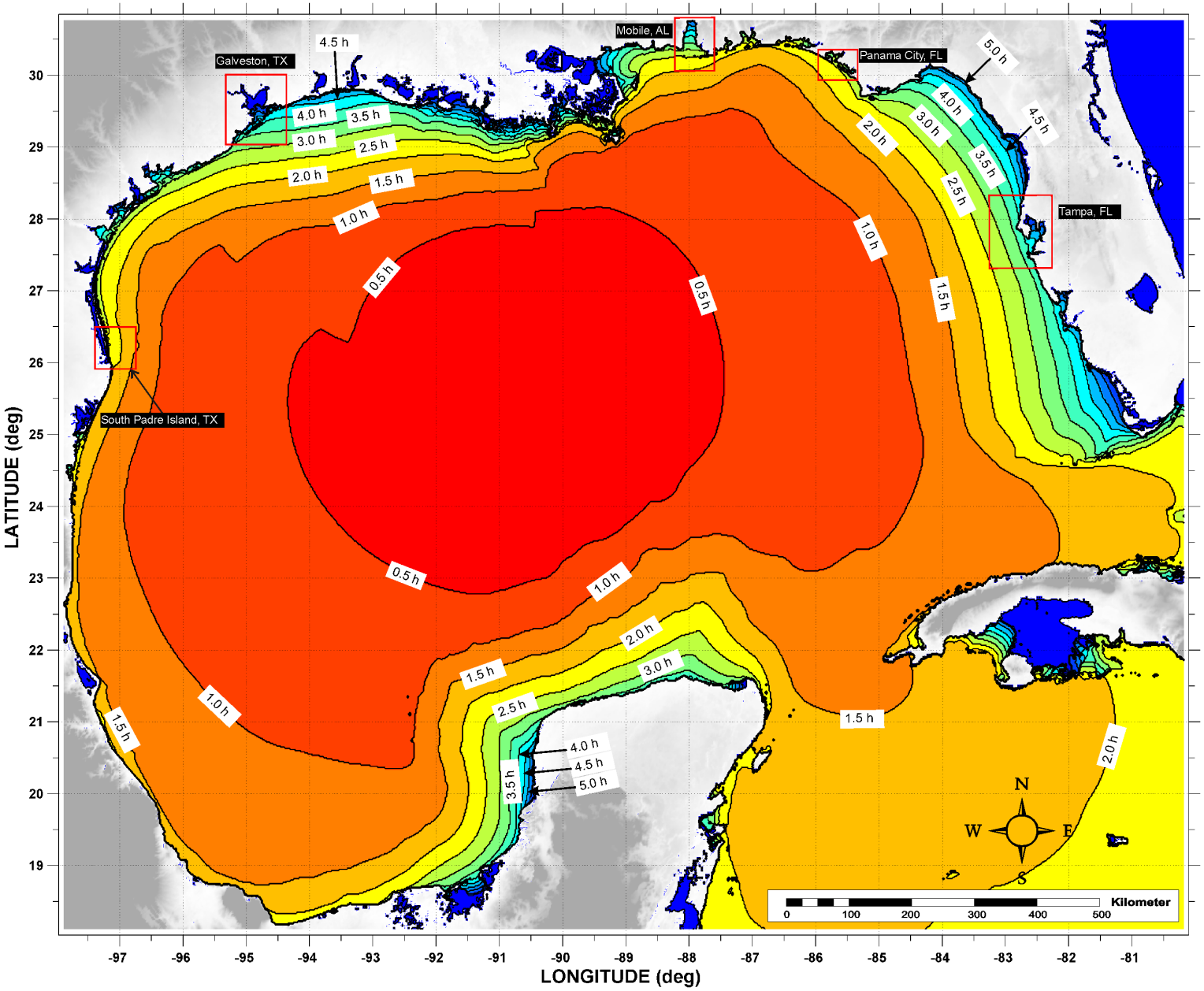

Figure 12: Tsunami arrival time for the Probabilistic Submarine Landslide -B2- (PSL-B2) scenario.

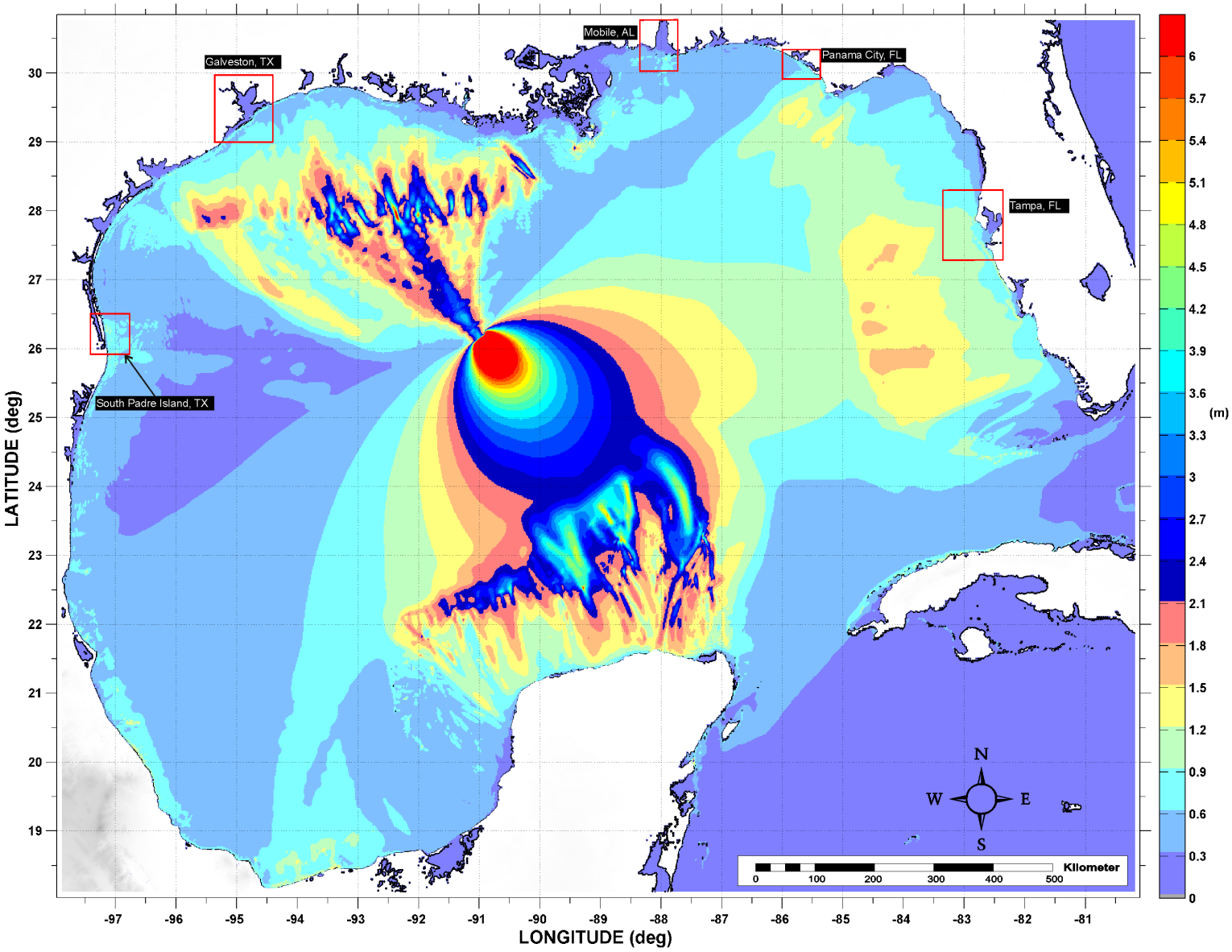

Figure 13: Maximum tsunami wave amplitude (one arcminute resolution) for the Probabilistic Submarine Landslide -B2- (PSL-B2) scenario.

Mississippi Canyon Submarine Landslide General Information

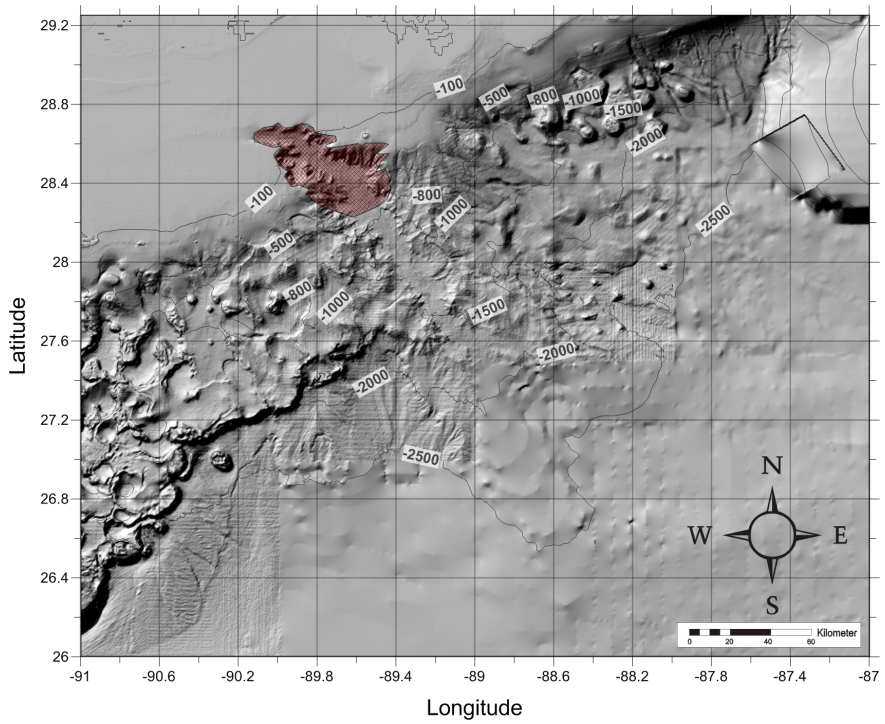

Figure 14: Mississippi Canyon submarine landslide location, excavation limits and surrounding bathymetry (in meters).

Table 10: Mississippi Canyon Submarine Landslide

Geologic Setting	Shelf-edge delta and fan system
Post Failure Sedimentation:	Canyon appears to be partially filled (failure deposits or post-failure sedimentation)
Age:	7500 - 11000 years
Maximum Credible Single Event:	Maximum: Volume: 425.54 km^3 Area: 3687.26 km^2
Other Reported Volumes:	1750km^3, 1500 - 2000 km^3
Excavation Depth:	$\sim$ 300 m (in the upper canyon)
Run-out Distance:	297 km from toe of the excavation area and 442 km from the headwall scarp
3D Model volume	425 km^3

Figure 15 depicts tsunami arrival time of the Mississippi Canyon Submarine Landslide scenario (one arcminute resolution) for the entire GOM. Figure 16 shows maximum tsunami wave amplitude using the same lower spatial resolution (one arcminute) to obtain on a global scale the energy focusing mechanisms along the continental shelf and the effect of predominant bathymetric features of the GOM like shelf break slopes, submarine escarpments, and submarine canyons.

Table 11: Coordinate limits for the Mississippi Canyon Submarine Landslide Domain to obtain initial dynamic tsunami wave source

Mississippi Canyon Submarine Landslide 3D Domain (Resolution 15 arcseconds)	
Longitude	$91.00°W$ - $87.00°W$
Latitude	$26.00°N$ - $29.25°N$
$dx = dy$ and dz	15 arcsec and 1 - 30 m
Max. Water Depth	$3,389$ m
dt (variable)	≤ 0.5 sec
# of Cells in the x, y, z-direction	$960 \times 780 \times 233$
Total # of Cells	$174,470,400$
Elapsed time of landslide deformation	1861 sec ($\sim$ 31 min)

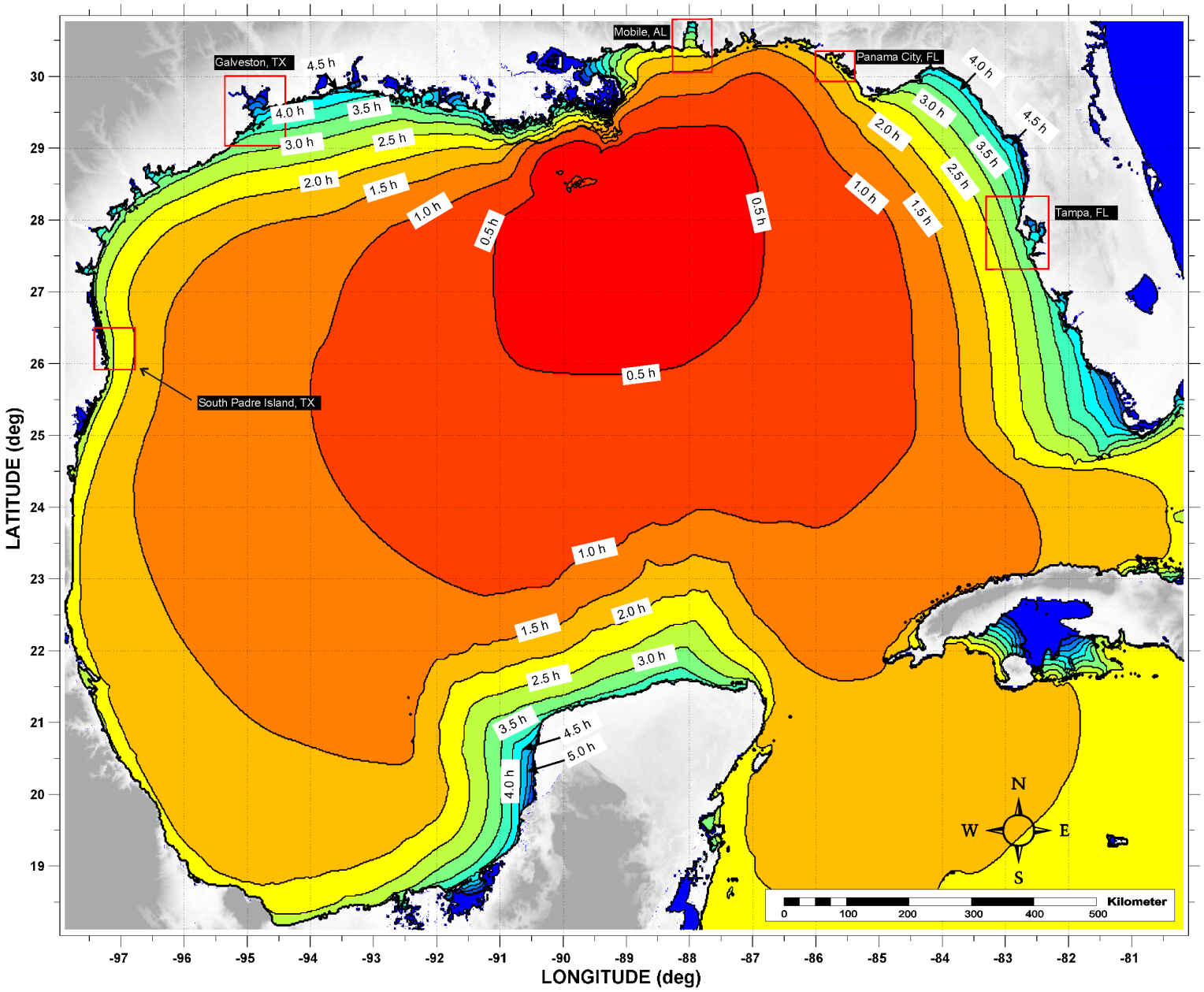

Figure 15: Tsunami arrival time for the Mississippi Canyon Submarine Landslide scenario.

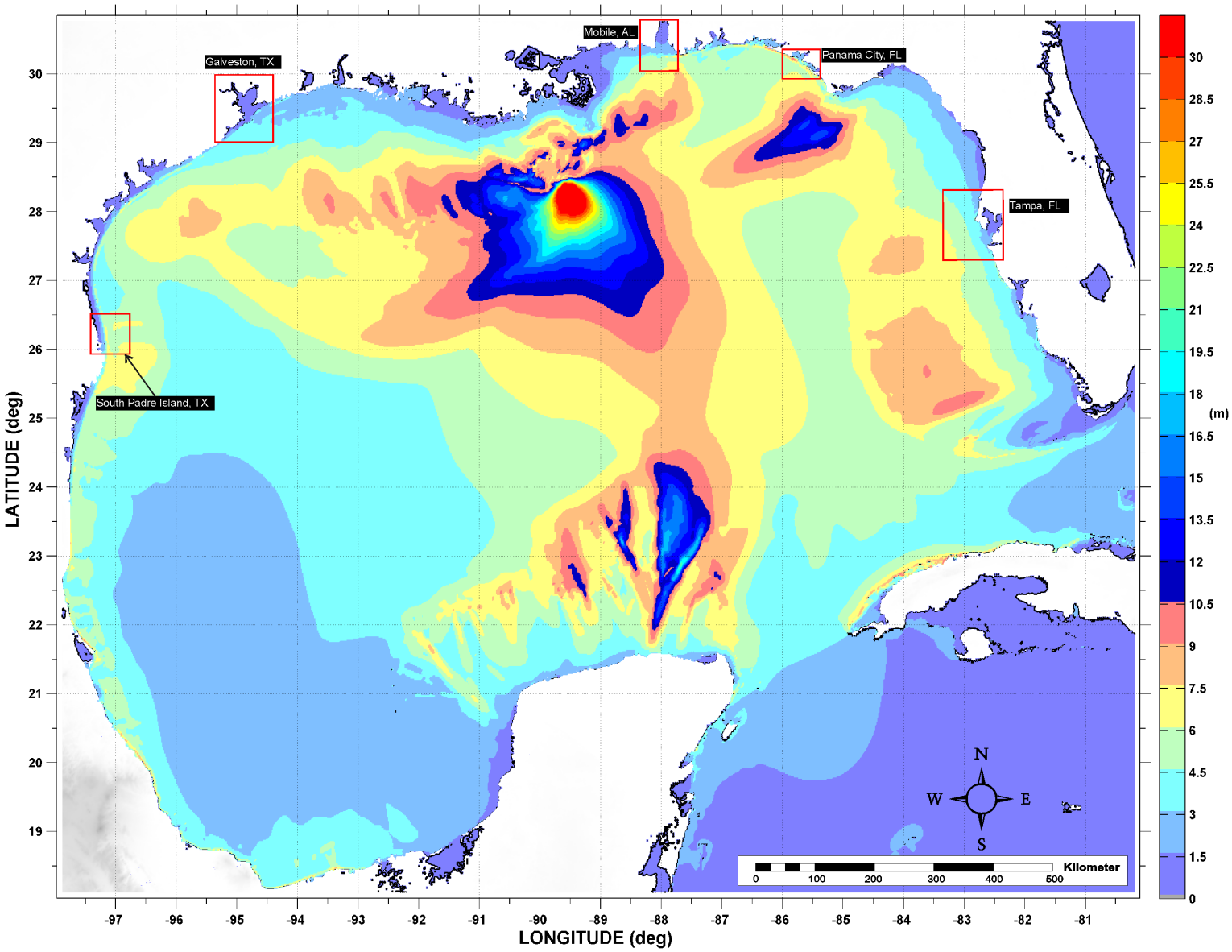

Figure 16: Maximum tsunami wave amplitude (one arcminute resolution) for the Mississippi Canyon Submarine Landslide scenario.

Probabilistic Submarine Landslide C (PSL-C) General Information

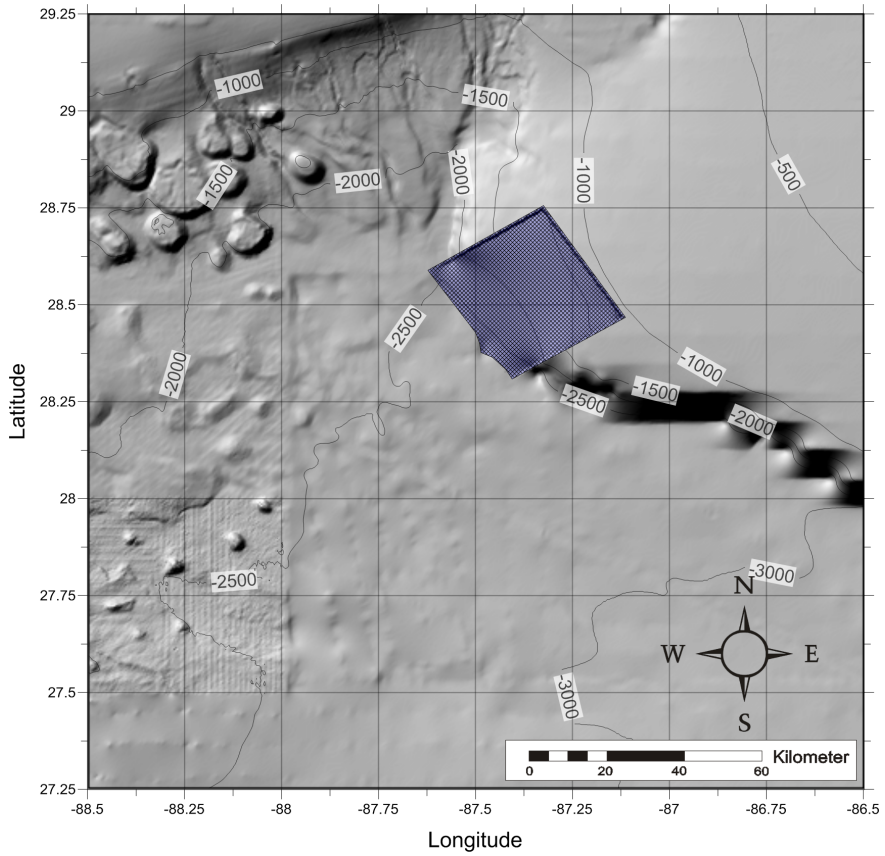

Figure 17: Probabilistic Submarine Landslide -C- location, excavation limits, and surrounding bathymetry (in meters).

Table 12: Probabilistic Submarine Landslide C

Geologic Setting	Shelf-slope
Predominant Sediment	Clay
Trigger Mechanism / Recurrence	Earthquake / $130 - 160$ years
Type of Sediment Failure	Translational
Probabilistic Tsunami Recurrence	$550 - 650$ years
Probabilistic Avg: Volume	315 km^3
Area	$1,529$ km^2
Excavation: Headscarp Thickness	~ 404 m
Length	~ 34 km
Width	~ 46 km
3D Model Volume	357 km^3

Figure 18 depicts tsunami arrival time of the Probabilistic Submarine Landslide C (PSL-C) scenario (one arcminute resolution) for the entire GOM. Figure 19 shows maximum tsunami wave amplitude using the same lower spatial resolution (one arcminute) to obtain on a global scale the energy focusing mechanisms along the continental shelf and the effect of predominant bathymetric features of the GOM like shelf break slopes, submarine escarpments, and submarine canyons.

Table 13: Coordinate limits for the PSL-C Submarine Landslide Domain to obtain initial dynamic tsunami wave source

PSL-C Submarine Landslide 3D Domain (Resolution 15 arcseconds)	
Longitude	$88.50°W$ - $86.50°W$
Latitude	$27.25°N$ - $29.25°N$
$dx = dy$ and dz	15 arcsec and 1 - 16 m
Max. Water Depth	$3,158$ m
dt (variable)	≤ 0.5 sec
# of Cells in the x, y, z-direction	$480 \times 480 \times 405$
Total # of Cells	$93,312,000$
Elapsed time of landslide deformation	600 sec (10 min)

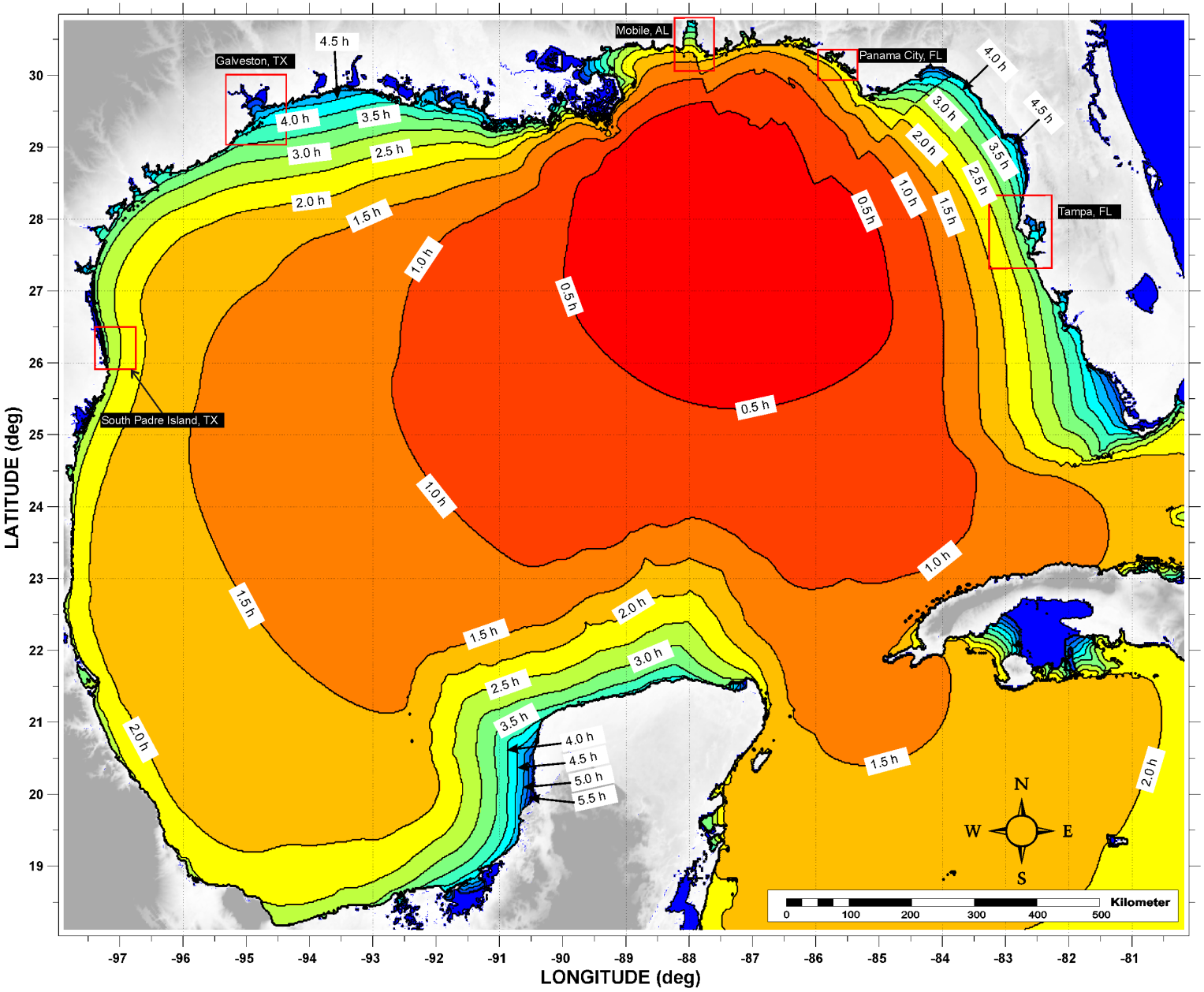

Figure 18: Tsunami arrival time for the Probabilistic Submarine Landslide -C- (PSL-C) scenario.

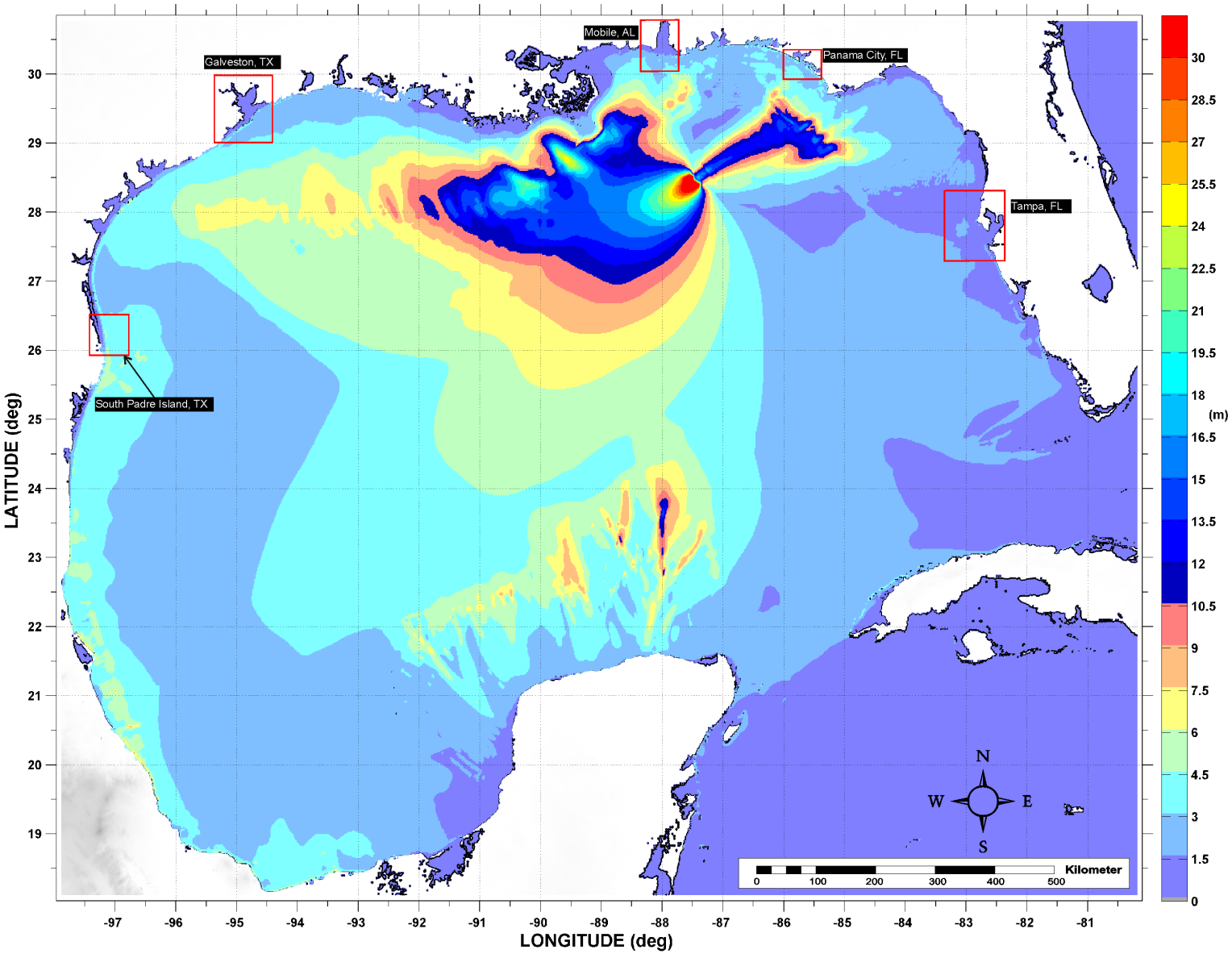

Figure 19: Maximum tsunami wave amplitude (one arcminute resolution) for the Probabilistic Submarine Landslide -C- (PSL-C) scenario.

West Florida Submarine Landslide General Information

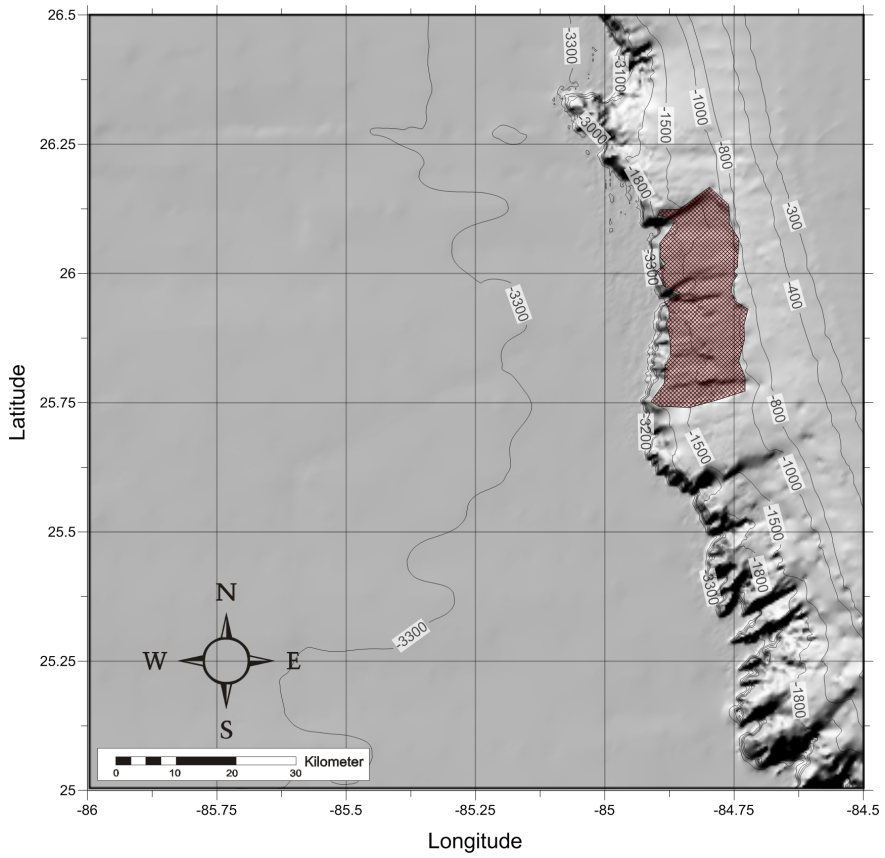

Figure 20: West Florida submarine landslide location, excavation limits and surrounding bathymetry (in meters).

Table 14: West Florida Submarine Landslide

Geologic Setting	Edge of a carbonate platform
Post Failure Sedimentation:	None visible on multi-beam images or on available high-resolution seismic profiles
Age:	Early Holocene or older ($>$ 10000) years
Maximum Credible Single Event:	Maximum Volume: 16.2 km^3 Area: 647.57 km^2
Excavation Depth:	$\sim$ 150 m
Run-out Distance:	Uncertain. The landslide deposit is at the base of the Florida Escarpment buried under younger Mississippi fan deposits
3D Model volume	18.4 km^3

Figure 21 depicts tsunami arrival time for the West Florida Submarine Landslide scenario (one arcminute resolution) for the entire GOM. Figure 22 shows maximum tsunami wave amplitude using the same lower spatial resolution (one arcminute) to obtain on a global scale the energy focusing mechanisms along the continental shelf and the effect of predominant bathymetric features of the GOM like shelf break slopes, submarine escarpments, and submarine canyons.

Table 15: Coordinate limits for the West Florida Submarine Landslide Domain to obtain initial dynamic tsunami wave source

West Florida Submarine Landslide 3D Domain (Resolution 15 arcseconds)	
Longitude	$86.00°W$ - $84.50°W$
Latitude	$25.00°N$ - $26.50°N$
$dx = dy$ and dz	15 arcsec and 1 - 29 m
Max. Water Depth	$3,437$ m
dt (variable)	≤ 0.10 sec.
# of Cells in the x, y, z-direction	$360 \times 360 \times 240$
Total # of Cells	$31,104,000$
Elapsed time of landslide deformation	300 sec (5 min)

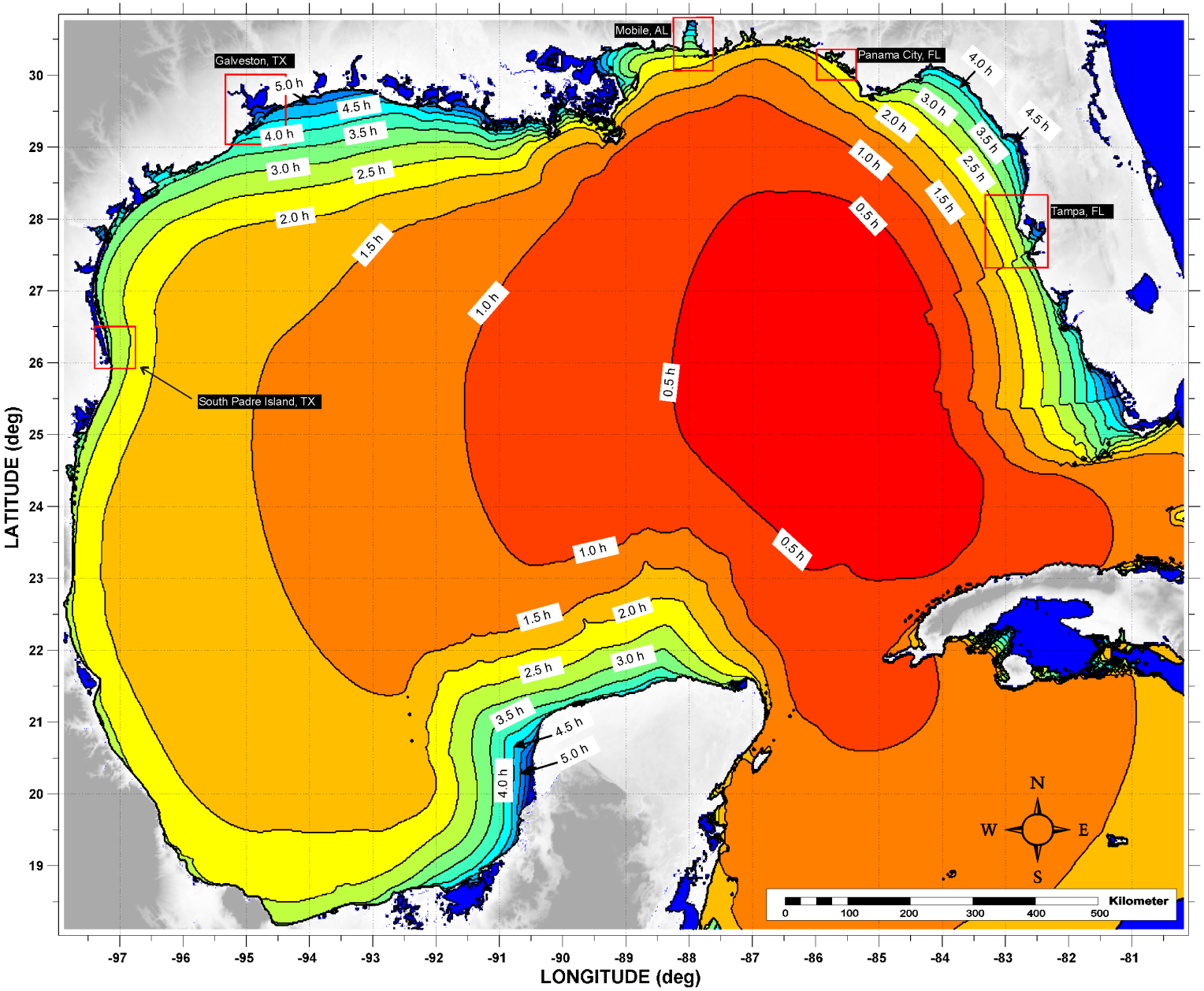

Figure 21: Tsunami arrival time for the West Florida Submarine Landslide scenario.

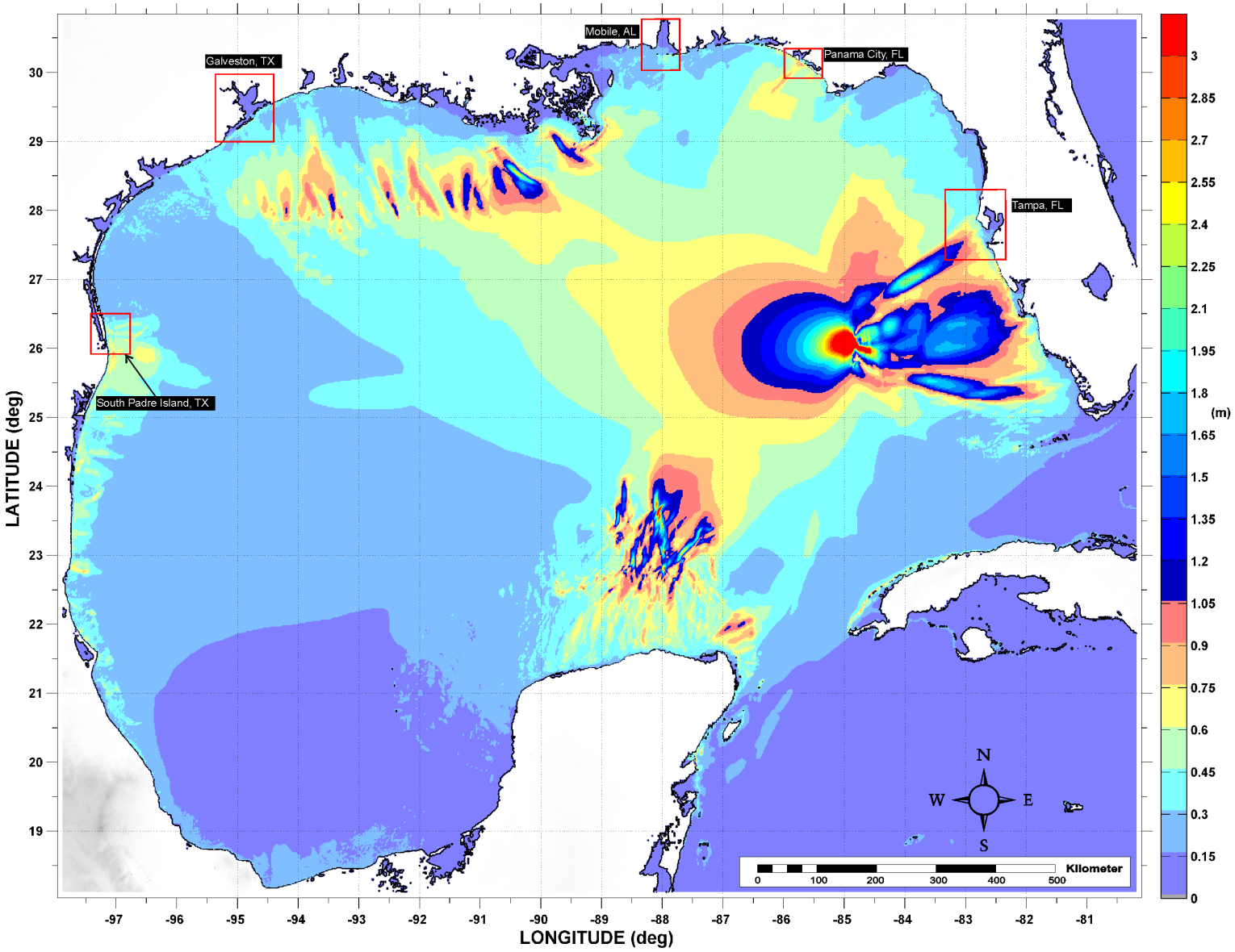

Figure 22: Maximum tsunami wave amplitude (one arcminute resolution) for the West Florida Submarine Landslide scenario.

Yucatan #3 Submarine Landslide General Information

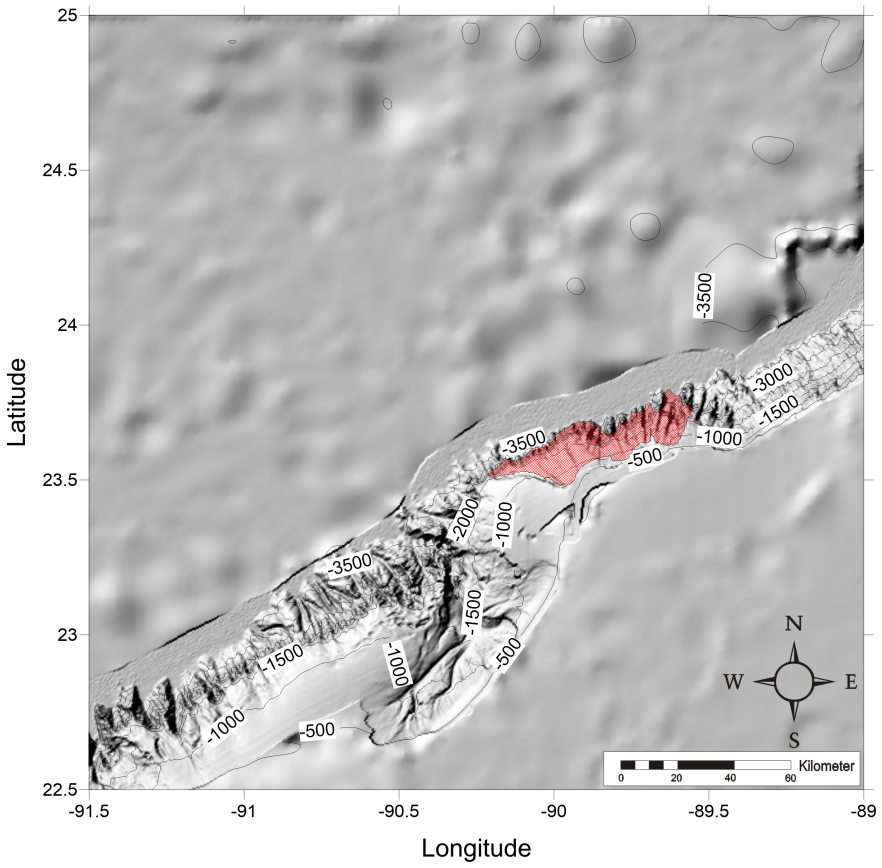

Figure 23: Yucatan #3 submarine landslide location, excavation limits and surrounding bathymetry (in meters).

Table 16: Yucatan #3 Submarine Landslide

Geologic Setting	Edge of a carbonate platform
Post Failure Sedimentation:	Not visible on multi-beam images or on available high-resolution seismic profiles
Age:	–
Maximum Credible Single Event:	Maximum Volume: 38.0 km^3 Area: 578 km^2
Excavation Depth:	< 278 m
Run-out Distance:	Uncertain. The landslide deposit is buried under younger deposits
3D Model volume	39.3 km^3

Figure 24 depicts tsunami arrival time for the Yucatan #3 Submarine Landslide scenario (one arcminute resolution) for the entire GOM. Figure 25 shows maximum tsunami wave amplitude using the same lower spatial resolution (one arcminute) to obtain on a global scale the energy focusing mechanisms along the continental shelf and the effect of predominant bathymetric features of the GOM like shelf break slopes, submarine escarpments, and submarine canyons.

Table 17: Coordinate limits for the Yucatan #3 Submarine Landslide Domain to obtain initial dynamic tsunami wave source

Yucatan #3 Submarine Landslide 3D Domain (Resolution 15 arcseconds)	
Longitude	$91.50°W$ - $89.00°W$
Latitude	$22.50°N$ - $25.00°N$
$dx = dy$ and dz	15 arcsec and 1 - 54 m
Max. Water Depth	1900 m
dt (variable)	≤ 0.10 sec.
# of Cells in the x, y, z-direction	$600 \times 600 \times 200$
Total # of Cells	$72,000,000$
Elapsed time of landslide deformation	480 sec (8 min)

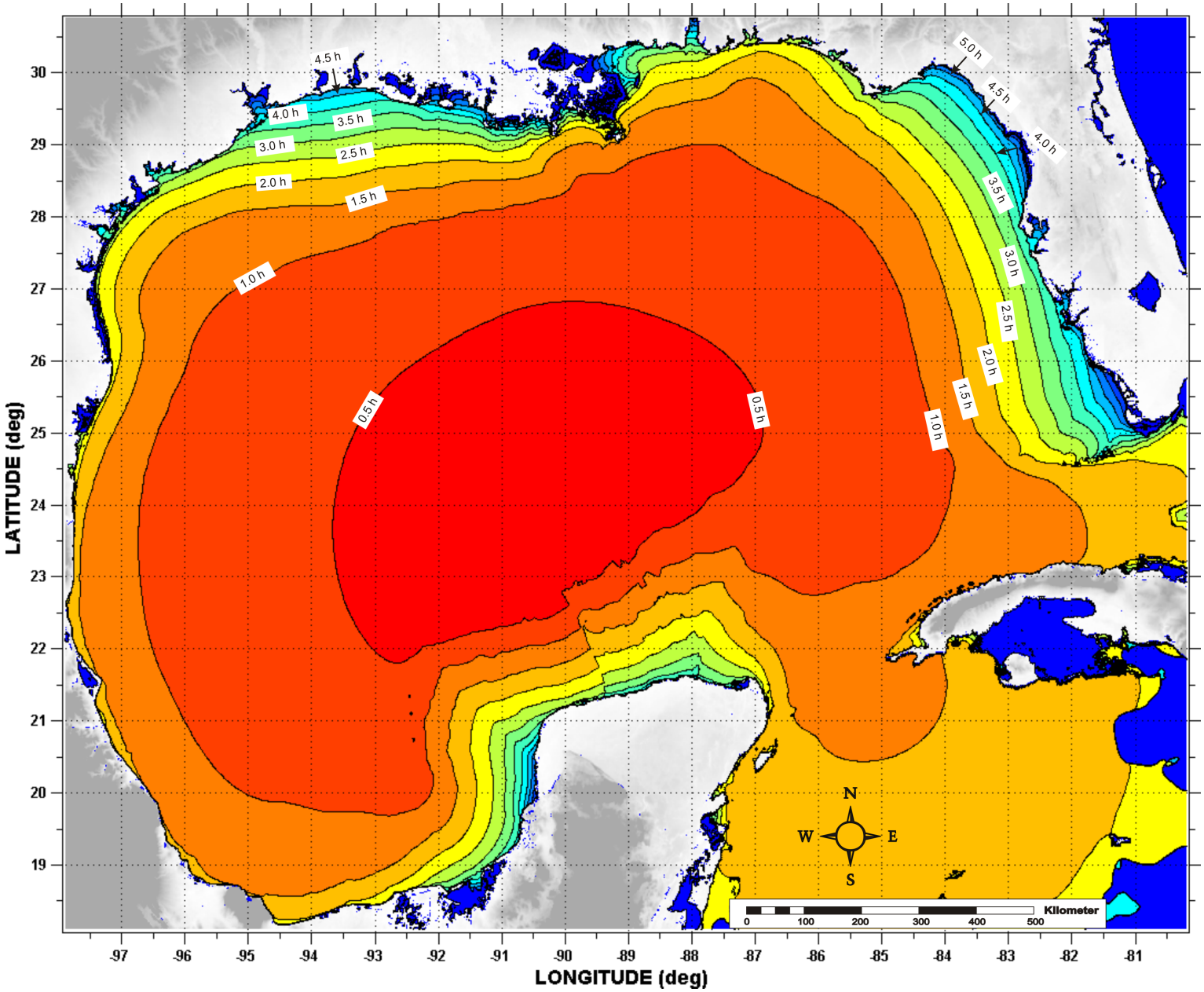

Figure 24: Tsunami arrival time for the Yucatan #3 Submarine Landslide scenario.

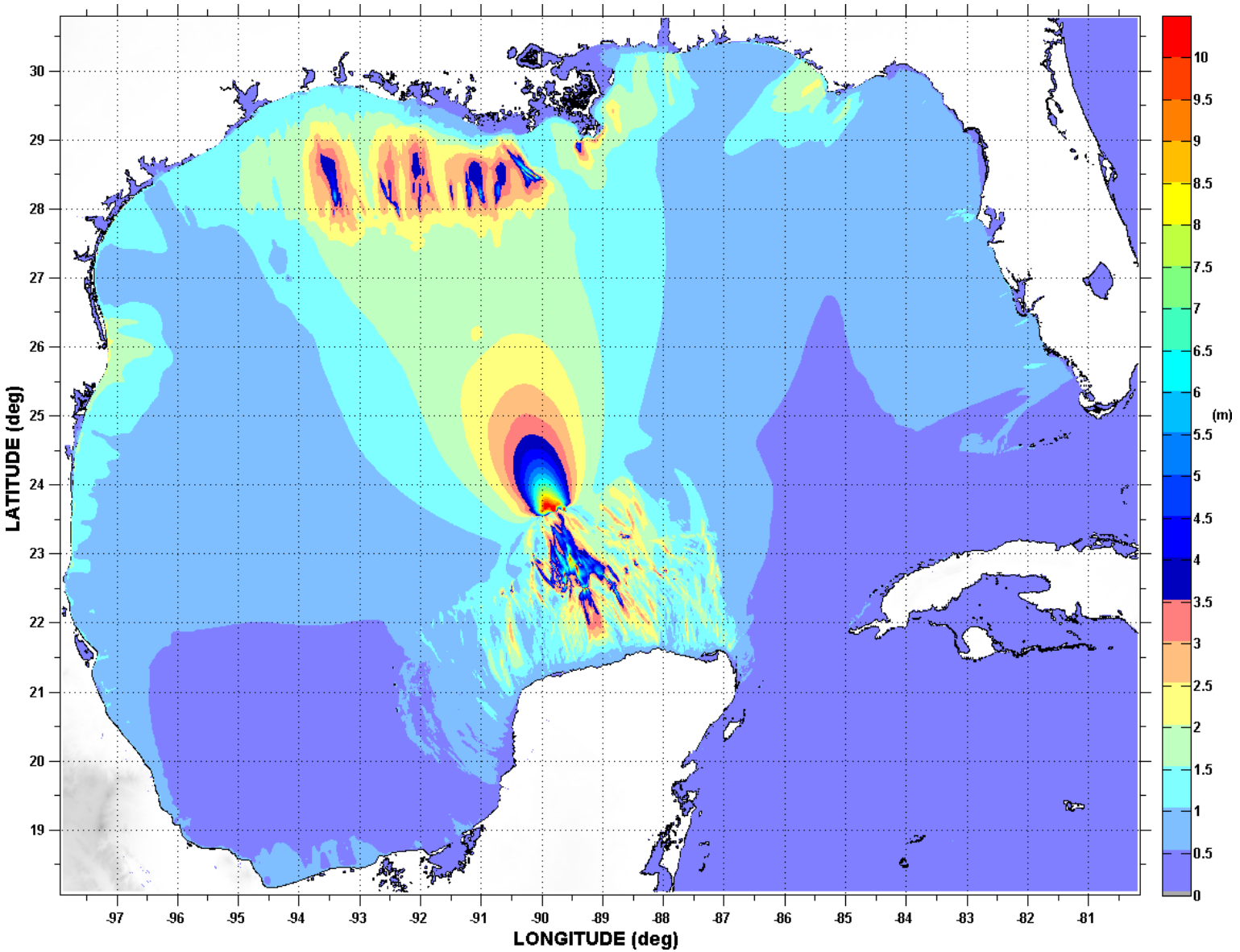

Figure 25: Maximum tsunami wave amplitude (one arcminute resolution) for the Yucatan #3 Submarine Landslide scenario.

Yucatan #5 Submarine Landslide General Information

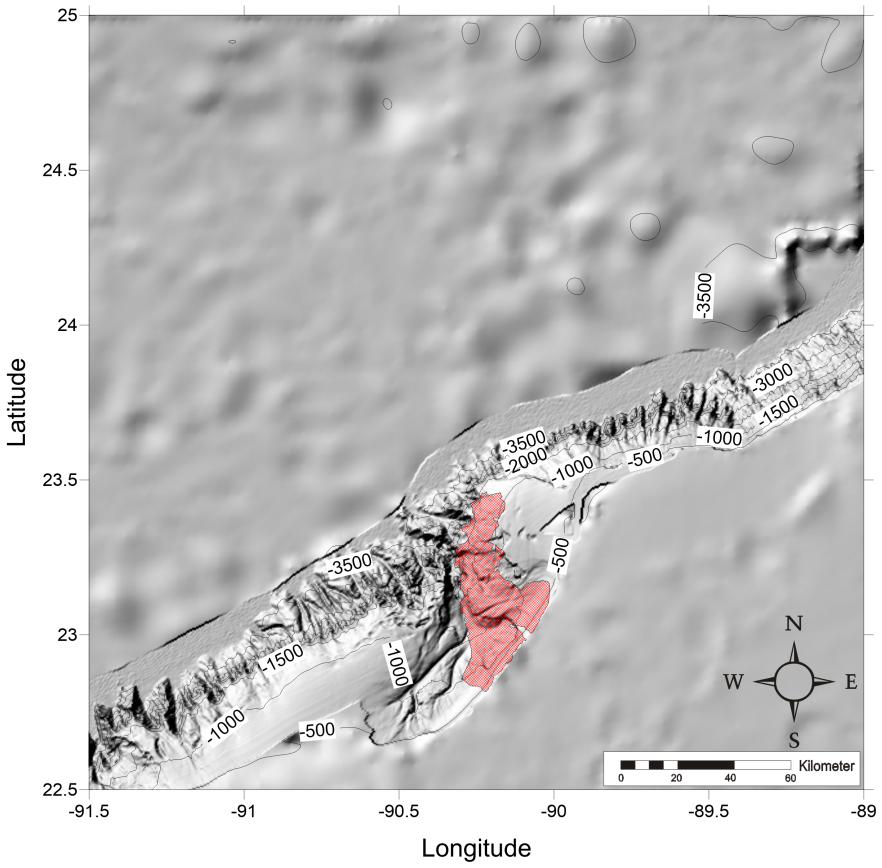

Figure 26: Yucatan #5 submarine landslide location, excavation limits and surrounding bathymetry (in meters).

Table 18: Yucatan #5 Submarine Landslide

Geologic Setting	Edge of a carbonate platform
Post Failure Sedimentation:	Not visible on multi-beam images or on available high-resolution seismic profiles
Age:	–
Maximum Credible Single Event:	Maximum Volume: 70.2 km^3 Area: 1094 km^2
Excavation Depth:	$<$ 385 m
Run-out Distance:	Uncertain. The landslide deposit is buried under younger deposits
3D Model volume	69.5 km^3

Figure 27 depicts tsunami arrival time for the Yucatan #3 Submarine Landslide scenario (one arcminute resolution) for the entire GOM. Figure 28 shows maximum tsunami wave amplitude using the same lower spatial resolution (one arcminute) to obtain on a global scale the energy focusing mechanisms along the continental shelf and the effect of predominant bathymetric features of the GOM like shelf break slopes, submarine escarpments, and submarine canyons.

Table 19: Coordinate limits for the Yucatan #5 Submarine Landslide Domain to obtain initial dynamic tsunami wave source

Yucatan #5 Submarine Landslide 3D Domain (Resolution 15 arcseconds)	
Longitude	$91.50°W$ - $89.00°W$
Latitude	$22.50°N$ - $25.00°N$
$dx = dy$ and dz	15 arcsec and 1 - 54 m
Max. Water Depth	1700 m
dt (variable)	≤ 0.10 sec.
# of Cells in the x, y, z-direction	$600 \times 600 \times 200$
Total # of Cells	$72,000,000$
Elapsed time of landslide deformation	720 sec (12 min)

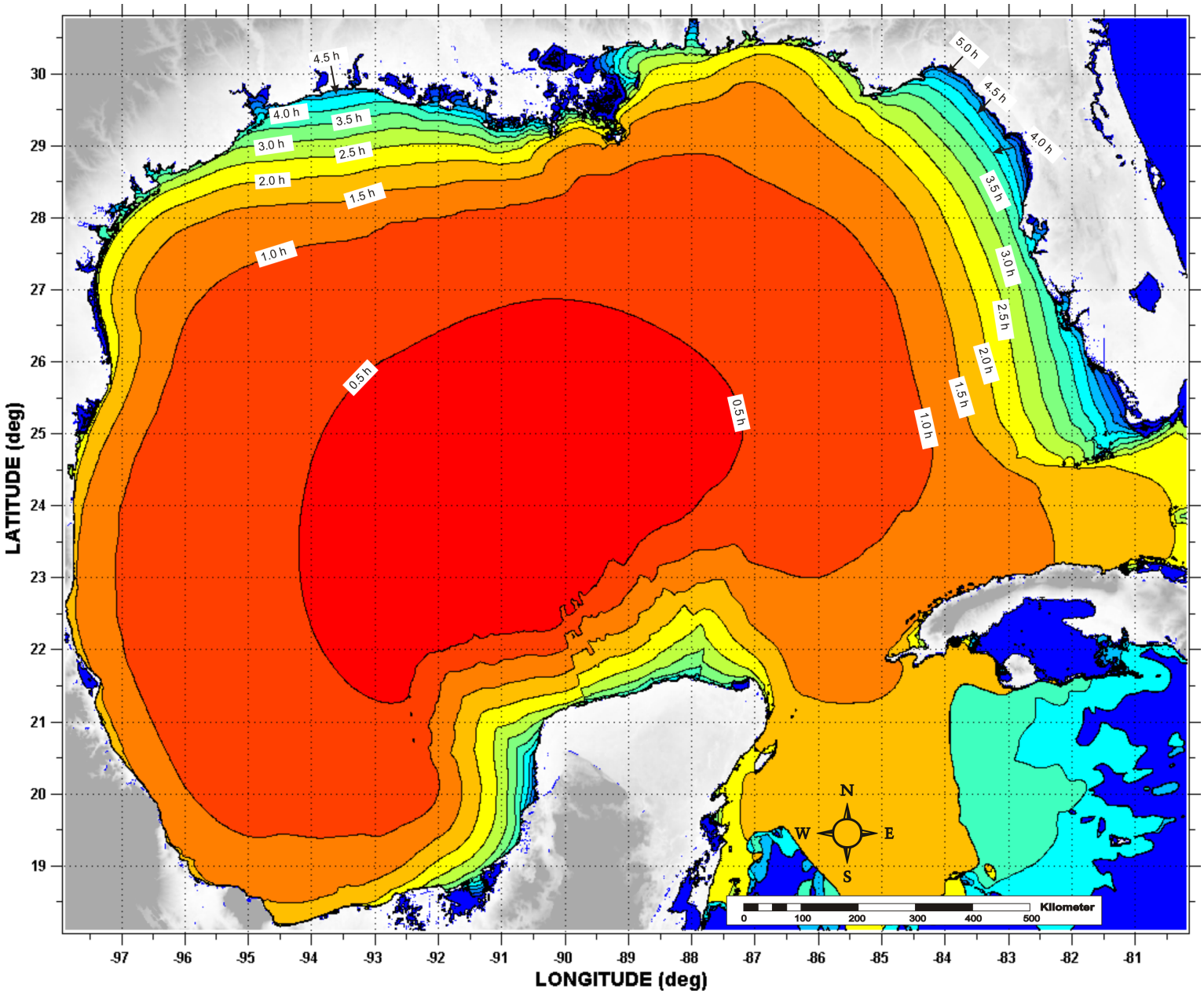

Figure 27: Tsunami arrival time for the Yucatan #5 Submarine Landslide scenario.

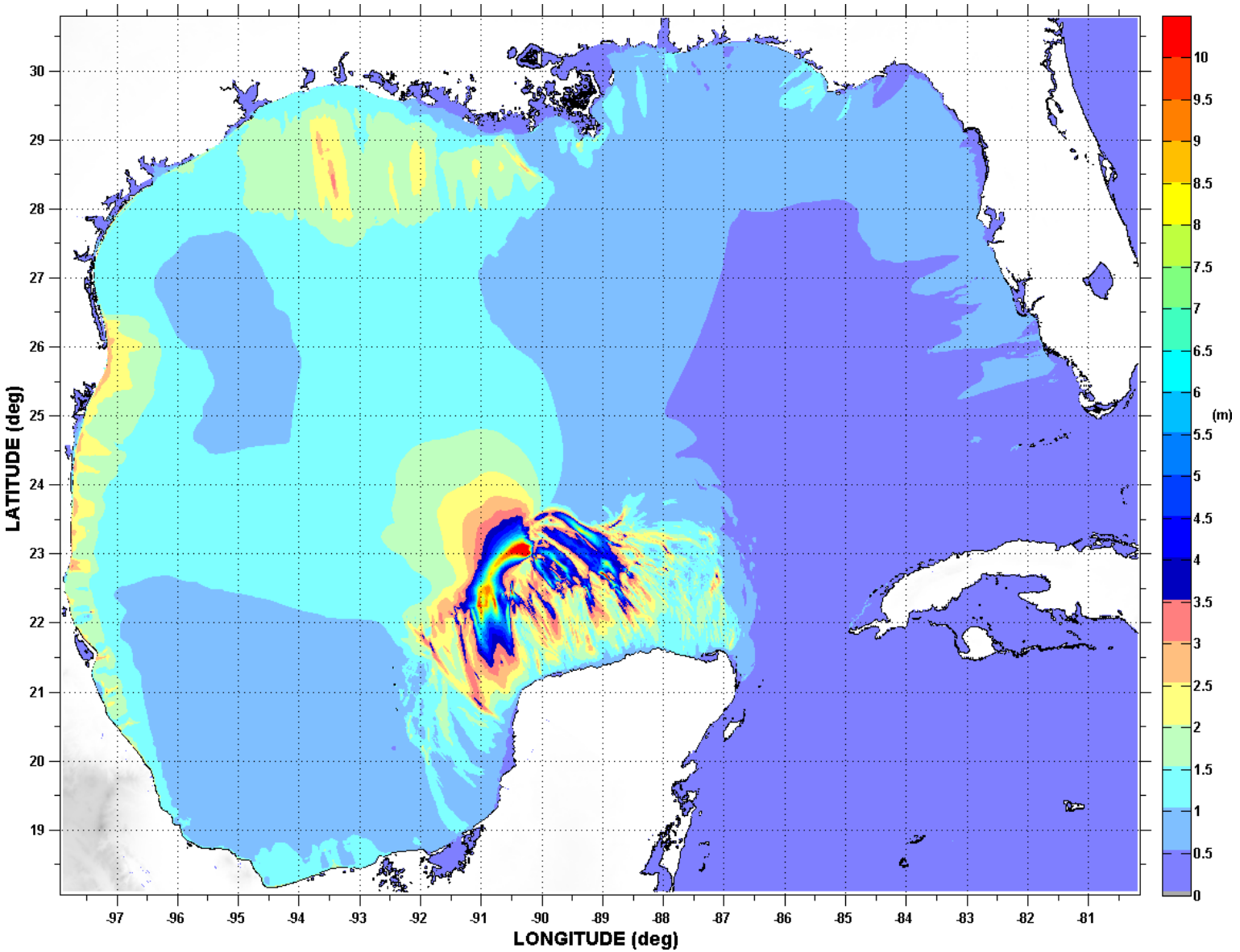

Figure 28: Maximum tsunami wave amplitude (one arcminute resolution) for the Yucatan #5 Submarine Landslide scenario.

3.2 Numerical Models

For the nine landslide tsunami sources considered here, tsunami wave development and subsequent propagation and inundation of coastal communities was modeled using coupled 3D and 2D numerical models [Horrillo et al., 2015]. The tsunami generation phase was modeled using the 3D model TSUNAMI3D [Horrillo, 2006, Horrillo et al., 2013], which solves the finite difference approximation of the full Navier-Stokes equations and the incompressibility (continuity) equation. Water and landslide material are represented as Newtonian fluids with different densities, and the landslide-water and water-air interfaces are tracked using the Volume of Fluid (VOF) method of Hirt and Nichols [1981], which is simplified to account for the large horizontal/vertical aspect ratio of the tsunami wave and the selected computational cell size required to construct an efficient 3D grid. The pressure term is split into hydrostatic and non-hydrostatic components. Although TSUNAMI3D has the capability of variable grids, the nesting capability necessary for modeling detailed inundation of coastal regions is too computationally intensive within the fully 3D model; thus, detailed inundation modeling is achieved by coupling the 3D model to a 2D model. Once the tsunami wave generated by the 3D model is fully developed, the wave is passed as an initial condition to the 2D model for modeling wave propagation and coastal inundation. The generated wave is considered fully developed when the total wave energy (potential plus kinetic) reaches a maximum and before the wave leaves the computational domain, as discussed in López-Venegas et al. [2015]. The 2D model used here is NEOWAVE [Yamazaki et al., 2008], a depth-integrated and non-hydrostatic model built on the nonlinear shallow water equations which includes a momentum-conserved advection scheme to model wave breaking and two-way nested grids for modeling higher-resolution wave runup and inundation. Propagation and inundation are calculated via a series of nested grids of increasing resolution, from 15 arcsecond (450 m) resolution for a domain encompassing the entire northern GOM (Fig. 1), to finer resolutions of 3 arcseconds (90 m, from NOAA NCEI Coastal Relief Models), 1 arcsecond (30 m), and 1/3 arcsecond (10 m, from NOAA NCEI Tsunami Inundation Digital Elevation Models [DEMs]) to model detailed inundation of the most populated/ inundation-prone areas of each coastal community. The 3 arcsecond (90 m) subdomains encompassing each coastal community studied here are shown by red rectangles in Fig. 1.

4 Tsunami Maps

Tsunami inundation depth and extent has been modeled for two selected coastal communities: Osprey-Venice-Englewood, FL and Sanibel Island-Naples, FL. Inundation (flooding) is determined by subtracting land elevation from water elevation, and elevations used are in reference to the Mean High Water (MHW) tidal datum. For this study, the tsunami inundation depth/extent modeled for each community is the maximum-of-maximums (MOM) inundation, which is calculated as the maximum inundation depth from an ensemble of inundation depths produced by each of the nine tsunami sources considered. That is, once inundation in a community has been modeled for each of the nine sources, the overall maximum inundation depth in each computational grid cell is taken as the MOM tsunami inundation in that cell. This approach gives a worst-case scenario perspective of estimated tsunami inundation for each coastal community.

In this section, the numerical results (inundation and momentum flux maps) for each landslide source are presented for Osprey-Venice-Englewood, FL and Sanibel Island-Naples, FL. The maximum of maximum inundation map from all sources and the maximum inundation map by source are also shown. A summary table of each location's numerical gauge (at an approximate water depth of 20 m) is presented, showing maximum wave amplitude and arrival time after landslide failure.

It is worth noting, however, that for both communities, the MOM tsunami inundation is produced solely by the Mississippi Canyon submarine landslide failure. That historical failure is the largest in both area and volume of material removed, and therefore produces the highest amplitude wave of all sources simulated. The newly added two sources, Yucatan #3 and Yucatan #5, made little impact to the selected communities.

4.1 Osprey-Venice-Englewood, FL

Table 20: Maximum tsunami wave amplitude and corresponding arrival time after landslide failure at Osprey-Venice-Englewood, FL numerical wave gauge: 26°56'19.22"N, 82°39'34.28"W (Fig. 1), approximate water depth 20 m.

Tsunami Source	Maximum Wave Amplitude (m)	Arrival Time After Landslide Failure (hr)
East Breaks	0.37	4.0
PSL-A	0.58	3.7
PSL-B1	0.64	3.0
PSL-B2	1.50	3.1
Mississippi Canyon	4.27	2.6
PSL-C	1.16	2.6
West Florida	1.14	2.2
Yucatan #3	0.52	3.1
Yucatan #5	0.26	3.1

Osprey-Venice-Englewood, FL
East Breaks submarine landslide
Maximum Momentum Flux

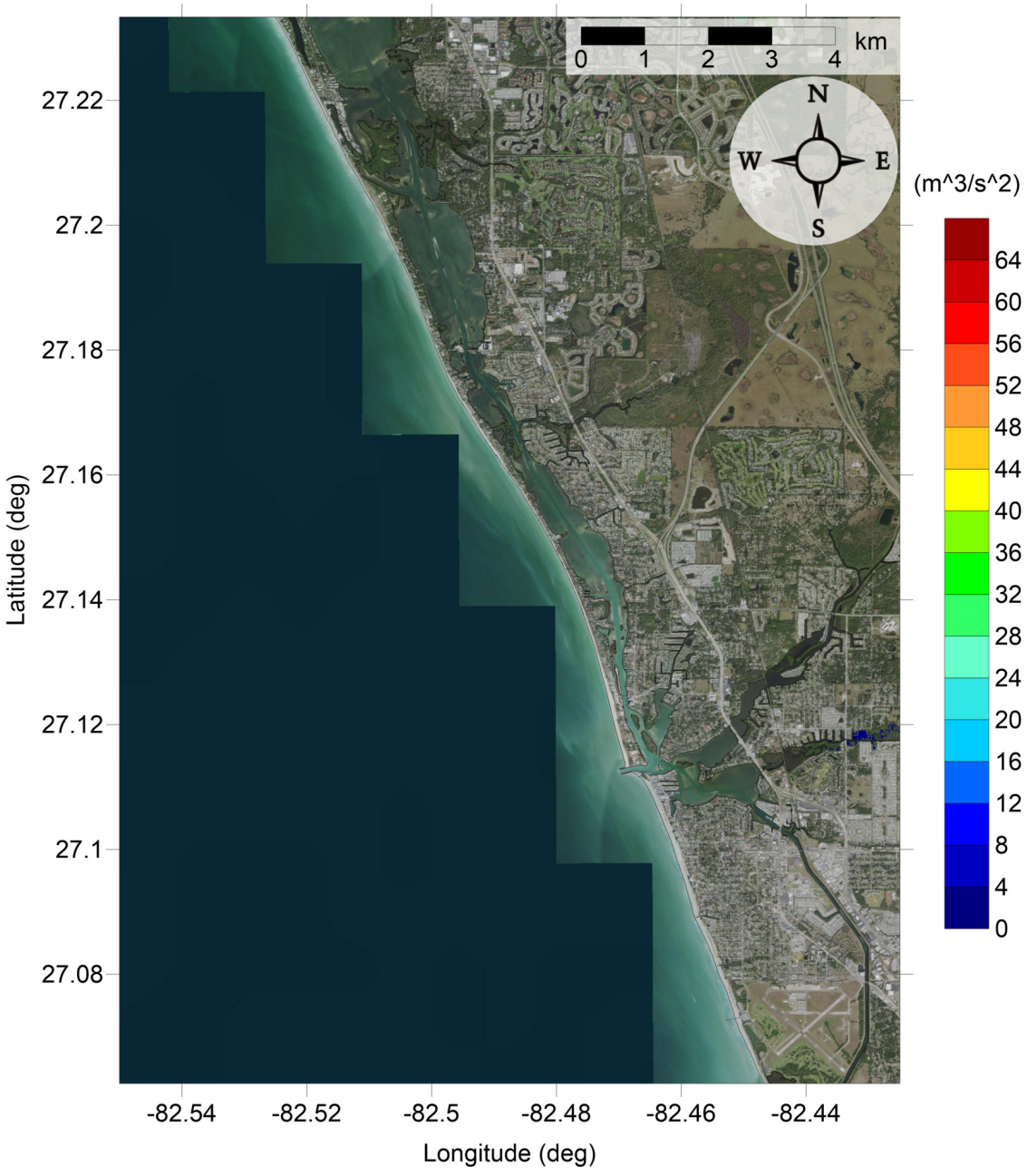

Figure 29: Maximum momentum flux (m^3/s^2) caused by the East Breaks submarine landslide in Osprey-Venice, FL. Arrows represent direction of maximum momentum flux. Contour drawn is the zero-meter contour for land elevation.

Osprey-Venice-Englewood, FL
East Breaks submarine landslide
Maximum Momentum Flux

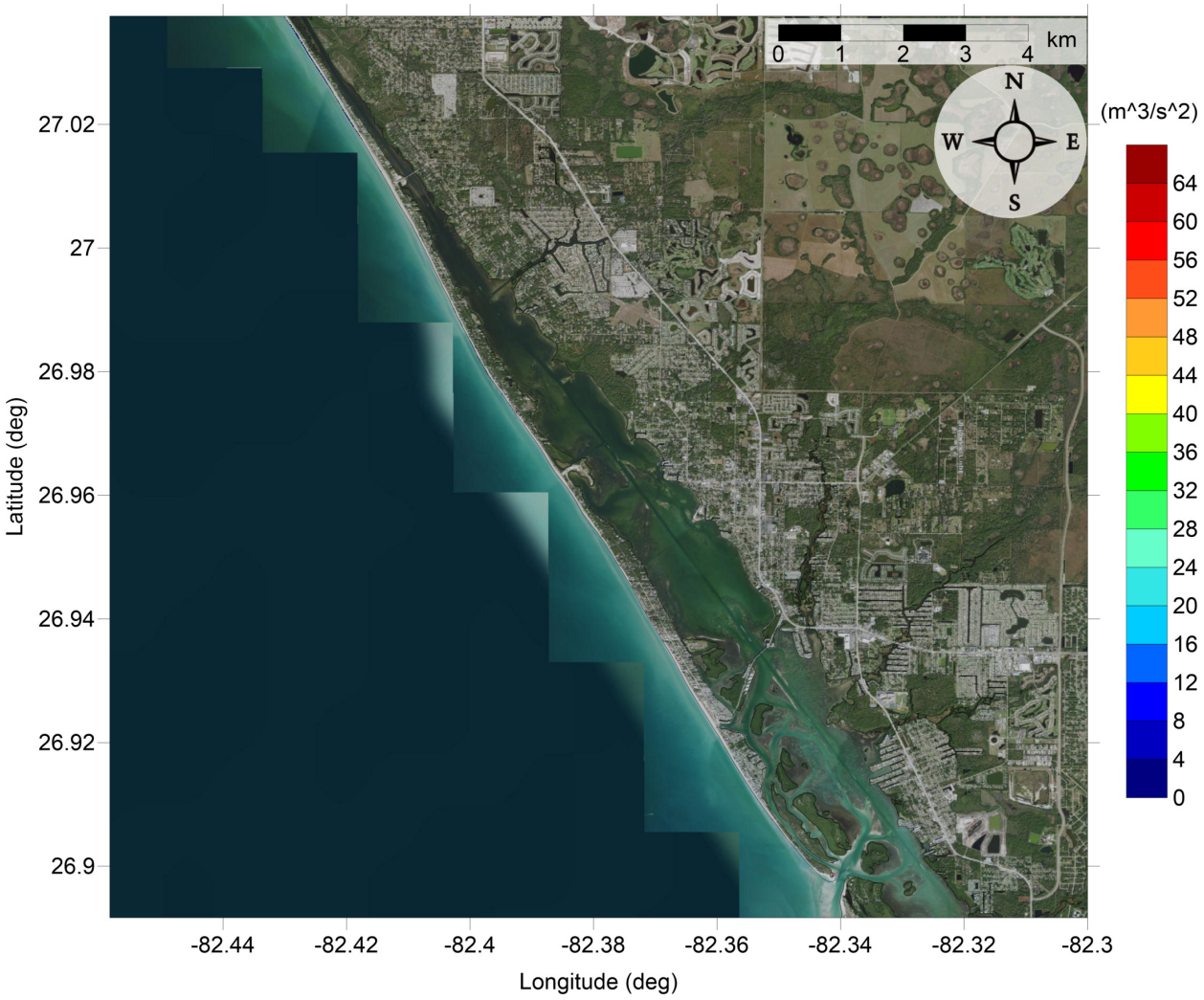

Figure 30: Maximum momentum flux (m^3/s^2) caused by the East Breaks submarine landslide in Englewood, FL. Arrows represent direction of maximum momentum flux. Contour drawn is the zero-meter contour for land elevation.

Osprey-Venice-Englewood, FL
East Breaks submarine landslide
Maximum Inundation Depth

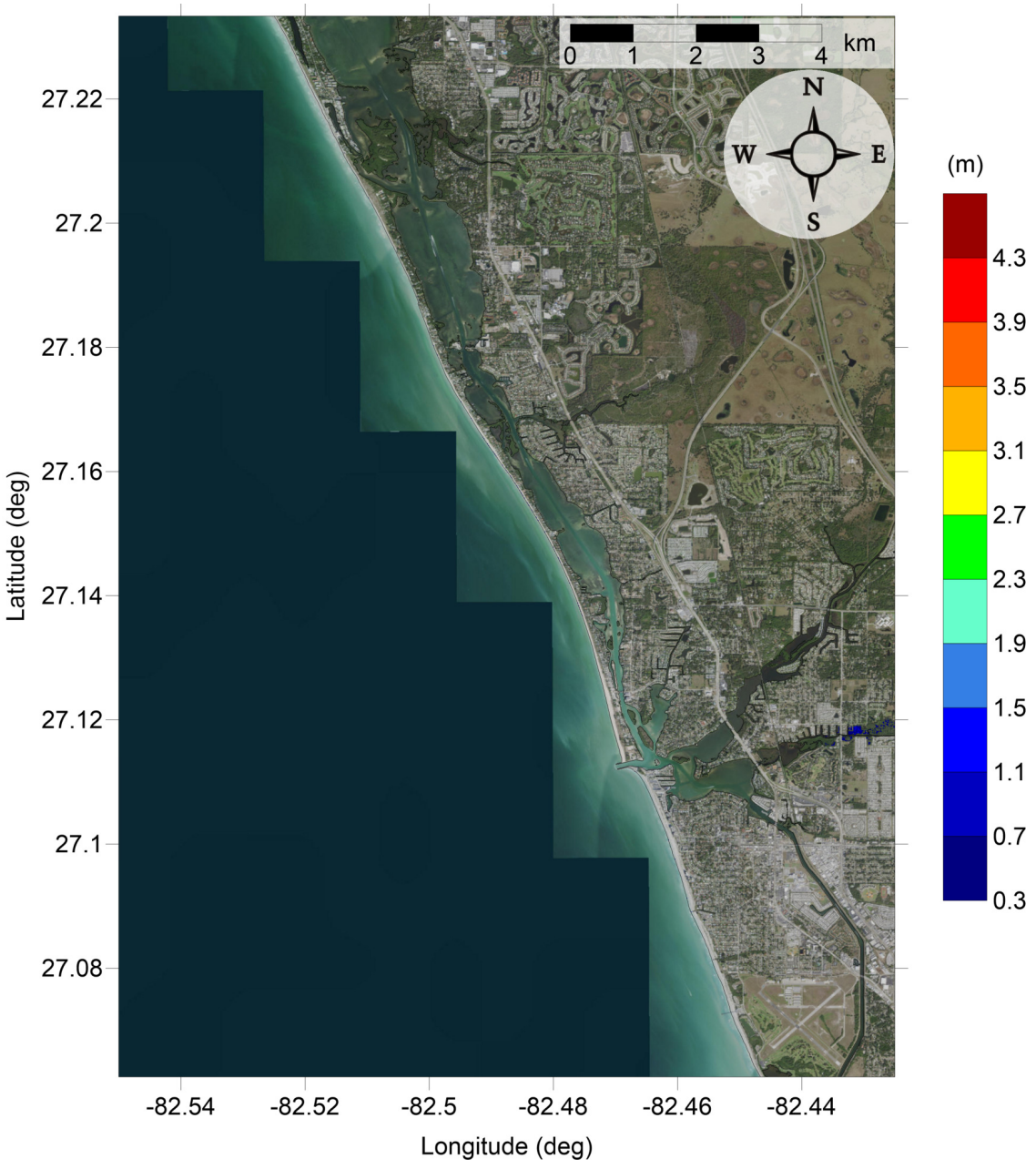

Figure 31: Maximum inundation depth (m) caused by the East Breaks submarine landslide in Osprey-Venice, FL. Contour drawn is the zero-meter contour for land elevation.

Osprey-Venice-Englewood, FL
East Breaks submarine landslide
Maximum Inundation Depth

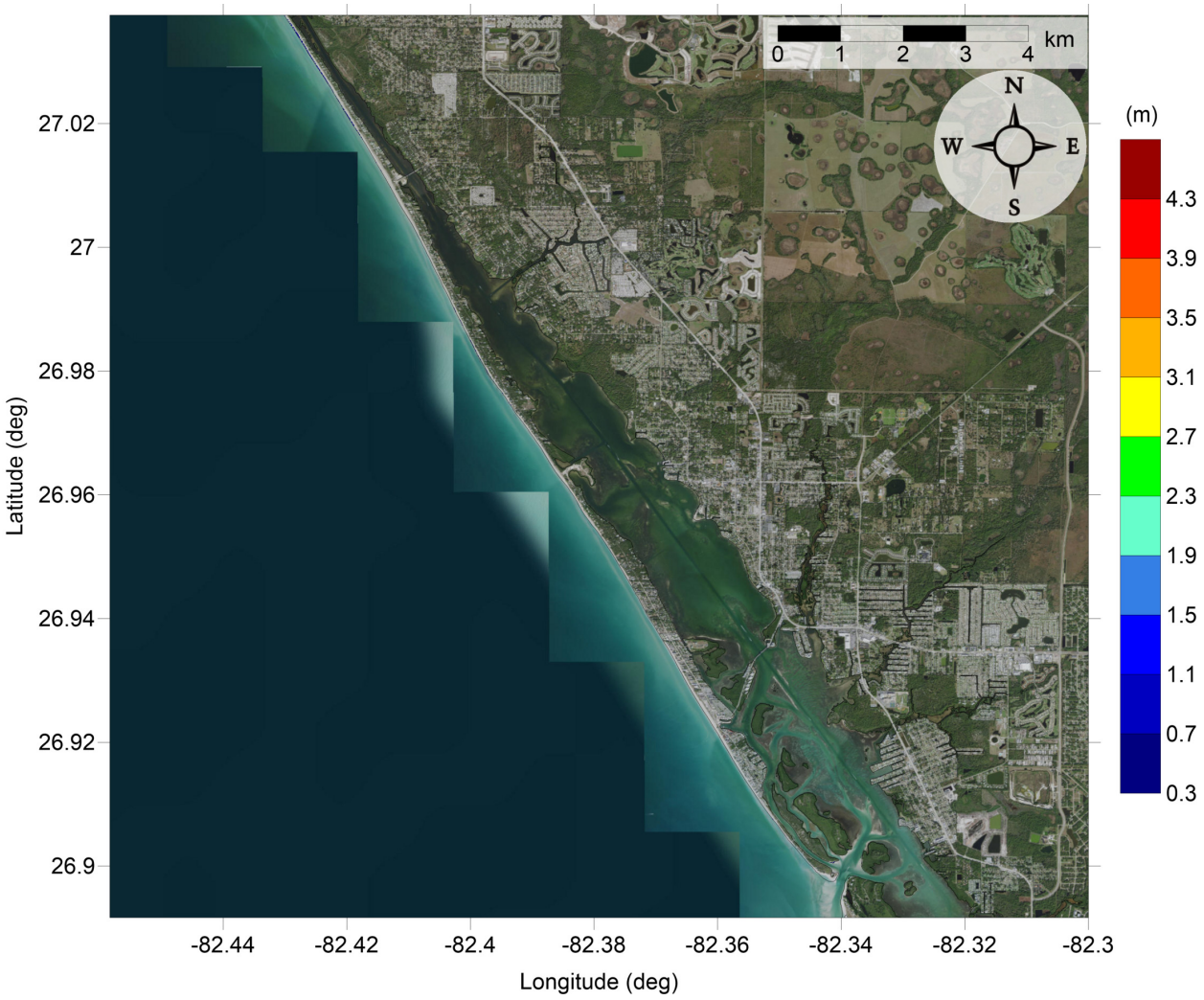

Figure 32: Maximum inundation depth (m) caused by the East Breaks submarine landslide in Englewood, FL. Contour drawn is the zero-meter contour for land elevation.

Osprey-Venice-Englewood, FL
Probabilistic Submarine Landslide A
Maximum Momentum Flux

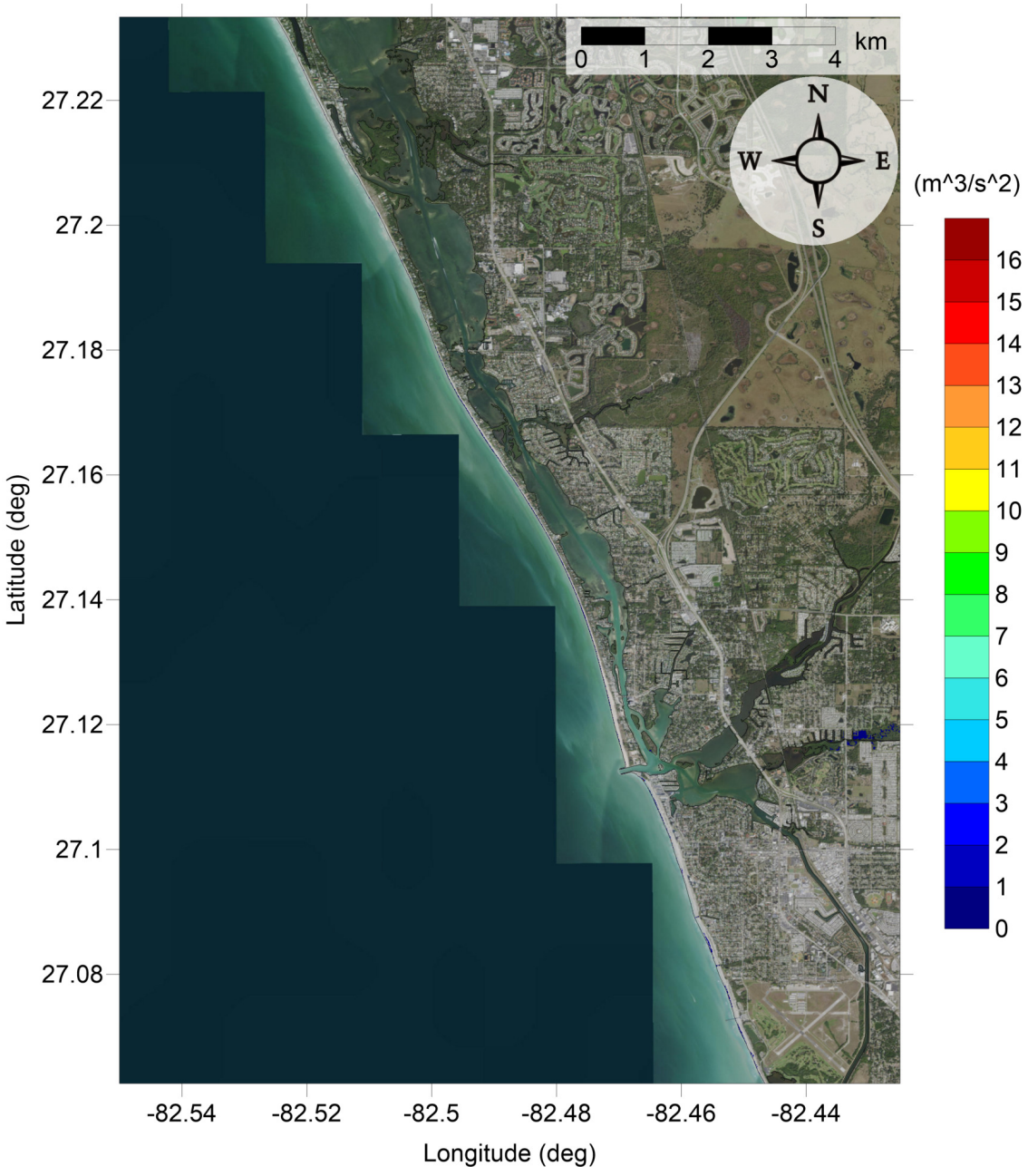

Figure 33: Maximum momentum flux (m^3/s^2) caused by the Probabilistic Submarine Landslide A in Osprey-Venice, FL. Arrows represent direction of maximum momentum flux. Contour drawn is the zero-meter contour for land elevation.

Osprey-Venice-Englewood, FL
Probabilistic Submarine Landslide A
Maximum Momentum Flux

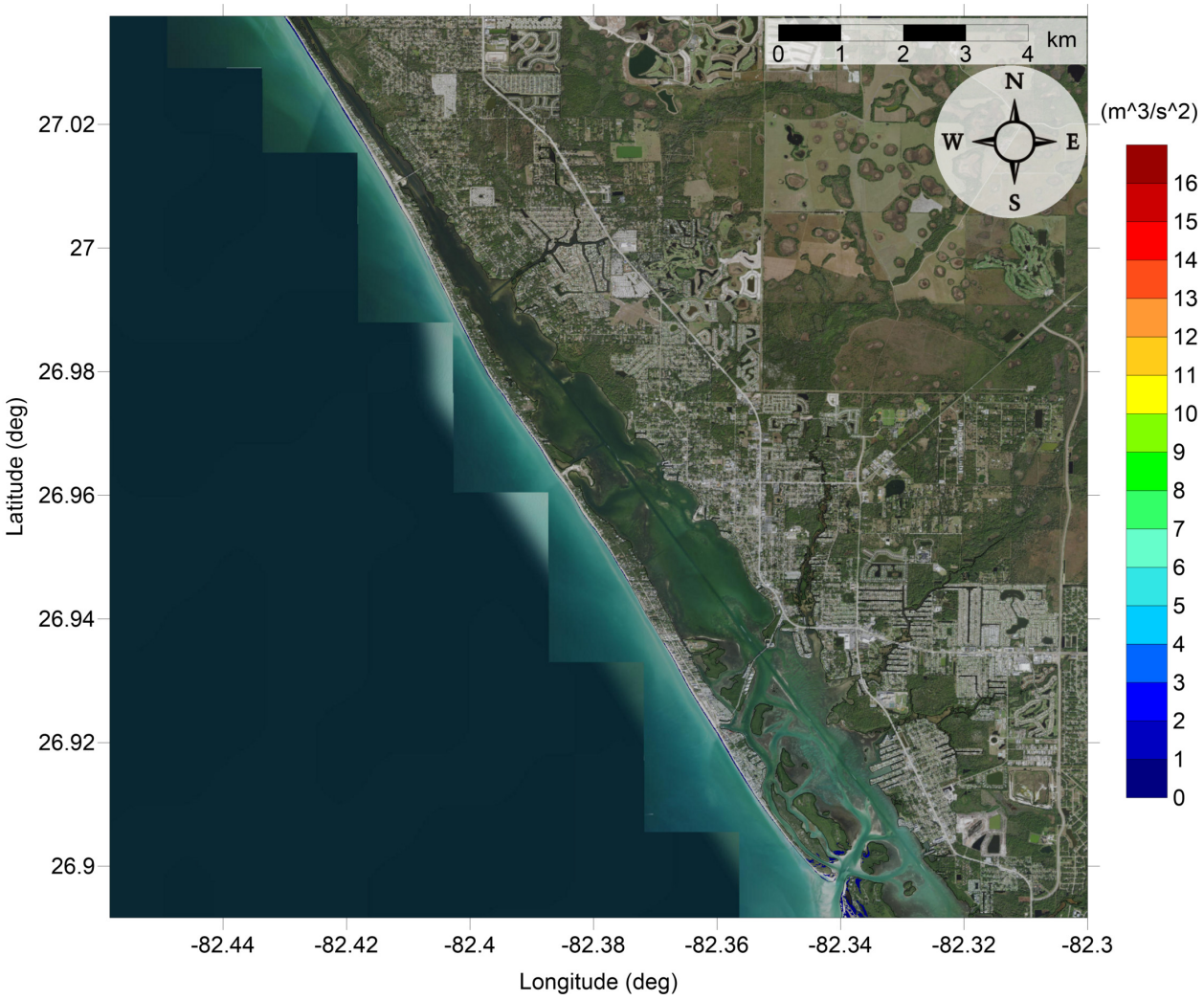

Figure 34: Maximum momentum flux (m^3/s^2) caused by the Probabilistic Submarine Landslide A in Englewood, FL. Arrows represent direction of maximum momentum flux. Contour drawn is the zero-meter contour for land elevation.

Osprey-Venice-Englewood, FL
Probabilistic Submarine Landslide A
Maximum Inundation Depth

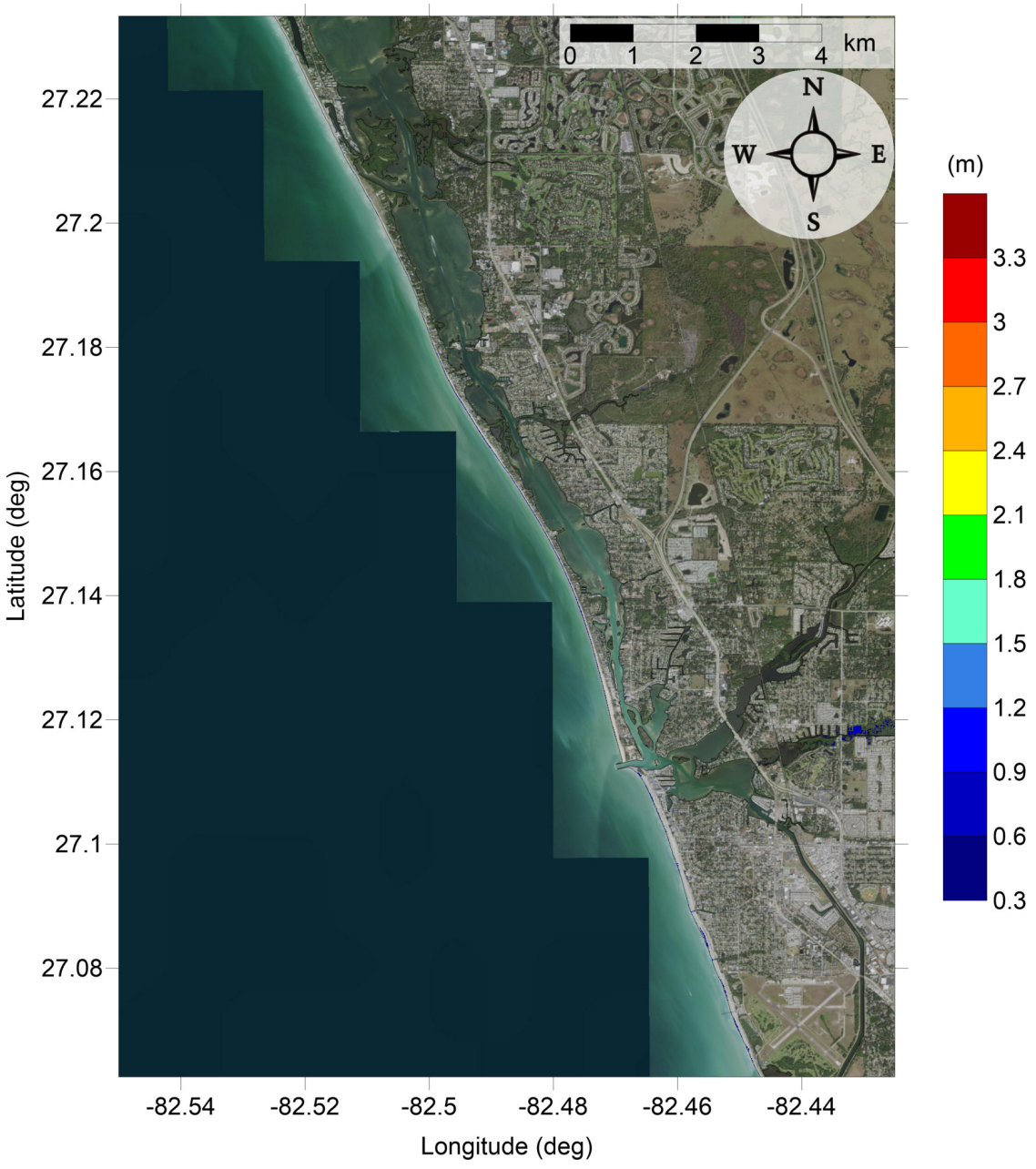

Figure 35: Maximum inundation depth (m) caused by the Probabilistic Submarine Landslide A in Osprey-Venice, FL. Contour drawn is the zero-meter contour for land elevation.

Osprey-Venice-Englewood, FL
Probabilistic Submarine Landslide A
Maximum Inundation Depth

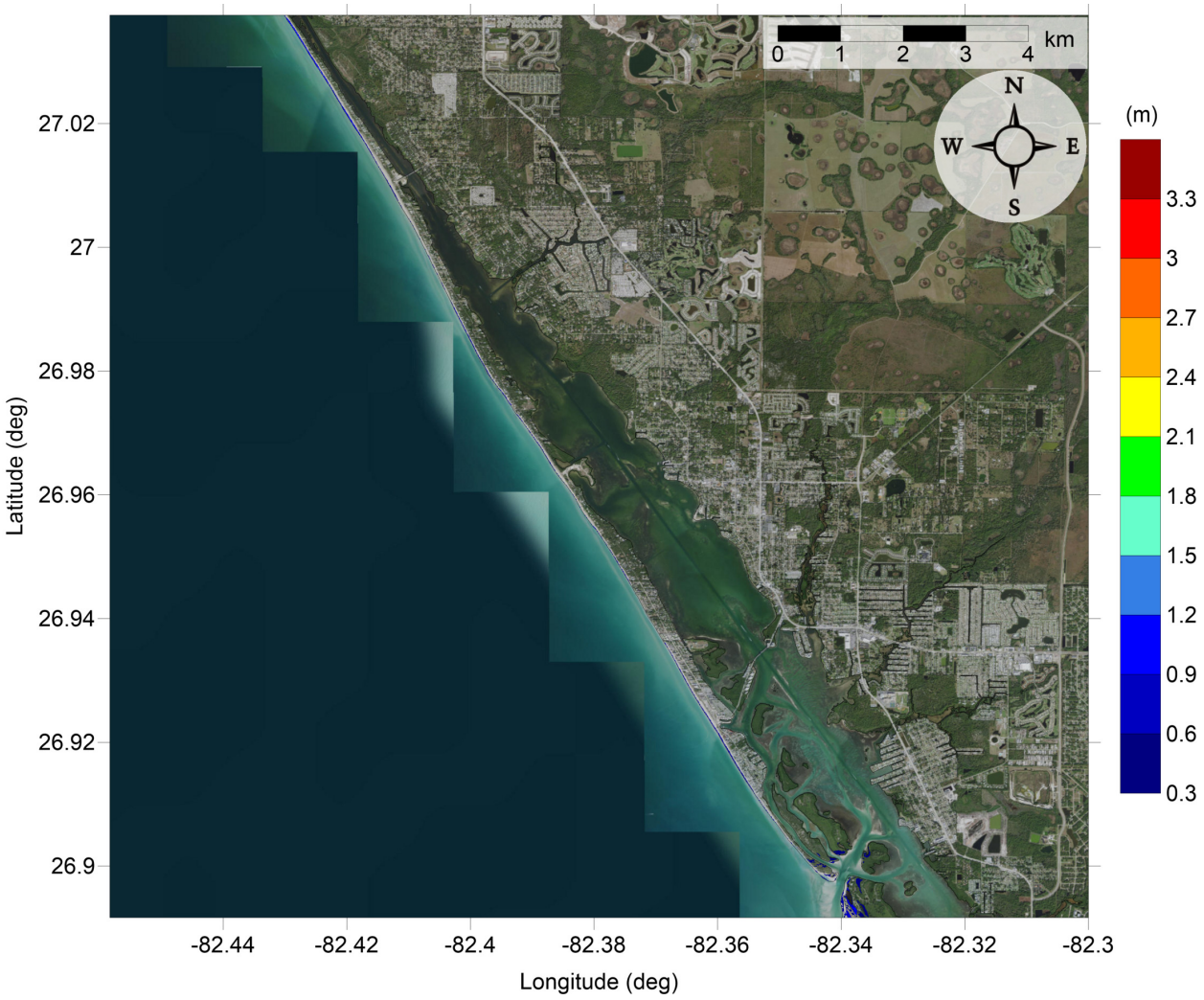

Figure 36: Maximum inundation depth (m) caused by the Probabilistic Submarine Landslide A in Englewood, FL. Contour drawn is the zero-meter contour for land elevation.

Osprey-Venice-Englewood, FL
Probabilistic Submarine Landslide B1
Maximum Momentum Flux

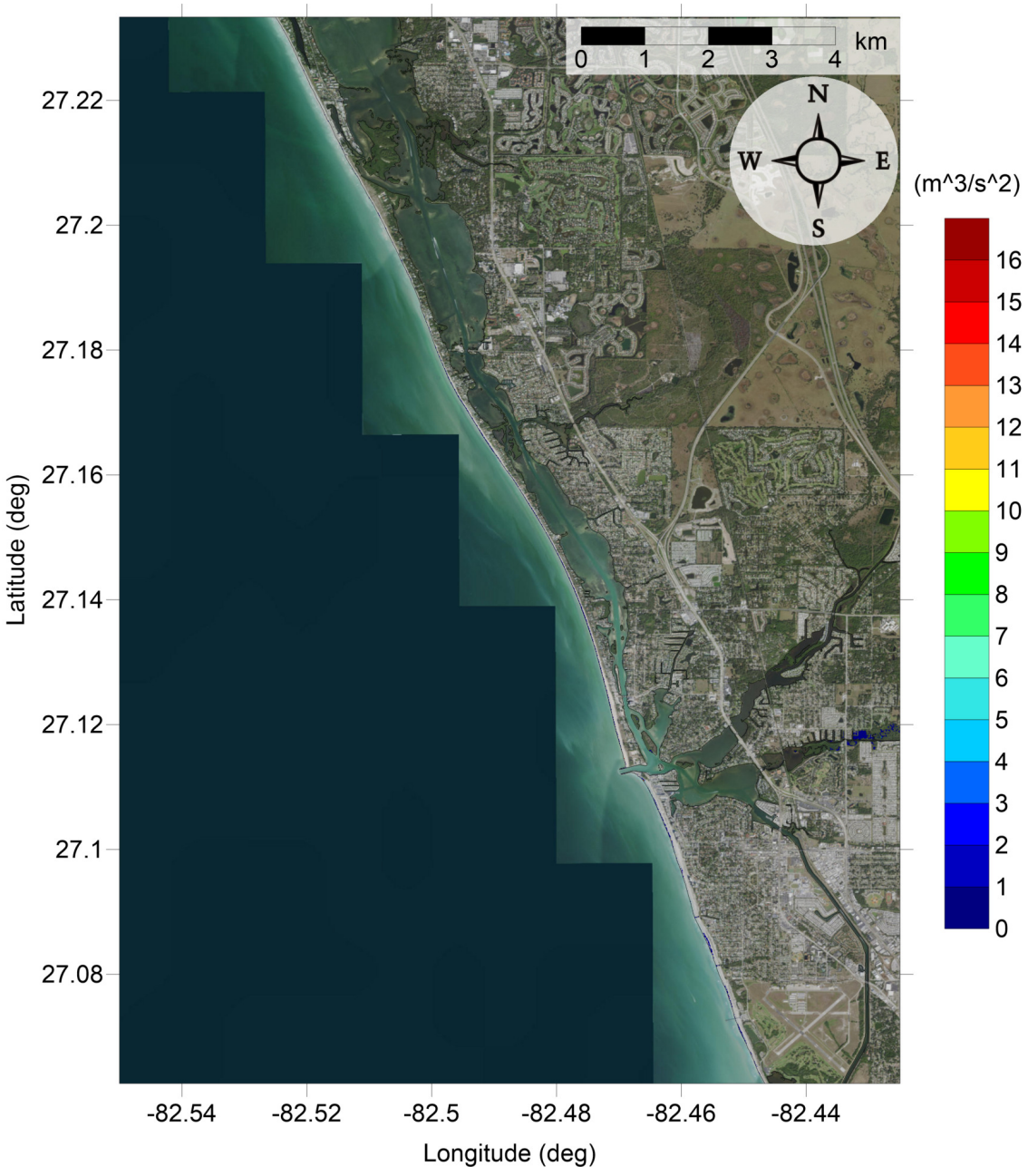

Figure 37: Maximum momentum flux (m^3/s^2) caused by the Probabilistic Submarine Landslide B1 in Osprey-Venice, FL. Arrows represent direction of maximum momentum flux. Contour drawn is the zero-meter contour for land elevation.

Osprey-Venice-Englewood, FL
Probabilistic Submarine Landslide B1
Maximum Momentum Flux

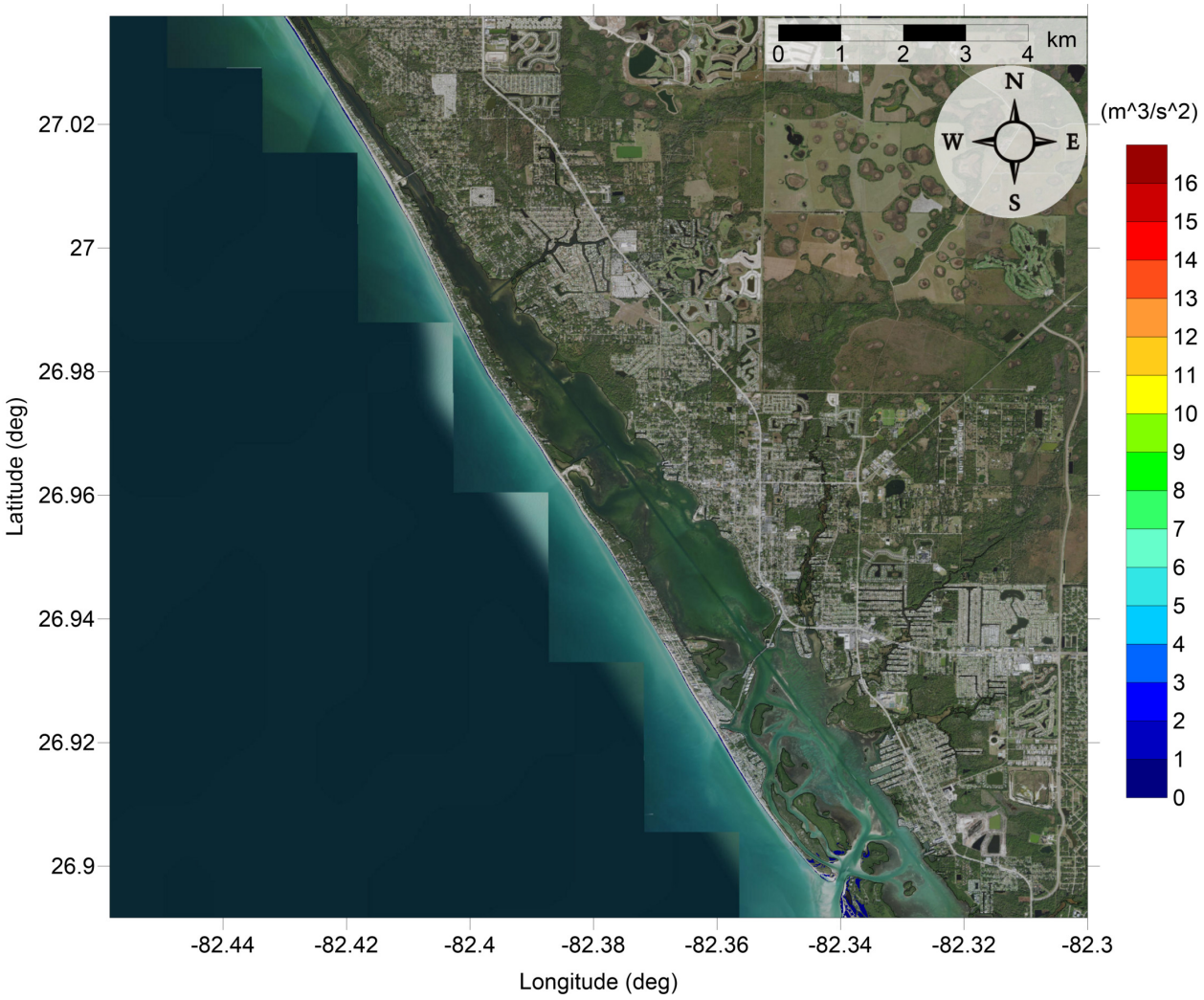

Figure 38: Maximum momentum flux (m^3/s^2) caused by the Probabilistic Submarine Landslide B1 in Englewood, FL. Arrows represent direction of maximum momentum flux. Contour drawn is the zero-meter contour for land elevation.

Osprey-Venice-Englewood, FL
Probabilistic Submarine Landslide B1
Maximum Inundation Depth

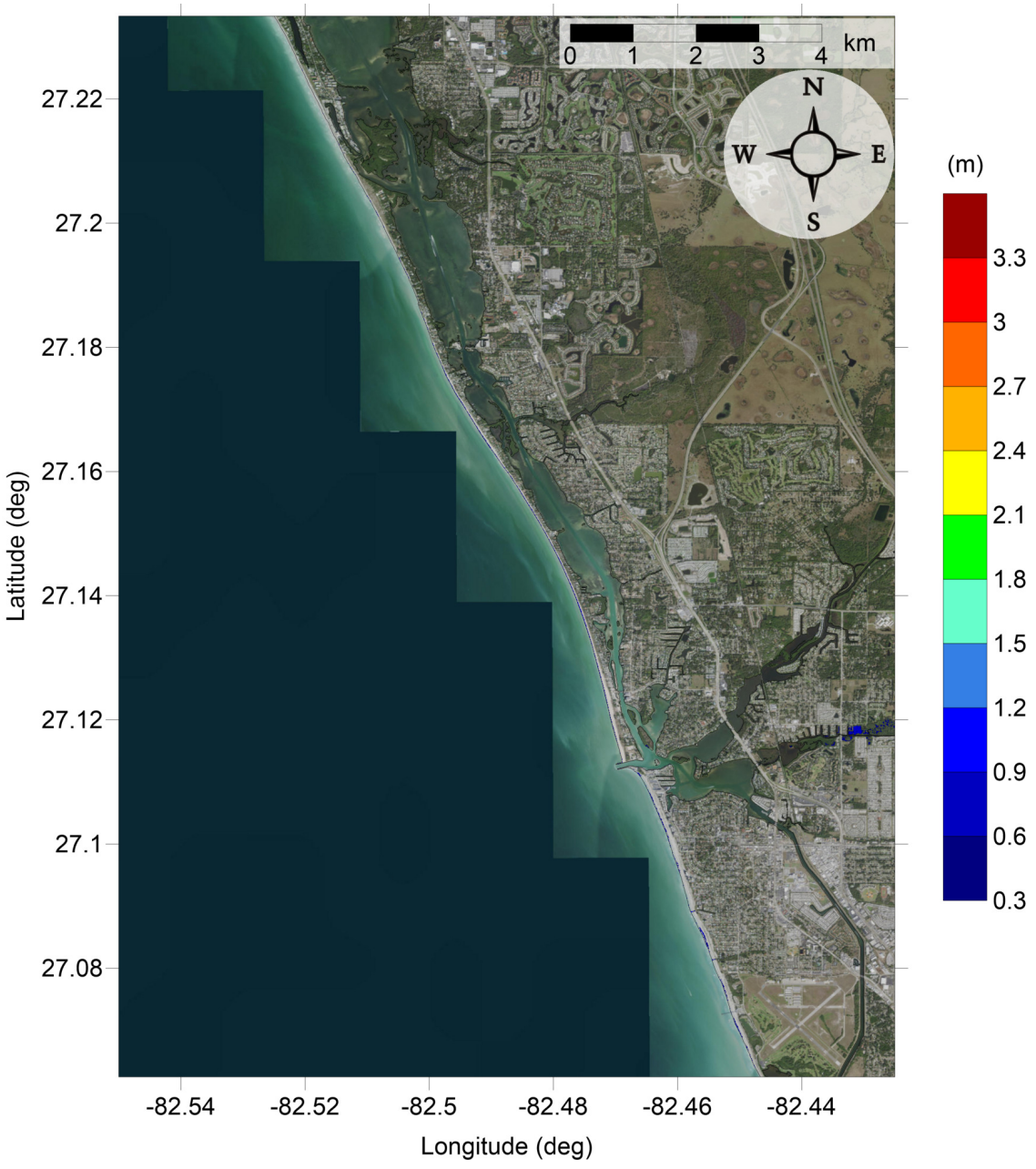

Figure 39: Maximum inundation depth (m) caused by the Probabilistic Submarine Landslide B1 in Osprey-Venice, FL. Contour drawn is the zero-meter contour for land elevation.

Osprey-Venice-Englewood, FL
Probabilistic Submarine Landslide B1
Maximum Inundation Depth

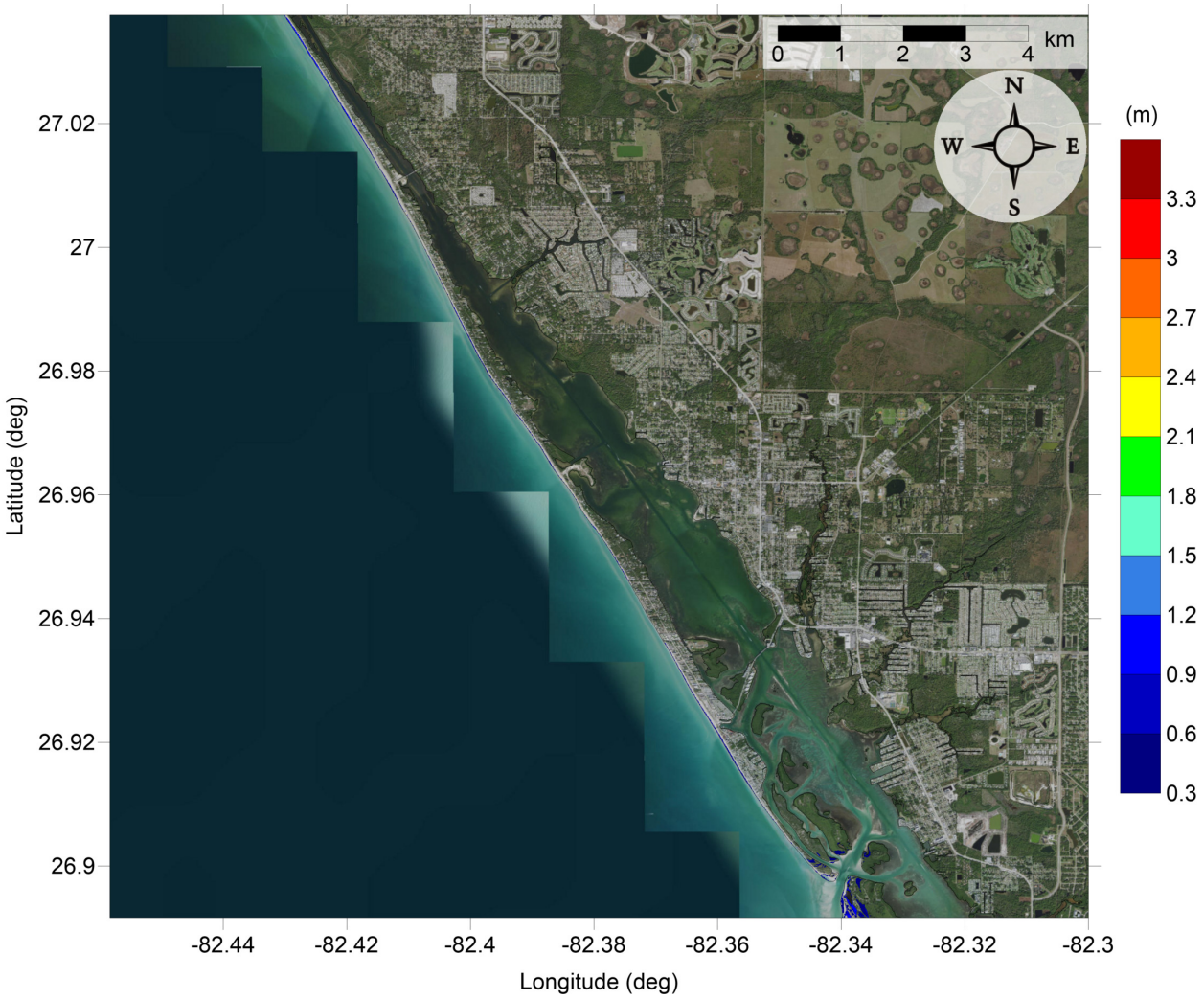

Figure 40: Maximum inundation depth (m) caused by the Probabilistic Submarine Landslide B1 in Englewood, FL. Contour drawn is the zero-meter contour for land elevation.

Osprey-Venice-Englewood, FL
Probabilistic Submarine Landslide B2
Maximum Momentum Flux

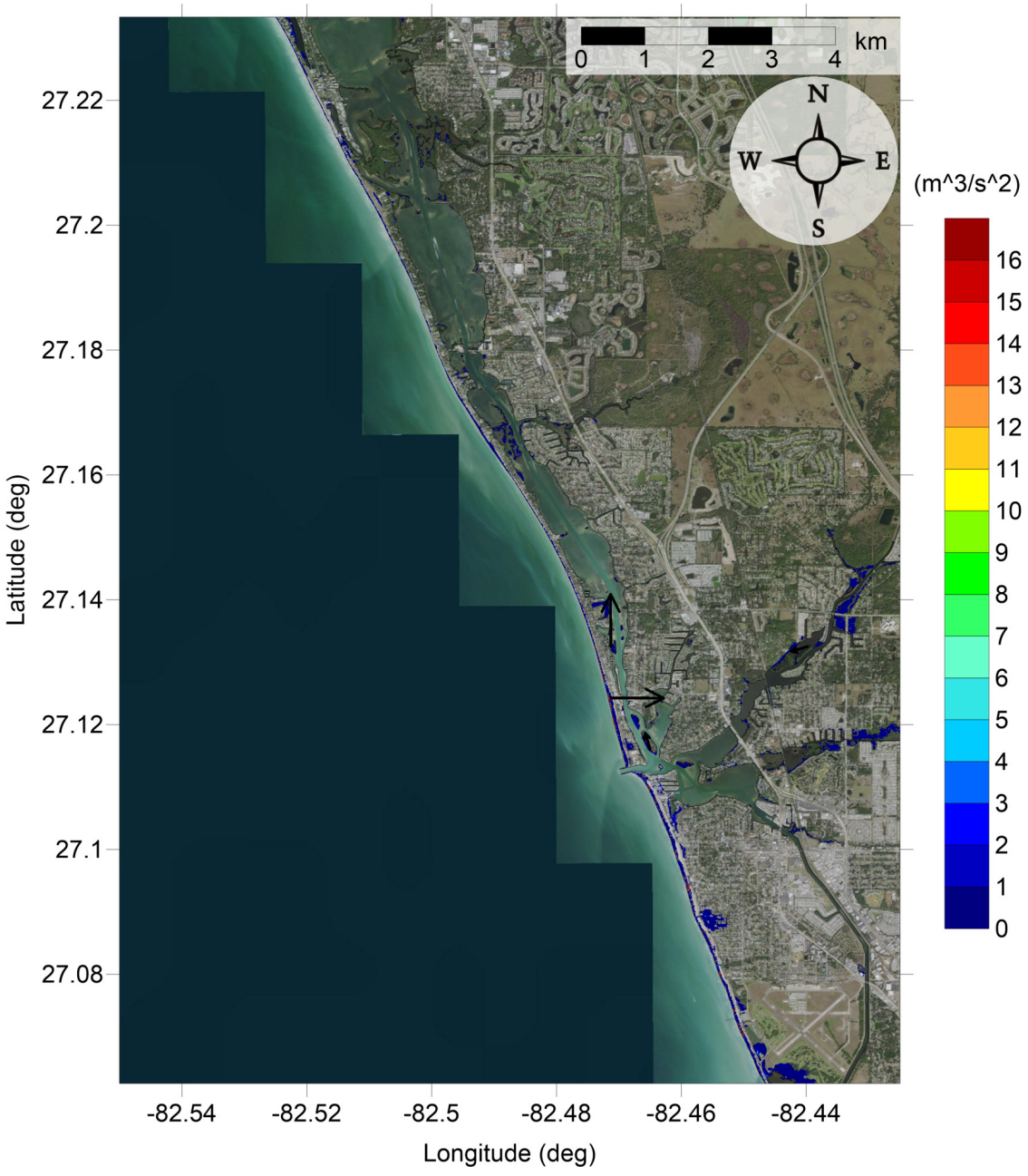

Figure 41: Maximum momentum flux (m^3/s^2) caused by the Probabilistic Submarine Landslide B2 in Osprey-Venice, FL. Arrows represent direction of maximum momentum flux. Contour drawn is the zero-meter contour for land elevation.

Osprey-Venice-Englewood, FL
Probabilistic Submarine Landslide B2
Maximum Momentum Flux

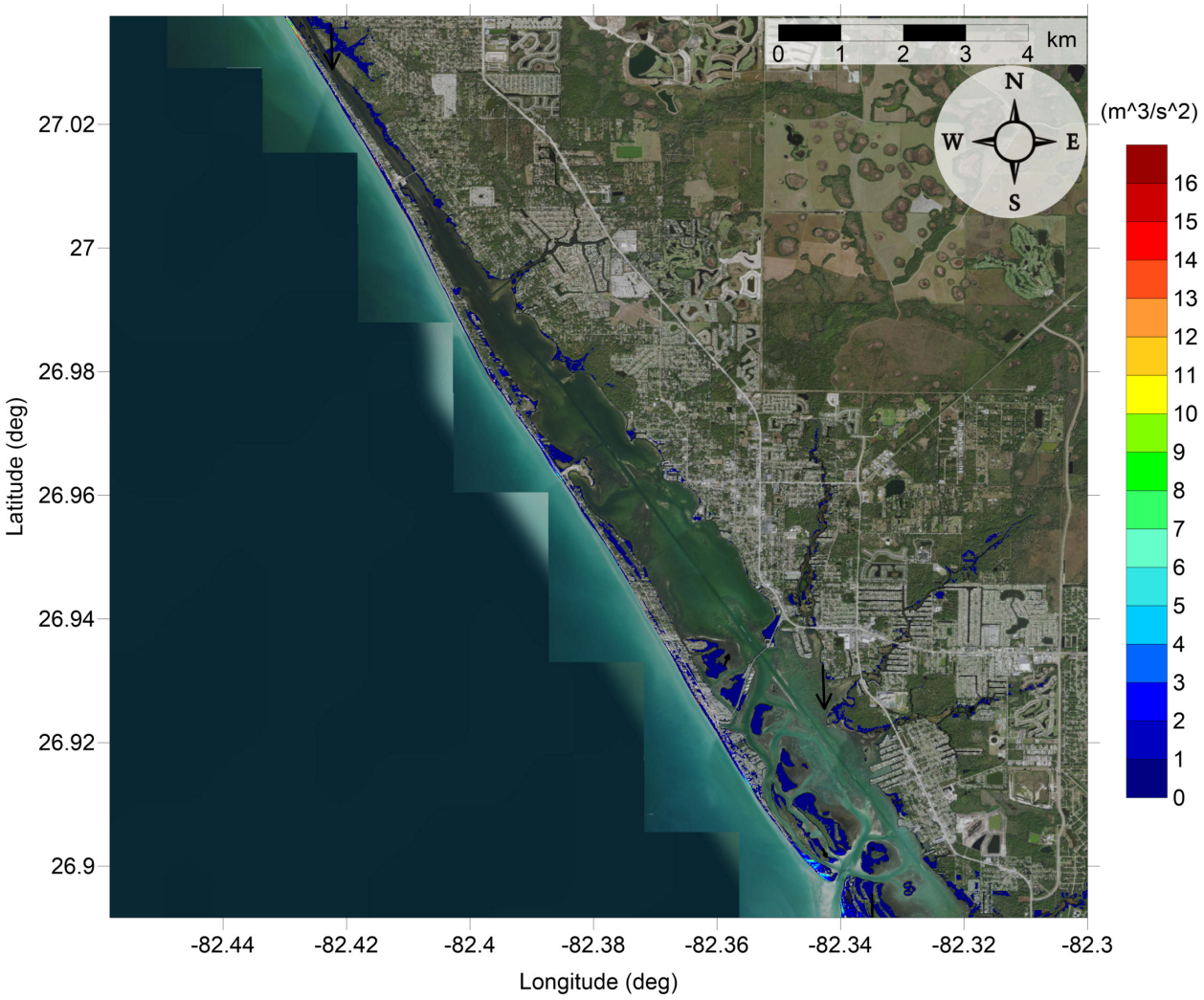

Figure 42: Maximum momentum flux (m^3/s^2) caused by the Probabilistic Submarine Landslide B2 in Englewood, FL. Arrows represent direction of maximum momentum flux. Contour drawn is the zero-meter contour for land elevation.

Osprey-Venice-Englewood, FL
Probabilistic Submarine Landslide B2
Maximum Inundation Depth

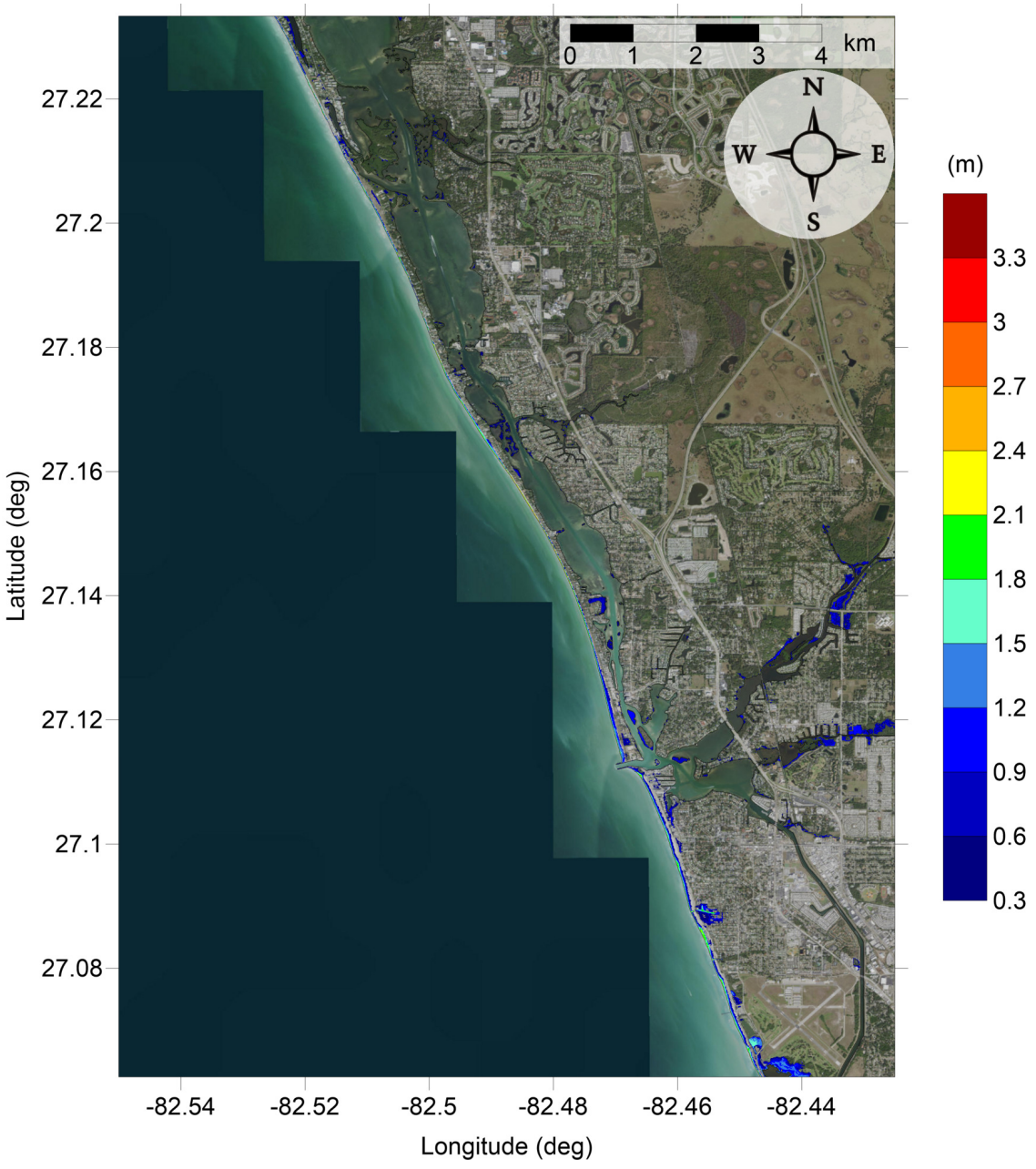

Figure 43: Maximum inundation depth (m) caused by the Probabilistic Submarine Landslide B2 in Osprey-Venice, FL. Contour drawn is the zero-meter contour for land elevation.

Osprey-Venice-Englewood, FL
Probabilistic Submarine Landslide B2
Maximum Inundation Depth

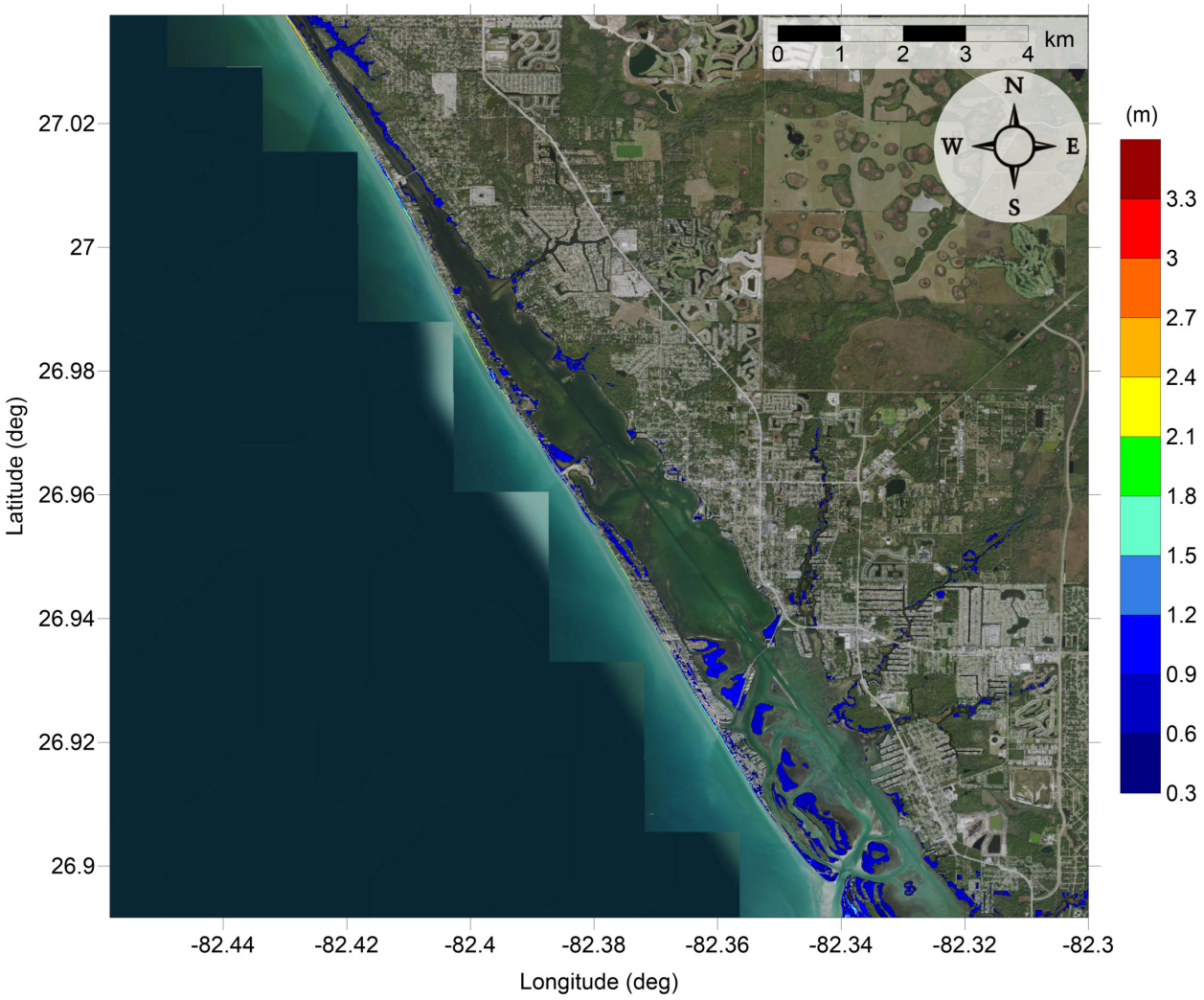

Figure 44: Maximum inundation depth (m) caused by the Probabilistic Submarine Landslide B2 in Englewood, FL. Contour drawn is the zero-meter contour for land elevation.

Osprey-Venice-Englewood, FL
Mississippi Canyon submarine landslide
Maximum Momentum Flux

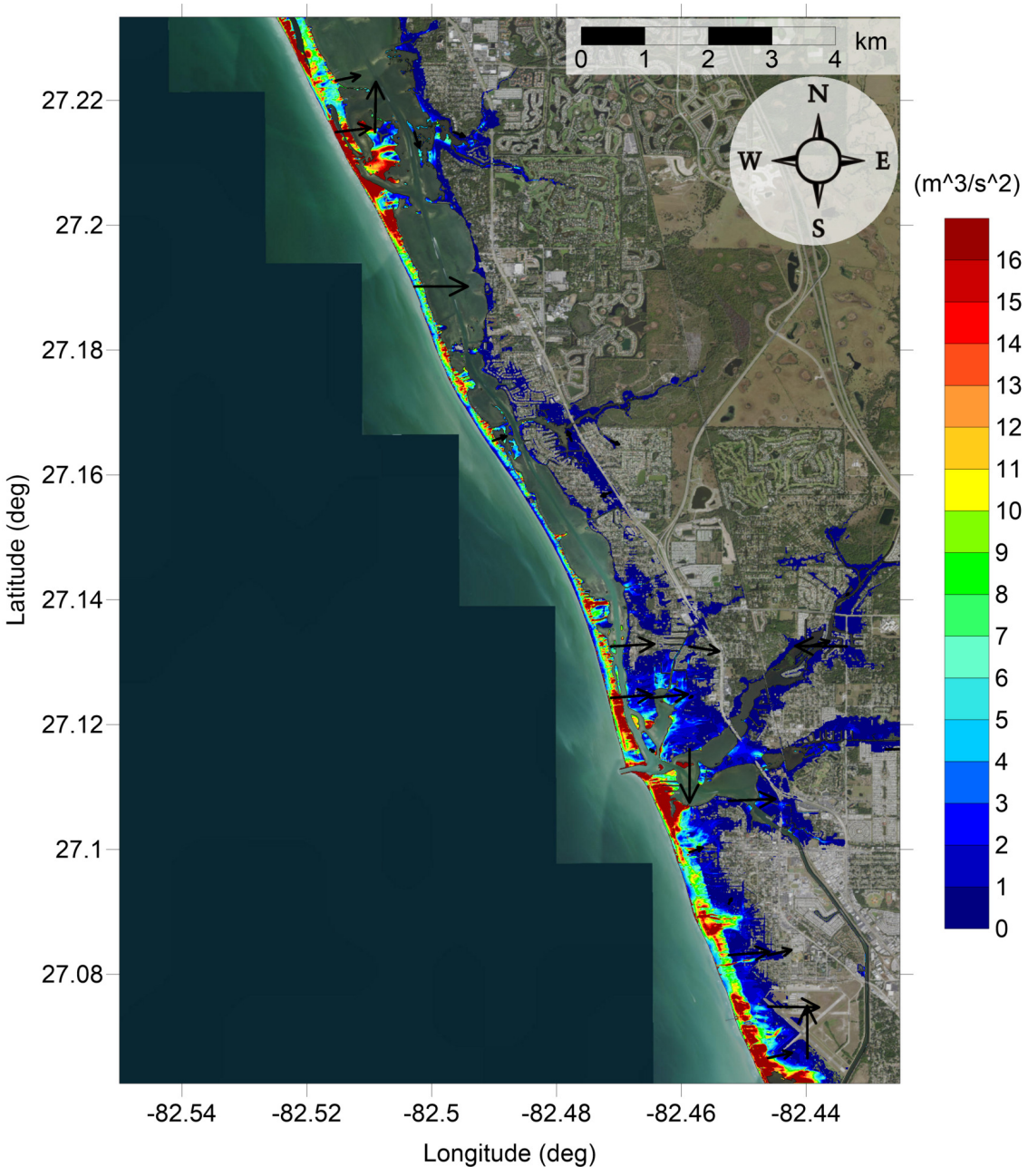

Figure 45: Maximum momentum flux (m^3/s^2) caused by the Mississippi Canyon submarine landslide in Osprey-Venice, FL. Arrows represent direction of maximum momentum flux. Contour drawn is the zero-meter contour for land elevation.

Osprey-Venice-Englewood, FL
Mississippi Canyon submarine landslide
Maximum Momentum Flux

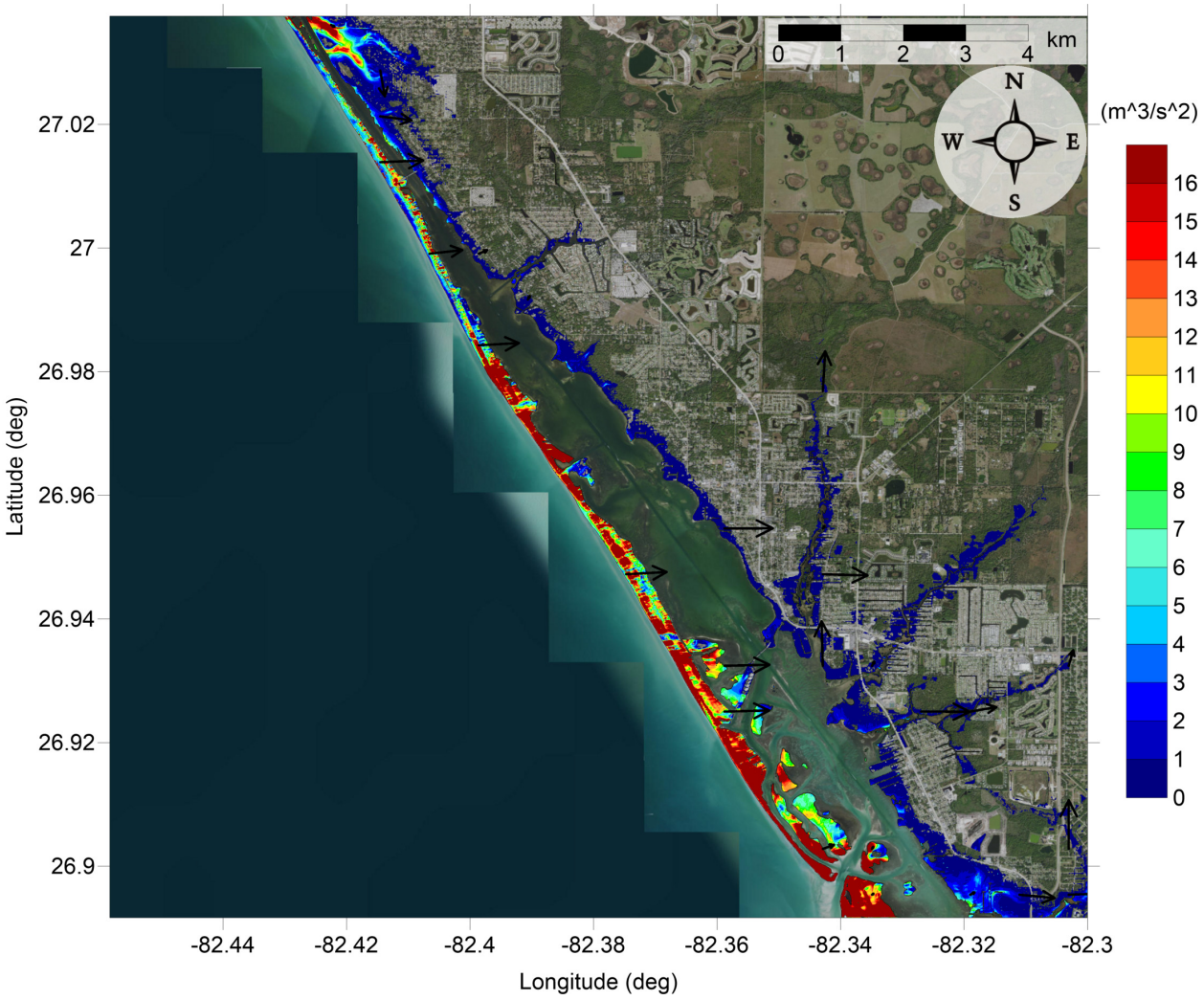

Figure 46: Maximum momentum flux (m^3/s^2) caused by the Mississippi Canyon submarine landslide in Englewood, FL. Arrows represent direction of maximum momentum flux. Contour drawn is the zero-meter contour for land elevation.

Osprey-Venice-Englewood, FL
Mississippi Canyon submarine landslide
Maximum Inundation Depth

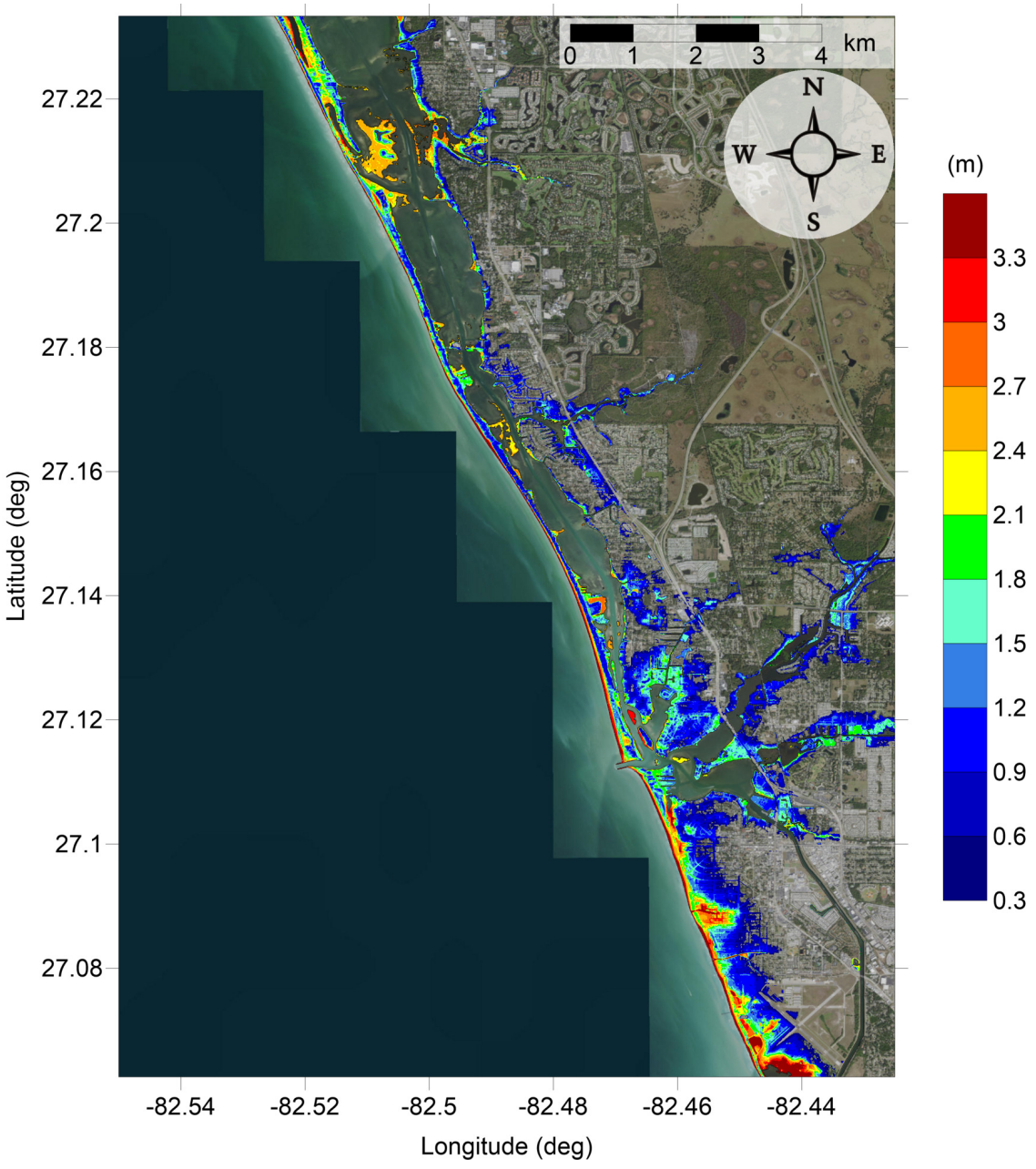

Figure 47: Maximum inundation depth (m) caused by the Mississippi Canyon submarine landslide in Osprey-Venice, FL. Contour drawn is the zero-meter contour for land elevation.

Osprey-Venice-Englewood, FL
Mississippi Canyon submarine landslide
Maximum Inundation Depth

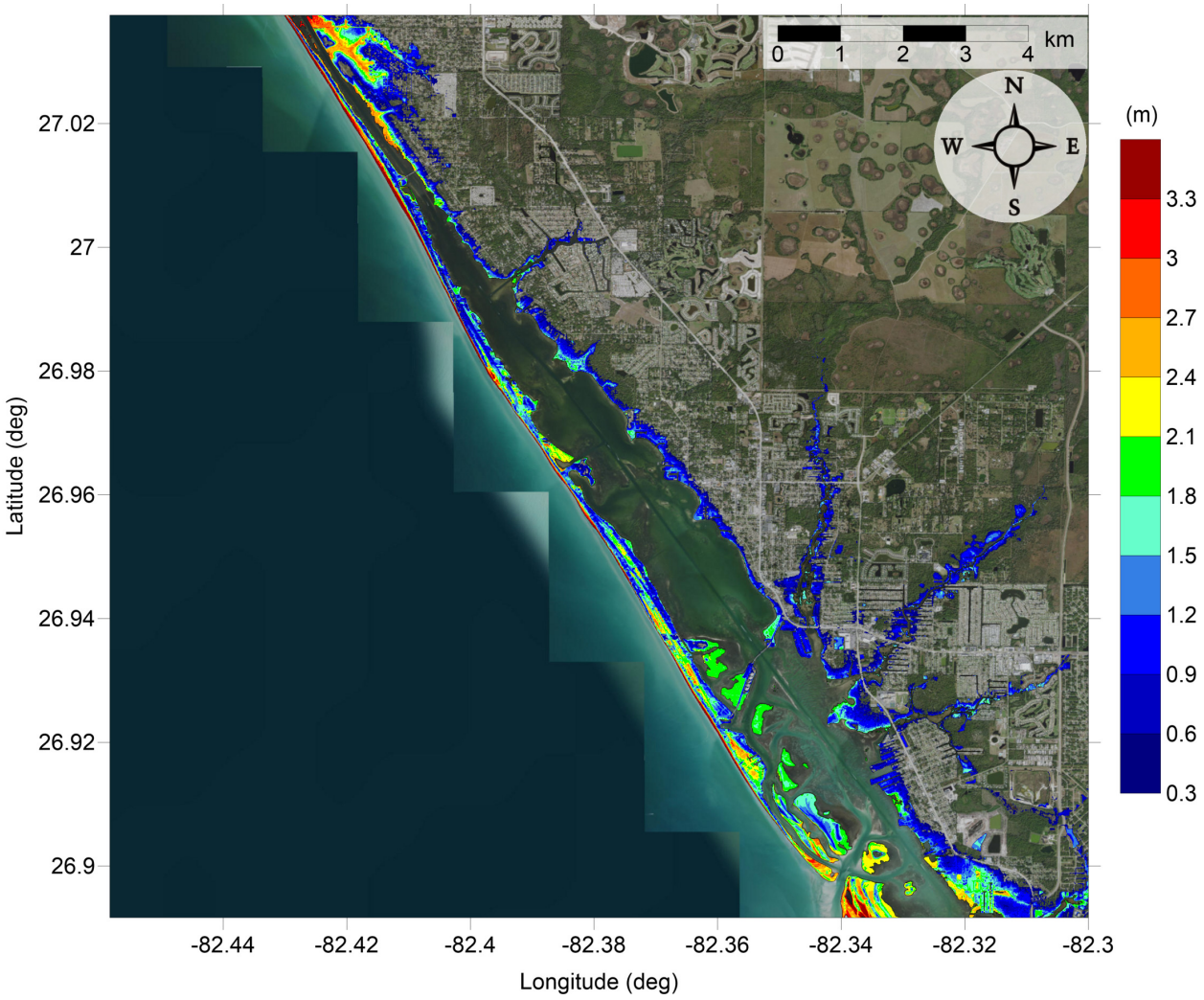

Figure 48: Maximum inundation depth (m) caused by the Mississippi Canyon submarine landslide in Englewood, FL. Contour drawn is the zero-meter contour for land elevation.

Osprey-Venice-Englewood, FL
Probabilistic Submarine Landslide C
Maximum Momentum Flux

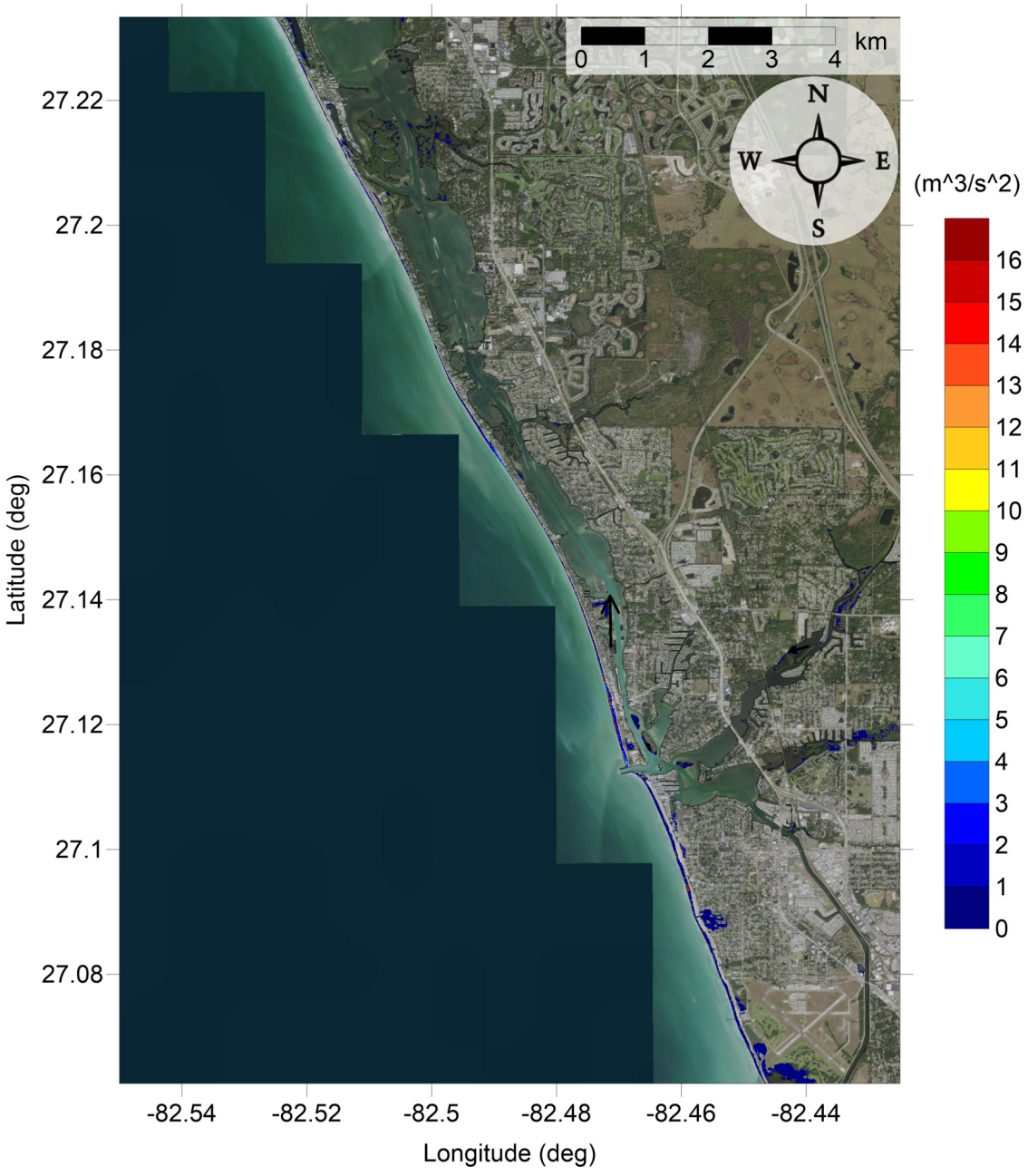

Figure 49: Maximum momentum flux (m^3/s^2) caused by the Probabilistic Submarine Landslide C in Osprey-Venice, FL. Arrows represent direction of maximum momentum flux. Contour drawn is the zero-meter contour for land elevation.

Osprey-Venice-Englewood, FL
Probabilistic Submarine Landslide C
Maximum Momentum Flux

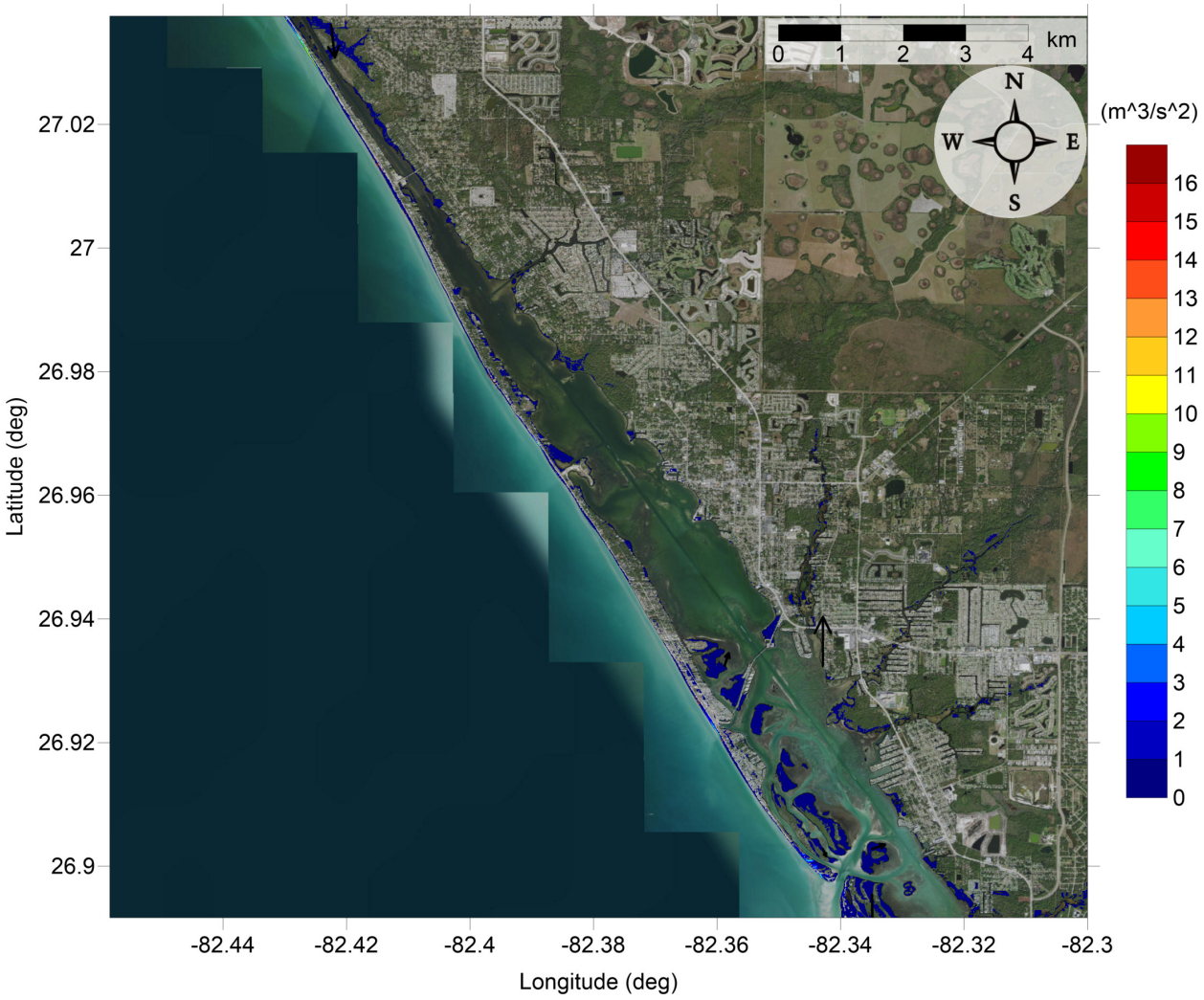

Figure 50: Maximum momentum flux (m^3/s^2) caused by the Probabilistic Submarine Landslide C in Englewood, FL. Arrows represent direction of maximum momentum flux. Contour drawn is the zero-meter contour for land elevation.

Osprey-Venice-Englewood, FL
Probabilistic Submarine Landslide C
Maximum Inundation Depth

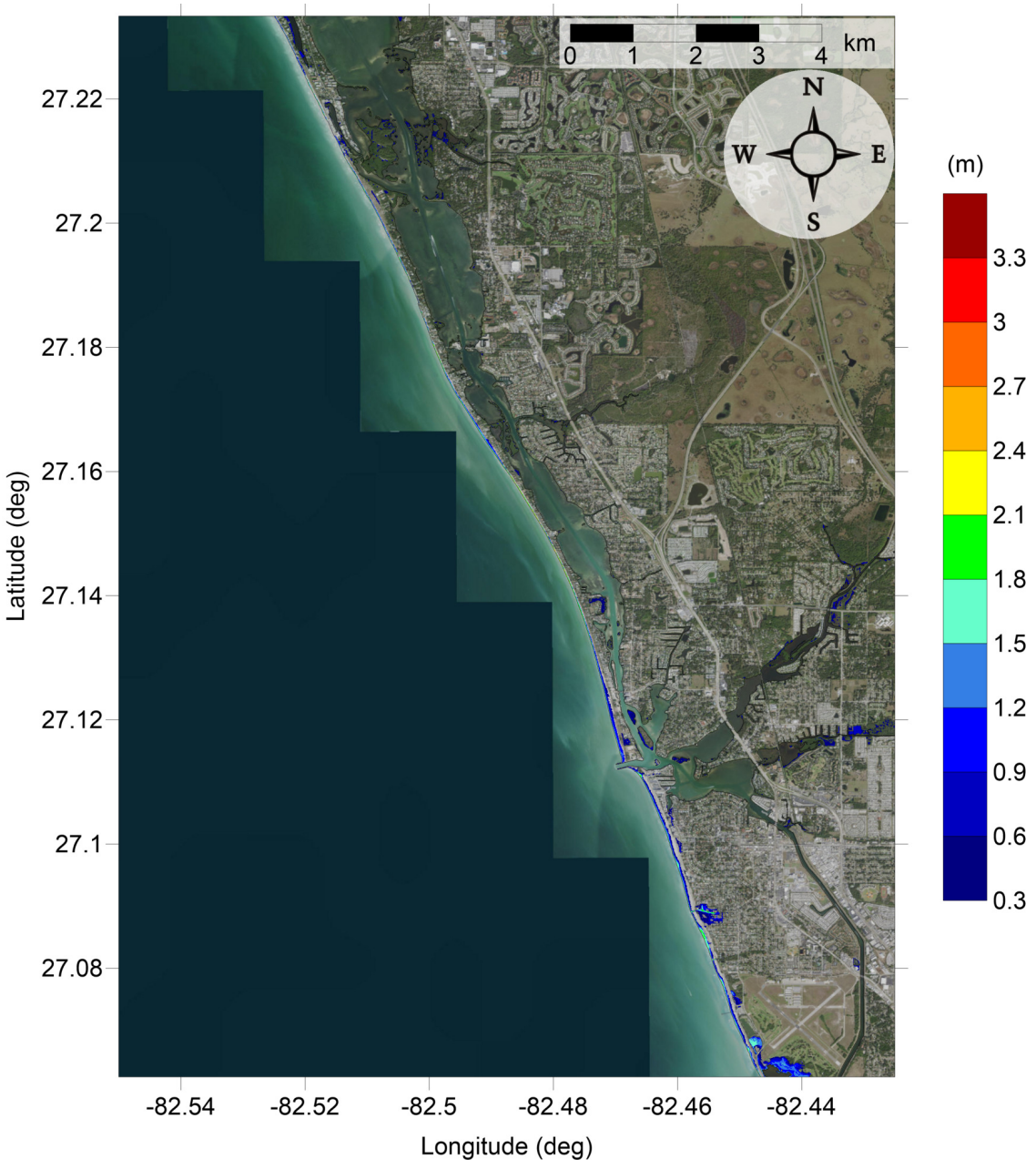

Figure 51: Maximum inundation depth (m) caused by the Probabilistic Submarine Landslide C in Osprey-Venice, FL. Contour drawn is the zero-meter contour for land elevation.

Osprey-Venice-Englewood, FL
Probabilistic Submarine Landslide C
Maximum Inundation Depth

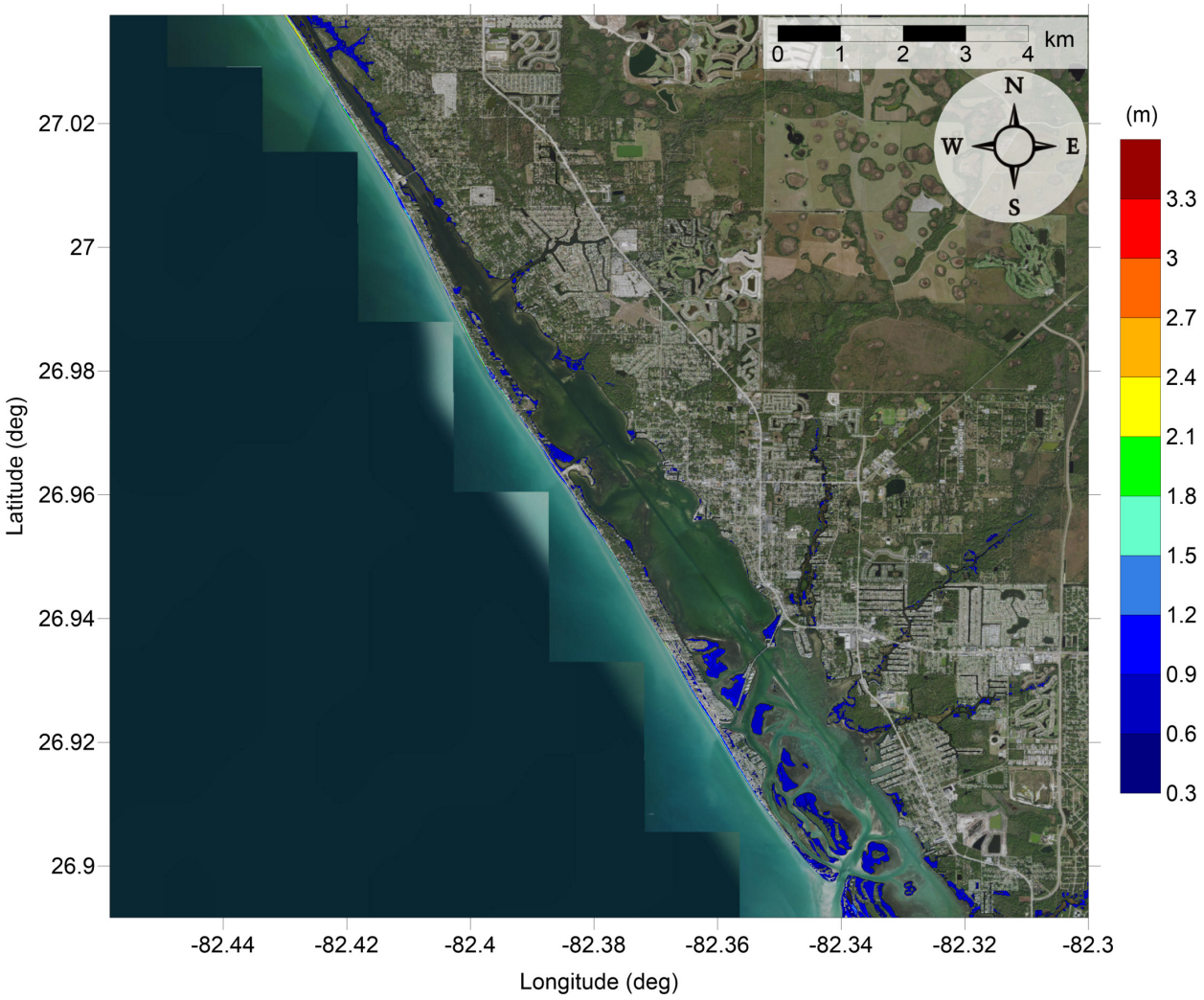

Figure 52: Maximum inundation depth (m) caused by the Probabilistic Submarine Landslide C in Englewood, FL. Contour drawn is the zero-meter contour for land elevation.

Osprey-Venice-Englewood, FL
West Florida submarine landslide
Maximum Momentum Flux

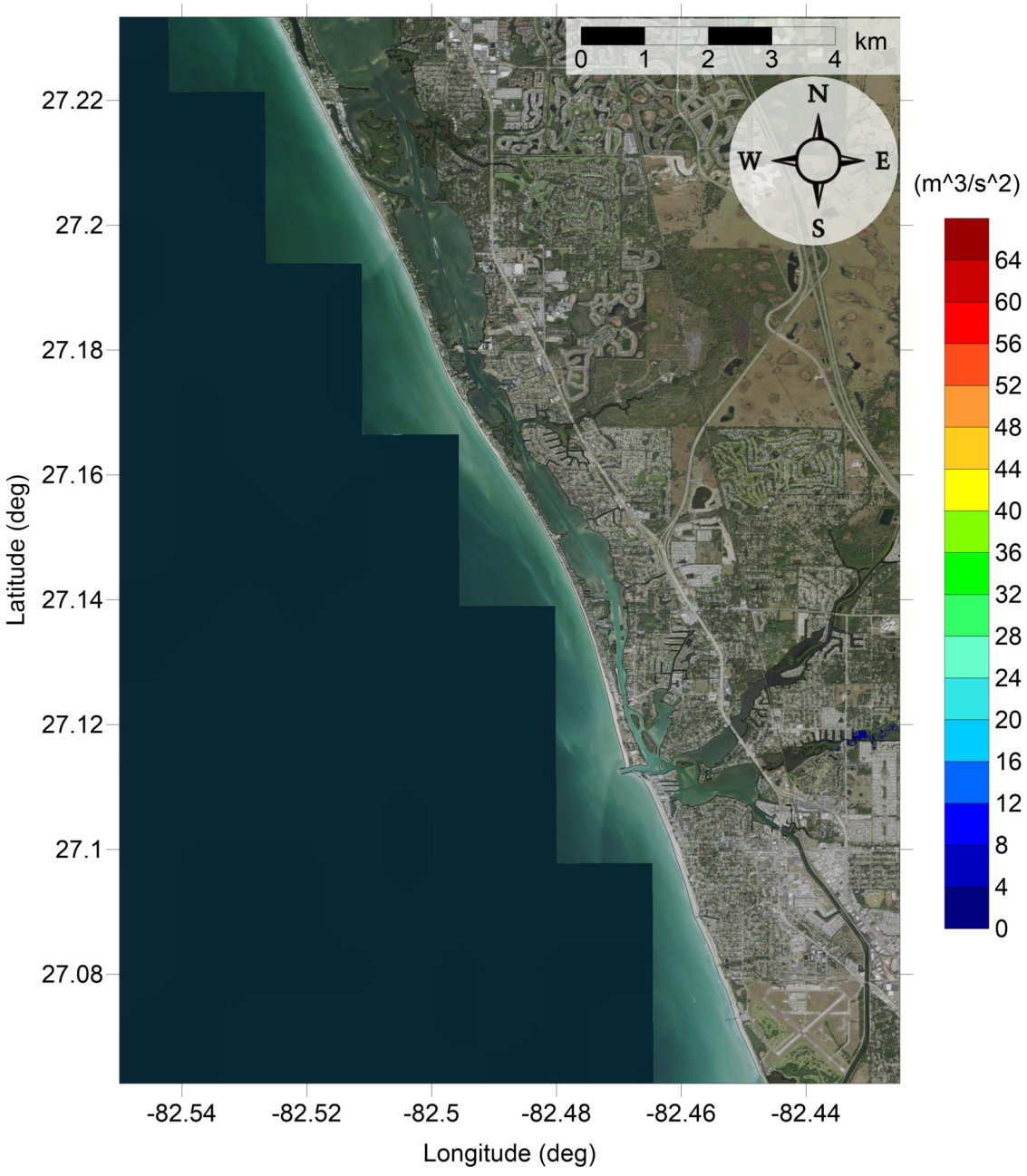

Figure 53: Maximum momentum flux (m^3/s^2) caused by the West Florida submarine landslide in Osprey-Venice, FL. Arrows represent direction of maximum momentum flux. Contour drawn is the zero-meter contour for land elevation.

Osprey-Venice-Englewood, FL
West Florida submarine landslide
Maximum Momentum Flux

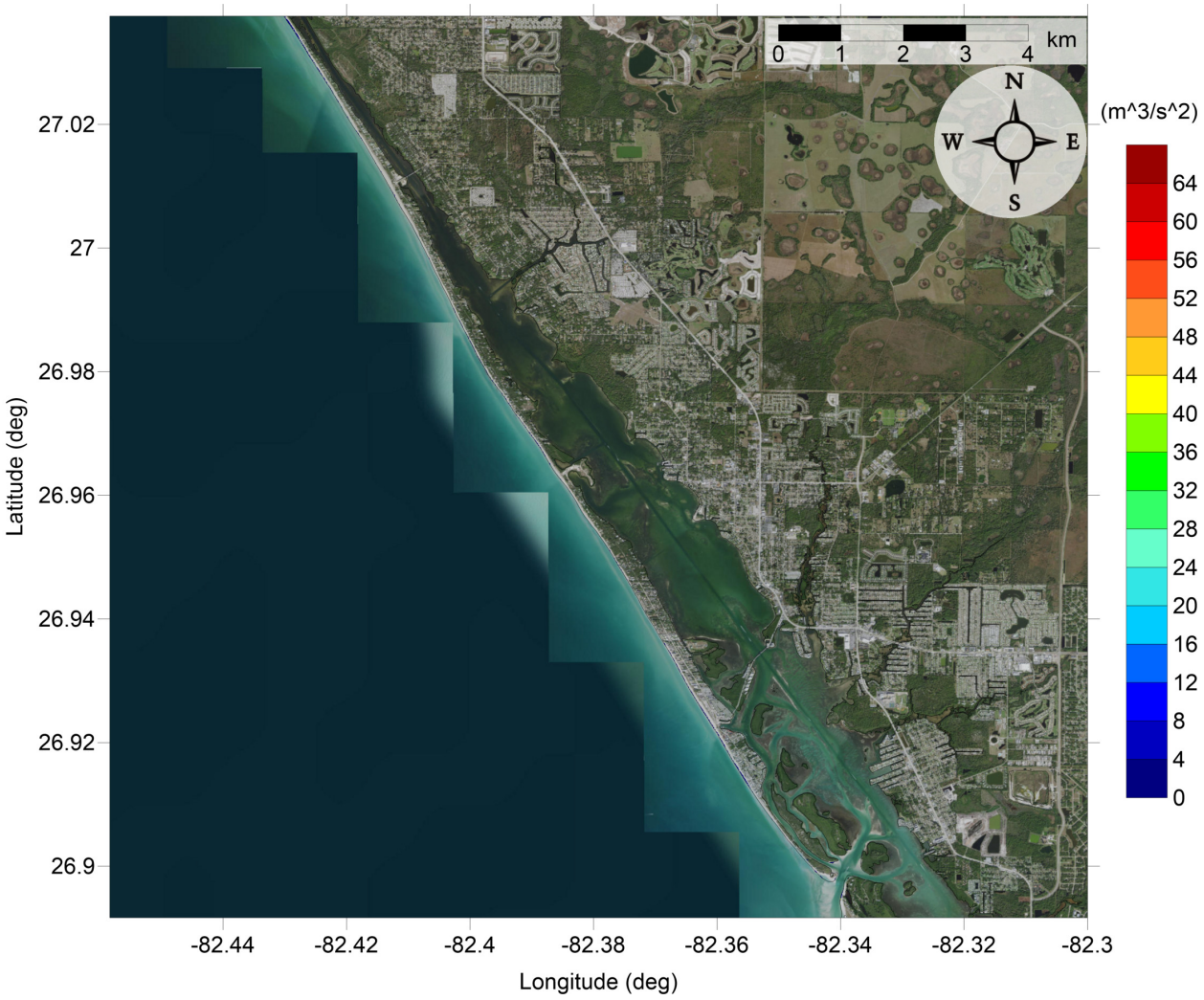

Figure 54: Maximum momentum flux (m^3/s^2) caused by the West Florida submarine landslide in Englewood, FL. Arrows represent direction of maximum momentum flux. Contour drawn is the zero-meter contour for land elevation.

Osprey-Venice-Englewood, FL
West Florida submarine landslide
Maximum Inundation Depth

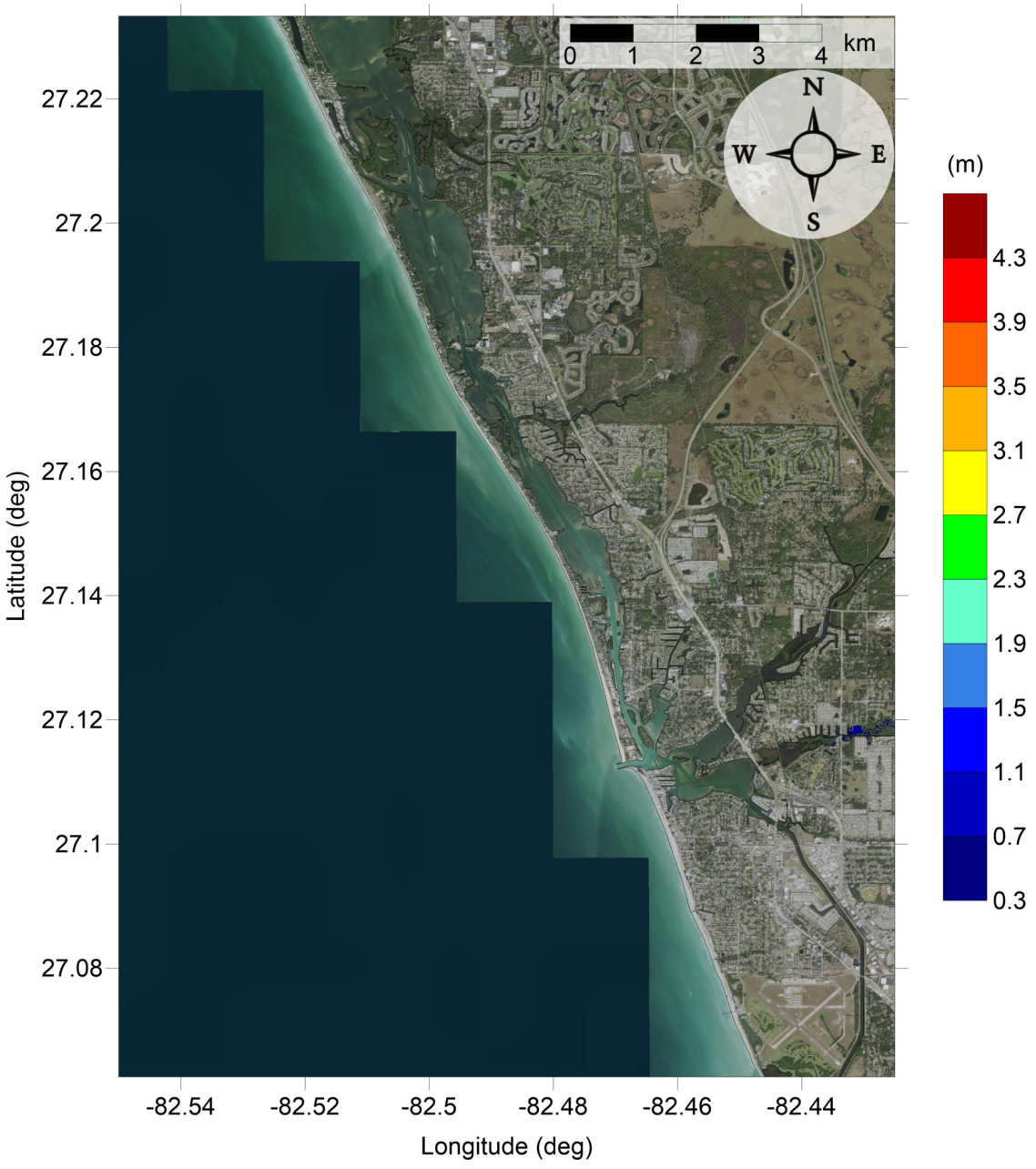

Figure 55: Maximum inundation depth (m) caused by the West Florida submarine landslide in Osprey-Venice, FL. Contour drawn is the zero-meter contour for land elevation.

Osprey-Venice-Englewood, FL
West Florida submarine landslide
Maximum Inundation Depth

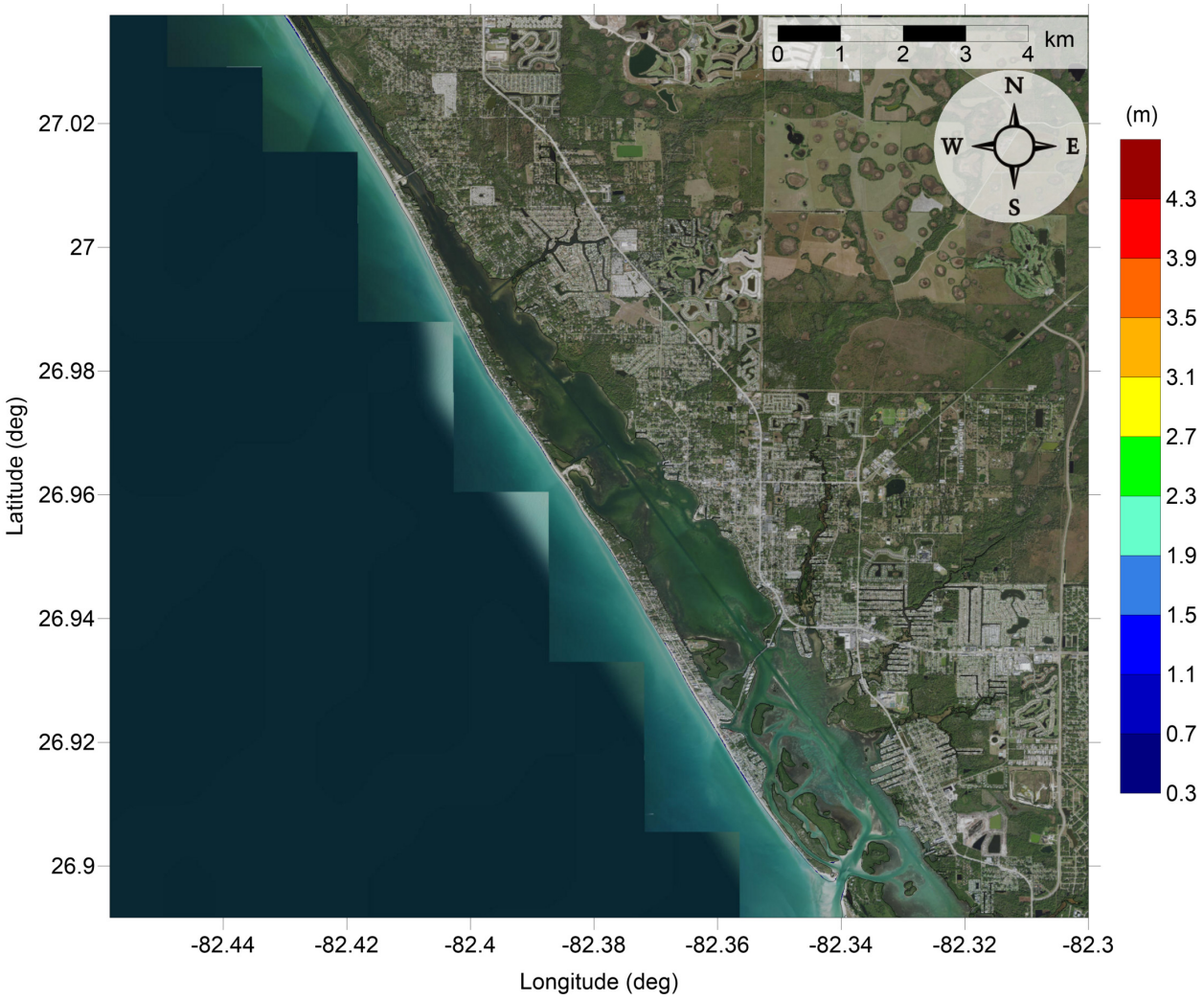

Figure 56: Maximum inundation depth (m) caused by the West Florida submarine landslide in Englewood, FL. Contour drawn is the zero-meter contour for land elevation.

Osprey-Venice-Englewood, FL
Yucatan #3 submarine landslide
Maximum Momentum Flux

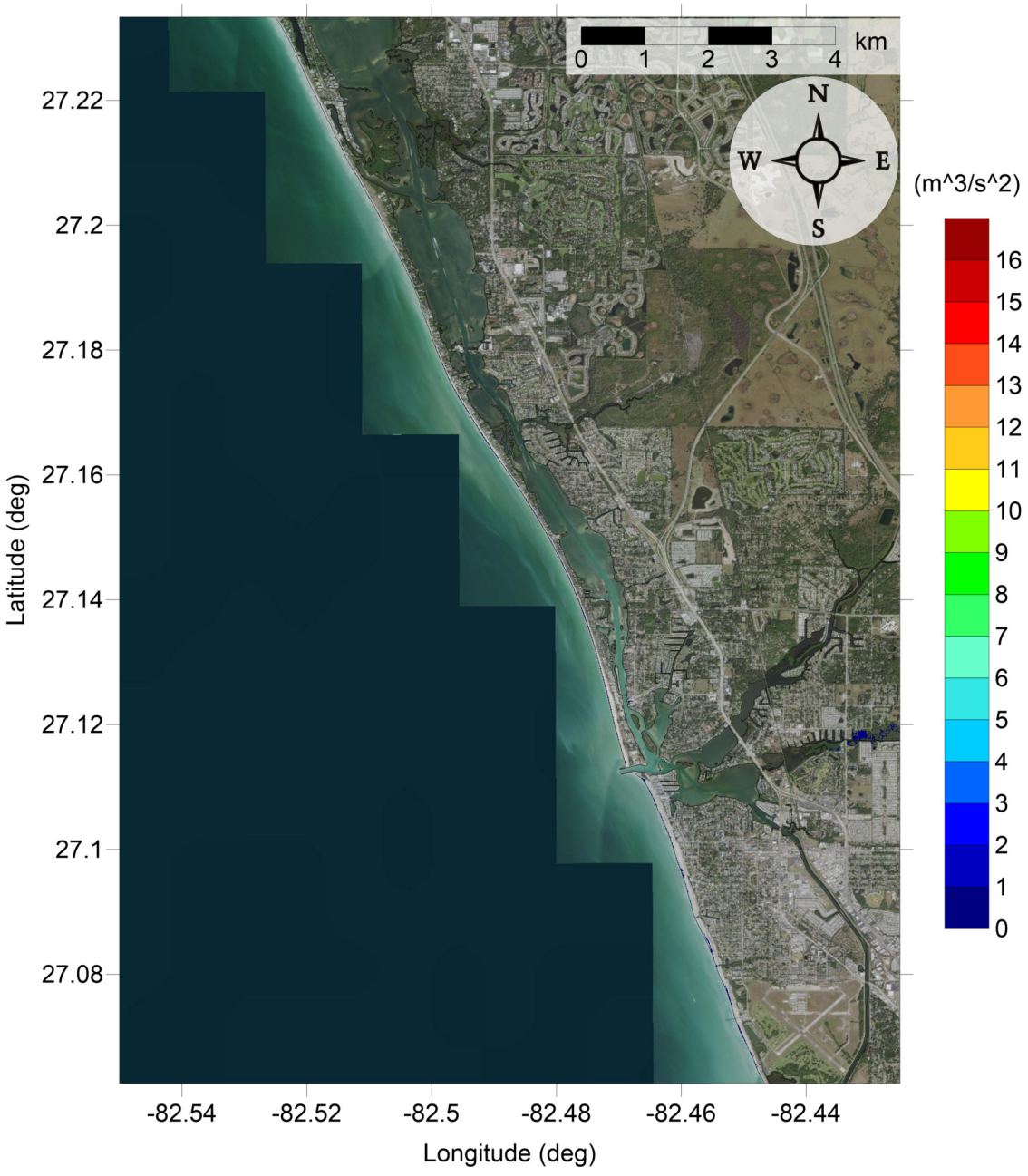

Figure 57: Maximum momentum flux (m^3/s^2) caused by the Yucatan #3 submarine landslide in Osprey-Venice, FL. Arrows represent direction of maximum momentum flux. Contour drawn is the zero-meter contour for land elevation.

Osprey-Venice-Englewood, FL
Yucatan #3 submarine landslide
Maximum Momentum Flux

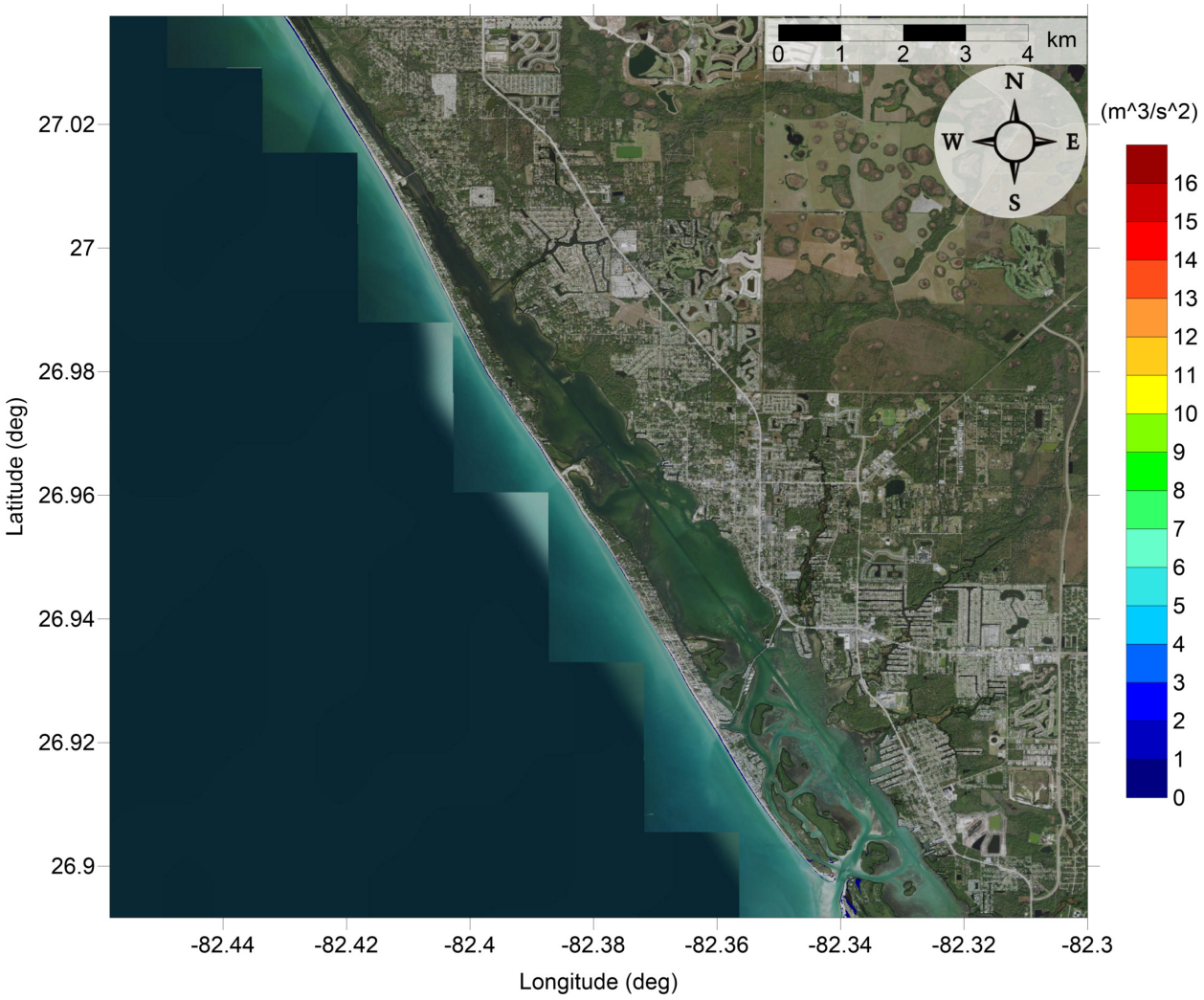

Figure 58: Maximum momentum flux (m^3/s^2) caused by the Yucatan #3 submarine landslide in Englewood, FL. Arrows represent direction of maximum momentum flux. Contour drawn is the zero-meter contour for land elevation.

Osprey-Venice-Englewood, FL
Yucatan #3 submarine landslide
Maximum Inundation Depth

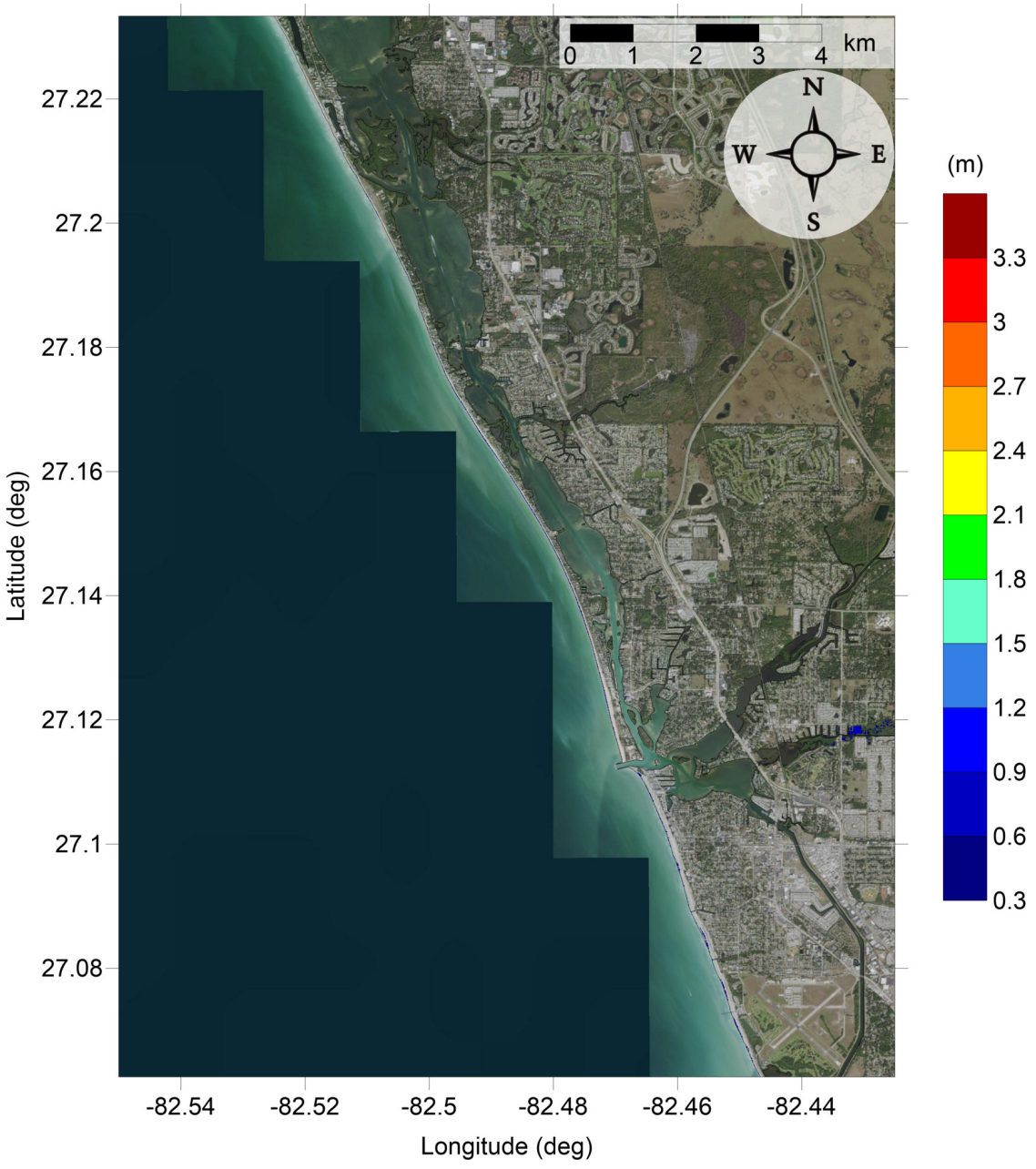

Figure 59: Maximum inundation depth (m) caused by the Yucatan #3 submarine landslide in Osprey-Venice, FL. Contour drawn is the zero-meter contour for land elevation.

Osprey-Venice-Englewood, FL
Yucatan #3 submarine landslide
Maximum Inundation Depth

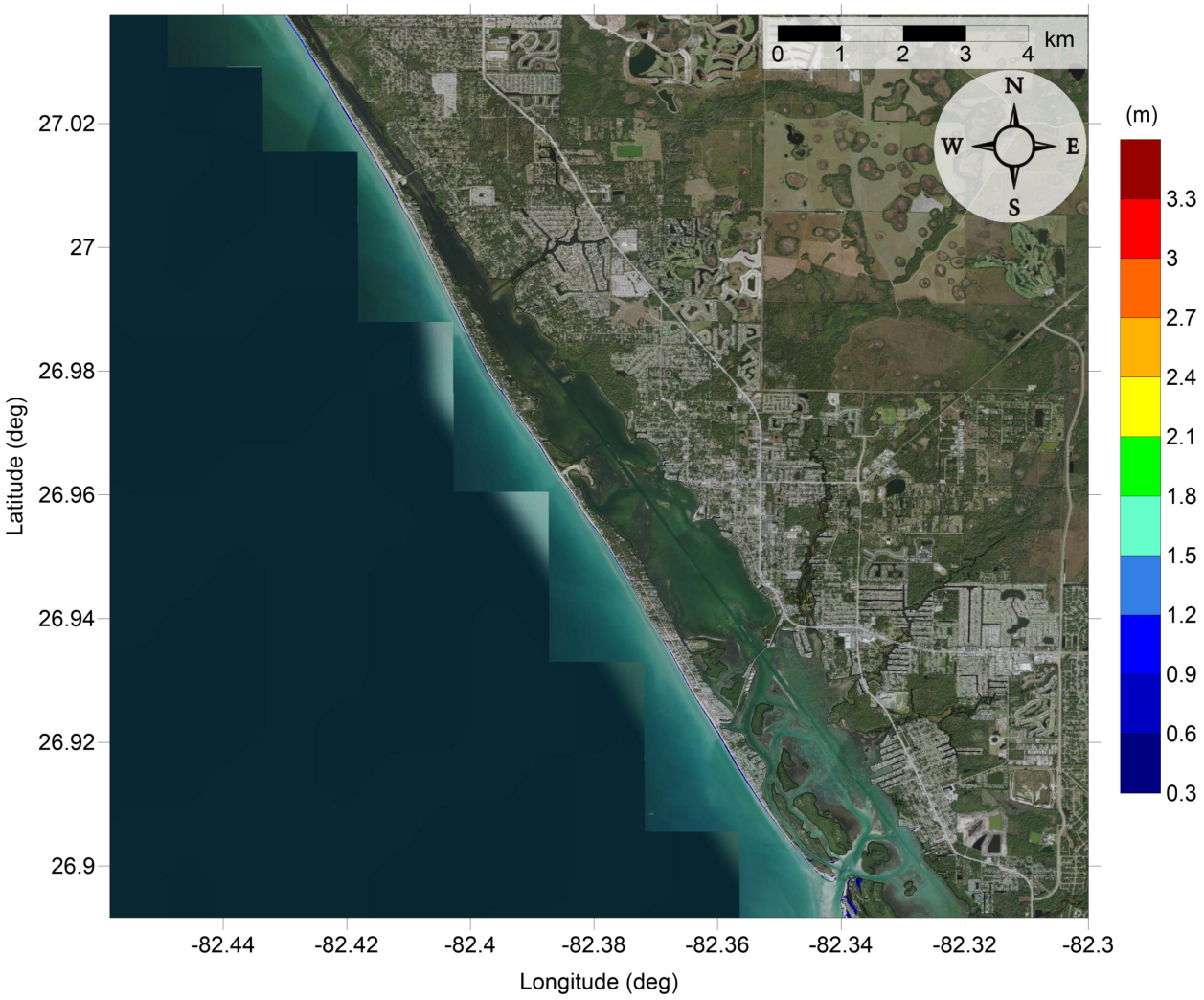

Figure 60: Maximum inundation depth (m) caused by the Yucatan #3 submarine landslide in Englewood, FL. Contour drawn is the zero-meter contour for land elevation.

Osprey-Venice-Englewood, FL
Yucatan #5 submarine landslide
Maximum Momentum Flux

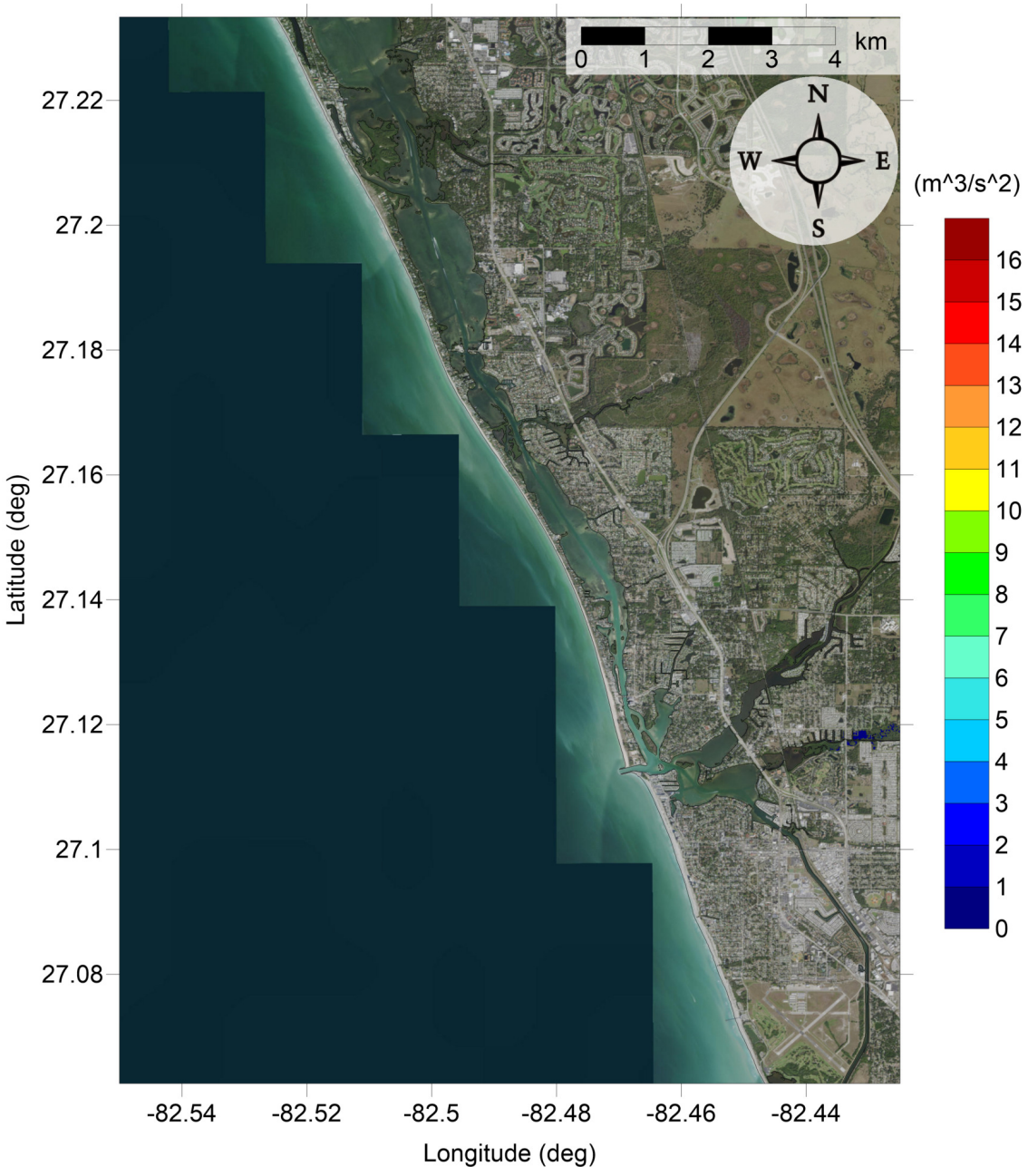

Figure 61: Maximum momentum flux (m^3/s^2) caused by the Yucatan #5 submarine landslide in Osprey-Venice, FL. Arrows represent direction of maximum momentum flux. Contour drawn is the zero-meter contour for land elevation.

Osprey-Venice-Englewood, FL
Yucatan #5 submarine landslide
Maximum Momentum Flux

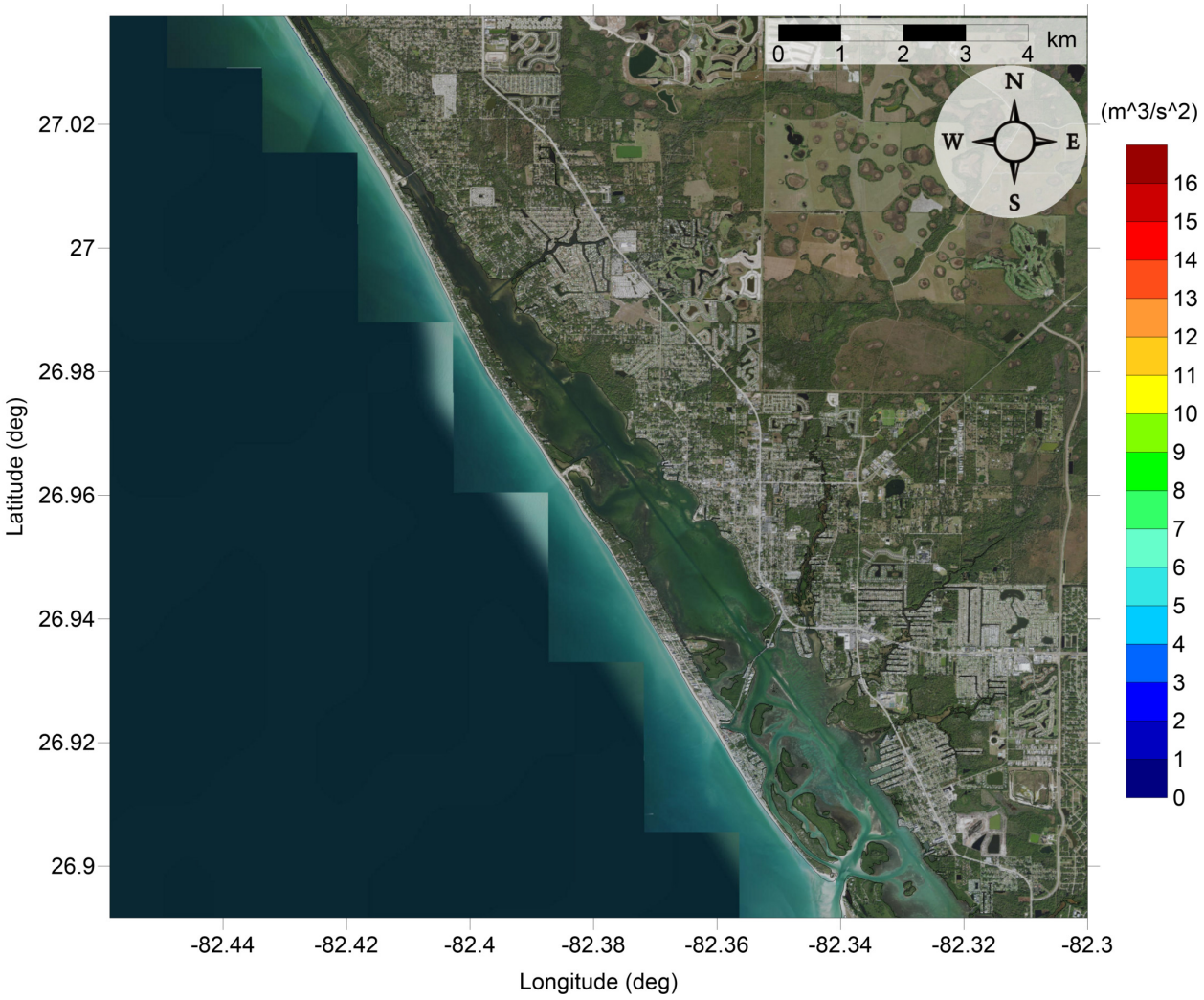

Figure 62: Maximum momentum flux (m^3/s^2) caused by the Yucatan #5 submarine landslide in Englewood, FL. Arrows represent direction of maximum momentum flux. Contour drawn is the zero-meter contour for land elevation.

Osprey-Venice-Englewood, FL
Yucatan #5 submarine landslide
Maximum Inundation Depth

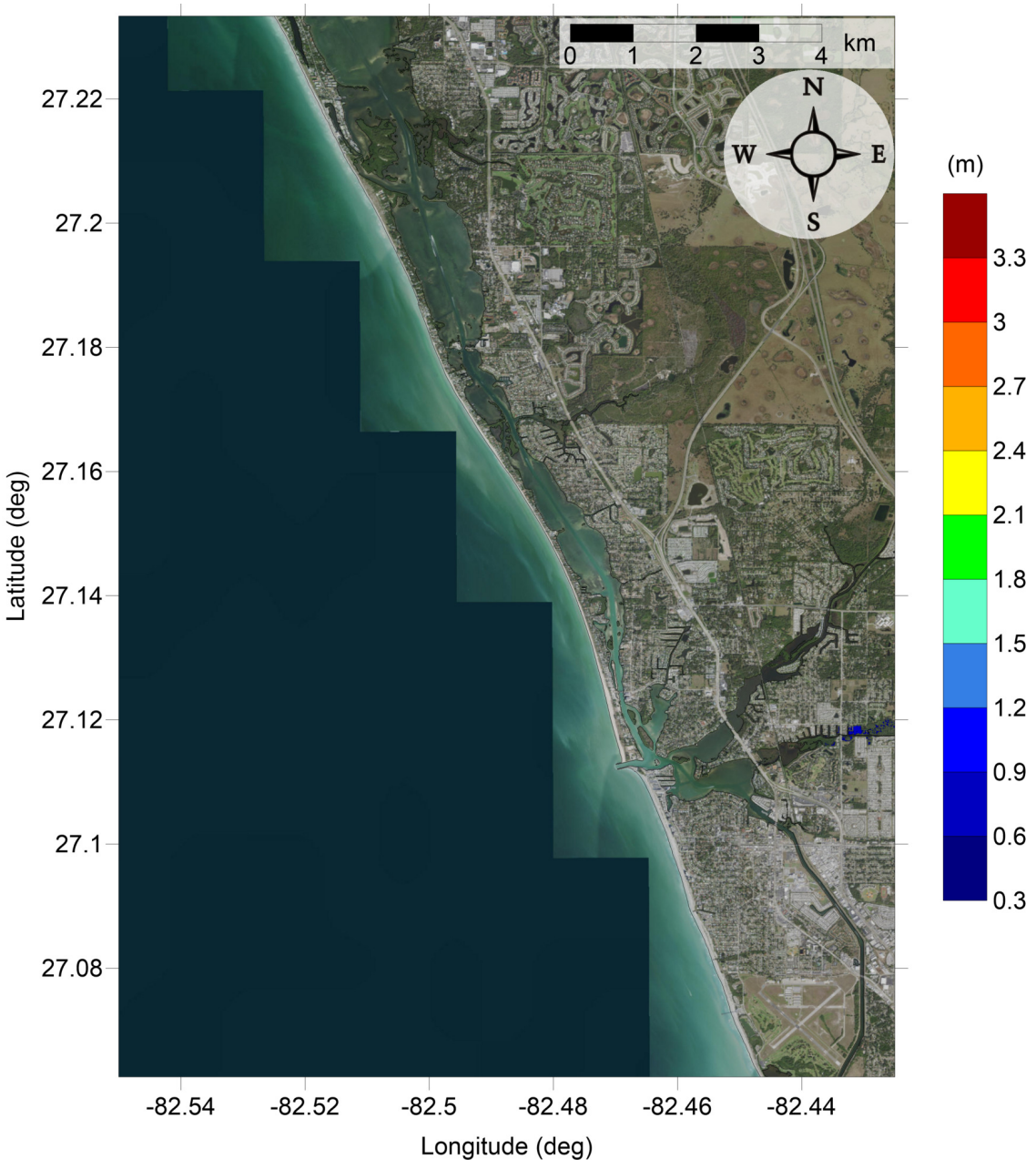

Figure 63: Maximum inundation depth (m) caused by the Yucatan #5 submarine landslide in Osprey-Venice, FL. Contour drawn is the zero-meter contour for land elevation.

Osprey-Venice-Englewood, FL
Yucatan #5 submarine landslide
Maximum Inundation Depth

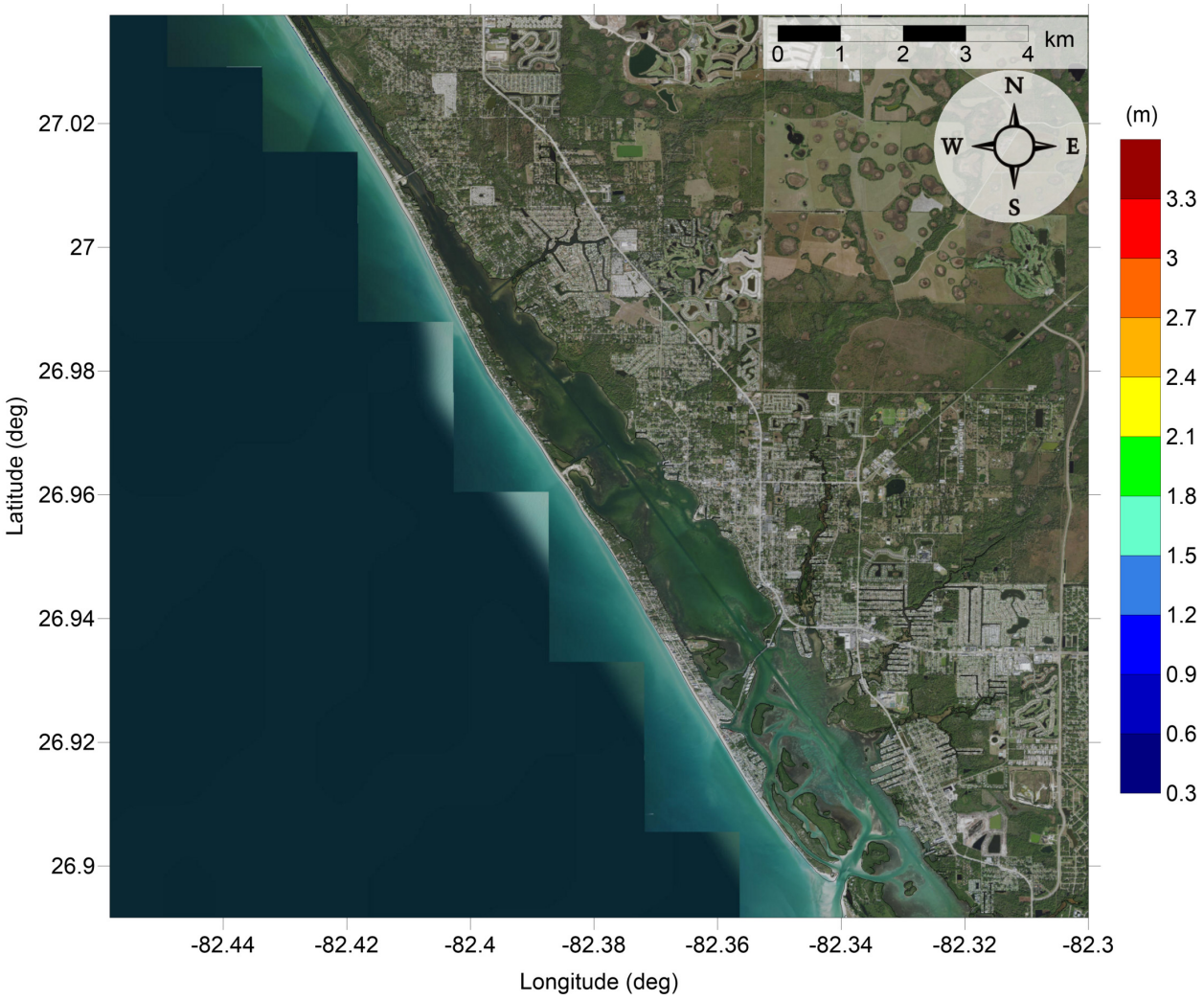

Figure 64: Maximum inundation depth (m) caused by the Yucatan #5 submarine landslide in Englewood, FL. Contour drawn is the zero-meter contour for land elevation.

Osprey-Venice-Englewood, FL
All Sources
Maximum of Maximum Inundation Depth

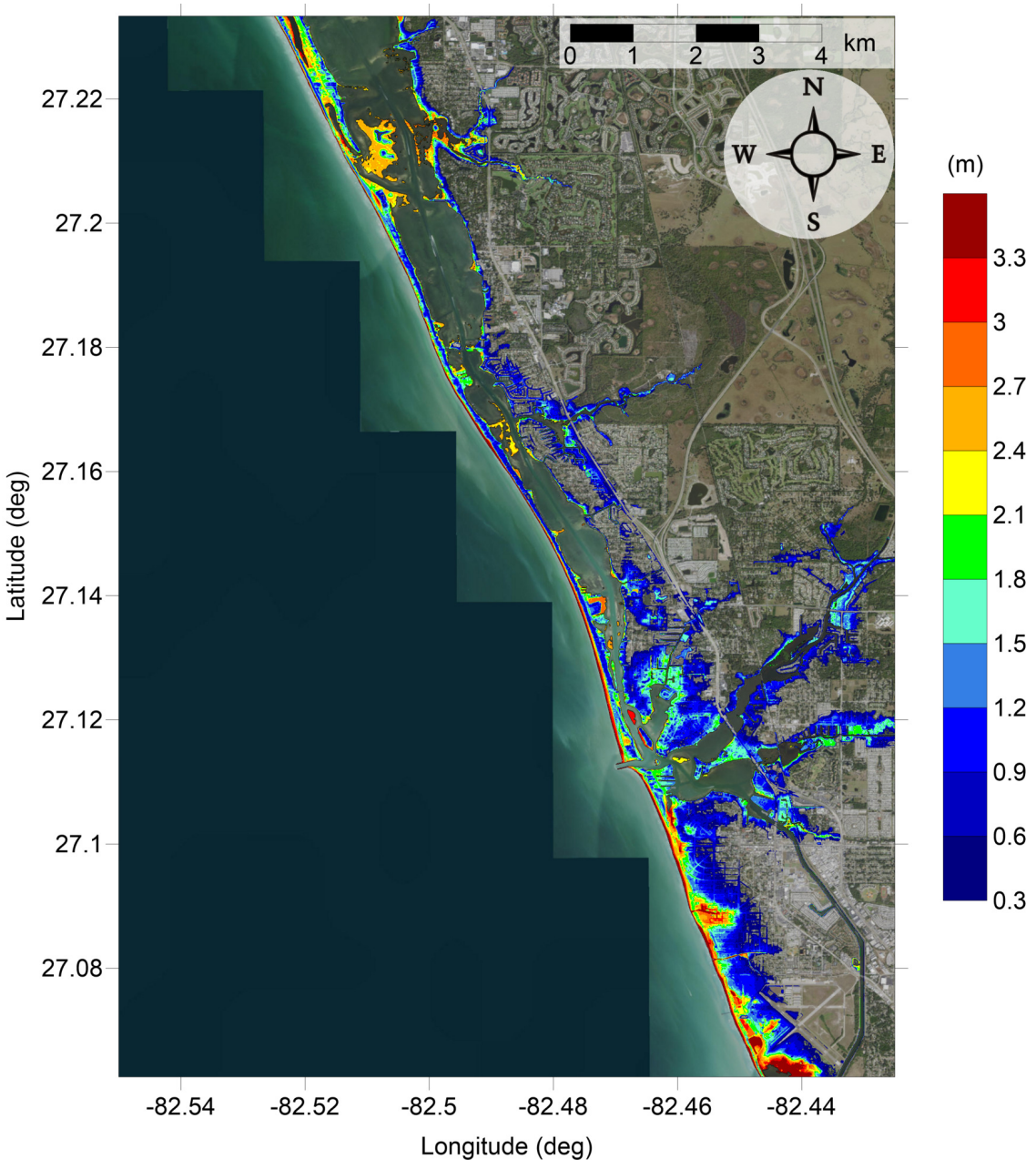

Figure 65: Maximum of maximums inundation depth (m) in Osprey-Venice, FL, calculated as the maximum inundation depth in each grid cell from an ensemble of all tsunami sources considered. Contour drawn is the zero-meter contour for land elevation.

Osprey-Venice-Englewood, FL
All Sources
Maximum of Maximum Inundation Depth

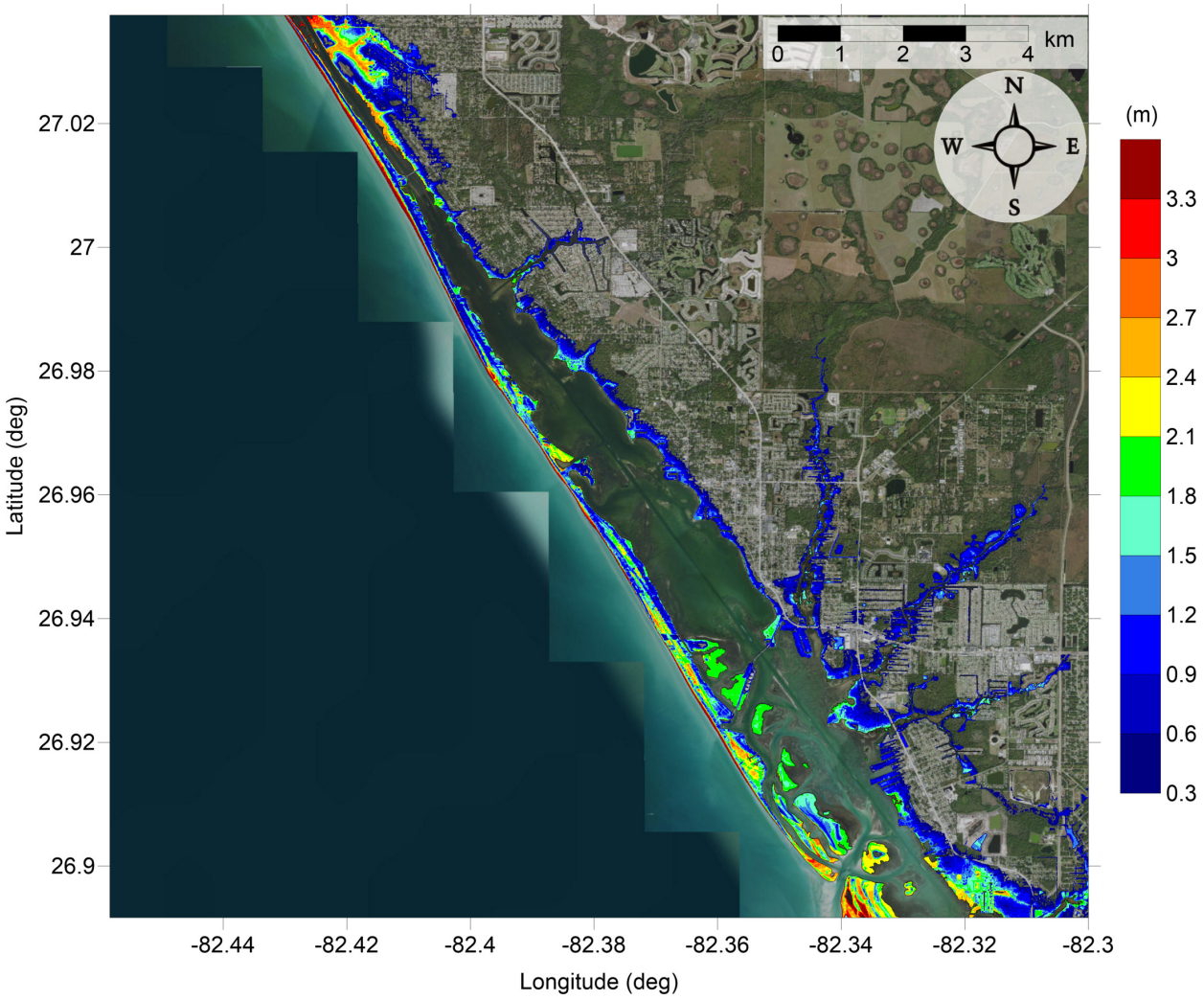

Figure 66: Maximum of maximums inundation depth (m) in Englewood, FL, calculated as the maximum inundation depth in each grid cell from an ensemble of all tsunami sources considered. Contour drawn is the zero-meter contour for land elevation.

Osprey-Venice-Englewood, FL
All Sources
Maximum Inundation Depth by Source

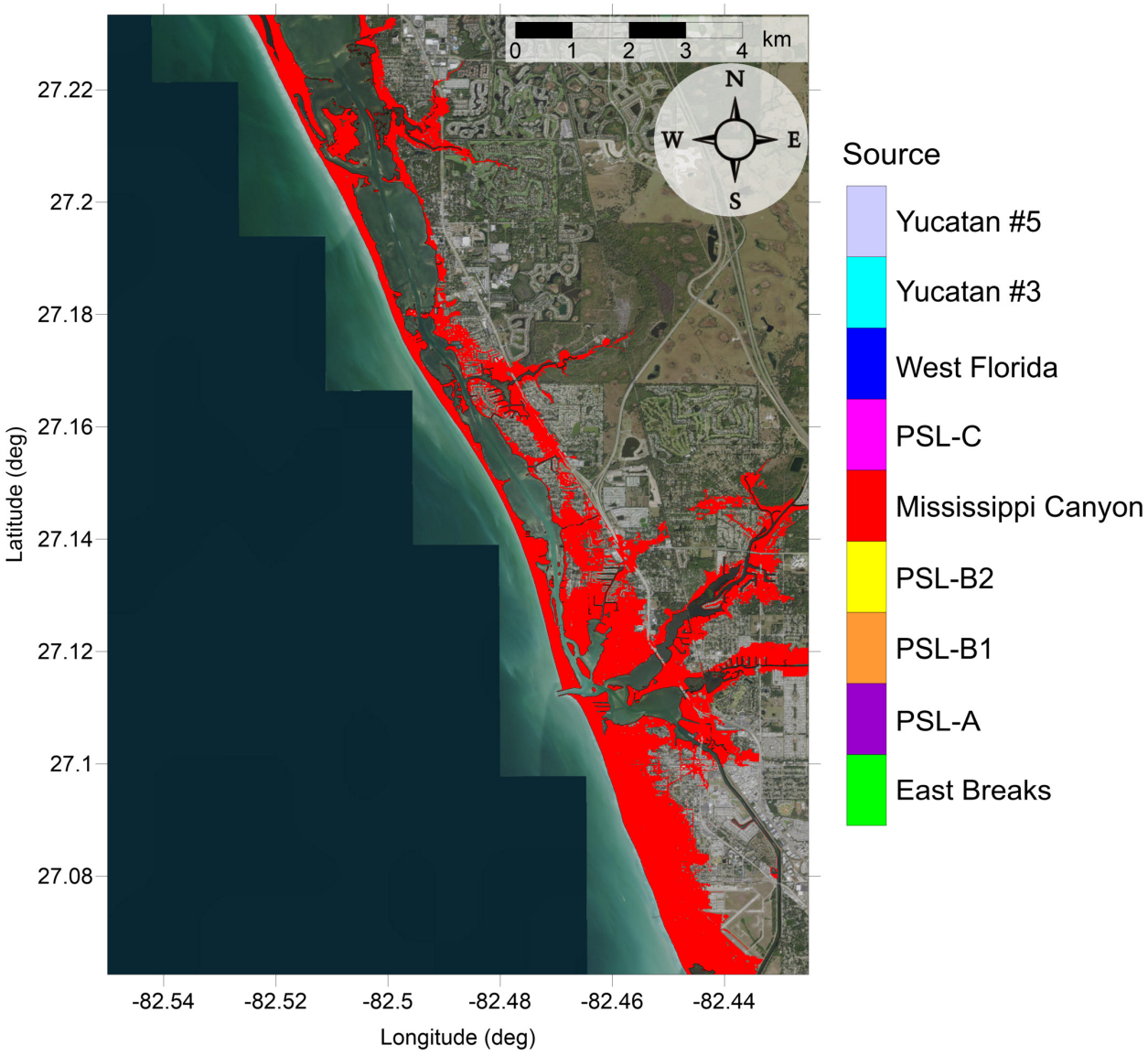

Figure 67: Indication of the tsunami source which causes the maximum of maximums inundation depth (m) in each grid cell from an ensemble of all tsunami sources in Osprey-Venice, FL. Contour drawn is the zero-meter contour for land elevation.

Osprey-Venice-Englewood, FL
All Sources
Maximum Inundation Depth by Source

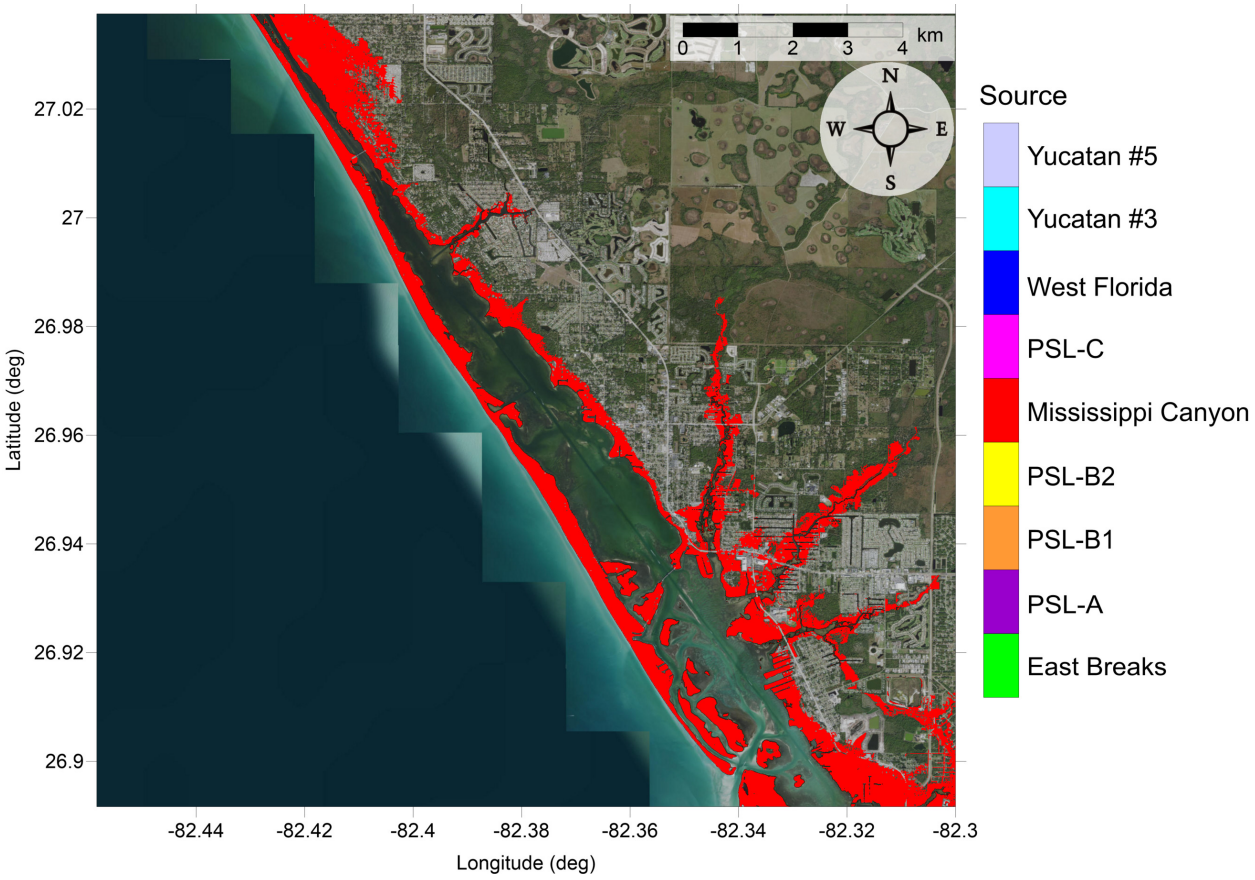

Figure 68: Indication of the tsunami source which causes the maximum of maximums inundation depth (m) in each grid cell from an ensemble of all tsunami sources in Englewood, FL. Contour drawn is the zero-meter contour for land elevation.

4.2 Sanibel Island-Naples, FL

Table 21: Maximum tsunami wave amplitude and corresponding arrival time after landslide failure at Sanibel Island-Naples, FL numerical wave gauge: 26°14'34.61"N, 82°25'32.45"W, approximate water depth 20 m.

Tsunami Source	Maximum Wave Amplitude (m)	Arrival Time After Landslide Failure (hr)
East Breaks	0.41	4.1
PSL-A	0.70	3.8
PSL-B1	0.78	3.1
PSL-B2	1.74	3.2
Mississippi Canyon	4.40	2.8
PSL-C	1.53	2.8
West Florida	0.85	2.3
Yucatan #3	0.62	3.2
Yucatan #5	0.30	3.2

Sanibel Island-Naples, FL
East Breaks submarine landslide
Maximum Momentum Flux

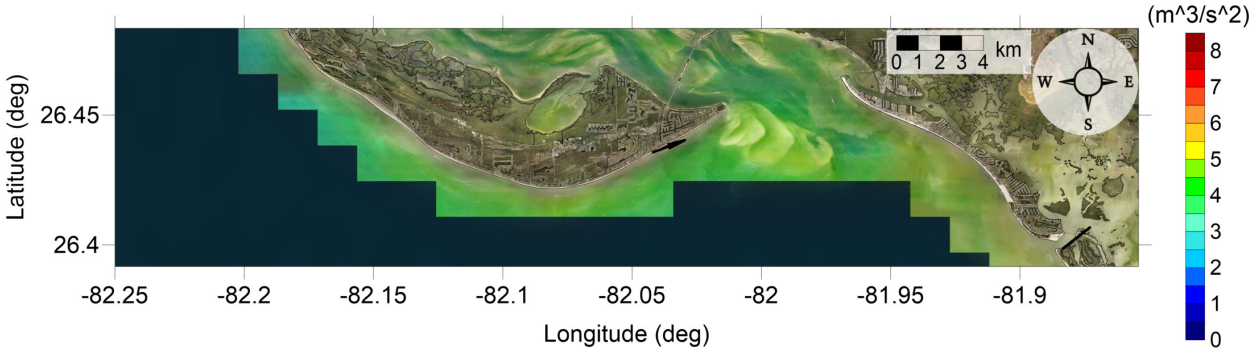

Figure 69: Maximum momentum flux (m^3/s^2) caused by the East Breaks submarine landslide in Sanibel Island, FL. Arrows represent direction of maximum momentum flux. Contour drawn is the zero-meter contour for land elevation.

Sanibel Island-Naples, FL
East Breaks submarine landslide
Maximum Momentum Flux

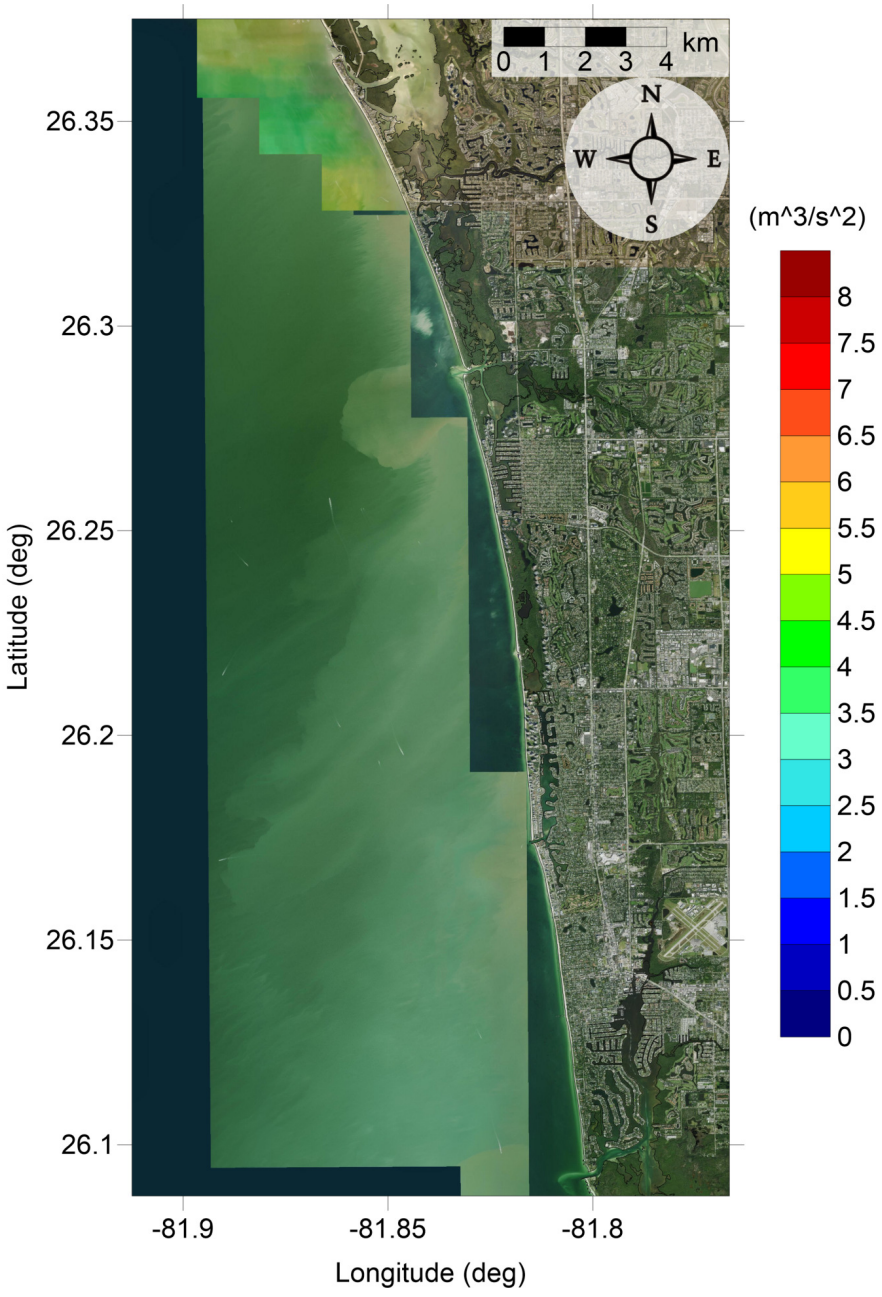

Figure 70: Maximum momentum flux (m^3/s^2) caused by the East Breaks submarine landslide in Naples, FL. Arrows represent direction of maximum momentum flux. Contour drawn is the zero-meter contour for land elevation.

Sanibel Island-Naples, FL
East Breaks submarine landslide
Maximum Inundation Depth

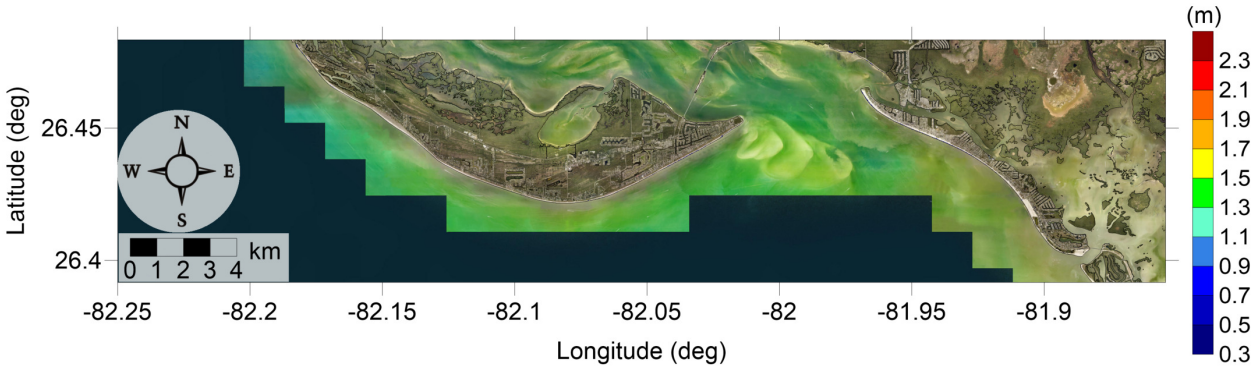

Figure 71: Maximum inundation depth (m) caused by the East Breaks submarine landslide in Sanibel Island, FL. Contour drawn is the zero-meter contour for land elevation.

Sanibel Island-Naples, FL
East Breaks submarine landslide
Maximum Inundation Depth

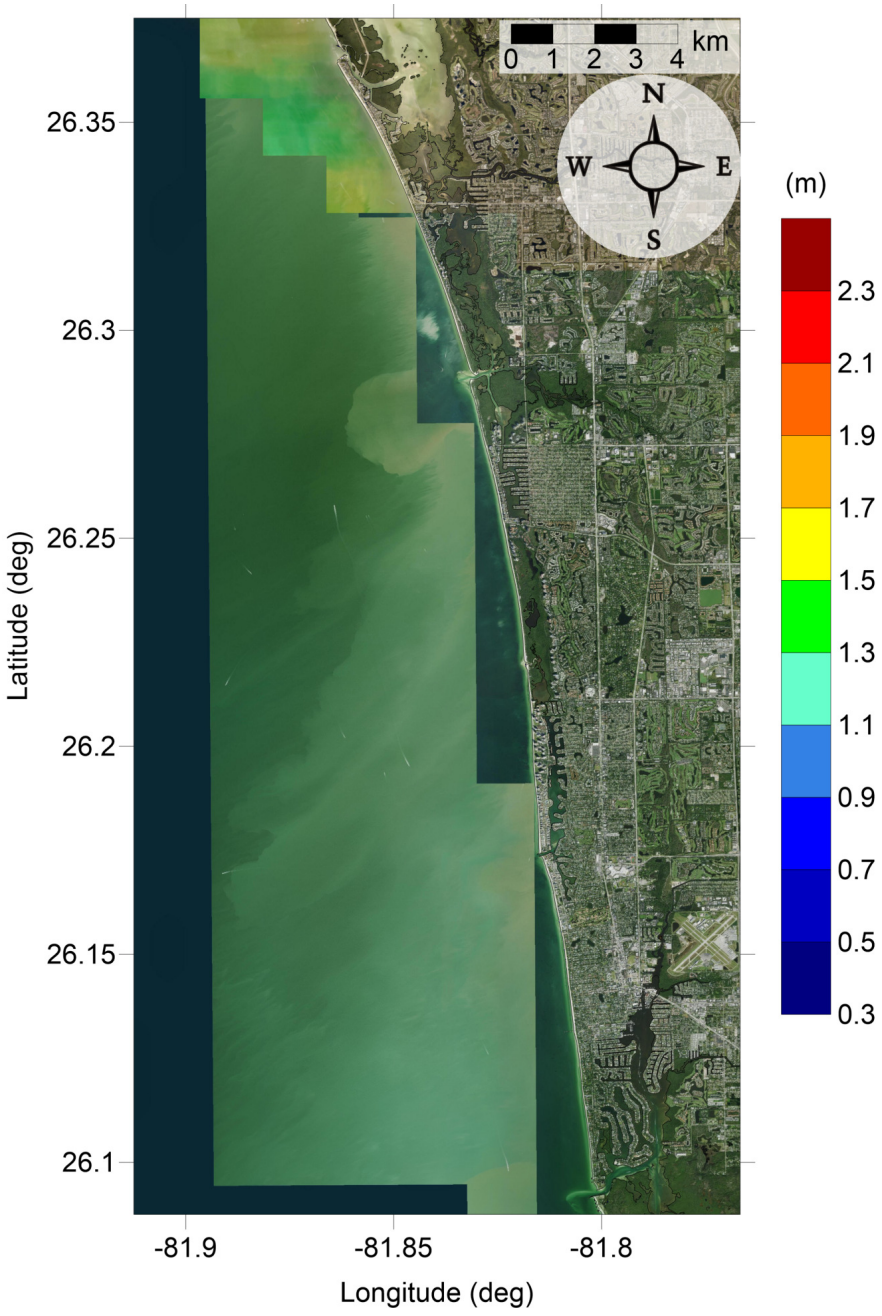

Figure 72: Maximum inundation depth (m) caused by the East Breaks submarine landslide in Naples, FL. Contour drawn is the zero-meter contour for land elevation.

Sanibel Island-Naples, FL
Probabilistic Submarine Landslide A
Maximum Momentum Flux

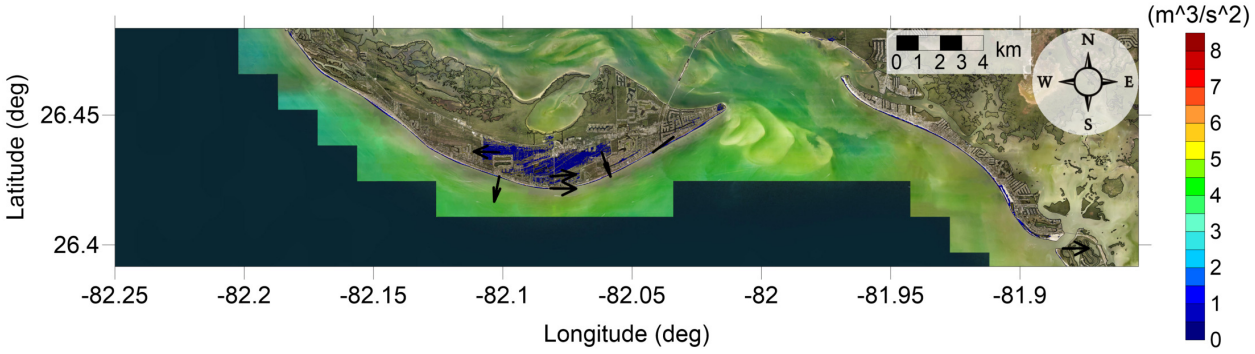

Figure 73: Maximum momentum flux (m^3/s^2) caused by the Probabilistic Submarine Landslide A in Sanibel Island, FL. Arrows represent direction of maximum momentum flux. Contour drawn is the zero-meter contour for land elevation.

Sanibel Island-Naples, FL
Probabilistic Submarine Landslide A
Maximum Momentum Flux

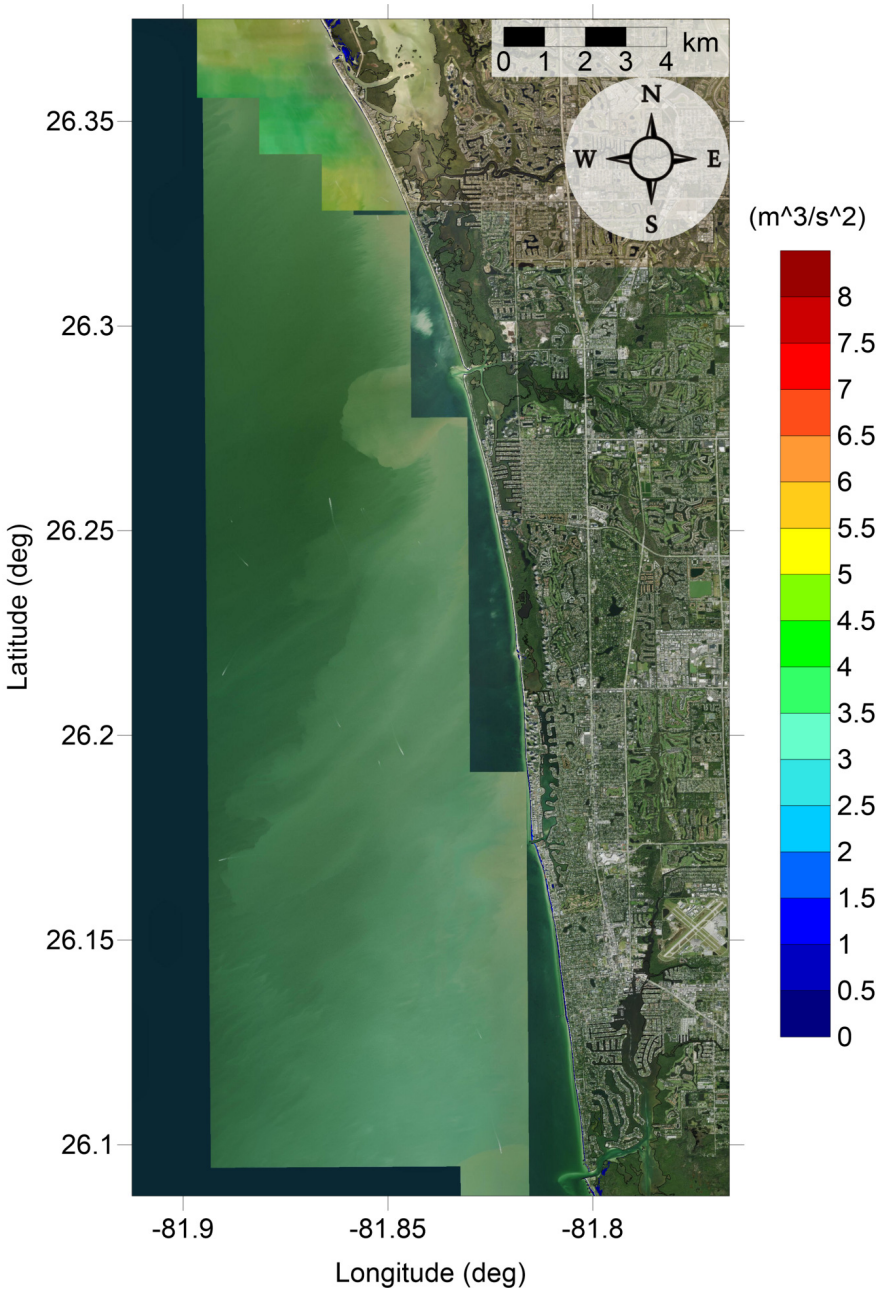

Figure 74: Maximum momentum flux (m^3/s^2) caused by the Probabilistic Submarine Landslide A in Naples, FL. Arrows represent direction of maximum momentum flux. Contour drawn is the zero-meter contour for land elevation.

Sanibel Island-Naples, FL
Probabilistic Submarine Landslide A
Maximum Inundation Depth

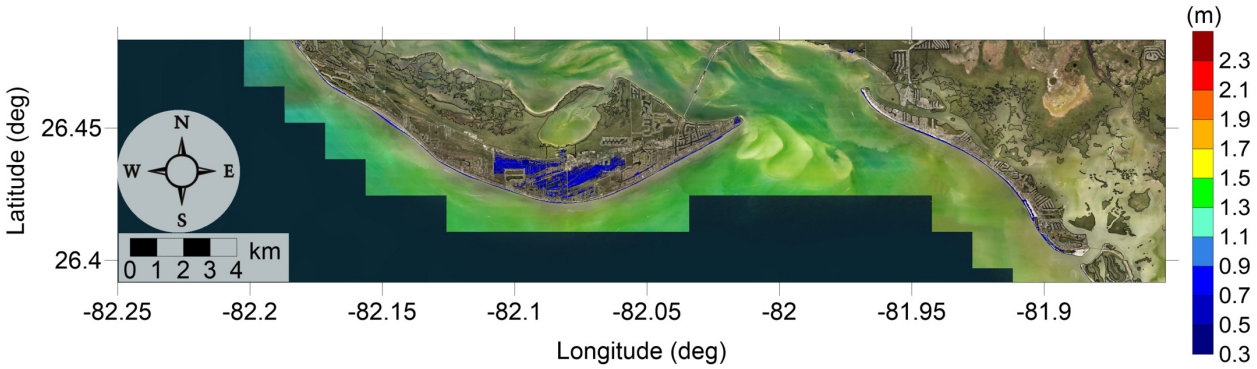

Figure 75: Maximum inundation depth (m) caused by the Probabilistic Submarine Landslide A in Sanibel Island, FL. Contour drawn is the zero-meter contour for land elevation.

Sanibel Island-Naples, FL
Probabilistic Submarine Landslide A
Maximum Inundation Depth

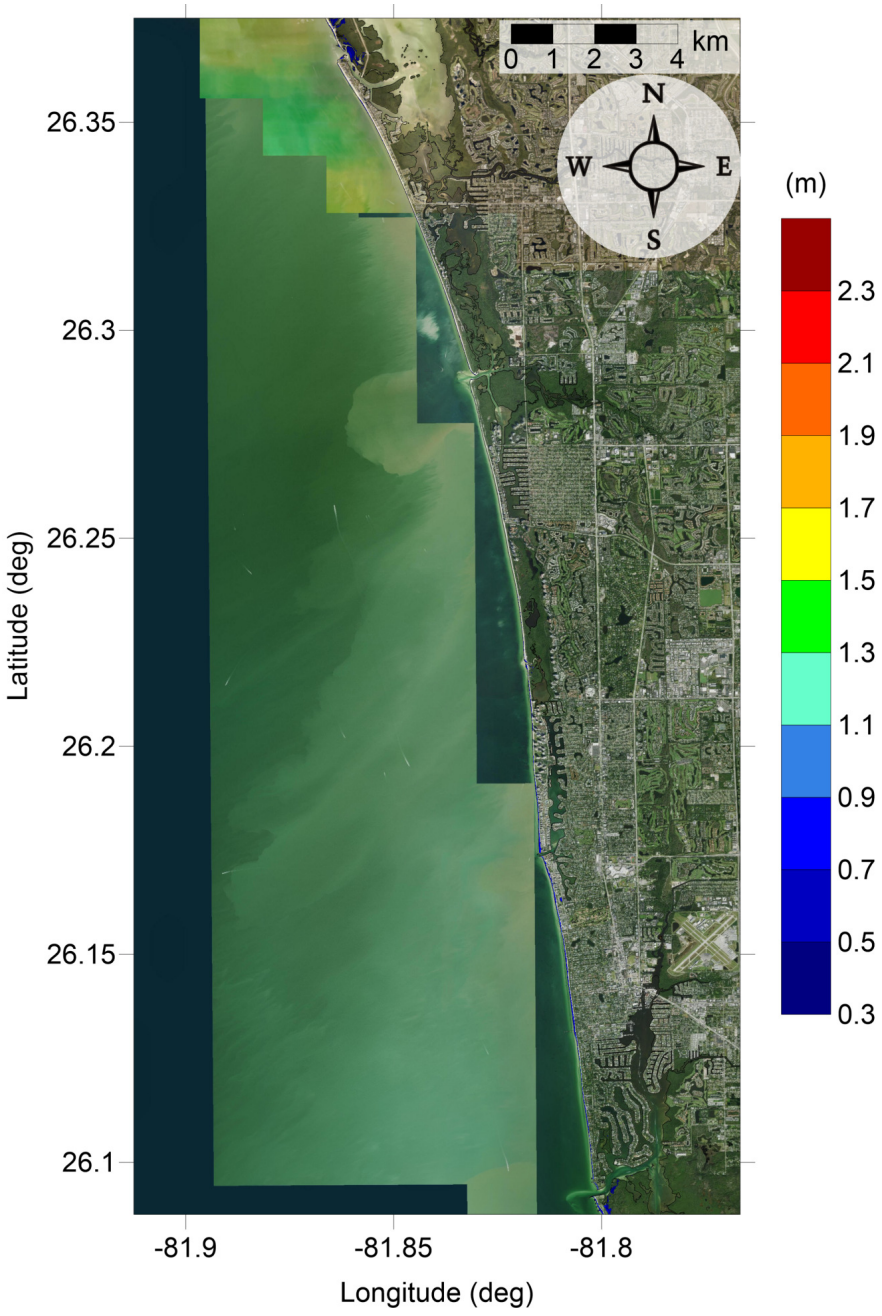

Figure 76: Maximum inundation depth (m) caused by the Probabilistic Submarine Landslide A in Naples, FL. Contour drawn is the zero-meter contour for land elevation.

Sanibel Island-Naples, FL
Probabilistic Submarine Landslide B1
Maximum Momentum Flux

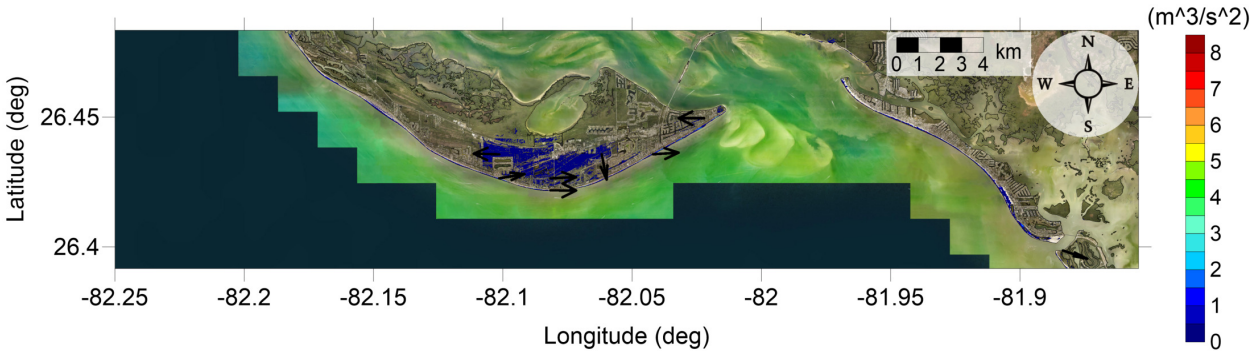

Figure 77: Maximum momentum flux (m^3/s^2) caused by the Probabilistic Submarine Landslide B1 in Sanibel Island, FL. Arrows represent direction of maximum momentum flux. Contour drawn is the zero-meter contour for land elevation.

Sanibel Island-Naples, FL
Probabilistic Submarine Landslide B1
Maximum Momentum Flux

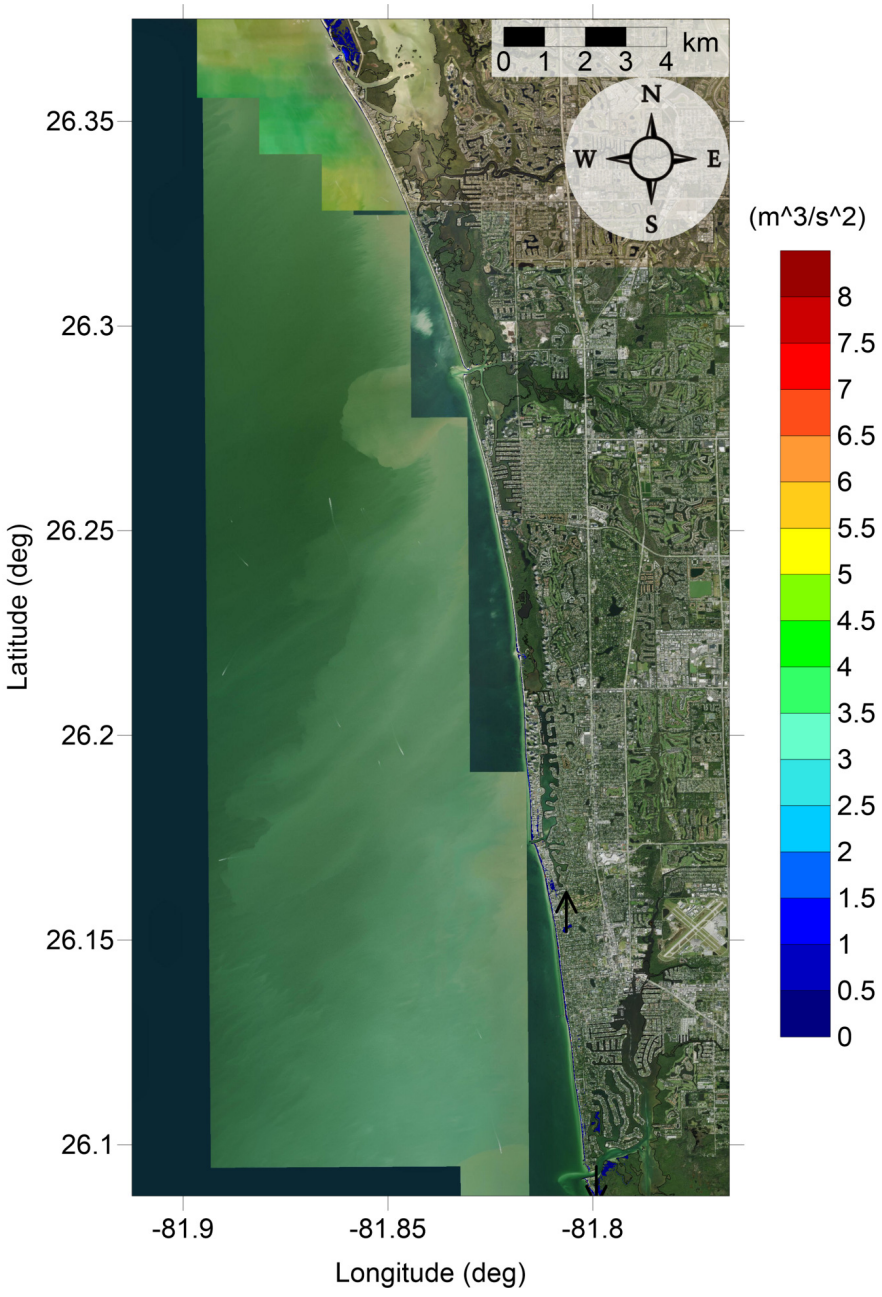

Figure 78: Maximum momentum flux (m^3/s^2) caused by the Probabilistic Submarine Landslide B1 in Naples, FL. Arrows represent direction of maximum momentum flux. Contour drawn is the zero-meter contour for land elevation.

Sanibel Island-Naples, FL
Probabilistic Submarine Landslide B1
Maximum Inundation Depth

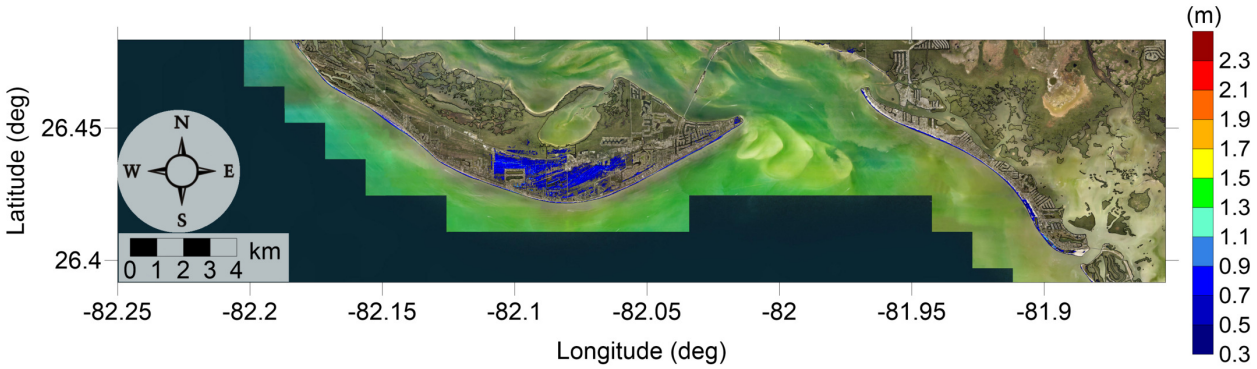

Figure 79: Maximum inundation depth (m) caused by the Probabilistic Submarine Landslide B1 in Sanibel Island, FL. Contour drawn is the zero-meter contour for land elevation.

Sanibel Island-Naples, FL
Probabilistic Submarine Landslide B1
Maximum Inundation Depth

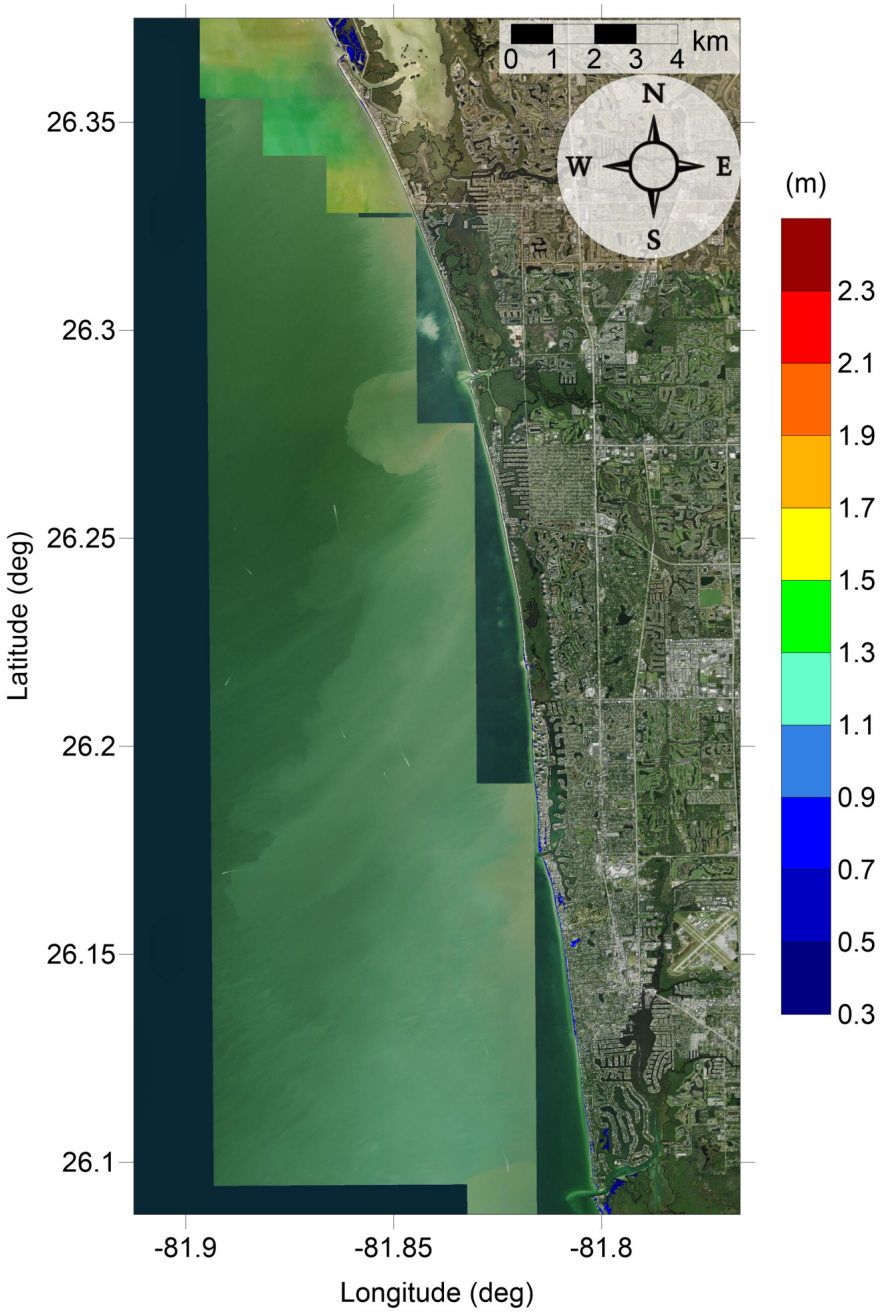

Figure 80: Maximum inundation depth (m) caused by the Probabilistic Submarine Landslide B1 in Naples, FL. Contour drawn is the zero-meter contour for land elevation.

Sanibel Island-Naples, FL
Probabilistic Submarine Landslide B2
Maximum Momentum Flux

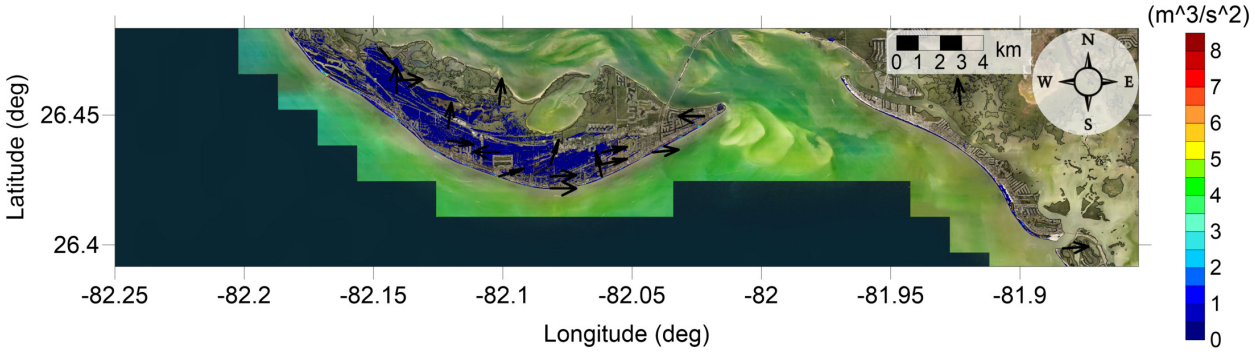

Figure 81: Maximum momentum flux (m^3/s^2) caused by the Probabilistic Submarine Landslide B2 in Sanibel Island, FL. Arrows represent direction of maximum momentum flux. Contour drawn is the zero-meter contour for land elevation.

Sanibel Island-Naples, FL
Probabilistic Submarine Landslide B2
Maximum Momentum Flux

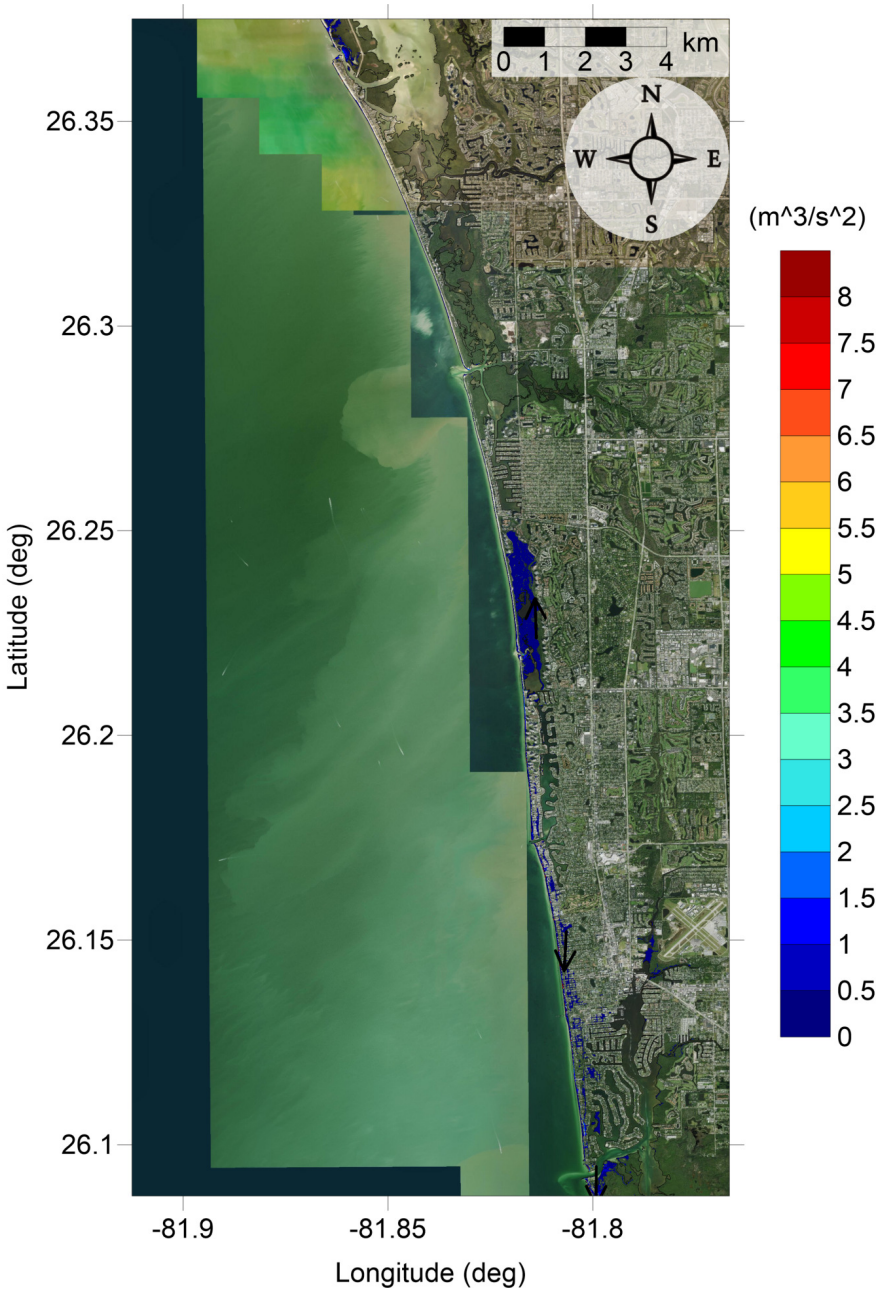

Figure 82: Maximum momentum flux (m^3/s^2) caused by the Probabilistic Submarine Landslide B2 in Naples, FL. Arrows represent direction of maximum momentum flux. Contour drawn is the zero-meter contour for land elevation.

Sanibel Island-Naples, FL
Probabilistic Submarine Landslide B2
Maximum Inundation Depth

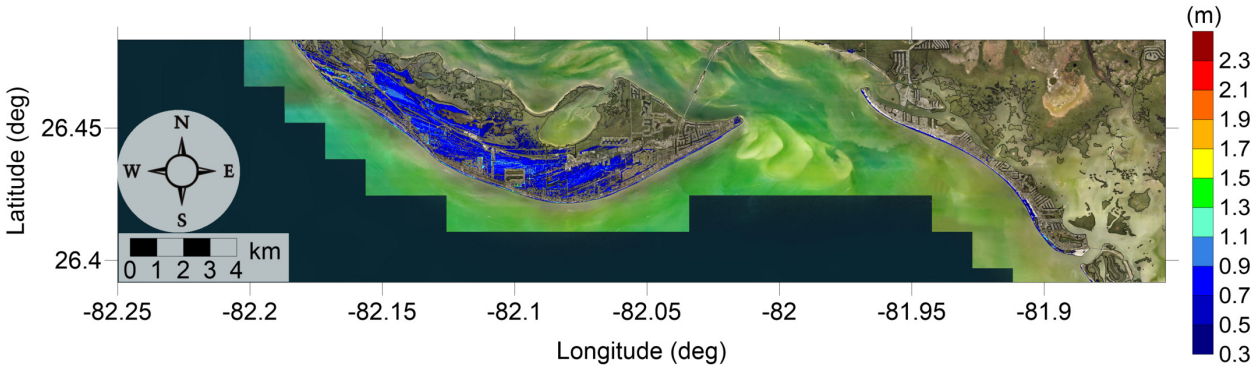

Figure 83: Maximum inundation depth (m) caused by the Probabilistic Submarine Landslide B2 in Sanibel Island, FL. Contour drawn is the zero-meter contour for land elevation.

Sanibel Island-Naples, FL
Probabilistic Submarine Landslide B2
Maximum Inundation Depth

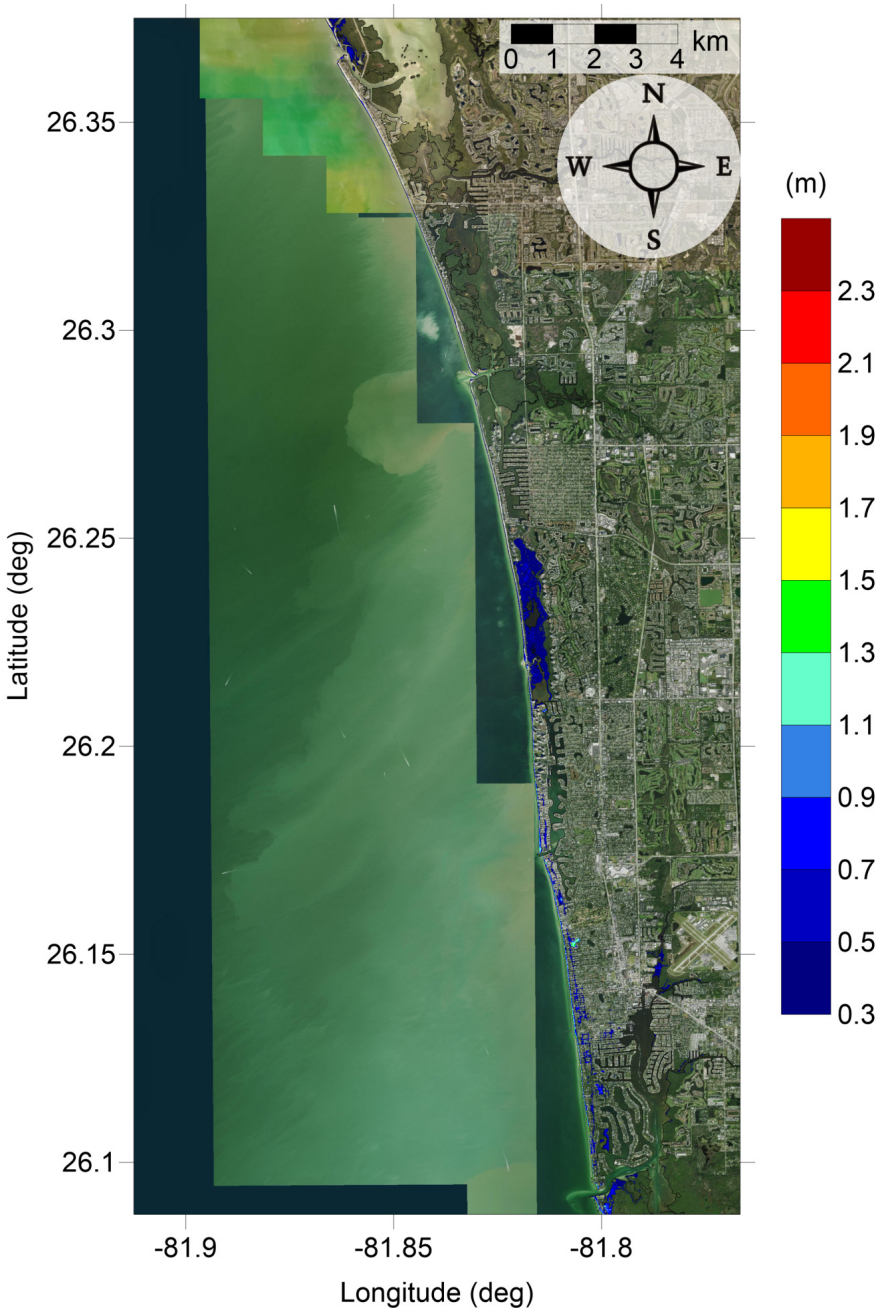

Figure 84: Maximum inundation depth (m) caused by the Probabilistic Submarine Landslide B2 in Naples, FL. Contour drawn is the zero-meter contour for land elevation.

Sanibel Island-Naples, FL
Mississippi Canyon submarine landslide
Maximum Momentum Flux

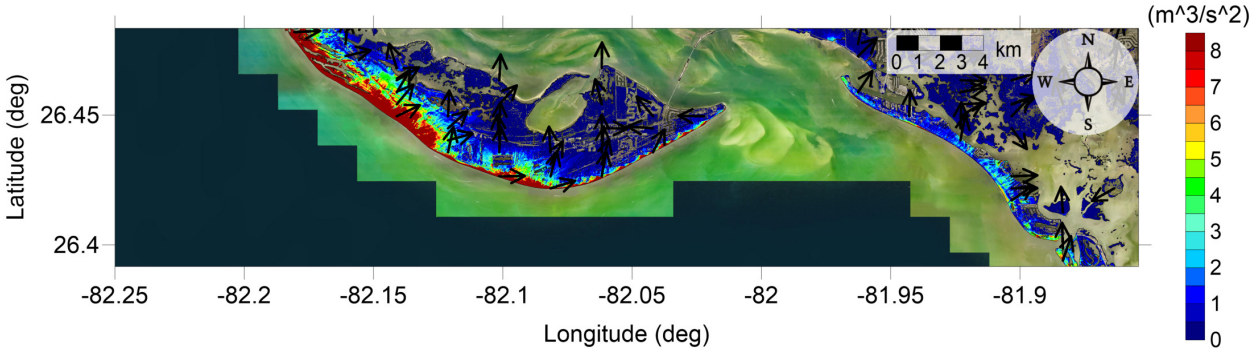

Figure 85: Maximum momentum flux (m^3/s^2) caused by the Mississippi Canyon submarine landslide in Sanibel Island, FL. Arrows represent direction of maximum momentum flux. Contour drawn is the zero-meter contour for land elevation.

Sanibel Island-Naples, FL
Mississippi Canyon submarine landslide
Maximum Momentum Flux

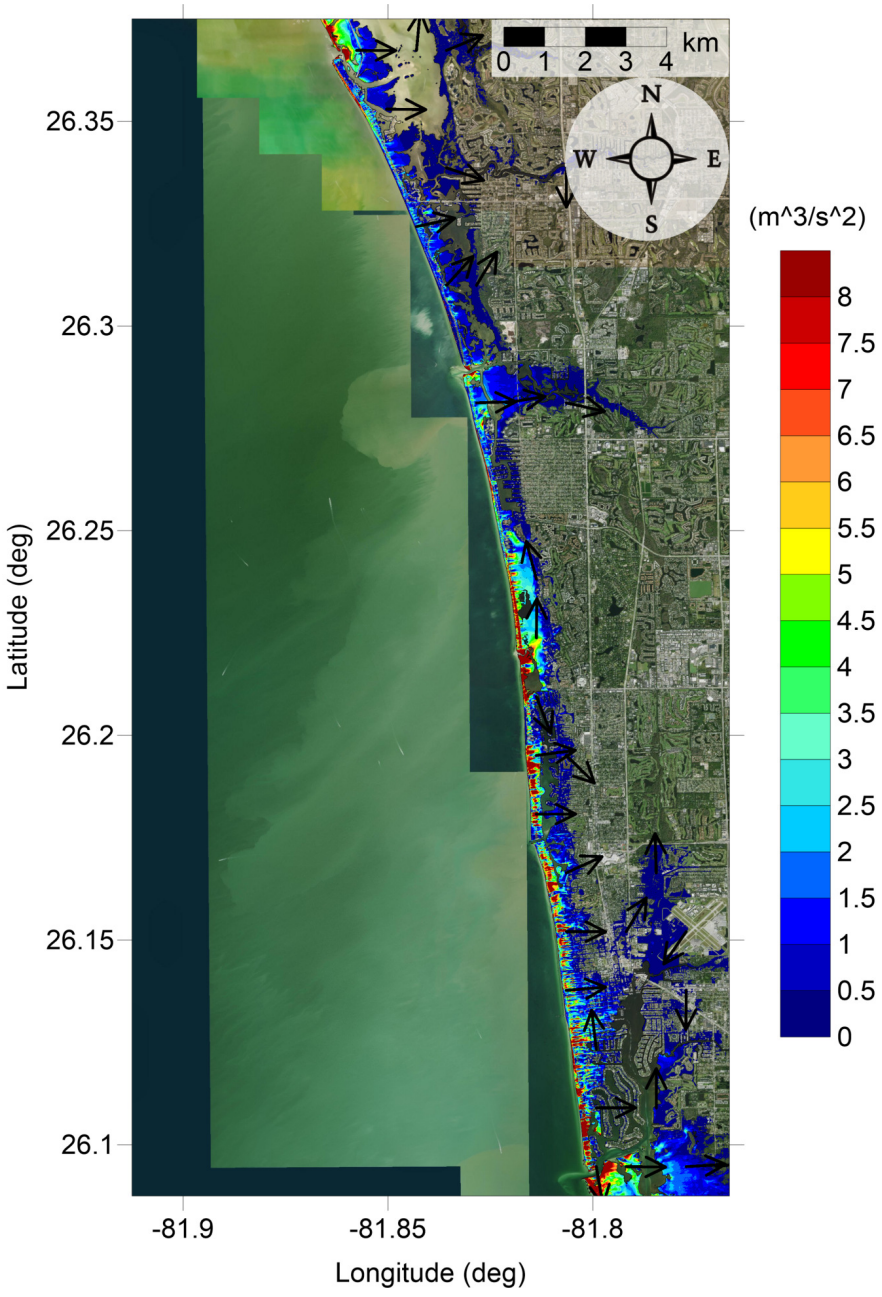

Figure 86: Maximum momentum flux (m^3/s^2) caused by the Mississippi Canyon submarine landslide in Naples, FL. Arrows represent direction of maximum momentum flux. Contour drawn is the zero-meter contour for land elevation.

Sanibel Island-Naples, FL
Mississippi Canyon submarine landslide
Maximum Inundation Depth

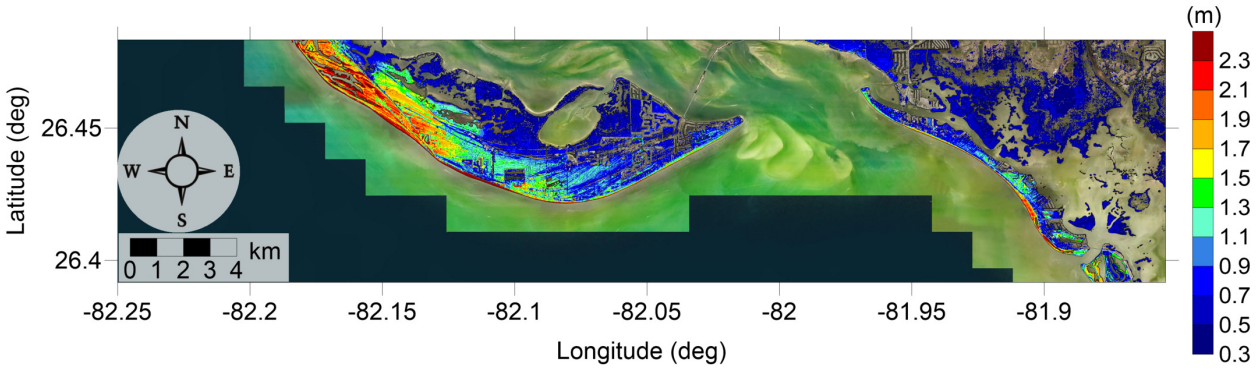

Figure 87: Maximum inundation depth (m) caused by the Mississippi Canyon submarine landslide in Sanibel Island, FL. Contour drawn is the zero-meter contour for land elevation.

Sanibel Island-Naples, FL
Mississippi Canyon submarine landslide
Maximum Inundation Depth

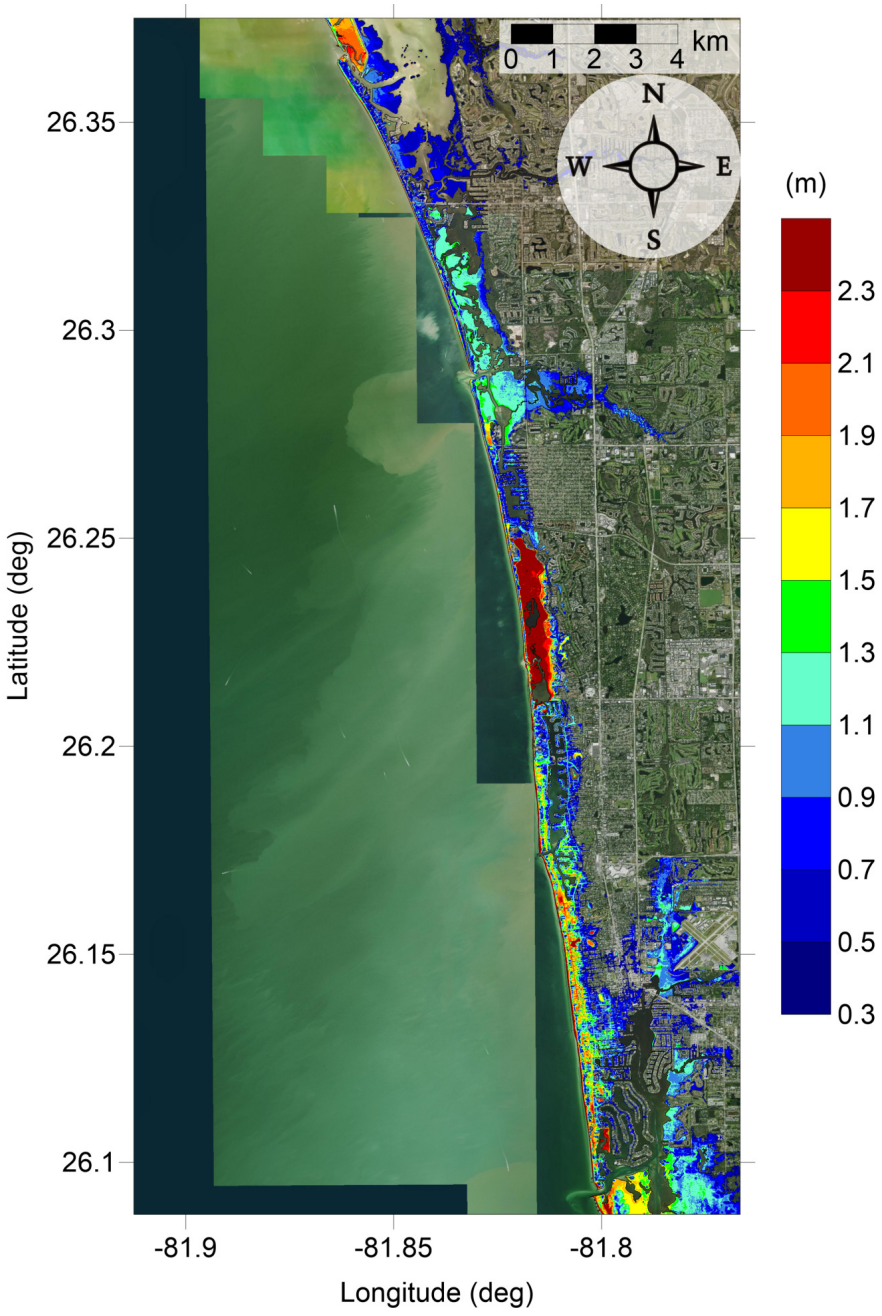

Figure 88: Maximum inundation depth (m) caused by the Mississippi Canyon submarine landslide in Naples, FL. Contour drawn is the zero-meter contour for land elevation.

Sanibel Island-Naples, FL
Probabilistic Submarine Landslide C
Maximum Momentum Flux

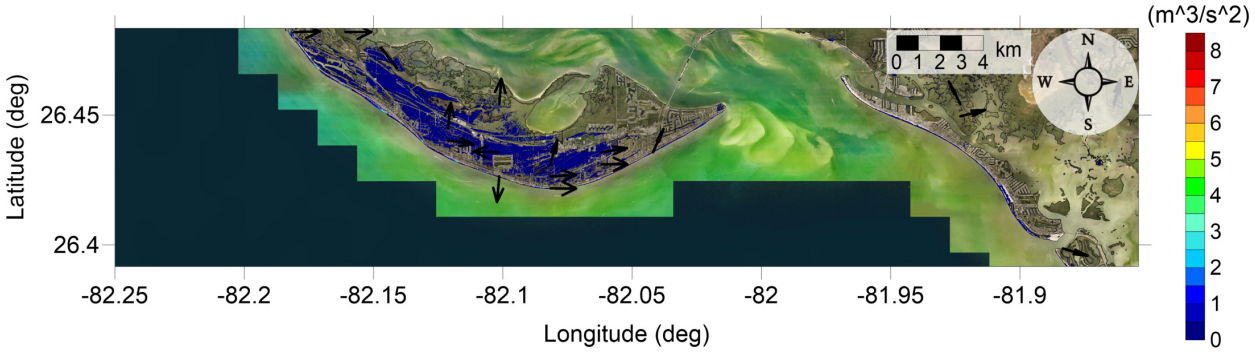

Figure 89: Maximum momentum flux (m^3/s^2) caused by the Probabilistic Submarine Landslide C in Sanibel Island, FL. Arrows represent direction of maximum momentum flux. Contour drawn is the zero-meter contour for land elevation.

Sanibel Island-Naples, FL
Probabilistic Submarine Landslide C
Maximum Momentum Flux

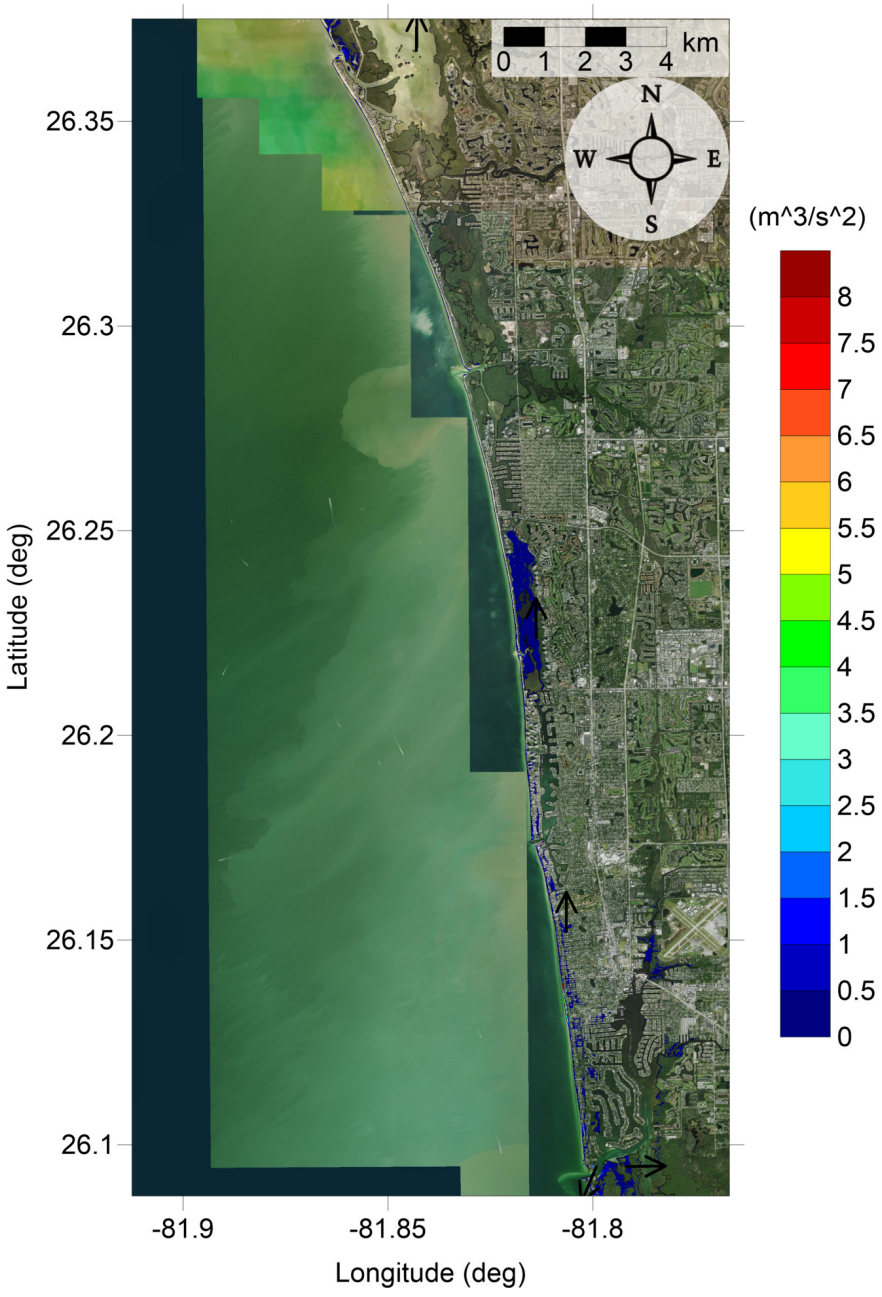

Figure 90: Maximum momentum flux (m^3/s^2) caused by the Probabilistic Submarine Landslide C in Naples, FL. Arrows represent direction of maximum momentum flux. Contour drawn is the zero-meter contour for land elevation.

Sanibel Island-Naples, FL
Probabilistic Submarine Landslide C
Maximum Inundation Depth

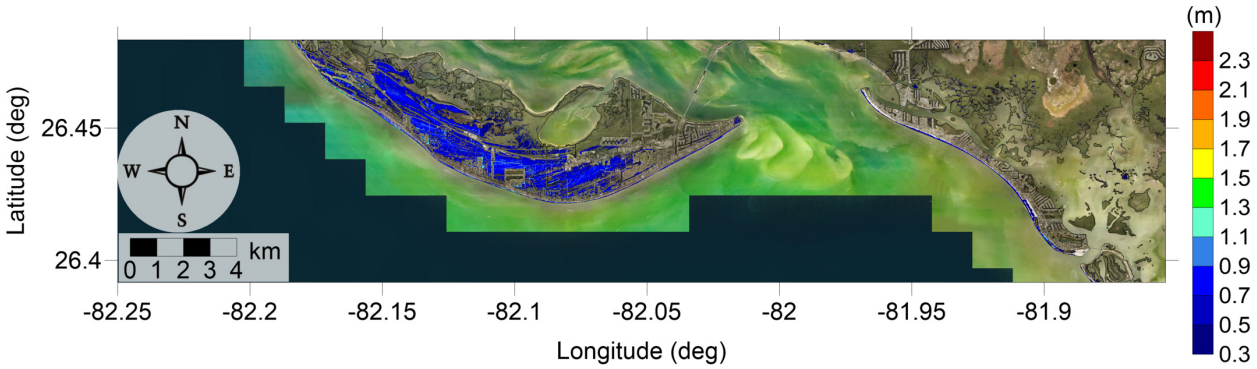

Figure 91: Maximum inundation depth (m) caused by the Probabilistic Submarine Landslide C in Sanibel Island, FL. Contour drawn is the zero-meter contour for land elevation.

Sanibel Island-Naples, FL
Probabilistic Submarine Landslide C
Maximum Inundation Depth

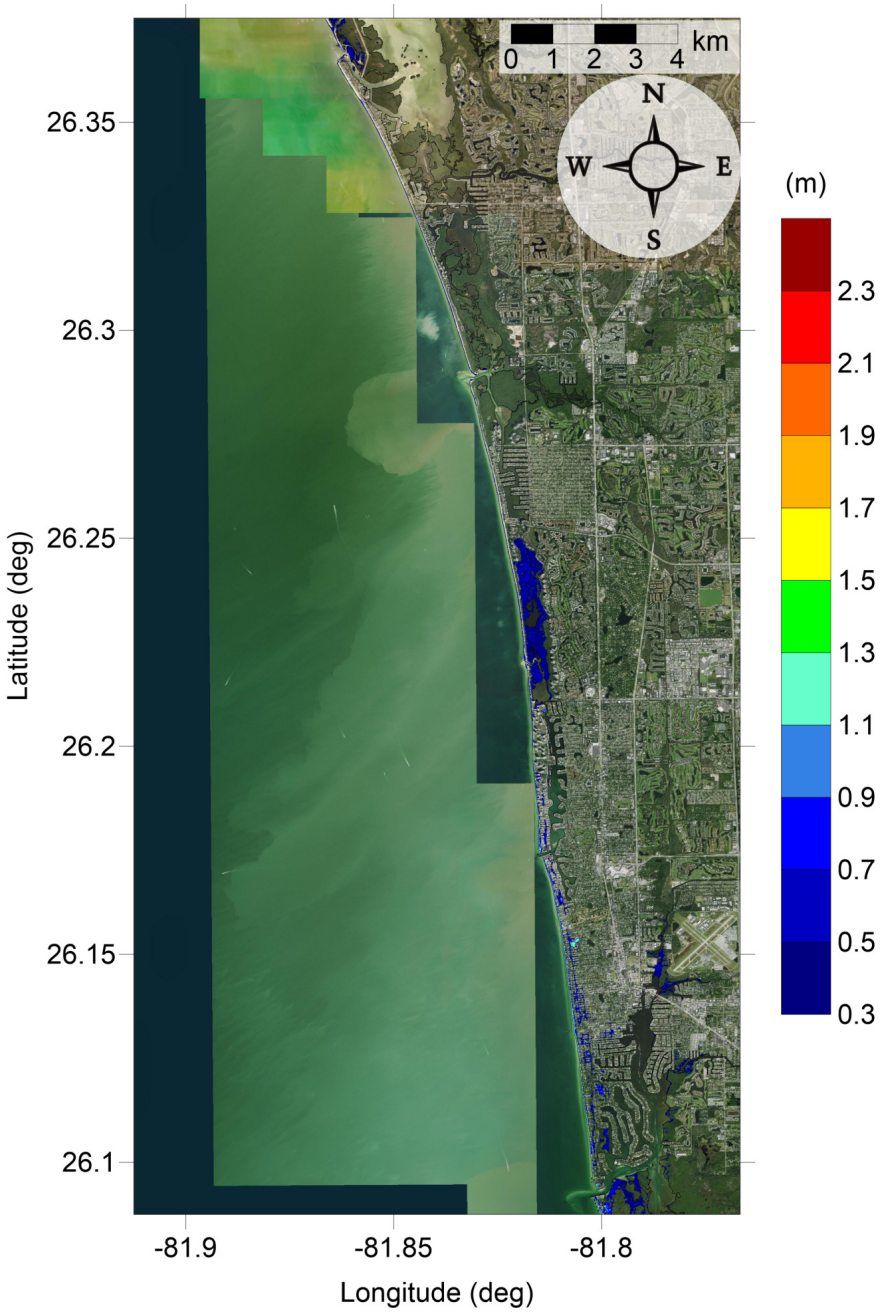

Figure 92: Maximum inundation depth (m) caused by the Probabilistic Submarine Landslide C in Naples, FL. Contour drawn is the zero-meter contour for land elevation.

Sanibel Island-Naples, FL
West Florida submarine landslide
Maximum Momentum Flux

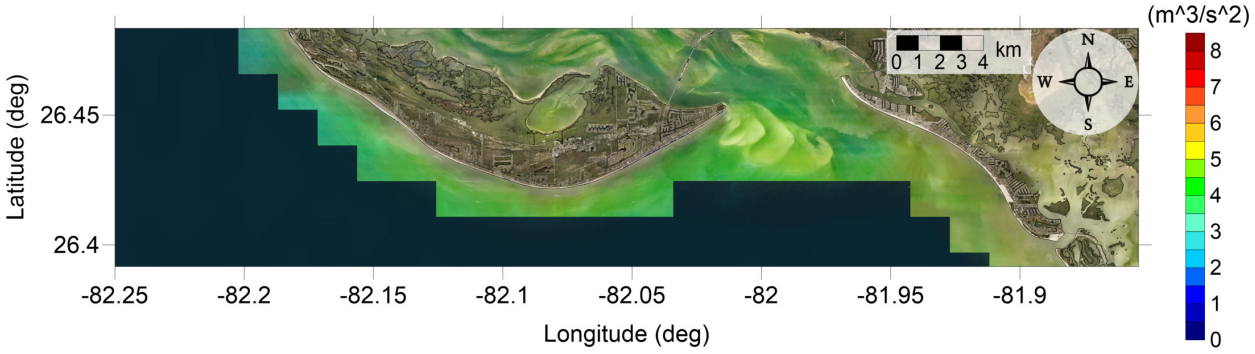

Figure 93: Maximum momentum flux (m^3/s^2) caused by the West Florida submarine landslide in Sanibel Island, FL. Arrows represent direction of maximum momentum flux. Contour drawn is the zero-meter contour for land elevation.

Sanibel Island-Naples, FL
West Florida submarine landslide
Maximum Momentum Flux

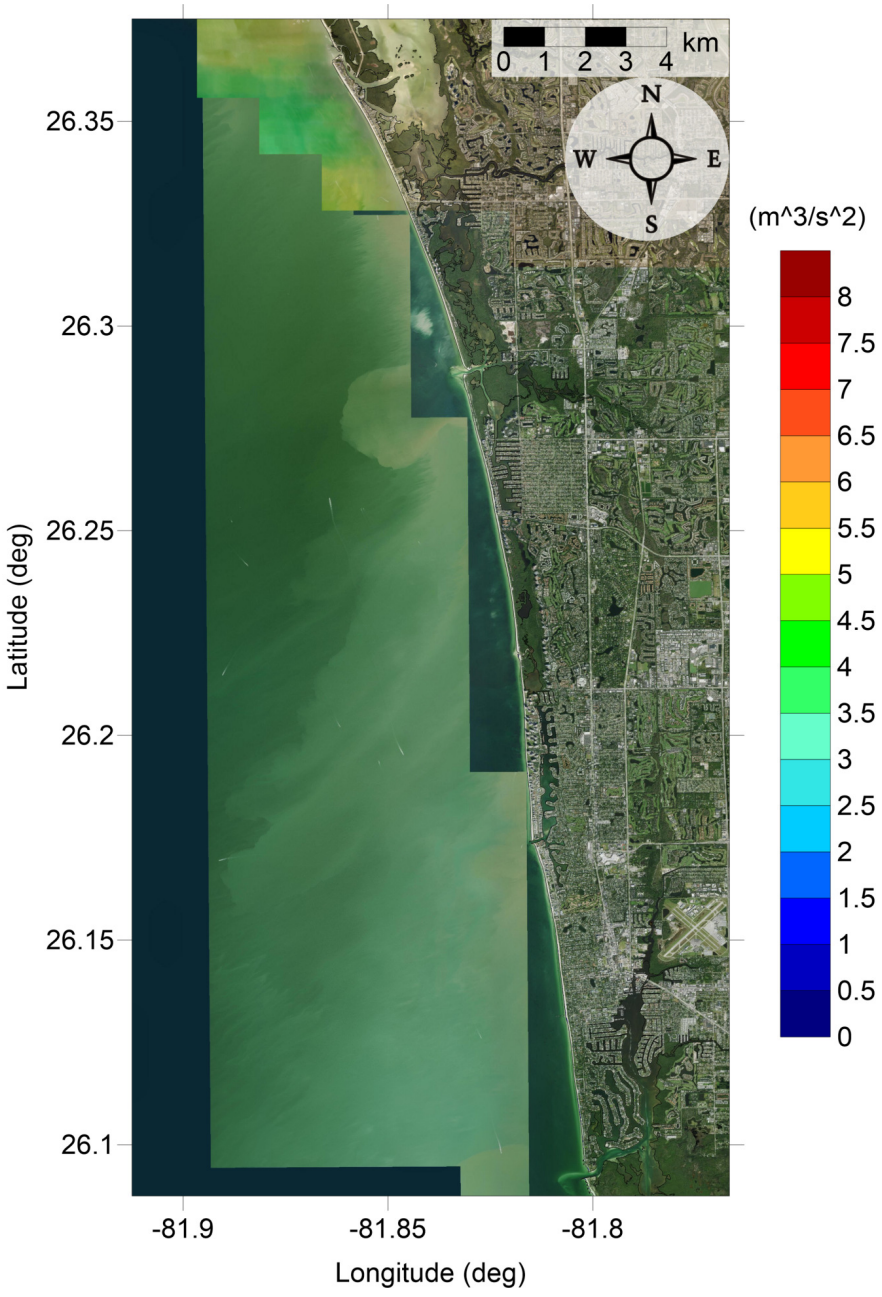

Figure 94: Maximum momentum flux (m^3/s^2) caused by the West Florida submarine landslide in Naples, FL. Arrows represent direction of maximum momentum flux. Contour drawn is the zero-meter contour for land elevation.

Sanibel Island-Naples, FL
West Florida submarine landslide
Maximum Inundation Depth

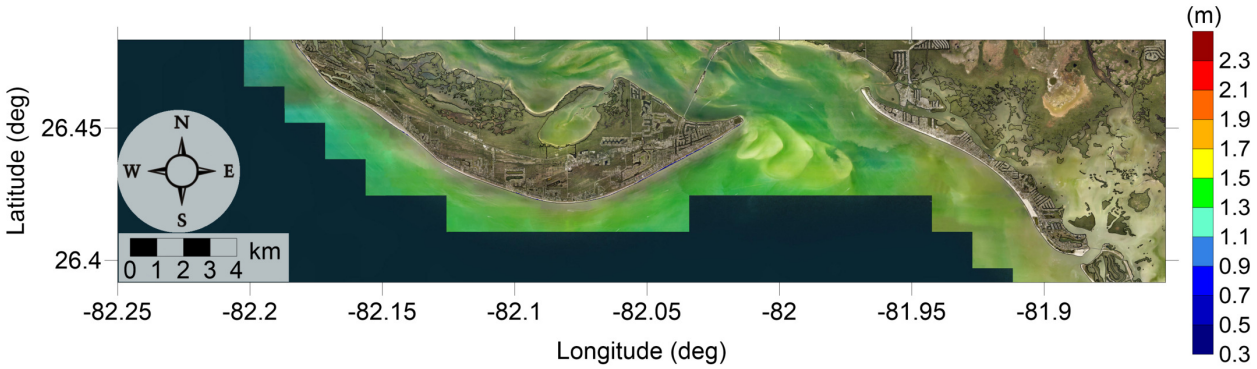

Figure 95: Maximum inundation depth (m) caused by the West Florida submarine landslide in Sanibel Island, FL. Contour drawn is the zero-meter contour for land elevation.

Sanibel Island-Naples, FL
West Florida submarine landslide
Maximum Inundation Depth

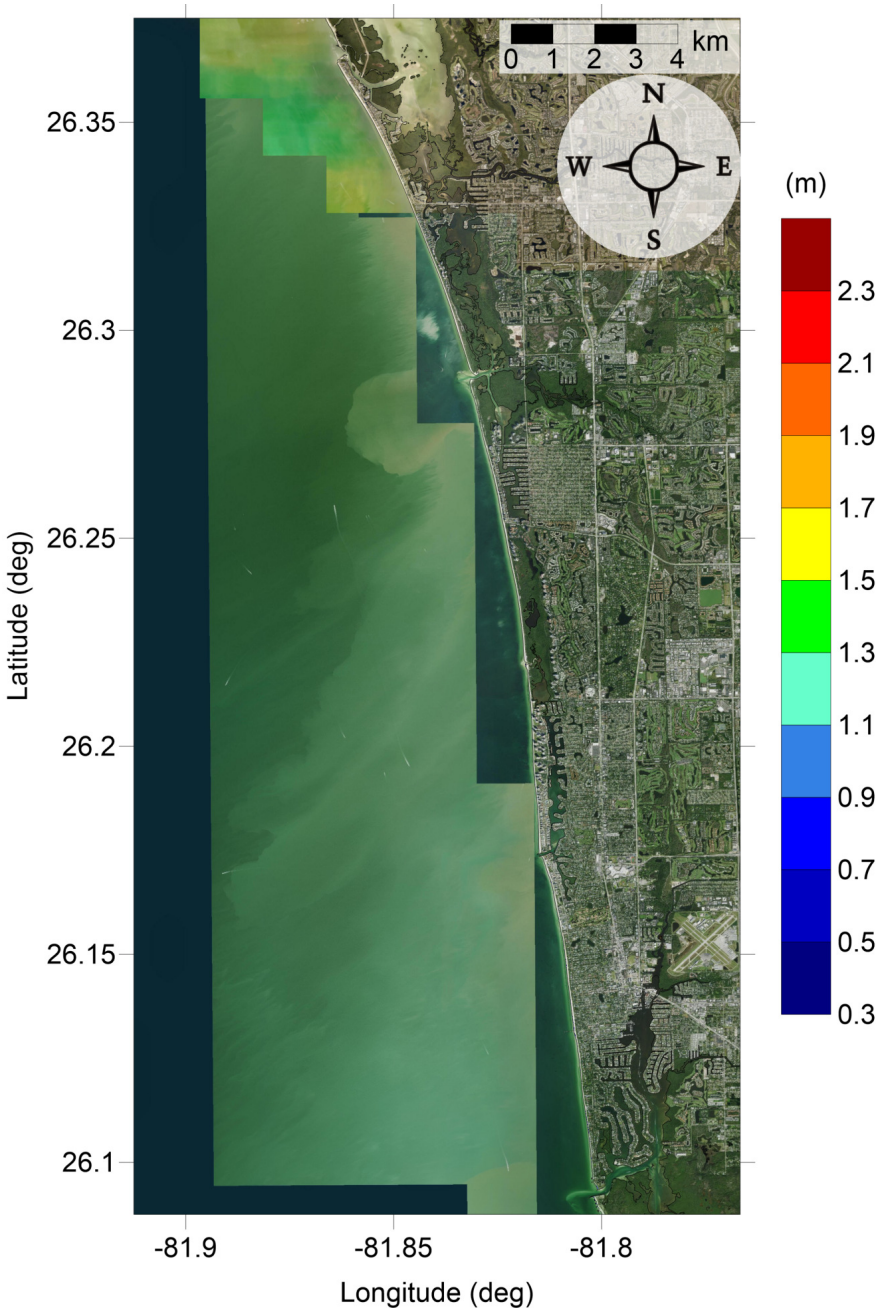

Figure 96: Maximum inundation depth (m) caused by the West Florida submarine landslide in Naples, FL. Contour drawn is the zero-meter contour for land elevation.

Sanibel Island-Naples, FL
Yucatan #3 submarine landslide
Maximum Momentum Flux

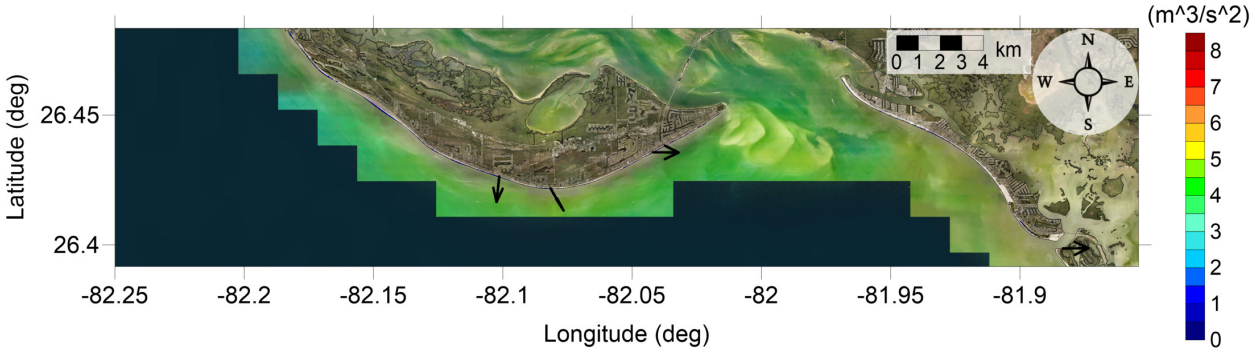

Figure 97: Maximum momentum flux (m^3/s^2) caused by the Yucatan #3 submarine landslide in Sanibel Island, FL. Arrows represent direction of maximum momentum flux. Contour drawn is the zero-meter contour for land elevation.

Sanibel Island-Naples, FL
Yucatan #3 submarine landslide
Maximum Momentum Flux

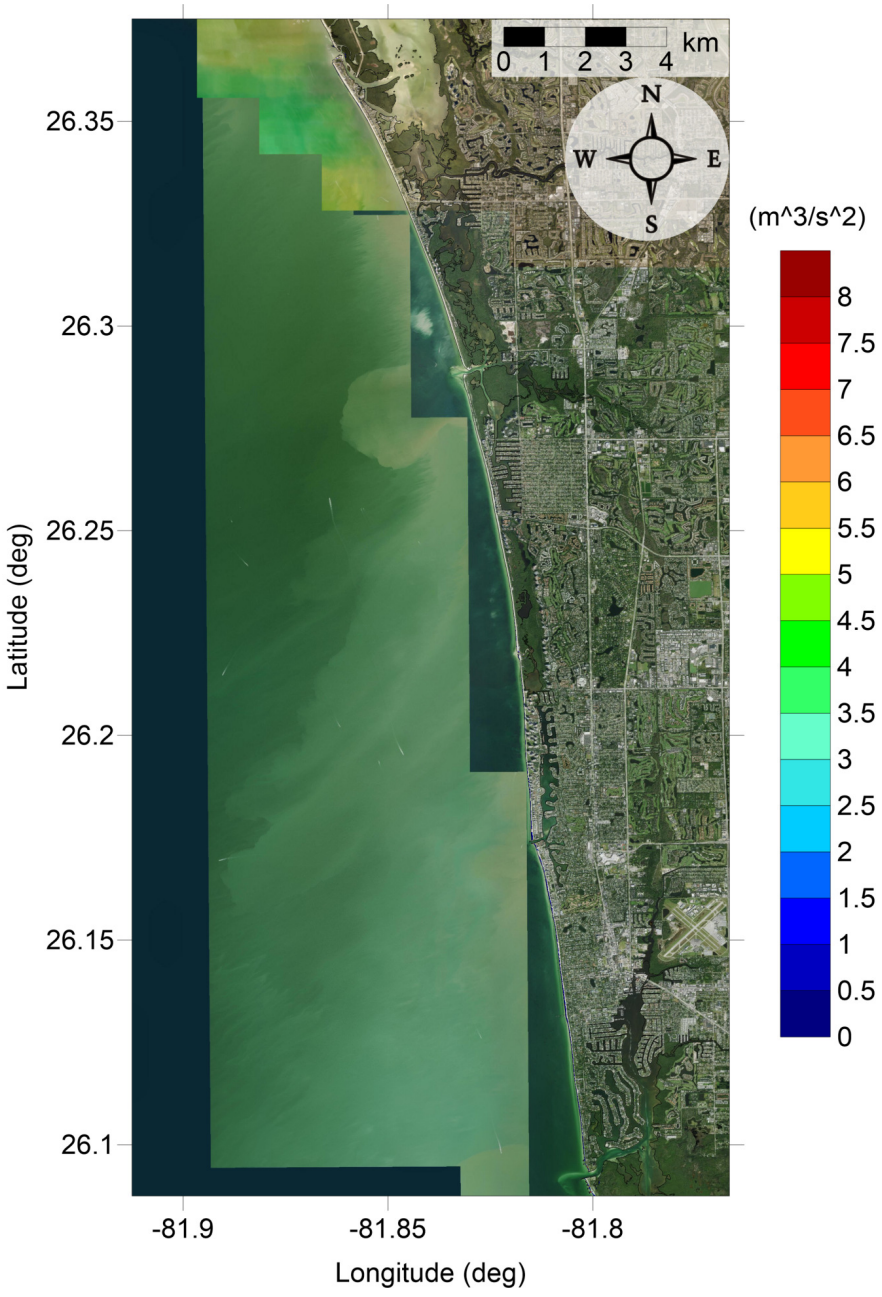

Figure 98: Maximum momentum flux (m^3/s^2) caused by the Yucatan #3 submarine landslide in Naples, FL. Arrows represent direction of maximum momentum flux. Contour drawn is the zero-meter contour for land elevation.

Sanibel Island-Naples, FL
Yucatan #3 submarine landslide
Maximum Inundation Depth

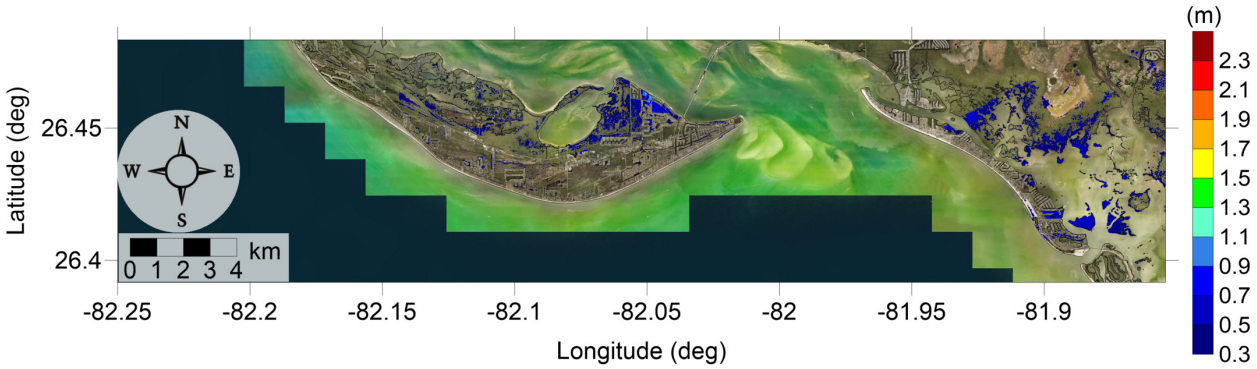

Figure 99: Maximum inundation depth (m) caused by the Yucatan #3 submarine landslide in Sanibel Island, FL. Contour drawn is the zero-meter contour for land elevation.

Sanibel Island-Naples, FL
Yucatan #3 submarine landslide
Maximum Inundation Depth

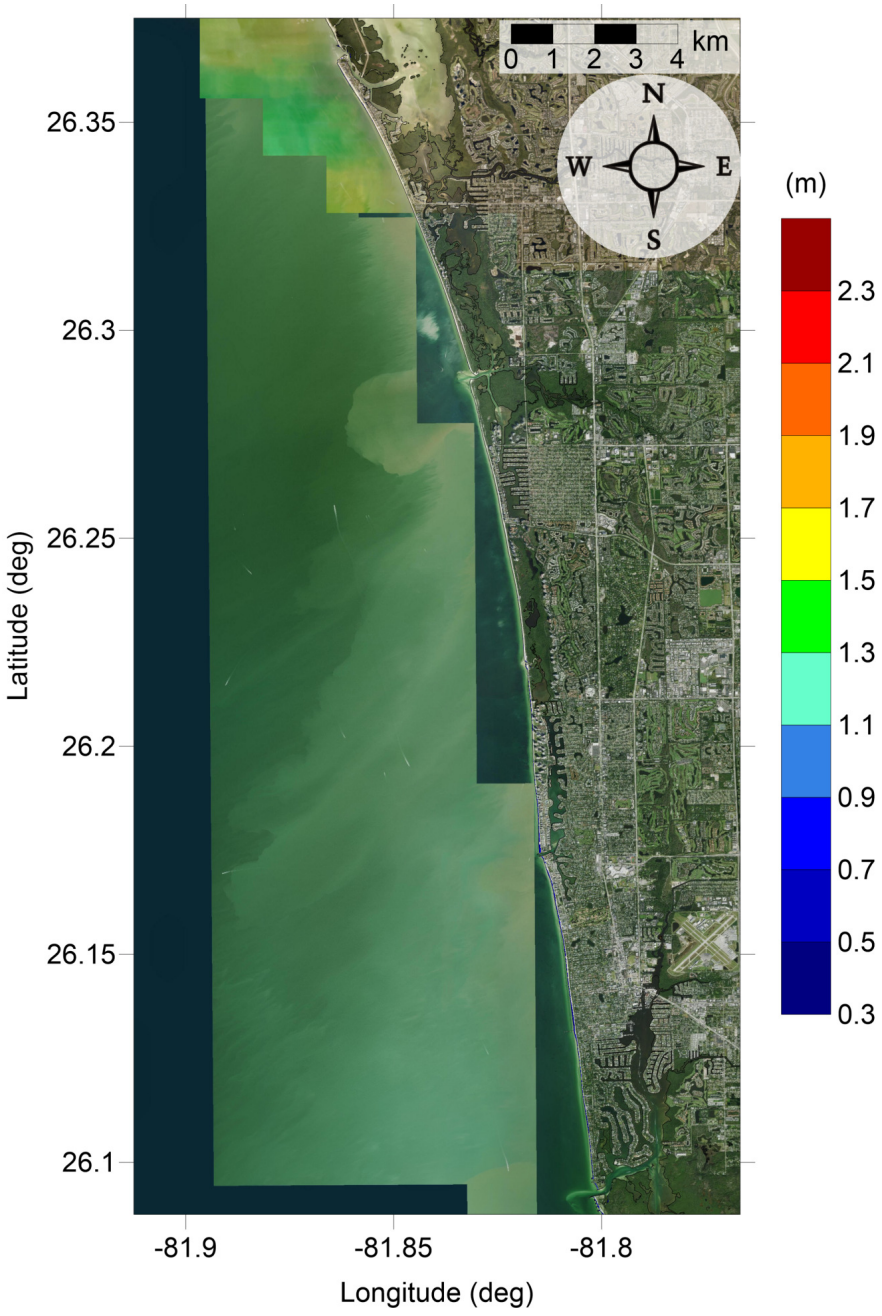

Figure 100: Maximum inundation depth (m) caused by the Yucatan #3 submarine landslide in Naples, FL. Contour drawn is the zero-meter contour for land elevation.

Sanibel Island-Naples, FL
Yucatan #5 submarine landslide
Maximum Momentum Flux

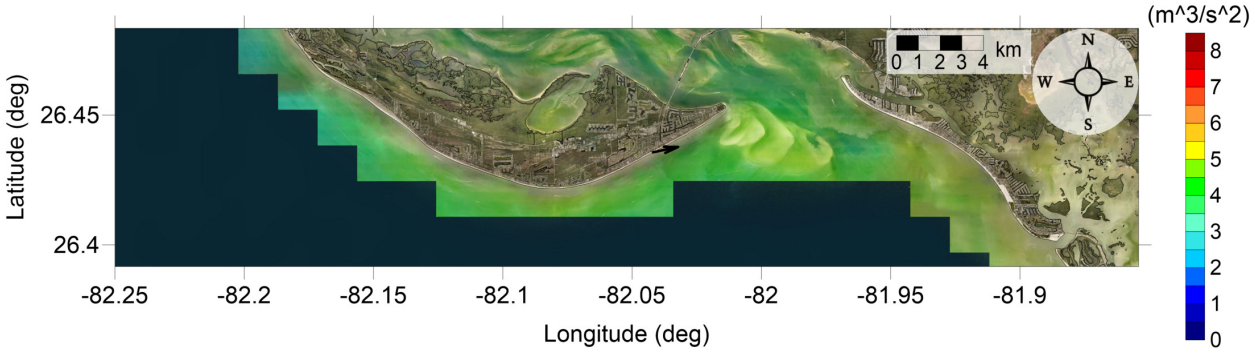

Figure 101: Maximum momentum flux (m^3/s^2) caused by the Yucatan #5 submarine landslide in Sanibel Island, FL. Arrows represent direction of maximum momentum flux. Contour drawn is the zero-meter contour for land elevation.

Sanibel Island-Naples, FL
Yucatan #5 submarine landslide
Maximum Momentum Flux

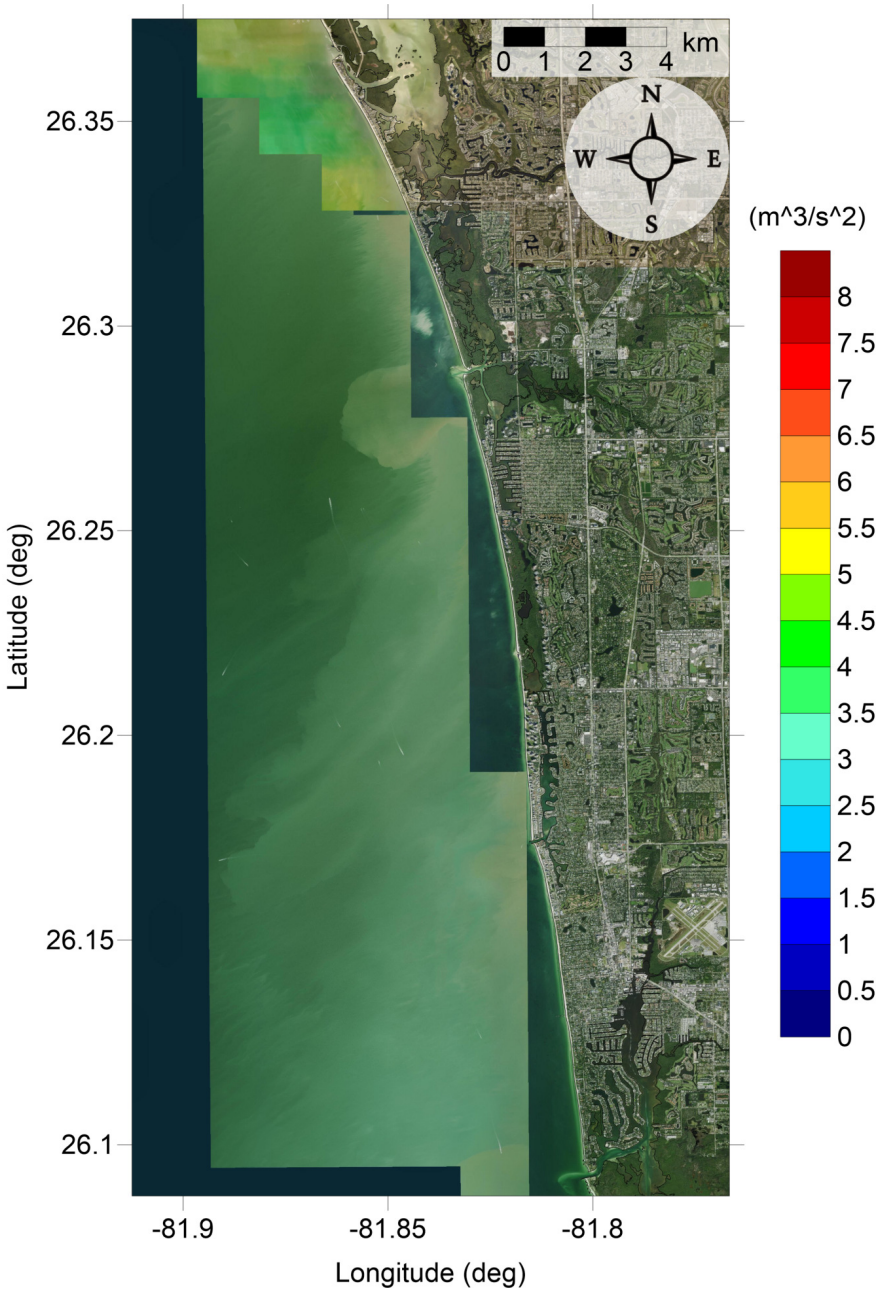

Figure 102: Maximum momentum flux (m^3/s^2) caused by the Yucatan #5 submarine landslide in Naples, FL. Arrows represent direction of maximum momentum flux. Contour drawn is the zero-meter contour for land elevation.

Sanibel Island-Naples, FL
Yucatan #5 submarine landslide
Maximum Inundation Depth

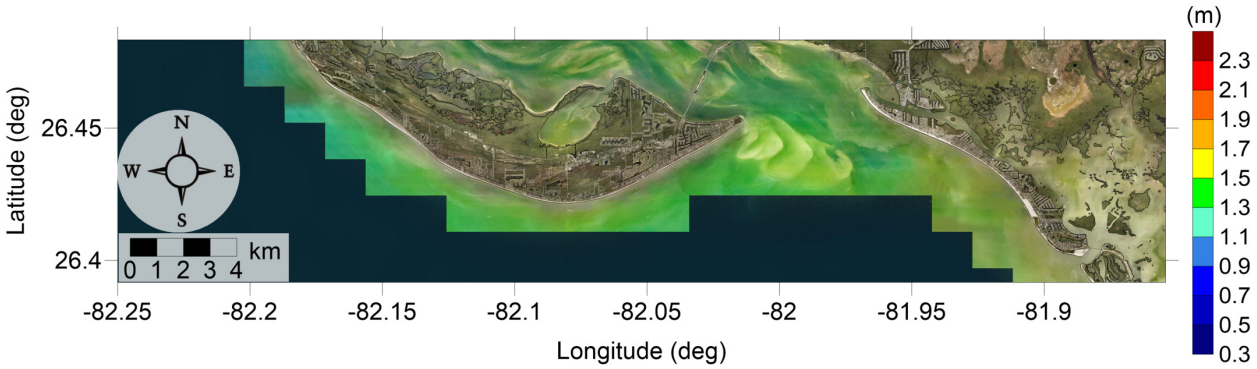

Figure 103: Maximum inundation depth (m) caused by the Yucatan #5 submarine landslide in Sanibel Island, FL. Contour drawn is the zero-meter contour for land elevation.

Sanibel Island-Naples, FL
Yucatan #5 submarine landslide
Maximum Inundation Depth

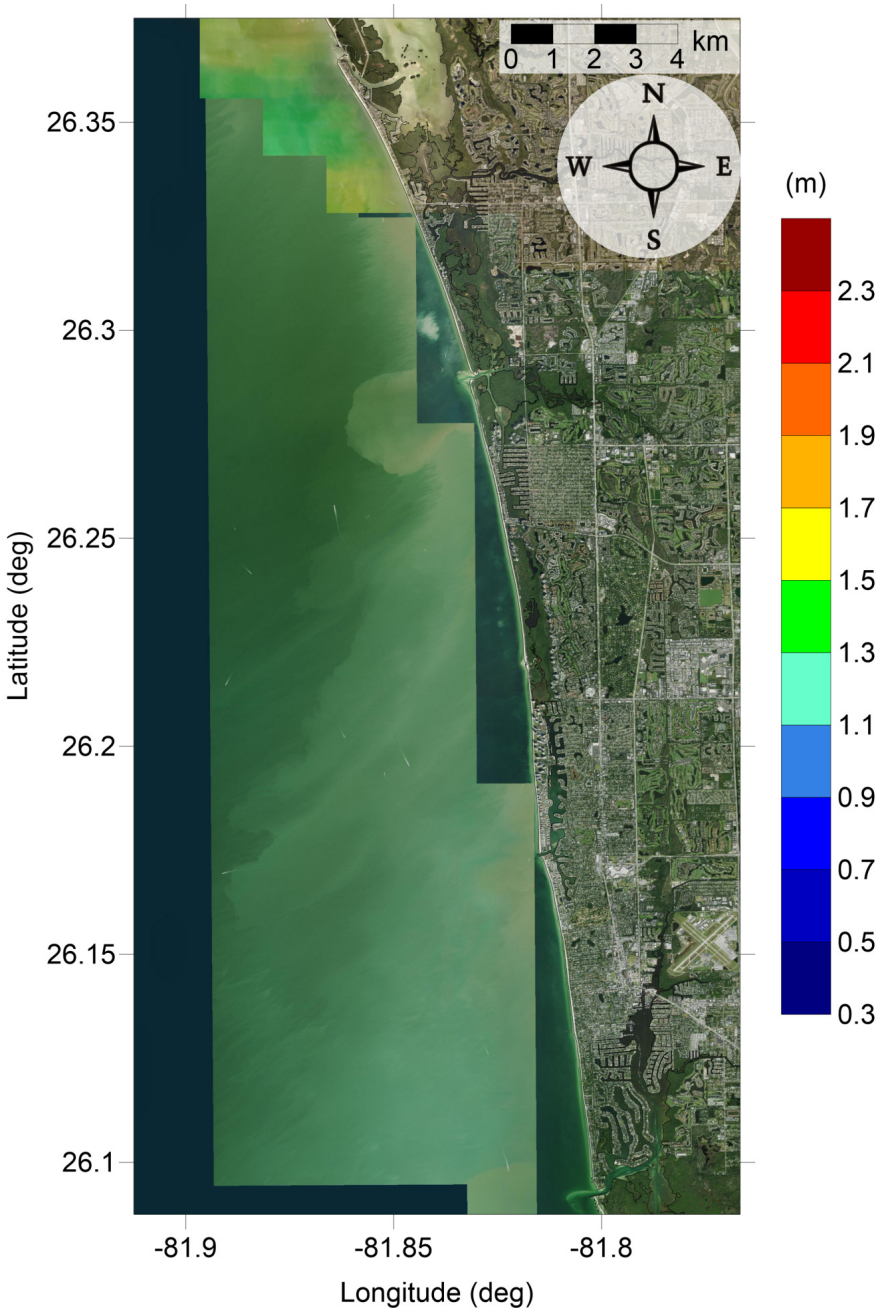

Figure 104: Maximum inundation depth (m) caused by the Yucatan #5 submarine landslide in Naples, FL. Contour drawn is the zero-meter contour for land elevation.

Sanibel Island-Naples, FL
All Sources
Maximum of Maximum Inundation Depth

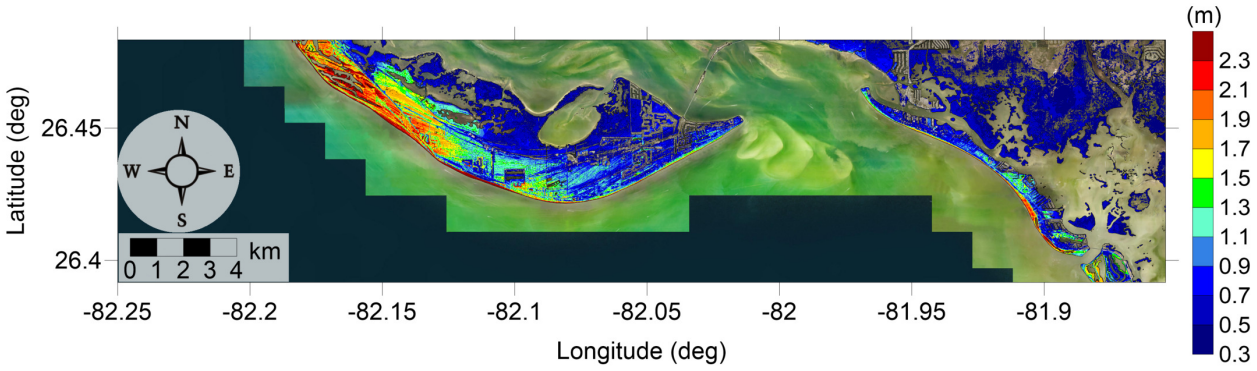

Figure 105: Maximum of maximums inundation depth (m) in Sanibel Island, FL, calculated as the maximum inundation depth in each grid cell from an ensemble of all tsunami sources considered. Contour drawn is the zero-meter contour for land elevation.

Sanibel Island-Naples, FL
All Sources
Maximum of Maximum Inundation Depth

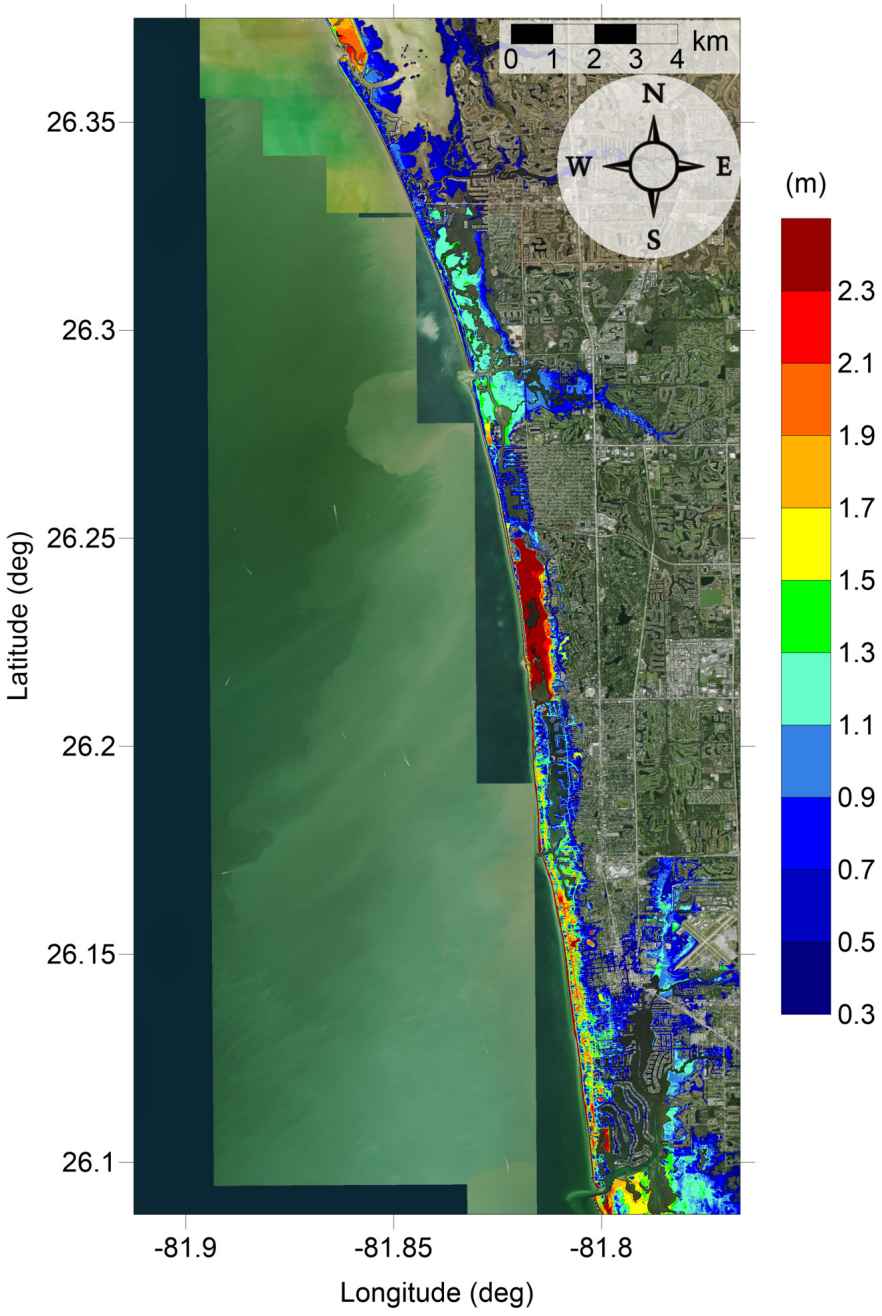

Figure 106: Maximum of maximums inundation depth (m) in Naples, FL, calculated as the maximum inundation depth in each grid cell from an ensemble of all tsunami sources considered. Contour drawn is the zero-meter contour for land elevation.

Sanibel Island-Naples, FL
All Sources
Maximum Inundation Depth by Source

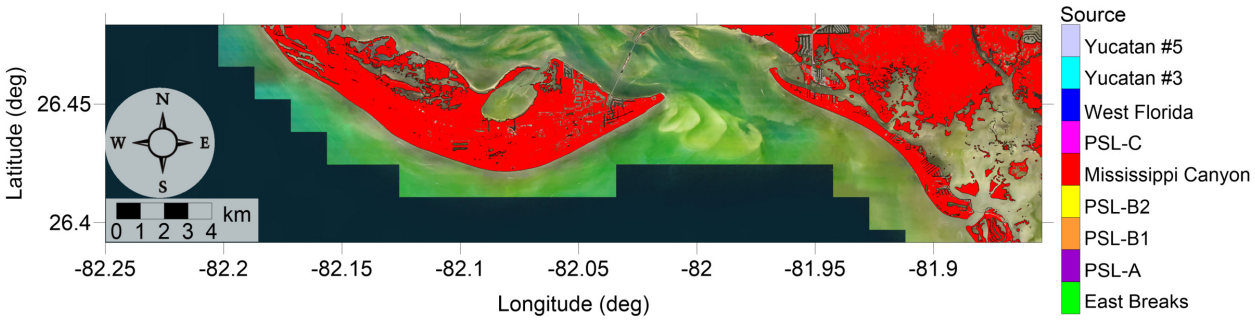

Figure 107: Indication of the tsunami source which causes the maximum of maximums inundation depth (m) in each grid cell from an ensemble of all tsunami sources in Sanibel Island, FL. Contour drawn is the zero-meter contour for land elevation.

Sanibel Island-Naples, FL
All Sources
Maximum Inundation Depth by Source

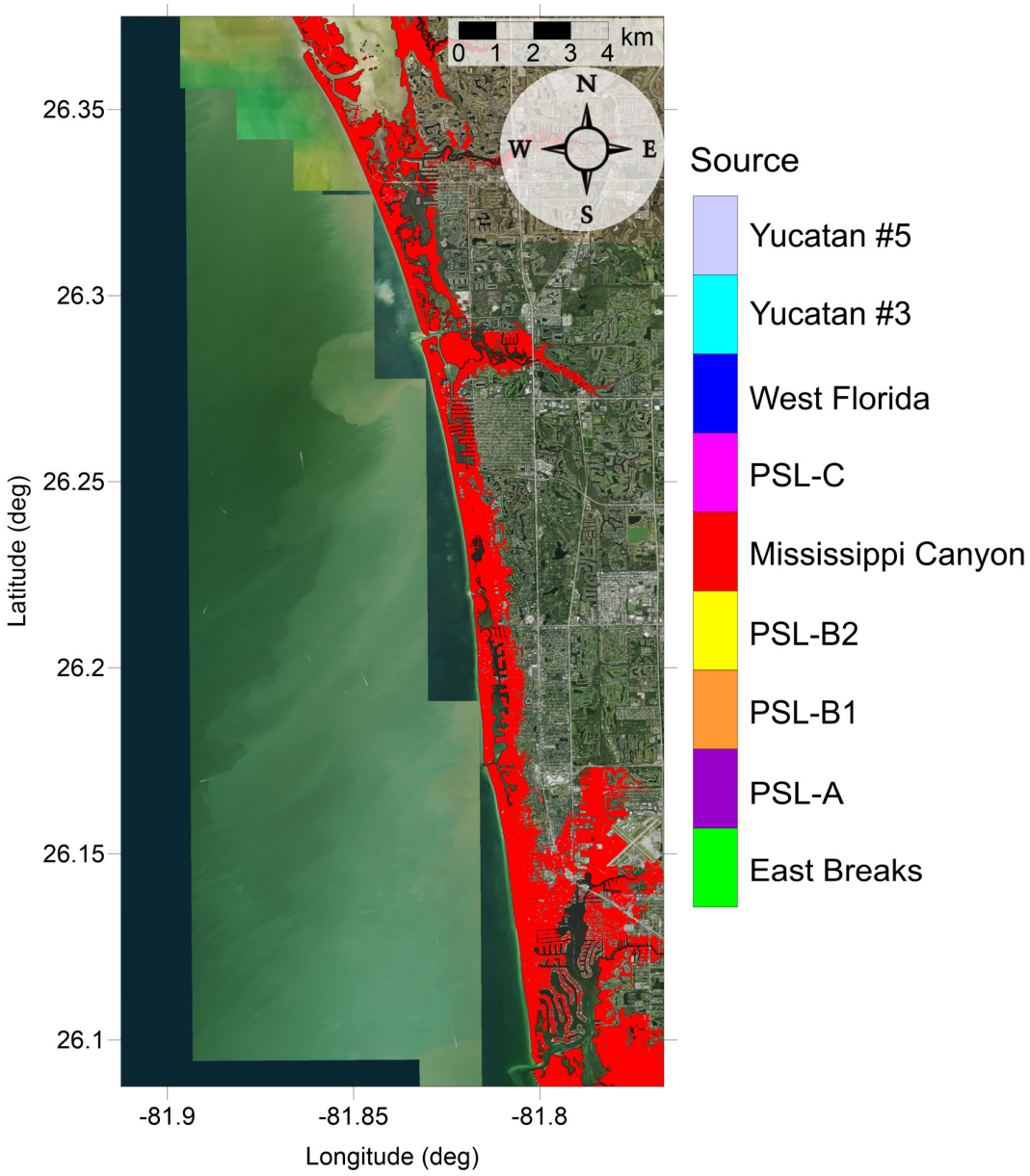

Figure 108: Indication of the tsunami source which causes the maximum of maximums inundation depth (m) in each grid cell from an ensemble of all tsunami sources in Naples, FL. Contour drawn is the zero-meter contour for land elevation.

5 Tsunami and Hurricane Storm Surge Inundation

Due to the limitations on availability of high-resolution (1/3 arcsecond) DEMs, detailed inundation maps for all communities along the Gulf Coast are not yet possible. In an effort to develop a first-order estimate of potential tsunami inundation for those locations where detailed inundation maps have not yet been developed, we compare tsunami inundation modeled for the communities mentioned above to hurricane storm surge modeled data. The motivation for and implications of this approach are twofold. It provides a way to assess tsunami inundation in un-mapped communities based on existing storm surge flood data and also relates the level of tsunami hazard to that of another hazard that is better defined in this region. Tsunamis are not well-understood as a threat along the Gulf Coast, making tsunami hazard mitigation efforts somewhat difficult. However, hurricane is a relatively well-understood threat in this region, and hurricane preparedness approaches are well-developed. As a result, comparisons of tsunami and hurricane storm surge inundation levels provide a more understandable and accessible idea of the level of hazard presented by potential tsunami events and can serve as a basis for tsunami preparedness efforts.

The hurricane storm surge data used here is available from the Sea, Lake, and Overland Surges from Hurricanes (SLOSH) model (http://www.nhc.noaa.gov/surge/slosh.php). The SLOSH model was developed by the National Weather Service (NWS) to provide estimates of storm surge heights caused by historical, predicted, or hypothetical hurricanes based on different values for atmospheric pressure, hurricane size, forward speed, and track. It uses a polar, elliptical, or hyperbolic grid for computations, leading to higher resolutions near coastal areas of interest. Some limitations of the SLOSH model should be acknowledged. Resolution of the model varies from tens of meters to a kilometer or more. Near the coastal communities of interest here, resolution is on the order of 1 km. Sub-grid scale water and topographic features such as channels, rivers, levees, and roads, are parameterized instead of being explicitly modeled. Despite these limitations, the hurricane storm surge data from the SLOSH model is currently the best data publicly available for our purposes, and efforts have been made to ensure the validity of the SLOSH data in performing comparisons with tsunami inundation.

The SLOSH MOM results provide the worst-case storm surge for a given hurricane category and initial tide level based on a set of model runs with various combinations of parameters such as forward speed, trajectory, and landfall location. To perform the storm surge and tsunami comparisons, SLOSH storm surge elevation data was first converted to meters and adjusted from the NAVD88 to the MHW vertical datum using NOAA's VDatum tool (http://vdatum.noaa.gov/). Due to the relatively low resolution of the SLOSH data as compared to the DEMs used for tsunami modeling, the SLOSH data was interpolated to 1/3 arcsecond (10 m) resolution using a kriging method. Inundation was then determined by subtracting land elevation from the storm surge elevation.

Here, an initial high tide level is used for the SLOSH MOM results in order to compare the worst-case tsunami inundation with a worst-case storm surge scenario. The high tide SLOSH MOM data includes effects of the highest predicted tide level at each location. In comparison, water elevations in the tsunami modeling are based on the MHW datum, which averages the high water levels over the National Tidal Datum Epoch (NTDE). Within the

GOM, tidal ranges are relatively small, with diurnal ranges on the order of 1.5 ft (0.5 m) for most of the communities studied here, and slightly higher at around 2.5 ft (0.8 m) for the west coast of Florida. Thus, differences between highest tide levels and the mean of the highest tide levels are expected to be relatively small, though local bathymetric effects combined with tidal effects can still be significant.

It should be noted that the updated Saffir-Simpson Hurricane Wind Scale which delineates hurricane categories 1-5 does not include storm surge as a component of the measure of hurricane intensity and that other methods may capture the physics of hurricane severity and damage in a more appropriate manner (e.g. Kantha [2006], Basco and Klentzman [2006], Irish and Resio [2010]). However, the SLOSH MOM results take into account thousands of scenarios for a given hurricane category, resulting in a composite worst-case storm surge scenario for each Saffir-Simpson hurricane category. Thus, since hurricane preparedness, storm surge evacuation zones, and hazard mitigation efforts are based on hurricane category assignment, we aim to determine the hurricane category which produces MOM storm surge inundation ζ_h that is a best match to the tsunami MOM inundation ζ_t. That is, we determine the hurricane category which satisfies

$$min_c(|\zeta_{h_c} - \zeta_t|), \qquad c = \text{Cat1,..,Cat5} \tag{1}$$

for each grid cell. The inundation level for the best-match category is denoted $\zeta_{h_{min}}$. The actual difference between hurricane and tsunami inundation levels $\Delta\zeta = \zeta_{h_{min}} - \zeta_t$ then indicates how close of a match the best-match category actually is. Thus, positive values of $\Delta\zeta$ indicate where hurricane storm surge inundation is higher than tsunami inundation, and negative values indicate where tsunami inundation is higher. A common local practice in tsunami modeling is to only consider inundation above a threshold of 0.3 m (1 ft) [Horrillo et al., 2011, 2015]. This is due to the extensive flat and low-lying elevation found along the Gulf Coast. All depths are calculated for tsunami inundation modeling, but inundation less than 0.3 m (1 ft) is considered negligible here for inundation mapping purposes. Thus, comparisons are only made where either the tsunami or hurricane MOM inundation is at least 0.3 m (1 ft). Results for the two selected Gulf Coast communities are given in the following subsections. It is possible that tsunami inundation zone has no hurricane flooding, therefore matching with hurricane category cannot be made.

5.1 Osprey-Venice-Englewood, FL

Osprey-Venice, FL

Fig. 65 shows the MOM tsunami inundation affecting Osprey-Venice, FL. Tsunami completely inundates the whole Casey Key barrier island, and water penetrates approximately 1 km inland at Venice. On the barrier island, water depth greater than 3 m can be seen along the immediate beachfront, and diminishes toward the inner island. At Venice, high water (>3 m) reaches farther inland, flooding a larger residential area. West of the Venice Municipal Airport is also severely flooded. On the mainland, only the coasts of Lyons Bay, Dona Bay and Roberts Bay have seen large areas inundated by tsunami waves, with water

as high as 2 m. Mississippi Canyon landslide is responsible for the MOM inundation (see Fig. 67).

Fig. 109 shows the hurricane category which best matches the tsunami inundation in Osprey-Venice, FL. Fig. 110 shows $\Delta\zeta$ for the best-match hurricane category satisfying equation 1 and shown in Fig. 109. The hurricane category that best matches tsunami inundation closely follow the MOM tsunami inundation trend.

Category 3 occurs only on the Casey Key barrier island and Venice, FL where there is maximum tsunami inundation water height (greater than 3 m). Category 2 appears on the rest of the barrier island. On the mainland, only Category 1 shows up. The difference between tsunami inundation and hurricane flooding is generally less than 0.5 m, indicating good matching with hurricane categories. There is no Category 4 or 5 present in this area.

Englewood, FL

Fig. 66 shows the MOM tsunami inundation affecting Englewood, FL. The inundation depth pattern is very similar to Casey Key barrier island. Tsunami inundation greater than 3 m appears on a thin strip of the Manasota Key beachfront, and water height diminishes toward the inland. Over at the mainland, tsunami inundation is limited to the vicinity of the Lemon Bay, with water height of no more than 2 m, except for the portions in South Venice where the bay is very narrow. Again, the Mississippi Canyon landslide is responsible for the MOM inundation (see Fig. 68).

Fig. 111 shows the hurricane category which best matches the tsunami inundation in Englewood, FL. Fig. 112 shows $\Delta\zeta$ for the best-match hurricane category satisfying equation 1 and shown in Fig. 111.

Category 3 and 4 occur only on the Manasota Key barrier island and Venice, FL where there is maximum tsunami inundation water height (greater than 3 m). Category 2 and 1 appears on the rest of the barrier island. On the mainland, only Category 1 shows up, with the exception of South Venice. The difference between tsunami inundation and hurricane flooding is generally less than 0.5 m, indicating good matching with hurricane categories. There is no Category 5 present in this area.

Osprey-Venice-Englewood, FL
All Sources
SLOSH Storm Surge and MOM Tsunami Inundation Comparison

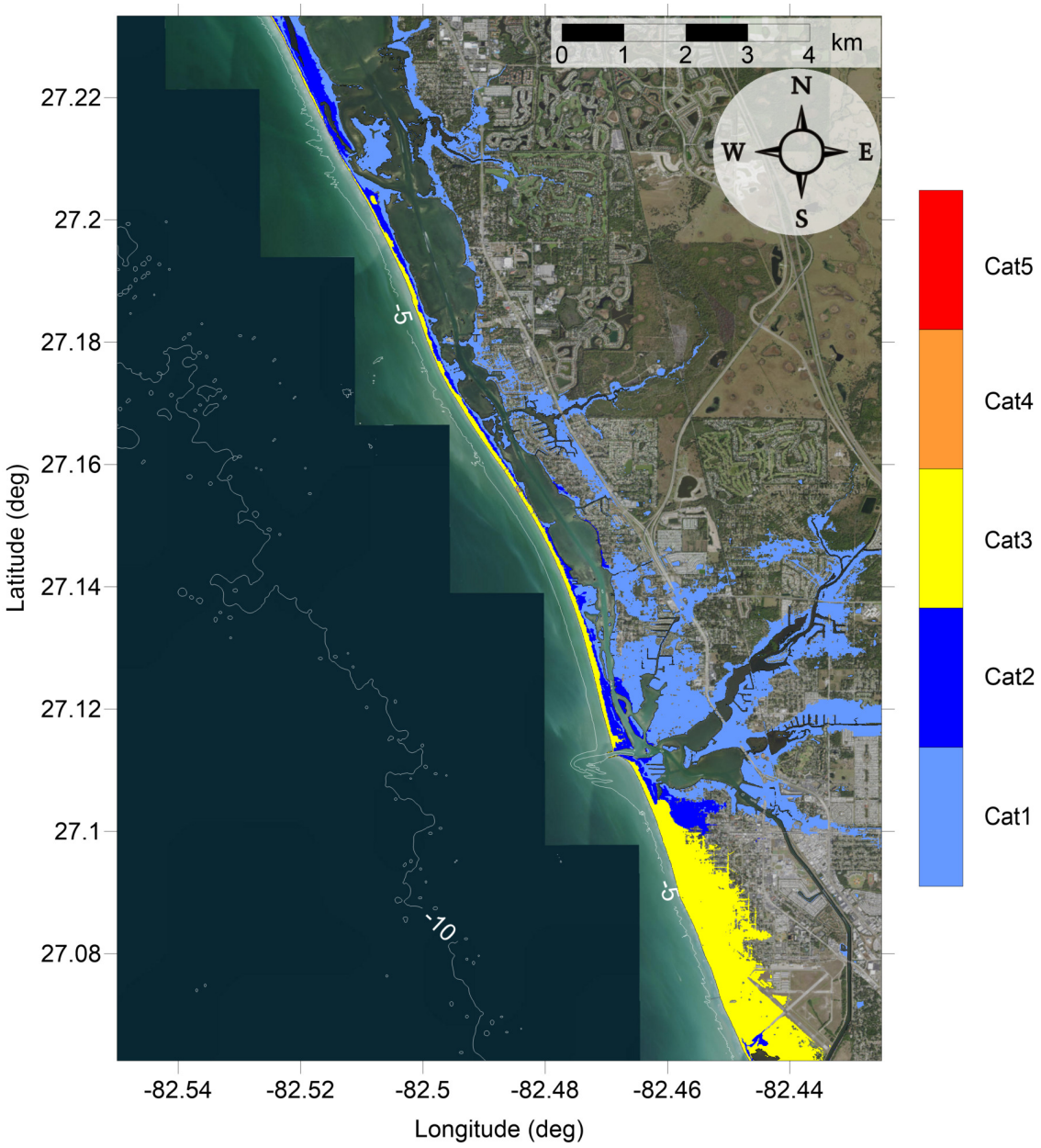

Figure 109: Hurricane category which produces inundation at high tide that best matches the MOM tsunami inundation shown in Figure 110 for Osprey-Venice, FL. The contours drawn and labeled are at -5 m, -10 m, and -15 m levels.

Osprey-Venice-Englewood, FL
All Sources
SLOSH Storm Surge and MOM Tsunami Inundation Comparison

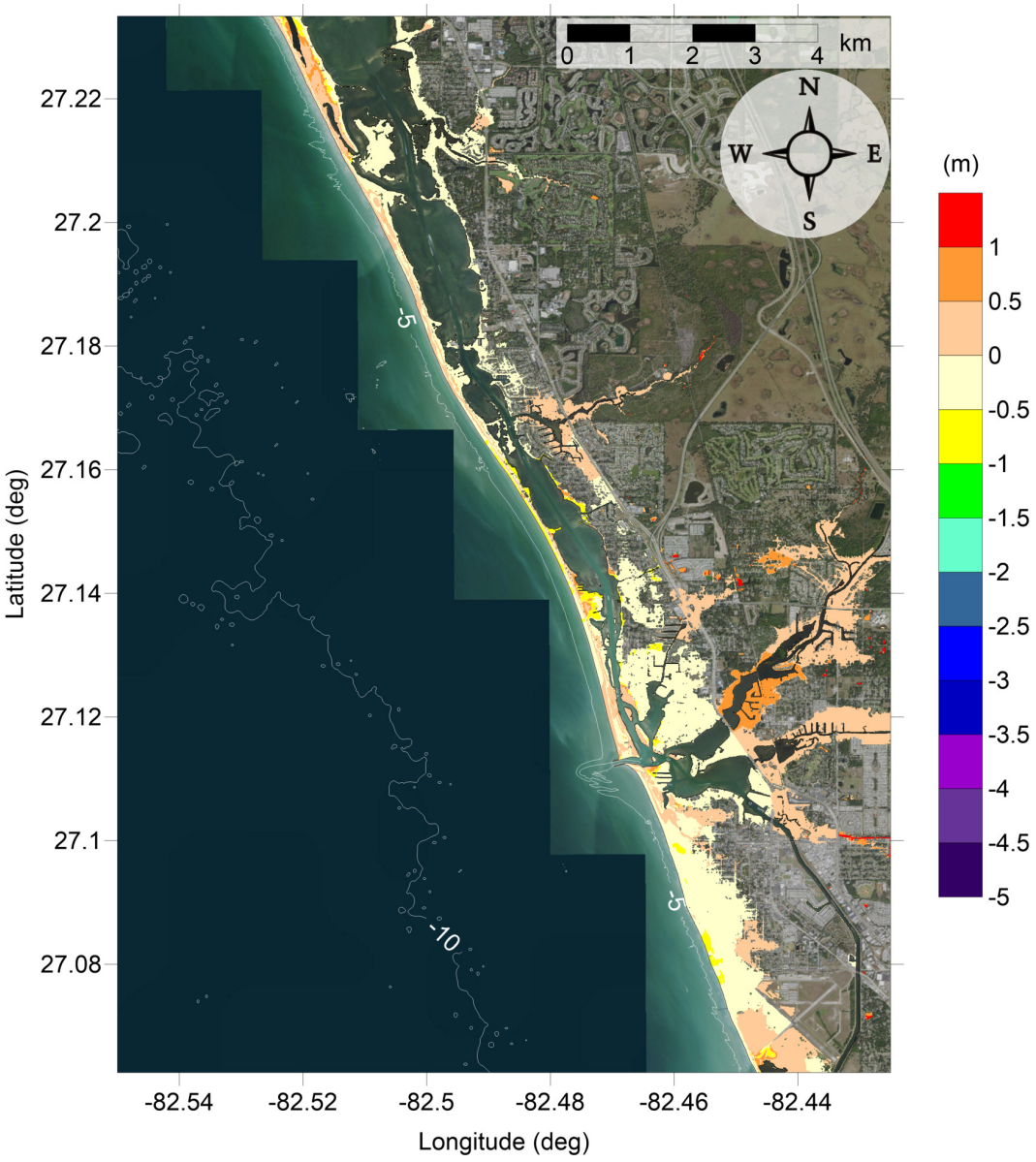

Figure 110: Actual difference $\Delta\zeta$ (in meters) between SLOSH MOM storm surge inundation and MOM tsunami inundation for the best-match hurricane category shown in Figure 109 for Osprey-Venice, FL. Note that negative values indicate where tsunami inundation is higher than hurricane inundation, and pale colors indicate relatively good agreement between tsunami and storm surge inundation, i.e. $|\Delta\zeta| \leq 0.5$ m. The contours drawn and labeled are at -5 m, -10 m, and -15 m levels.

Osprey-Venice-Englewood, FL
All Sources
SLOSH Storm Surge and MOM Tsunami Inundation Comparison

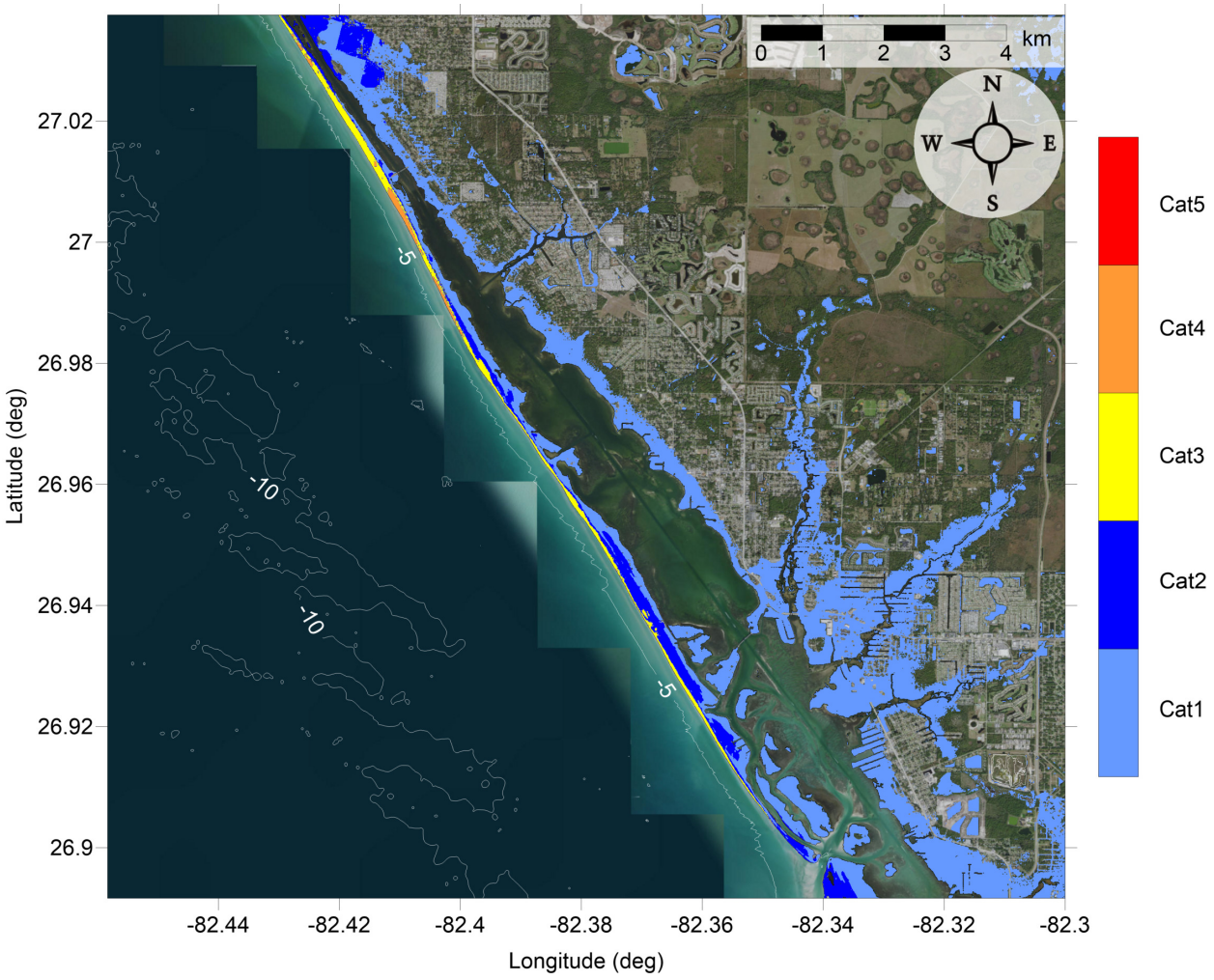

Figure 111: Hurricane category which produces inundation at high tide that best matches the MOM tsunami inundation shown in Figure 112 for Englewood, FL. The contours drawn and labeled are at -5 m, -10 m, and -15 m levels.

Osprey-Venice-Englewood, FL
All Sources
SLOSH Storm Surge and MOM Tsunami Inundation Comparison

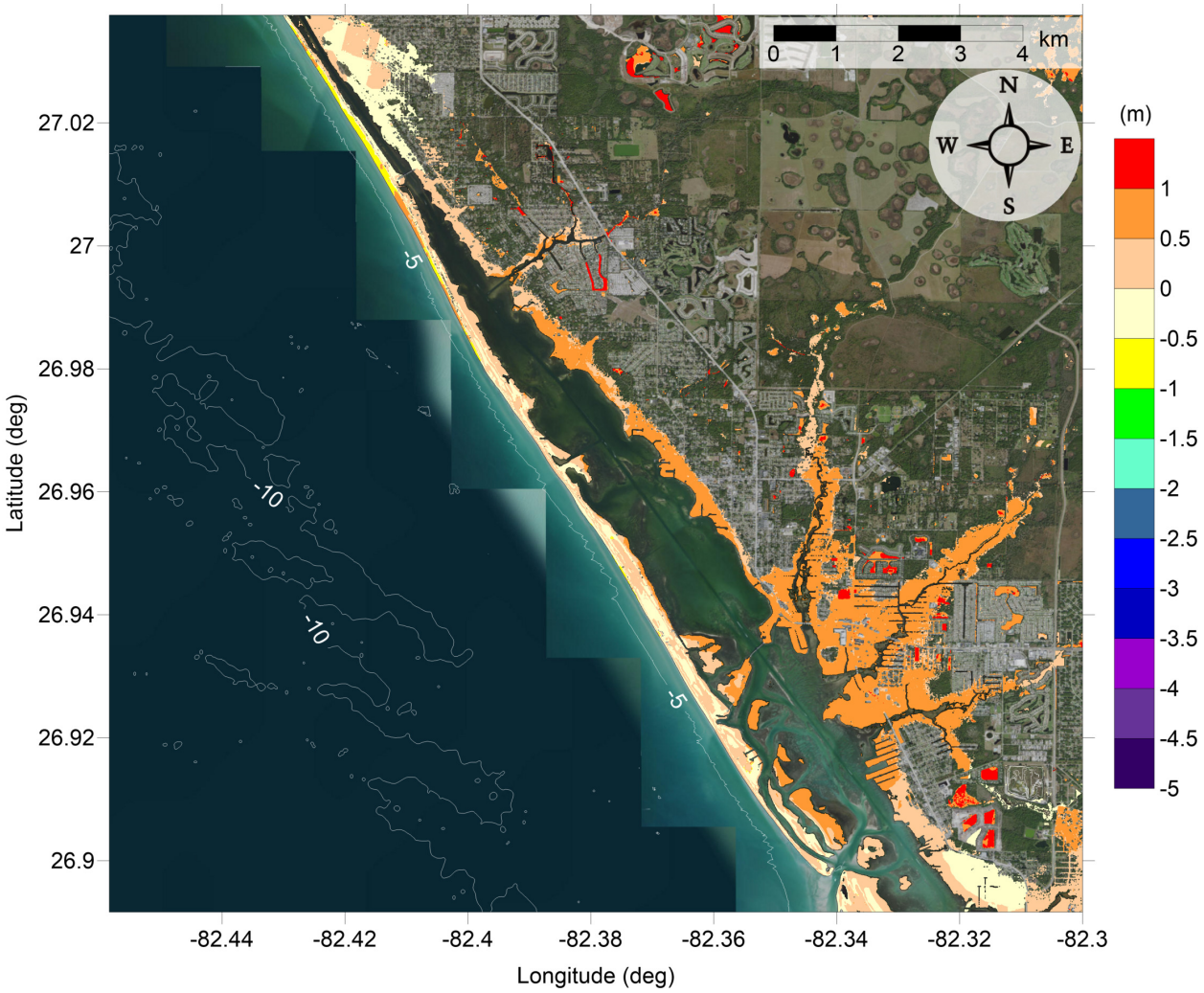

Figure 112: Actual difference $\Delta\zeta$ (in meters) between SLOSH MOM storm surge inundation and MOM tsunami inundation for the best-match hurricane category shown in Figure 111 for Englewood, FL. Note that negative values indicate where tsunami inundation is higher than hurricane inundation, and pale colors indicate relatively good agreement between tsunami and storm surge inundation, i.e. $|\Delta\zeta| \leq 0.5$ m. The contours drawn and labeled are at -5 m, -10 m, and -15 m levels.

5.2 Sanibel Island-Naples, FL

Sanibel Island, FL

Fig. 105 shows the MOM tsunami inundation affecting Sanibel Island, FL. Sanibel island is completely inundated, with water depth up to 2 m. While the trend of decreasing inundation depth from the coast to inland still exists, there is another distinct trend from west to east, because the tsunami waves come from the west. As a result, by the time tsunami reaches Estero Island, wave energy is further dissipated, causing less severe inundation than Sanibel Island. The Mississippi Canyon landslide is responsible for the MOM inundation (see Fig. 107).

Fig. 113 shows the hurricane category which best matches the tsunami inundation in Sanibel Island, FL. Fig. 114 shows $\Delta\zeta$ for the best-match hurricane category satisfying equation 1 and shown in Fig. 113. The hurricane category that best matches tsunami inundation is Category 1 everywhere, except for the west side of Sanibel Island facing the tsunami waves where best match is Category 2. Category 3 is also spotted, but in few beachfront locations. The difference between hurricane flooding and tsunami inundation $\Delta\zeta$ gradually changes from -0.5 m at the west side of Sanibel Island to +1 m, which coincides with the tsunami inundation trend. The same trend can also be observed at Estero Island.

Naples, FL

Fig. 106 shows the MOM tsunami inundation affecting Naples, FL. Naples is also significantly impacted, with $>$ 2 m water depth reaching to 500 m inland. Tsunami also flooded a relatively large area in the vicinity of Naples Bay. North of the Inner Clam Bay tsunami causes less than 1 m inundation at the Little Hickory Island and Vanderbilt Beach, and very limited area surrounding Little Hickory Bay. The Mississippi Canyon landslide is also responsible for the MOM inundation (see Fig. 108). The marsh of Inner Clam Bay is flooded with water depth greater than 2 m, but this area is not populated.

Fig. 115 shows the hurricane category which best matches the tsunami inundation in Naples, FL. Fig. 116 shows $\Delta\zeta$ for the best-match hurricane category satisfying equation 1 and shown in Fig. 115. The hurricane category that best matches tsunami inundation is uniformly Category 1, except for the coast of Naples where there is a thin strip of Category 2. The difference between hurricane flooding and tsunami inundation is larger than 1 m (hurricane $>$ tsunami) around the Estero Bay, Inner Clam Bay and Naples Bay, and less than 0.5 m (absolute value) for the other inundated areas.

Sanibel Island-Naples, FL
All Sources
SLOSH Storm Surge and MOM Tsunami Inundation Comparison

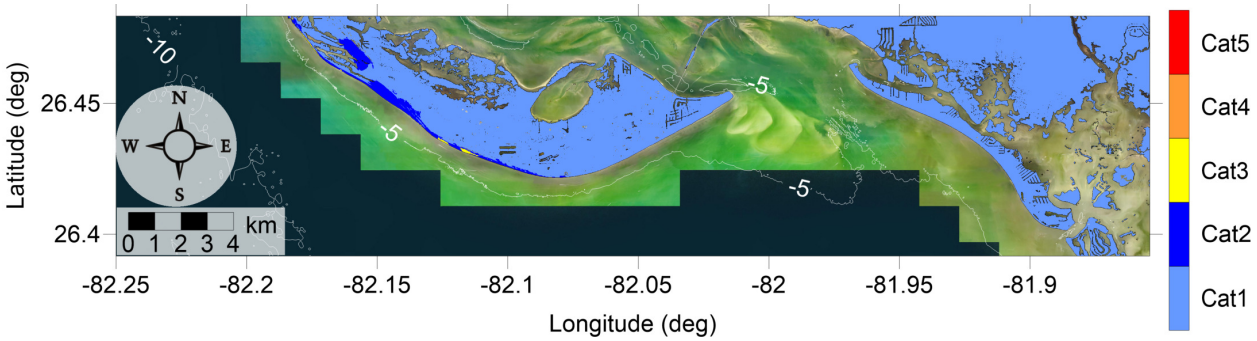

Figure 113: Hurricane category which produces inundation at high tide that best matches the MOM tsunami inundation shown in Figure 114 for Sanibel Island, FL. The contours drawn and labeled are at -5 m, -10 m, and -15 m levels.

Sanibel Island-Naples, FL
All Sources
SLOSH Storm Surge and MOM Tsunami Inundation Comparison

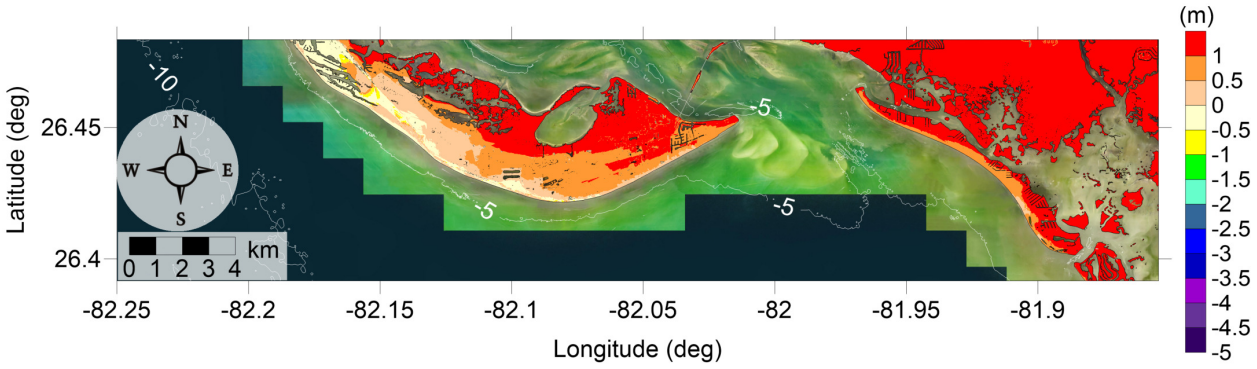

Figure 114: Actual difference $\Delta\zeta$ (in meters) between SLOSH MOM storm surge inundation and MOM tsunami inundation for the best-match hurricane category shown in Figure 115 for Sanibel Island, FL. Note that negative values indicate where tsunami inundation is higher than hurricane inundation, and pale colors indicate relatively good agreement between tsunami and storm surge inundation, i.e. $|\Delta\zeta| \leq 0.5$ m. The contours drawn and labeled are at -5 m, -10 m, and -15 m levels.

Sanibel Island-Naples, FL
All Sources
SLOSH Storm Surge and MOM Tsunami Inundation Comparison

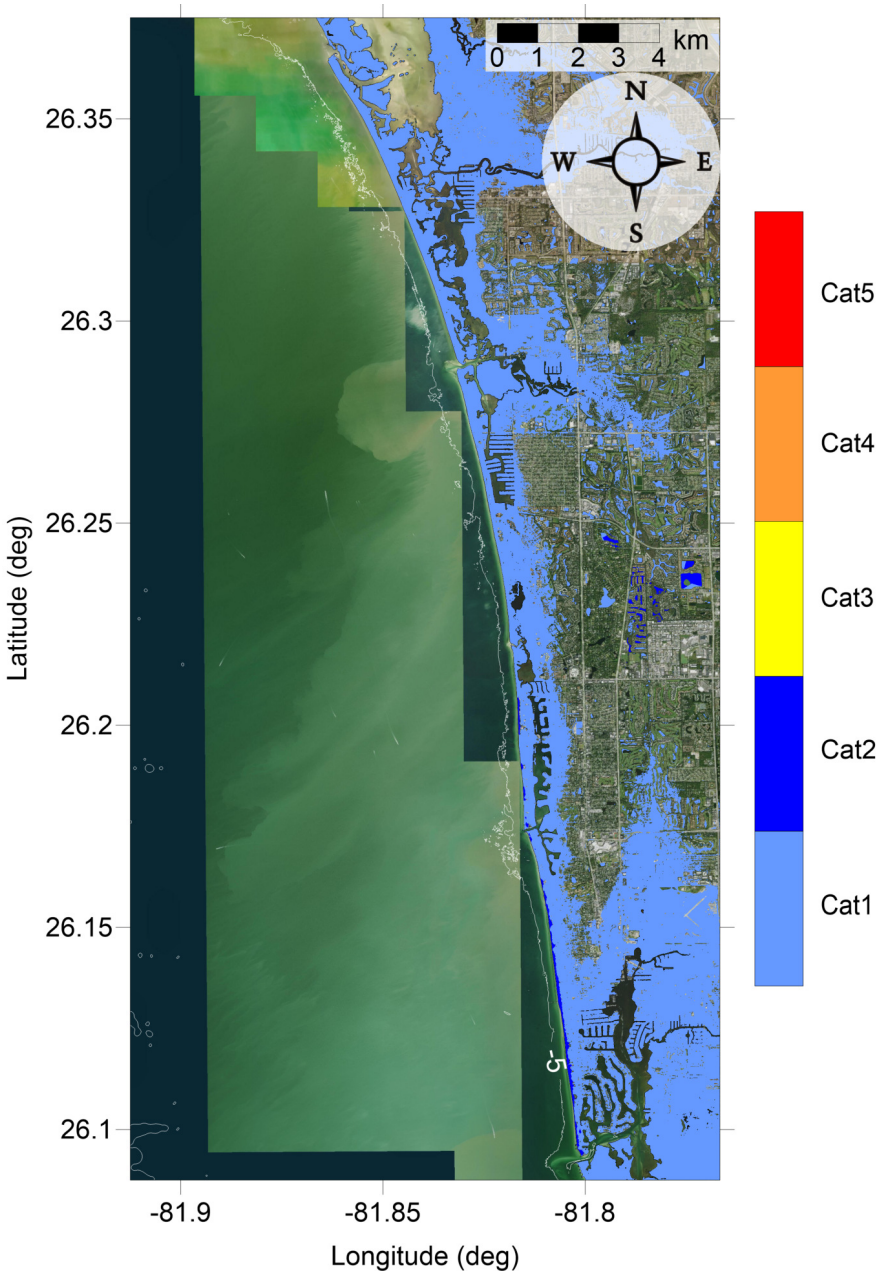

Figure 115: Hurricane category which produces inundation at high tide that best matches the MOM tsunami inundation shown in Figure 116 for Naples, FL. The contours drawn and labeled are at -5 m, -10 m, and -15 m levels.

Sanibel Island-Naples, FL
All Sources
SLOSH Storm Surge and MOM Tsunami Inundation Comparison

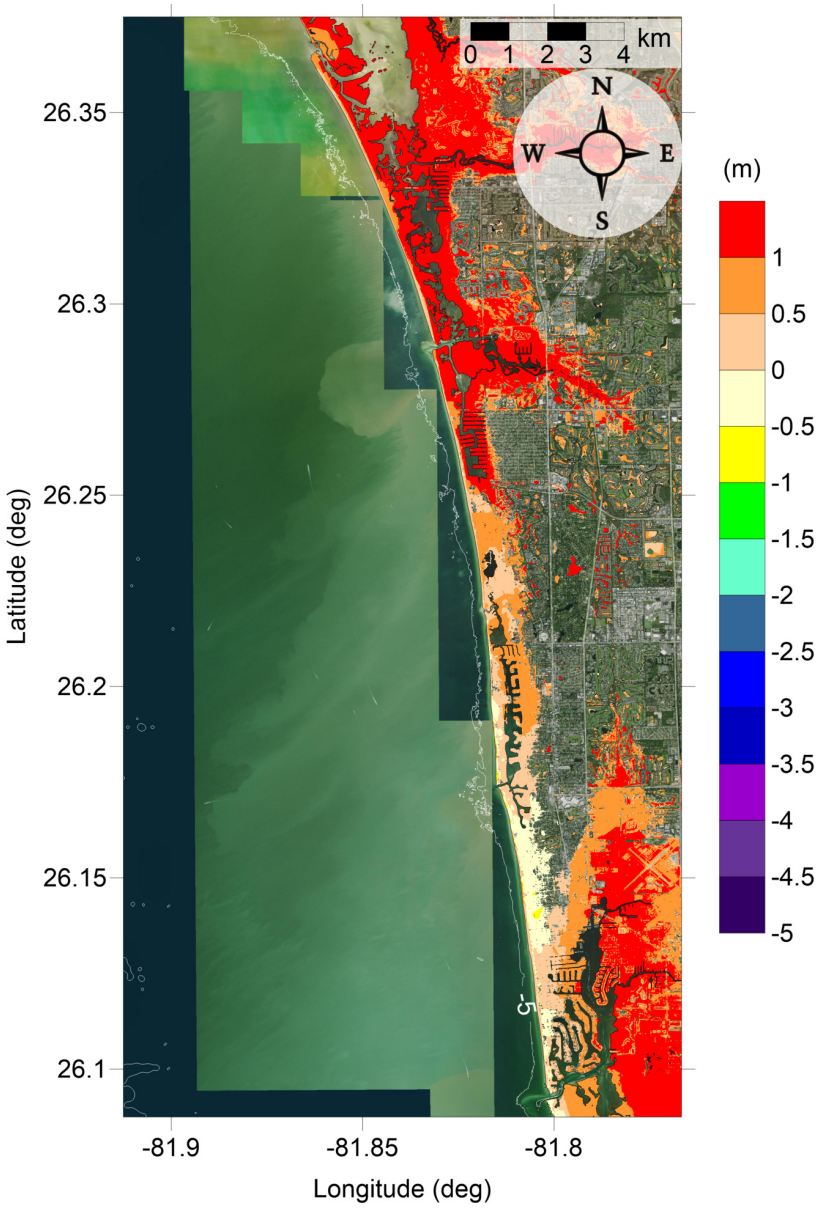

Figure 116: Actual difference $\Delta\zeta$ (in meters) between SLOSH MOM storm surge inundation and MOM tsunami inundation for the best-match hurricane category shown in Figure 115 for Naples, FL. Note that negative values indicate where tsunami inundation is higher than hurricane inundation, and pale colors indicate relatively good agreement between tsunami and storm surge inundation, i.e. $|\Delta\zeta| \leq 0.5$ m. The contours drawn and labeled are at -5 m, -10 m, and -15 m levels.

6 Tsunami Maritime Products

Accurate estimates of tsunami wave amplitude do not necessarily equate to the prediction of localized damaging currents in a basin or harbor [Lynett et al., 2012]. Furthermore, damage potential in ports is strongly related to the current speed. Therefore, tsunami hazard mitigation products need to be advanced to predict damage potential in basins or harbors. Recent tsunamis have shown that the maritime community requires additional information and guidance about tsunami hazards and post-tsunami recovery [Wilson et al., 2012, 2013]. To accomplish mapping and modeling activities to meet NTHMP's planning/response purposes for the maritime community and port emergency management and other customer requirements, it is necessary to continue the process to include maritime products in our current inundation map development. These maritime products will help identify impact specifically on ship channels, bay inlets, harbors, marinas, and oil infrastructures (e.g., designated lightering and oil tanker waiting zones).

In this study, Osprey-Venice-Englewood, FL and Sanibel Island-Naples, FL are added to the maritime portfolio, where tsunami hazard maritime products such as tsunami current magnitude, vorticity, safe/hazard zones are included. This work is based on our pilot tsunami maritime study conducted in the Galveston Bay in Horrillo et al. [2016], and later extended to another nine locations, South Padre Island, TX, Mobile, AL, Panama City, FL, and Tampa, FL, Pensacola, FL, Key West, FL, Okaloosa County, FL, Santa Rosa County, FL and Mustang Island, TX, which were reported in project NA15NWS4670031 and NA16NWS4670039 [Horrillo et al., 2017].

Lynett et al. [2014] complied a general relationship between tsunami current speed and harbor damage based on observational data, in which the current speed is divided into four ranges of damaging potential, 0 - 3 knots means unharmful currents, 3 - 6 knots corresponds to minor-to-moderate damage, 6 - 9 knots moderate-to-major damage, and over 9 knots extreme damage. Since the extent of damage is very location-dependent, to make the text concise, we associate 0 - 3 knots to unharmful currents, 3 - 6 knots to minor damage, 6 - 9 knots to moderate damage, and finally over 9 knots to major damage. The four levels are denoted with white, blue, yellow and red colors, respectively, for all the velocity contour plots within our velocity maritime products.

Using this damage-to-speed relationship, we have plotted the maximum of maximum depth-averaged velocity for each computational subdomain of the two new communities. Fig. 117 shows the minimum offshore safe depth (approximately 200 m or 100 fathoms), and the maximum of maximum velocity magnitude contour plot across the entire Gulf of Mexico (15 arcsecond resolution) for all landslide scenarios (Eastbreaks, PSL-A, PSL-B1, PSL-B2, Mississippi Canyon, PSL-C, West Florida, Yucatan #3 and Yucatan #5). Potential damaging currents ($>$ 3 knots, blue, yellow and red areas) tend to be present in most of the area shallower than the minimum offshore safe depth. However, damaging currents could reach areas deeper than 200 m close to most of the landslide generation regions. Major damaging currents ($>$ 9 knots, red) can be expected in most of the landslide generation regions, in the continental shelf adjacent to Mississippi Canyon, offshore northwest Florida, and Yucatan shelf. Moderate ($>$ 6 knots and $<$ 9 knots, yellow) damaging current areas are scattered over the continental shelf, but mostly close to areas with major damage currents.

All locations
All Sources
Maximum of Maximum Velocity Magnitude

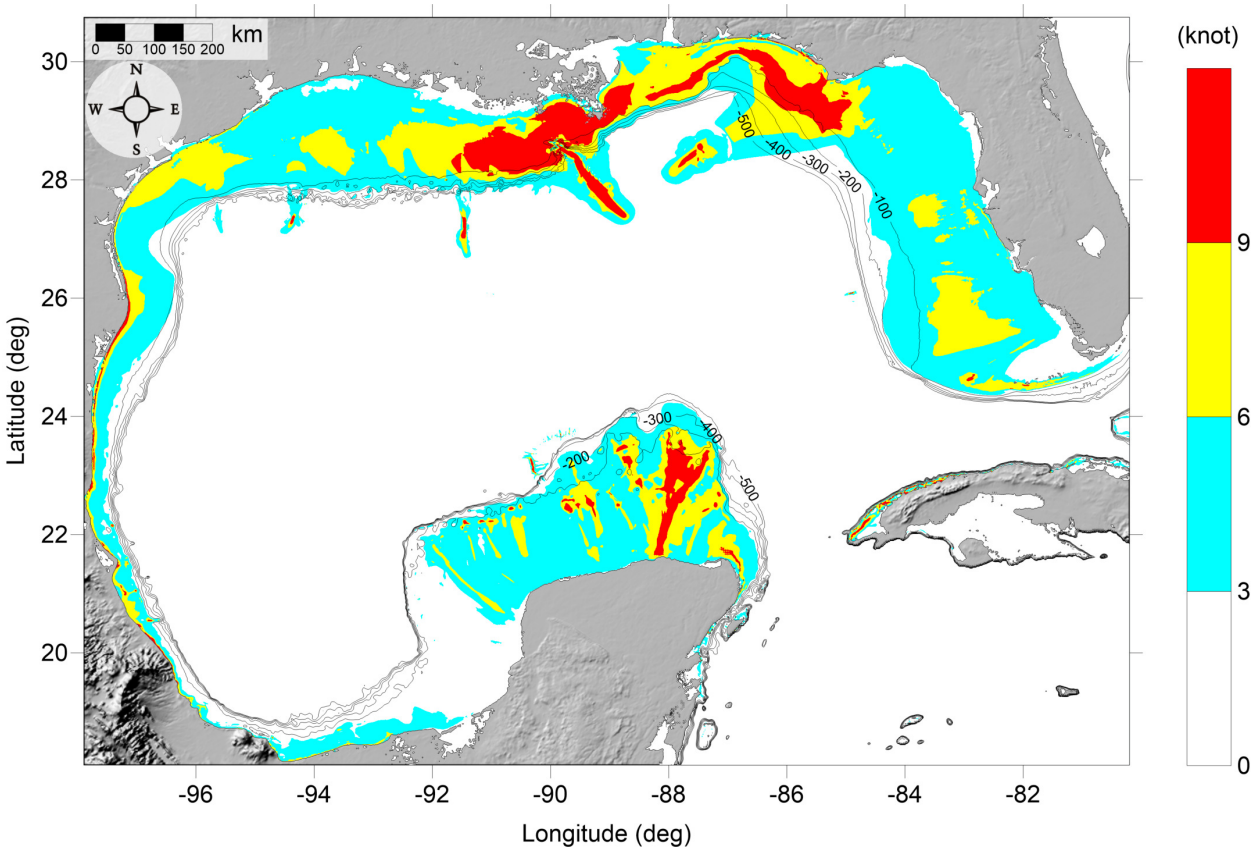

Figure 117: Maximum of maximum velocity magnitude contour in GOM for all landslide scenarios and all locations.

The MOM velocity magnitude (damaging potential) contour maps and the MOM vorticity magnitude contour maps for the finer computational subdomains of Osprey-Venice-Englewood, FL and Sanibel Island-Naples, FL are presented from Fig. 118 to Fig. 131.

General trends can be observed from all of the MOM velocity and vorticity maps of the subdomains. In the nearshore region of the subdomains, there are mostly moderate damaging currents ($>$ 6 knots and $<$ 9 knots, yellow). In the surf zone of the islands, there are major damaging currents ($>$ 9 knots, red) in Ospary-Venice-Englewood, but not in Sanibel Island-Naples, FL. There are usually strong currents flowing through the inlets (some with jetties) which connects the GOM and internal water bodies, for example, Venice Inlet (Fig. 120) and the inlet south of Estero Island (Fig. 127). For internal channel/lagoons, minor damaging currents ($>$ 3 knots and $<$ 6 knots, blue) are most common. In the interior bays, the tsunami currents are less severe which can be used as shelter to minimize tsunami impact.

Comparing to the other GOM locations previously mapped, there is less current impact in the nearshore, surf zone, inlet and channels/lagoons in the Osprey-Venice-Englewood and Sanibel Island-Naples, FL, probably because the wider continental shelf dissipates more tsunami energy, and also the long distance from the most influential Mississippi submarine landslide source.

6.1 Osprey-Venice-Englewood, FL

Osprey-Venice-Englewood, FL
All Sources
Maximum of Maximum Velocity Magnitude

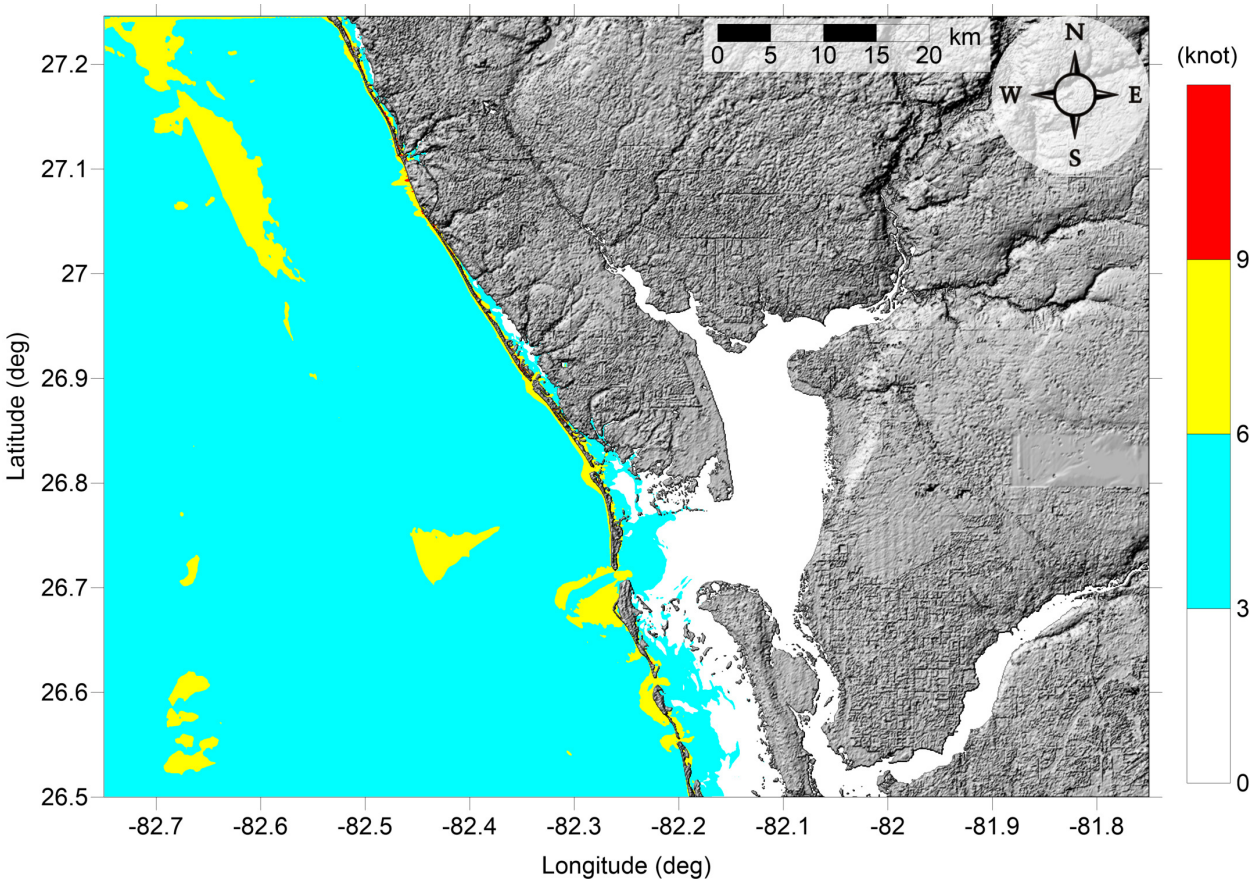

Figure 118: Maximum of maximum velocity magnitude contour in Osprey-Venice-Englewood, FL (Grid 2 - 3 arcsecond) for all landslide scenarios.

Osprey-Venice-Englewood, FL
All Sources
Maximum of Maximum Velocity Magnitude

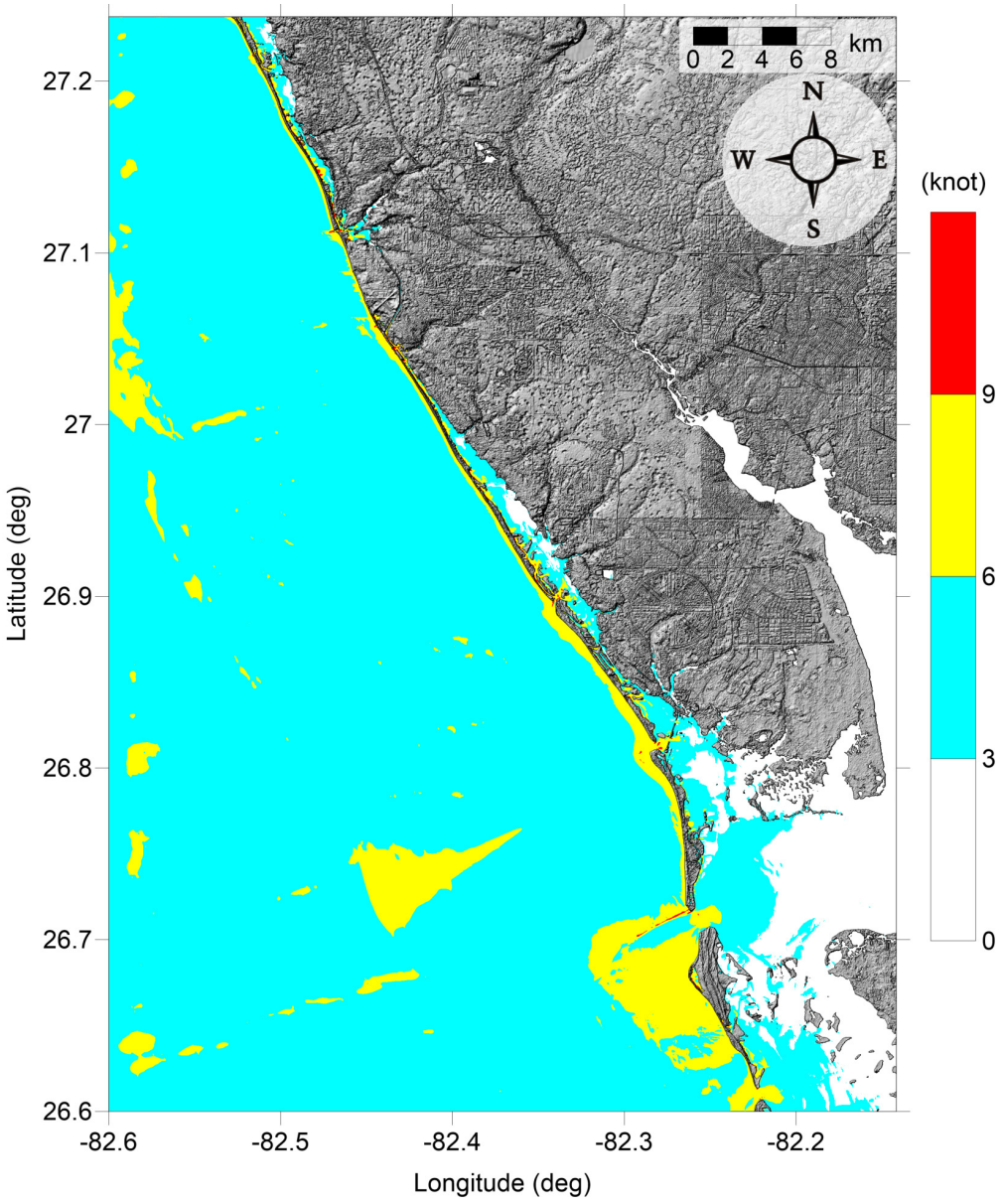

Figure 119: Maximum of maximum velocity magnitude contour in Osprey-Venice-Englewood, FL (Grid 3 - 1 arcsecond) for all landslide scenarios.

Osprey-Venice-Englewood, FL
All Sources
Maximum of Maximum Velocity Magnitude

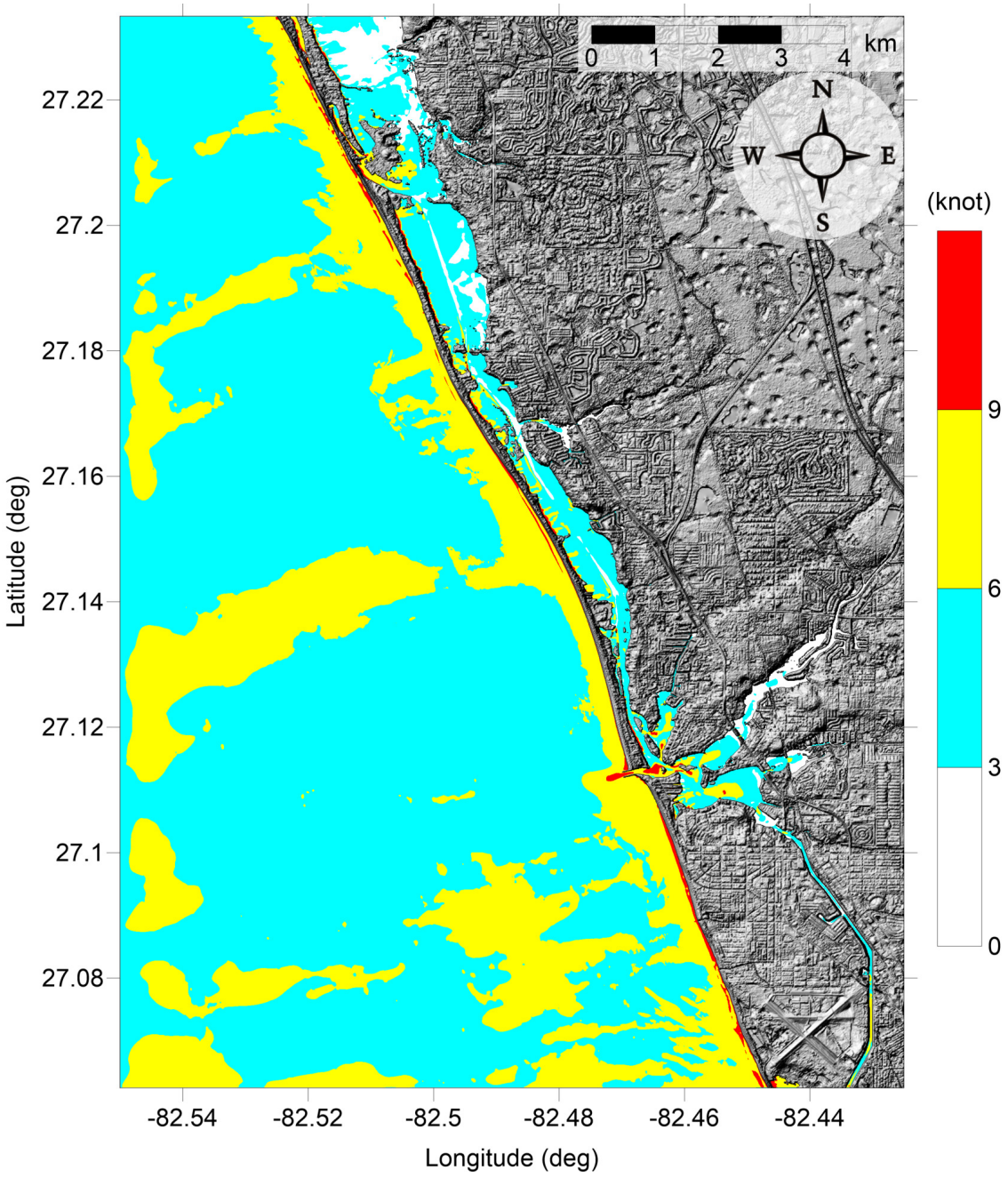

Figure 120: Maximum of maximum velocity magnitude contour in Osprey-Venice, FL (Grid 4 - 1/3 arcsecond) for all landslide scenarios.

Osprey-Venice-Englewood, FL
All Sources
Maximum of Maximum Velocity Magnitude

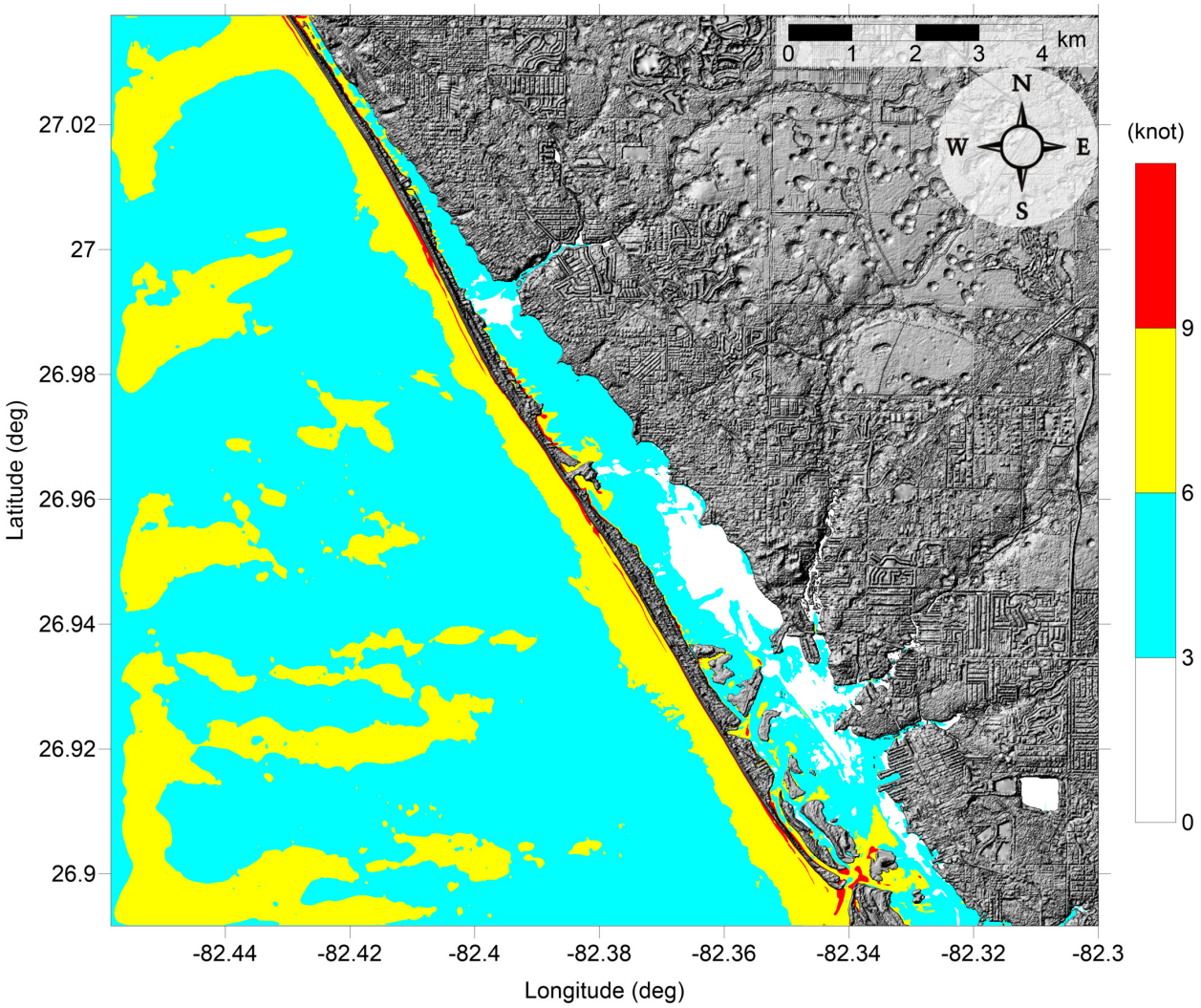

Figure 121: Maximum of maximum velocity magnitude contour in Englewood, FL (Grid 5 - 1/3 arcsecond) for all landslide scenarios.

Osprey-Venice-Englewood, FL
All Sources
Maximum of Maximum Vorticity Magnitude

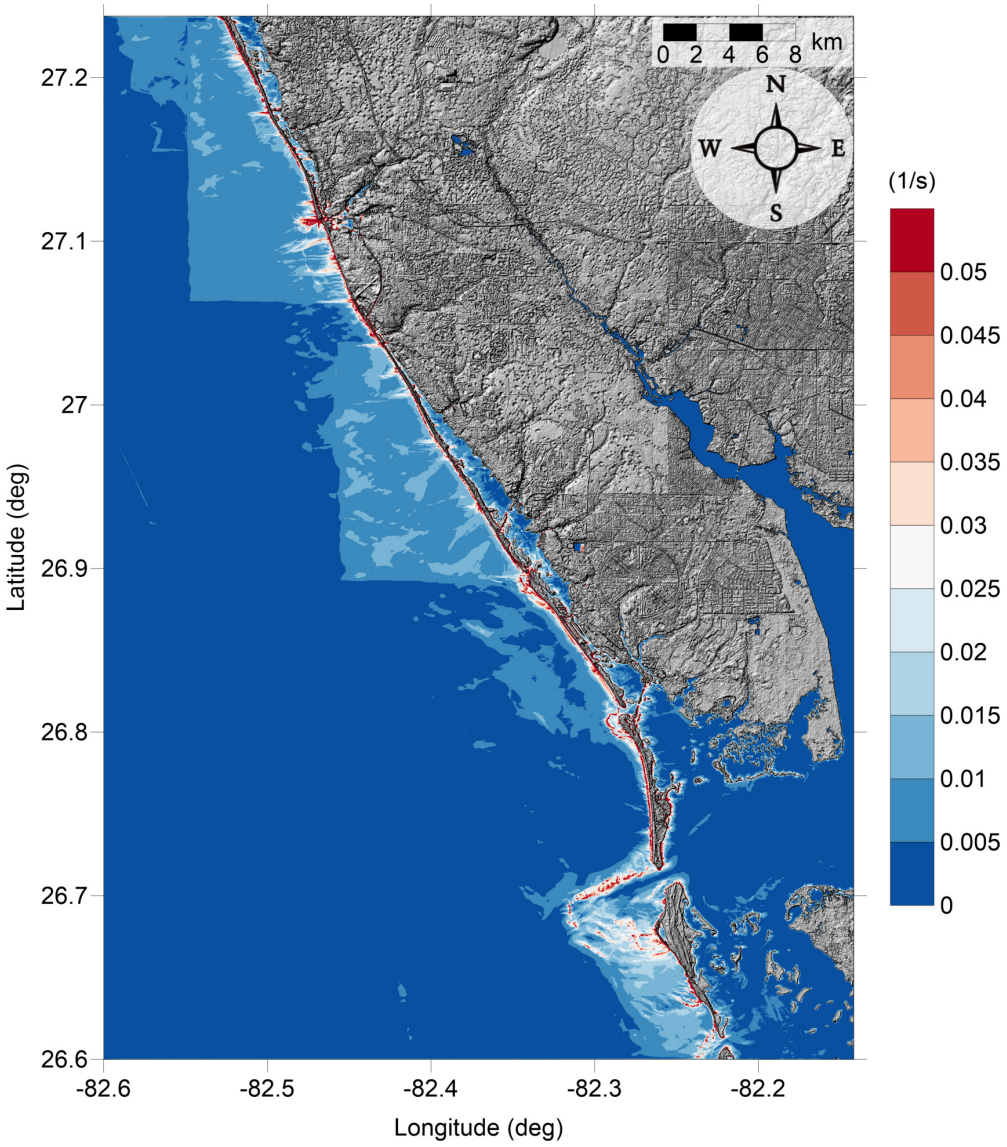

Figure 122: Maximum of maximum vorticity magnitude contour in Osprey-Venice-Englewood, FL Grid 3 (1 arcsecond) for all landslide scenarios.

Osprey-Venice-Englewood, FL
All Sources
Maximum of Maximum Vorticity Magnitude

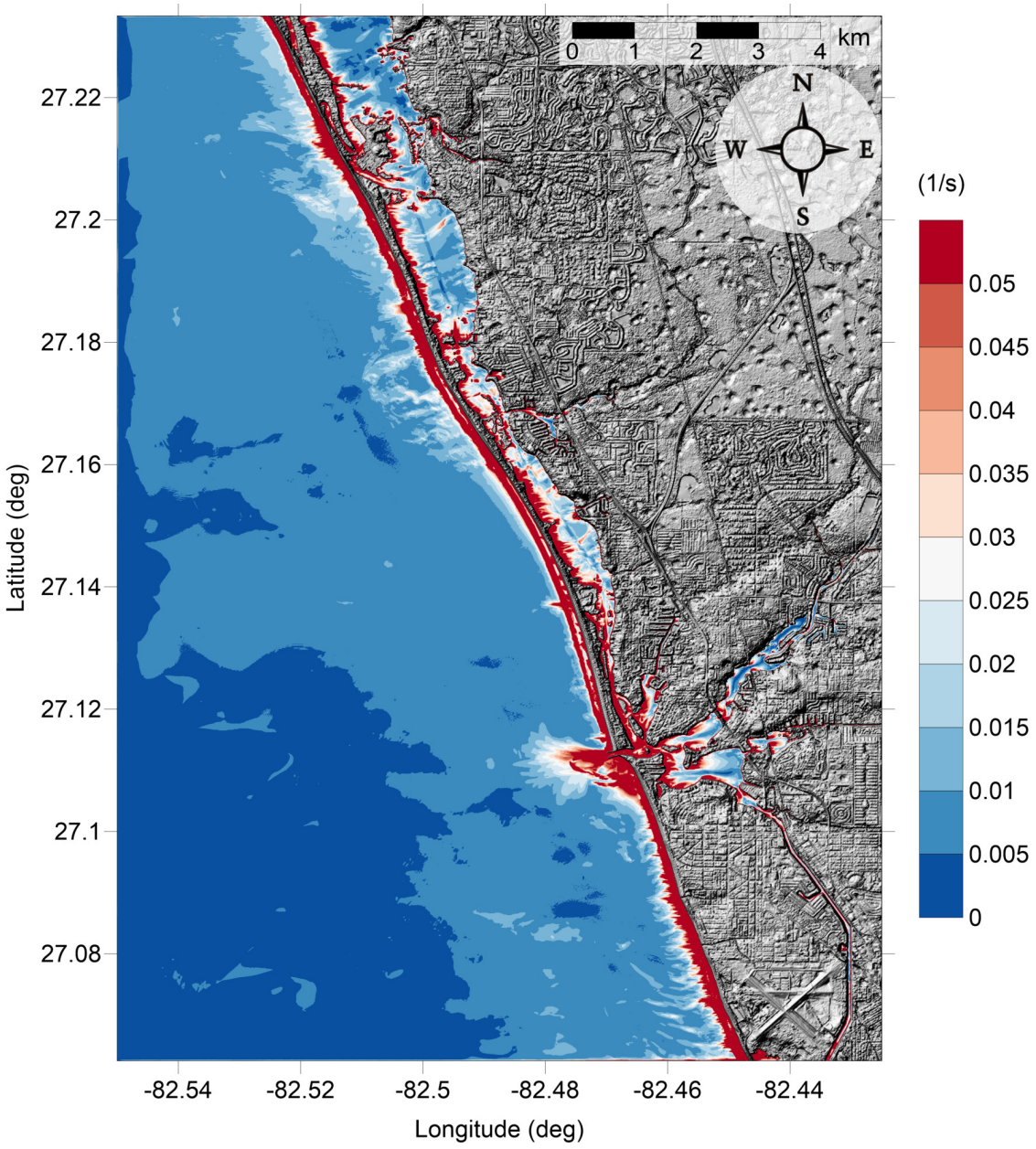

Figure 123: Maximum of maximum vorticity magnitude contour in Osprey-Venice, FL Grid 4 (1/3 arcsecond) for all landslide scenarios.

Osprey-Venice-Englewood, FL
All Sources
Maximum of Maximum Vorticity Magnitude

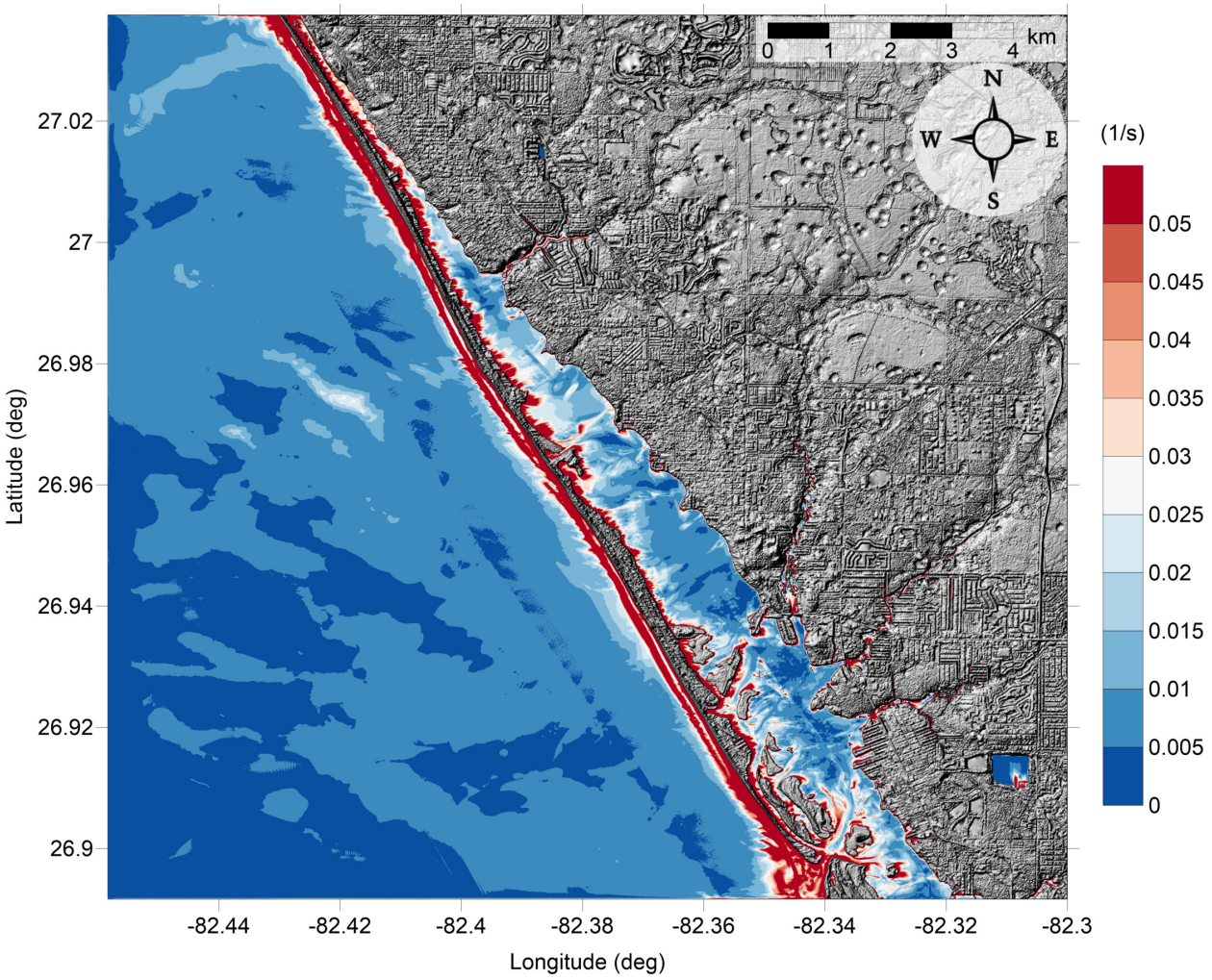

Figure 124: Maximum of maximum vorticity magnitude contour in Englewood, FL Grid 5 (1/3 arcsecond) for all landslide scenarios.

6.2 Sanibel Island-Naples, FL

Sanibel Island-Naples, FL
All Sources
Maximum of Maximum Velocity Magnitude

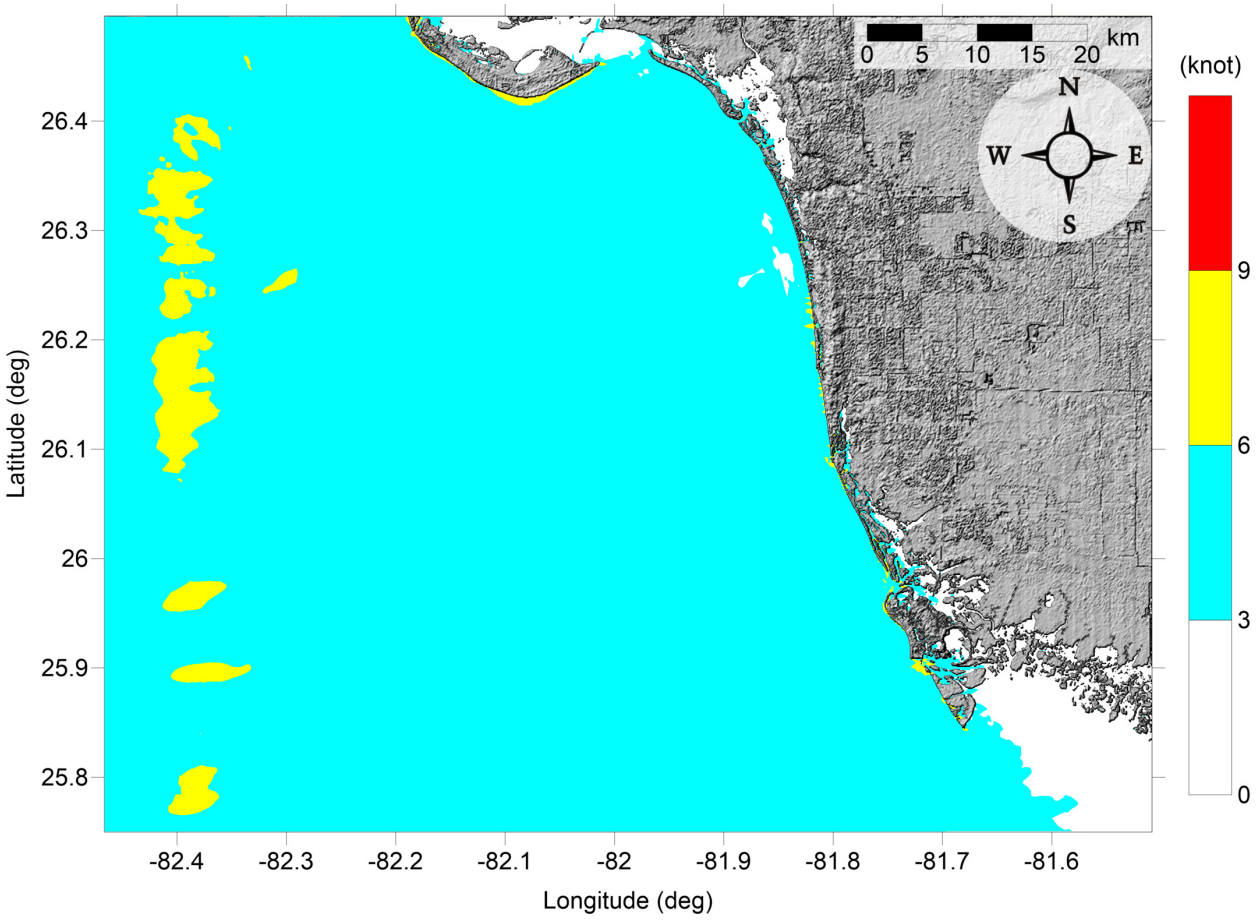

Figure 125: Maximum of maximum velocity magnitude contour in Sanibel Island-Naples, FL (Grid 2 - 3 arcsecond) for all landslide scenarios.

Sanibel Island-Naples, FL
All Sources
Maximum of Maximum Velocity Magnitude

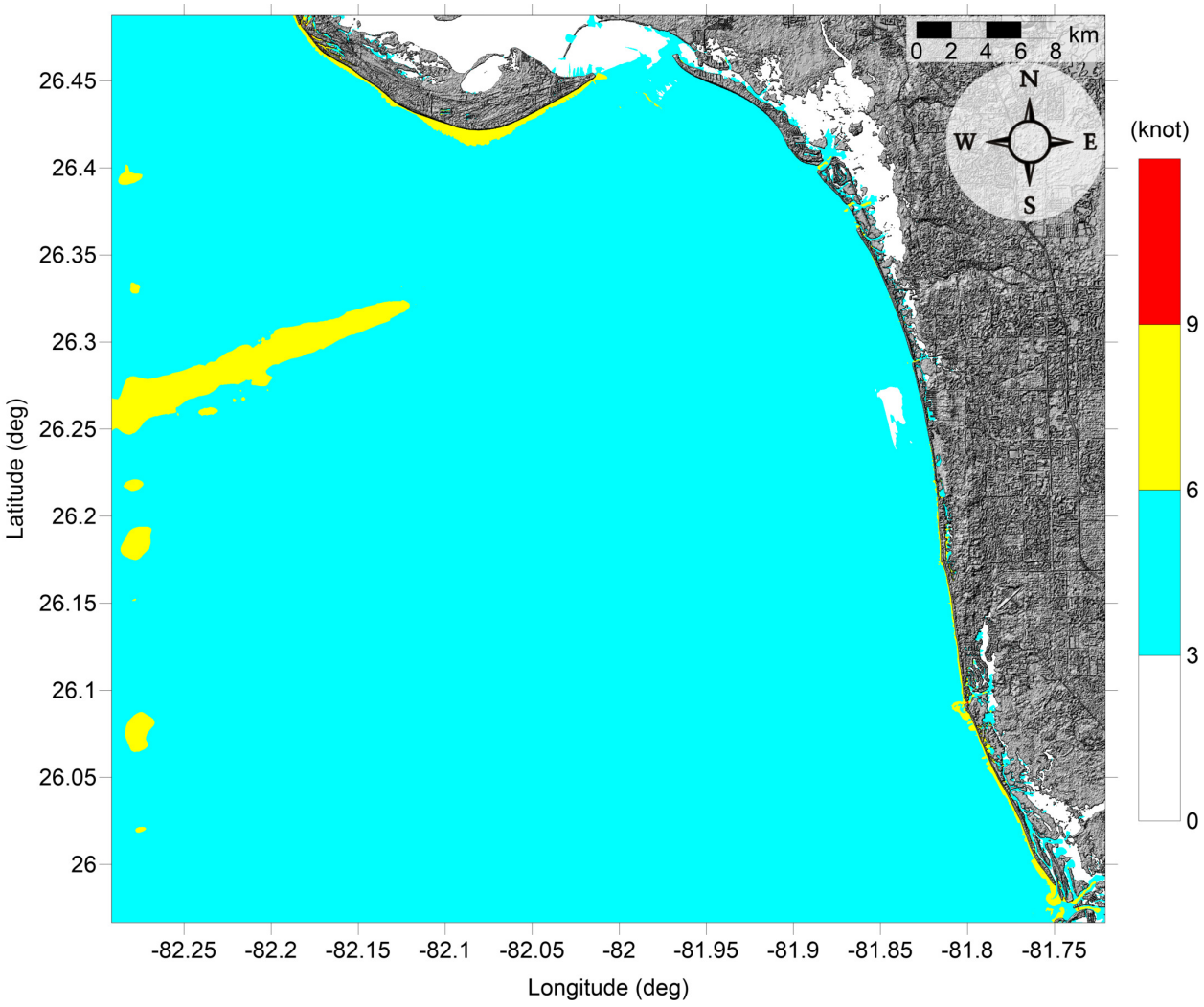

Figure 126: Maximum of maximum velocity magnitude contour in Sanibel Island-Naples, FL (Grid 3 - 1 arcsecond) for all landslide scenarios.

Sanibel Island-Naples, FL
All Sources
Maximum of Maximum Velocity Magnitude

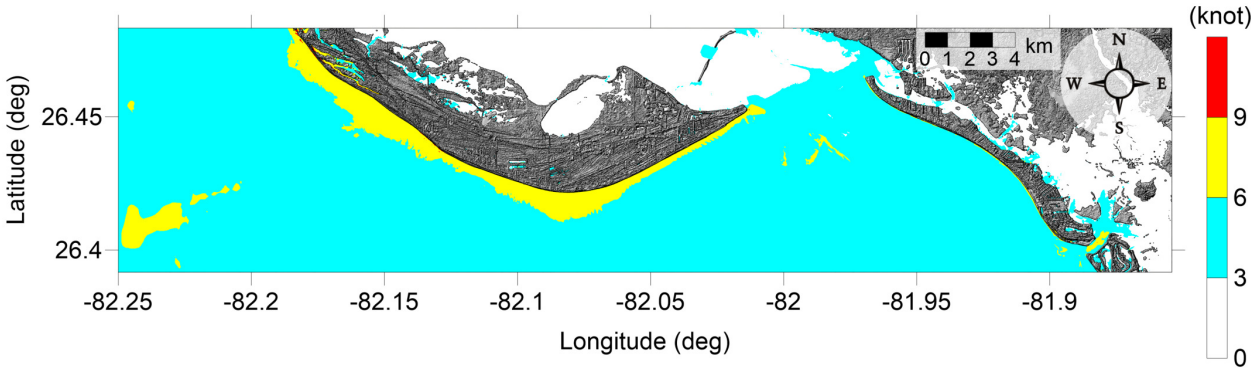

Figure 127: Maximum of maximum velocity magnitude contour in Sanibel Island, FL (Grid 4 - 1/3 arcsecond) for all landslide scenarios.

Sanibel Island-Naples, FL
All Sources
Maximum of Maximum Velocity Magnitude

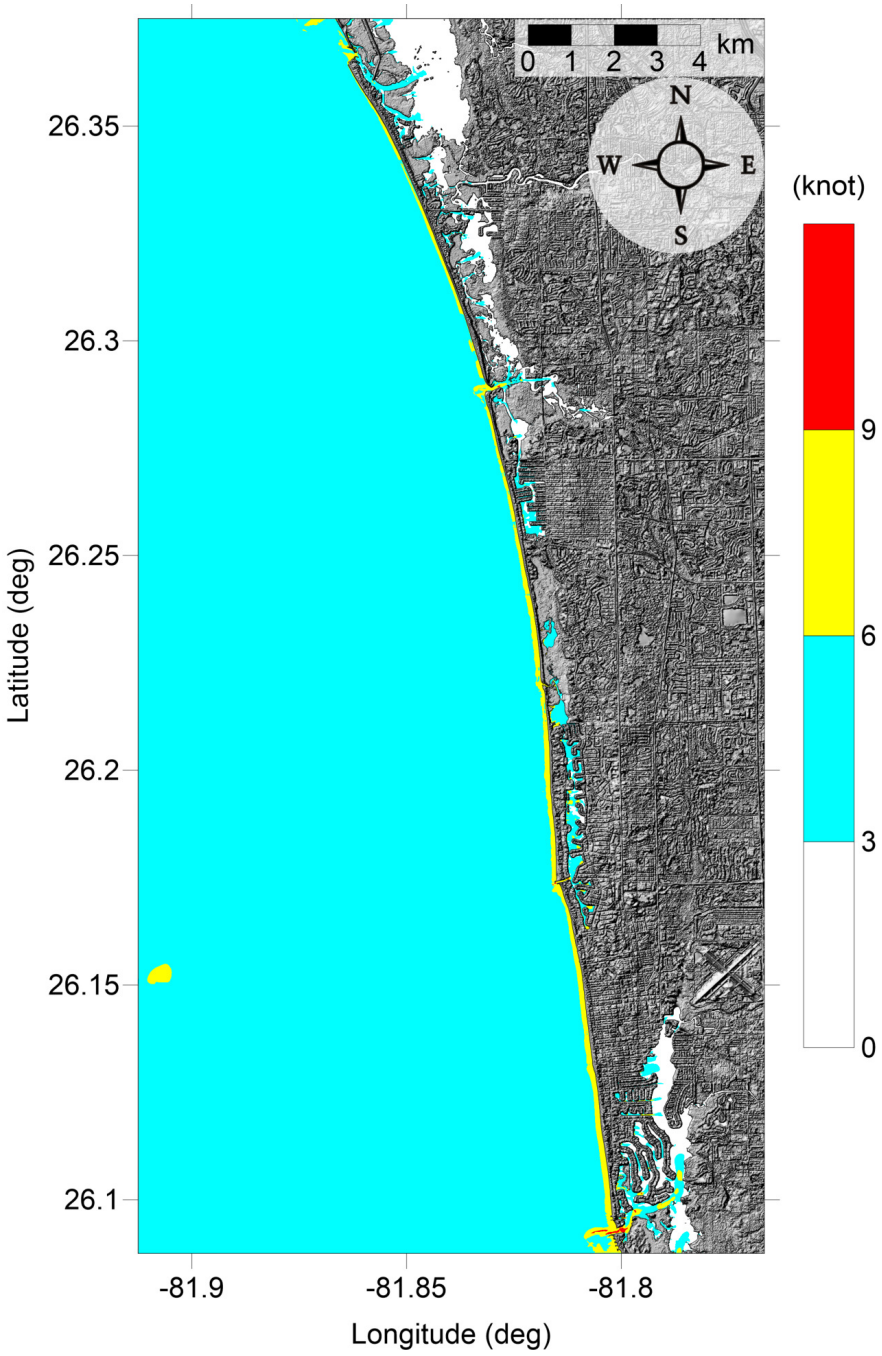

Figure 128: Maximum of maximum velocity magnitude contour in Naples, FL (Grid 5 - 1/3 arcsecond) for all landslide scenarios.

Sanibel Island-Naples, FL
All Sources
Maximum of Maximum Vorticity Magnitude

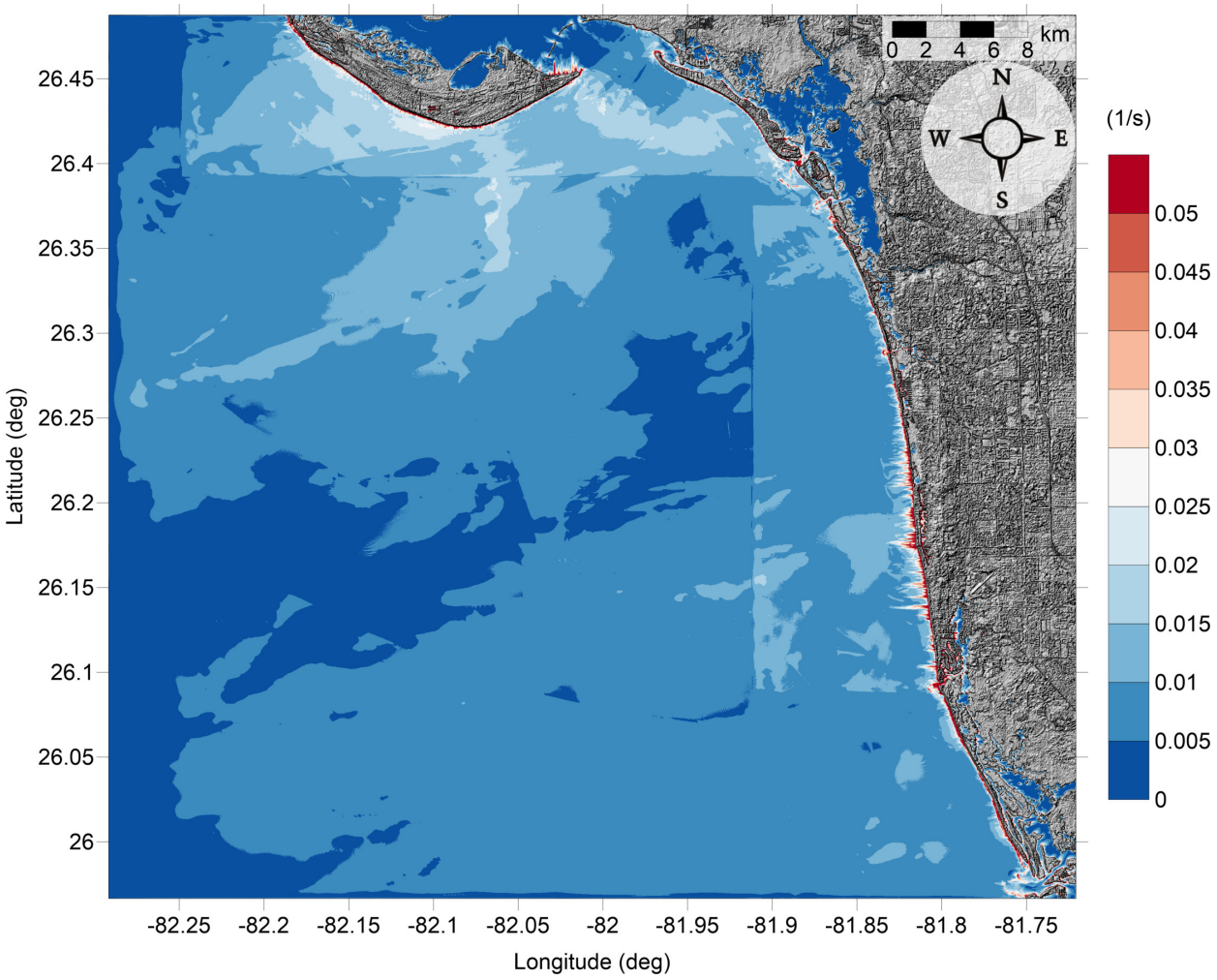

Figure 129: Maximum of maximum vorticity magnitude contour in Sanibel Island-Naples, FL Grid 3 (1 arcsecond) for all landslide scenarios.

Sanibel Island-Naples, FL
All Sources
Maximum of Maximum Vorticity Magnitude

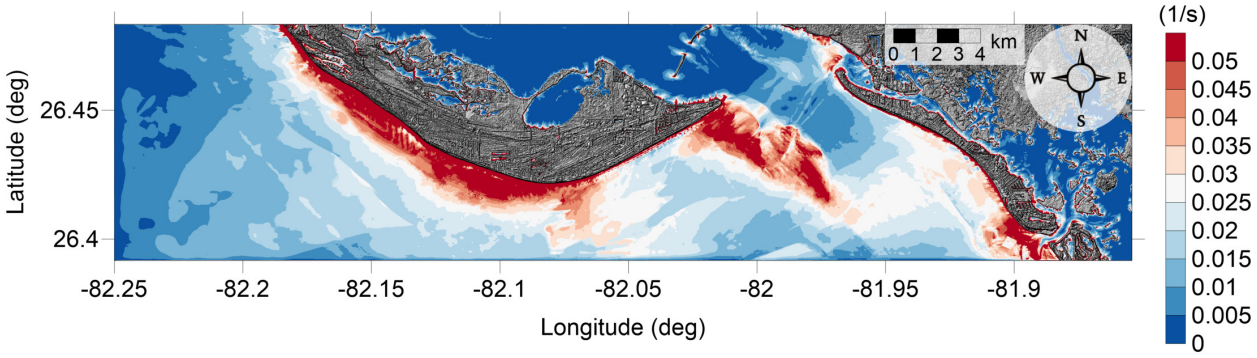

Figure 130: Maximum of maximum vorticity magnitude contour in Sanibel Island, FL Grid 4 (1/3 arcsecond) for all landslide scenarios.

Sanibel Island-Naples, FL
All Sources
Maximum of Maximum Vorticity Magnitude

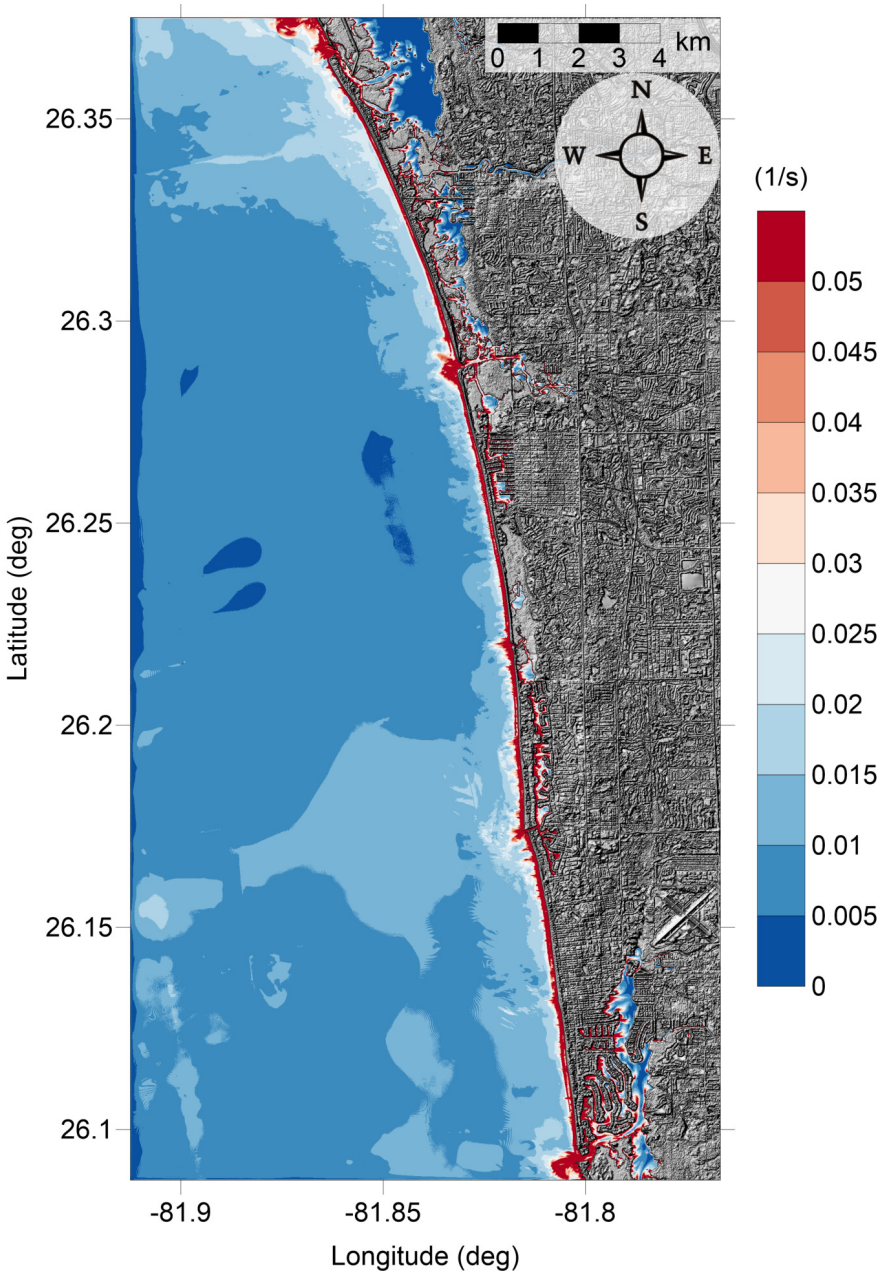

Figure 131: Maximum of maximum vorticity magnitude contour in Naples, FL Grid 5 (1/3 arcsecond) for all landslide scenarios.

7 Conclusions

This project focused on the implementation of recent developments in the tsunami science recommended by the National Tsunami Hazard Mitigation Program - Modeling Mapping Subcommittee - Strategic Plan (NTHMP-MMS-SP) into our current Gulf of Mexico (GOM) tsunami mitigation products. Three main developments for tsunami mitigation have been created under this project for two new communities in the GOM (Osprey-Venice-Englewood, FL and Sanibel Island-Naples, FL) that will provide guidance to state emergency managers for tsunami hazard mitigation and warning purposes. The first task is the development of tsunami inundation maps for the two selected communities with the addition of two new Yucatan landslide sources. The second is the comparison between existing SLOSH hurricane flooding data and our tsunami inundation result for the two new communities in order to facilitate temporal-low-order estimate for tsunami hazard areas (community) where inundation studies have not yet been assigned/executed or where little bathymetric and elevation data exists. The third is to produce maritime products (maximum of maximum (MOM) velocity and velocity magnitude maritime maps) for both communities to help identify impact specifically on ship channels, bay inlets, harbors, marinas, and other infrastructures.

We developed the two new landslide sources based on the source characterization of submarine landslides along the Yucatan Shelf/Campeche Escarpment by Chaytor et al. [2016]. The Yucatan Shelf/Campeche Escarpment was the last remaining area of the GOM that had not been evaluated for landslide tsunami hazards, until high-resolution mapping data collected in 2013 [Paull et al., 2014] shows that the Yucatan Shelf/Campeche Escarpment margin has been subjected to intense modifications by Cenozoic mass wasting processes. Although no known tsunami events have been linked to these Yucatan sources, numerical modeling result shows that they are capable of generating tsunamis that could propagate throughout the GOM Basin [Chaytor et al., 2016]. Our simulation results show that the two new Yucatan sources can generate some impact on South Padre Island, TX and Panama City, FL regions, with maximum wave amplitude of 1 - 3 m (Fig. 25 and Fig. 28).

Tsunami wave propagation and inundation in Osprey-Venice-Englewood, FL and Sanibel Island-Naples, FL was also modeled to obtain inundation, momentum flux, current velocity and vorticity maps considering the entire suite of landslide sources, including the two new Yucatan sources.

We observed similar patterns from the MOM inundation maps for both communities, that is, barrier islands are completely overtopped by tsunami waves. Also, barrier islands provide excellent protection for the mainland against direct tsunami impact, as a result, mainland only suffers from minor inundation. However, important differences exist between the two communities. For instance, the highest tsunami inundation depth in Osprey-Venice-Englewood, FL area is approximately 1 m higher than Sanibel Island-Naples, FL due to being closer to major landslide sources and having narrower continental shelf. In addition, while the trend of decreasing inundation depth from the coast to inland still exists for Sanibel Island, there is another distinct decreasing trend from west to east, because major tsunami waves come from the west. For both communities, MOM tsunami inundation is produced solely by the Mississippi Canyon failure. This historical failure is the largest in both area and volume of material removed, and therefore produces the highest amplitude wave of all

simulated sources. Other landslide sources, including the two new Yucatan sources, do not generate much inundation.

At Osprey-Venice, FL, tsunami completely inundates the whole Casey Key barrier island, and water penetrates approximately 1 km inland at Venice. On the barrier island, water depth greater than 3 m can be seen along the immediate beachfront, and diminishes toward the inner island. At Venice, high water (>3 m) reaches farther inland, flooding a larger residential area. West of the Venice Municipal Airport is also severely flooded. On the mainland, only the coasts of Lyons Bay, Dona Bay and Roberts Bay have seen large areas inundated by tsunami waves, with water as high as 2 m. The inundation depth pattern of Englewood, FL is very similar to Casey Key barrier island. Tsunami inundation greater than 3 m appears on a thin strip of the Manasota Key beachfront, and water height diminishes toward the inland. Over at the mainland, tsunami inundation is limited to the vicinity of the Lemon Bay, with water height of no more than 2 m, except for the portions in South Venice where the bay is very narrow. Sanibel island is completely inundated, with water depth up to 2 m. While the trend of decreasing inundation depth from the coast to inland still exists, there is another distinct trend from west to east, because major sources generate tsunami waves coming from the west. As a result, by the time tsunami reaches Estero Island, wave energy is further dissipated, causing less severe inundation than Sanibel Island. Naples is also significantly impacted, with > 2 m water depth reaching to 500 m inland. Tsunami also floods a relatively large area in the vicinity of Naples Bay. North of the Inner Clam Bay tsunami causes less than 1 m inundation at the Little Hickory Island and Vanderbilt Beach, and very limited area surrounding Little Hickory Bay.

Comparisons of MOM tsunami inundation results with the SLOSH MOM high tide storm surge inundation indicate that while the details of referencing tsunami inundation to hurricane storm surge is dependent on local topographic effects, general regional trends can be identified. For both communities, category 1-comparable tsunami inundation dominates, especially in the mainland. Immediate beachfront areas are inundated at levels comparable to major hurricanes (Category 2 or 3) at Osprey-Venice-Englewood and west side of Sanibel Island, but very little in Naples, FL. For most locations, the difference between tsunami inundation and hurricane flooding depth is within 1 m, indicating good matching. However, around Estero Bay, Inner Clam Bay and Naples Bay, the difference is larger than 1 m (hurricane > tsunami). The good matching shows that it is possible to provide temporal-low-order estimate for tsunami hazard areas (community) where inundation studies have not yet been executed or where little bathymetric and elevation data exists.

Since even general, low-resolution inundation information is useful for hazard mitigation efforts, we believe that these results can be extended to provide a preliminary, first-order estimate of potential tsunami hazard zones for other Gulf Coast communities that is accessible and understandable to regional emergency managers and more appropriate for the low-lying Gulf Coast than methods such as the 10 m (33 ft) elevation contour line. We anticipate that communities which lack detailed tsunami inundation maps, but which have modeled hurricane storm surge information, would be able to use the results presented here to estimate their potential tsunami hazard level based on their regional topographical/bathymetric features. We stress, however, that such results should be used only in a broad, regional sense given the differences seen among and within communities based on local details of

bathymetry, topography, and geographical location within the GOM basin. There is no guarantee that comparison results will be identical in areas with similar topography, and comparisons should only be made after understanding the limitations and simplifications of the methodology presented here. Improvements to the methodology would clearly improve the reliability of comparisons. For example, given the large difference in resolution of the SLOSH model data (1 km) and tsunami inundation data (1/3 arcsecond $\approx$ 10 m), the comparison between the two datasets would be greatly improved with increased resolution of the SLOSH model runs, or alternate data on category-specific hurricane storm surge. Additionally, a more detailed comparison could also be accomplished by comparison with probabilistic storm surge parameters, e.g. 100-year or 500-year hurricane surge events, which may provide more/better information in areas where there are large differences between the modeled tsunami inundation and that of the best-match hurricane category. Successful implementation of this approach would certainly require the availability of probabilistic data for the locations of interest in order to develop a generalized probabilistic tsunami - storm surge comparison.

Finally, we produced the MOM velocity and velocity magnitude maps for all the landslide scenarios, for Osprey-Venice-Englewood, FL and Sanibel Island-Naples, FL, based on a simplified current velocity damage scale where we associate 0 - 3 knots to unharmful currents, 3 - 6 knots to minor damage, 6 - 9 knots to moderate damage, and over 9 knots to major damage. The four damage levels are denoted with white, blue, yellow and red colors, respectively.

From the MOM velocity magnitude results in the entire Gulf of Mexico (Fig. 117), it can be observed that, potential damaging currents ($>$ 3 knots, blue, yellow and red areas) tend to be present in most of the area shallower than the minimum offshore safe depth. However, damaging currents could reach areas deeper than 200 m close to most of the landslide generation regions. Major damaging currents ($>$ 9 knots, red) can be expected in most of the landslide generation regions, in the continental shelf adjacent to Mississippi Canyon, offshore northwest Florida, and Yucatan shelf. Moderate ($>$ 6 knots and $<$ 9 knots, yellow) damaging current areas are scattered over the continental shelf, but mostly close to areas with major damage currents.

General trends can be observed from all of the MOM velocity and vorticity maps of the subdomains. In the nearshore region of the subdomains, there are mostly moderate damaging currents ($>$ 6 knots and $<$ 9 knots, yellow). In the surf zone of the islands, there are major damaging currents ($>$ 9 knots, red) in Ospary-Venice-Englewood, but not in Sanibel Island-Naples, FL. There are usually strong currents flowing through the inlets (some with jetties) which connects the GOM and internal water bodies, for example, Venice Inlet (Fig. 120) and the inlet south of Estero Island (Fig. 127). For internal channel/lagoons, minor damaging currents ($>$ 3 knots and $<$ 6 knots, blue) are most common. In the interior bays, tsunami currents are less severe which can be used as shelter to minimize tsunami impact.

Comparing to the other GOM locations previously mapped, there is less current impact in the nearshore, surf zone, inlet and channels/lagoons in Osprey-Venice-Englewood and Sanibel Island-Naples, FL, probably because the wider continental shelf dissipates more tsunami energy and also of the long distance from the most influential Mississippi submarine landslide source.

Tsunami hazard maritime products such as tsunami current magnitude, vorticity, safe/hazard zones would be central for future developments of maritime hazard maps, maritime emergency response and as well as infrastructure planning.

Although the recurrence of destructive tsunami events have been verified to be quite low in the GOM, our work has confirmed that submarine landslide events with similar characteristics to those used here, have indeed the potential to cause severe damage to GOM coastal communities. Therefore, this work is intended to provide guidance to local emergency managers to help managing urban growth, evacuation planning, and public education with the final objective to mitigate potential tsunami hazards in the GOM.

Acknowledgments

This work was supported by the National Tsunami Hazard Mitigation Program (NTHMP) under awards NA17NWS4670015, "Development of two tsunami inundation maps in the GOM and inclusion of the USGS' Yucatan landslide tsunami sources". The authors wish to thank all NTHMP modeling and Mapping Subcommittee members and GOM's emergency manager representatives for their helpful insights. Special thanks go to Jason Chaytor, Brad Baker and Daniel Hahn for their helpful insight and support. Also thank Kelly Carignan and Kelly Stroker for providing the DEMs. High resolution inundation maps are available from `http://www.tamug.edu/tsunami/NTHMP/NTHMP.html` or by contacting corresponding author upon request.

References

D. Basco and C. Klentzman. On the classification of coastal storms using principles of momentum conservation. In *Proc. 31st Int. Conf. on Coastal Eng.* ASCE, 2006.

J. D. Chaytor, E. L. Geist, C. K. Paull, D. W. Caress, R. Gwiazda, J. U. Fucugauchi, and M. R. Vieyra. Source characterization and tsunami modeling of submarine landslides along the yucatán shelf/campeche escarpment, southern gulf of mexico. *Pure and Applied Geophysics*, 173(12):4101–4116, Dec 2016. ISSN 1420-9136. doi: 10.1007/s00024-016-1363-3. URL `https://doi.org/10.1007/s00024-016-1363-3`.

B. Dugan and J. Stigall. Origin of overpressure and slope failure in the Ursa region, northern Gulf of Mexico. In D. C. Mosher, R. C. Shipp, L. Moscardelli, J. D. Chaytor, C. D. P. Baxter, H. J. Lee, and R. Urgeles, editors, *Submarine Mass Movements and Their Consequences*, pages 167–178. Springer Netherlands, 2010.

P. K. Dunbar and C. S. Weaver. *U.S. States and Territories National Tsunami Hazard Assessment: Historical Record and Sources for Waves.* U.S. Department of Commerce, National Oceanic and Atmospheric Administration, National Geophysical Data Center Tech. Rep.No. 3, 2008.

E. L. Geist, J. D. Chaytor, T. Parsons, and U. ten Brink. Estimation of submarine mass failure probability from a sequence of deposits with age dates. *Geosphere*, 9(2):287–298, 2013.

S. T. Grilli, O.-D. S. Taylor, C. D. P. Baxter, and S. Maretzki. A probabilistic approach for determining submarine landslide tsunami hazard along the upper east coast of the United States. *Mar. Geol.*, 264:74–97, 2009.

C. B. Harbitz, F. Løvholt, and H. Bungum. Submarine landslide tsunamis: How extreme and how likely? *Nat. Hazards*, 72(3):1341–1374, 2014.

C. W. Hirt and B. D. Nichols. Volume of fluid method for the dynamics of free boundaries. *J. Comput. Phys.*, 39:201–225, 1981.

J. Horrillo. *Numerical Method for Tsunami calculations using Full Navier-Stokes equations and the Volume of Fluid method.* PhD thesis, University of Alaska Fairbanks, 2006.

J. Horrillo, A. Wood, C. Williams, A. Parambath, and G. Kim. Construction of tsunami inundation maps in the Gulf of Mexico. Technical report, Award Number: NA09NWS4670006 to the National Tsunami Hazard Mitigation Program (NTHMP), National Weather Service Program Office, NOAA, 2011. avail. from http://www.tamug.edu/tsunami/NTHMP.html.

J. Horrillo, A. Wood, G.-B. Kim, and A. Parambath. A simplified 3-D Navier-Stokes numerical model for landslide-tsunami: Application to the Gulf of Mexico. *J. Geophys. Res.-Oceans*, 118:6934–6950, 2013. doi:10.1002/2012JC008689.

J. Horrillo, A. Pampell-Manis, C. Sparagowski, L. Parambath, and Y. Shigihara. Construction of five tsunami inundation maps for the Gulf of Mexico. Technical report, Award Number: NA12NWS4670014 and NA13NWS4670018 to the National Tsunami Hazard Mitigation Program (NTHMP), National Weather Service Program Office, NOAA, 2015. avail. from http://www.tamug.edu/tsunami/NTHMP.html.

J. Horrillo, W. Cheng, A. Pampell-Manis, and J. Figlus. Implementing nthmp-mms strategic plan in tsunami hazard mitigation products for the Gulf of Mexico. Technical report, Award Number: NA14NWS4670049 to the National Tsunami Hazard Mitigation Program (NTHMP), National Weather Service Program Office, NOAA, 2016. avail. from http://www.tamug.edu/tsunami/NTHMP.html.

J. Horrillo, W. Cheng, and J. Figlus. Development of four additional tsunami inundation maps with revision of Port Aransas, TX and updating existing ones with maritime products. Technical report, Award Number: NA15NWS4670031 and NA16NWS4670039 to the National Tsunami Hazard Mitigation Program (NTHMP), National Weather Service Program Office, NOAA, 2017. avail. from http://www.tamug.edu/tsunami/NTHMP.html.

J. L. Irish and D. T. Resio. A hydrodynamics-based surge scale for hurricanes. *Ocean Eng.*, 37:69–81, 2010.

L. Kantha. Time to replace the Saffir-Simpson hurricane scale? *Eos, Transactions American Geophysical Union*, 87(1):3–6, 2006.

W. Knight. Model predictions of Gulf and Southern Atlantic Coast tsunami impacts from a distribution of sources. *Sci. of Tsunami Hazards*, 24:304–312, 2006.

A. M. López-Venegas, J. Horrillo, A. Pampell-Manis, V. Huérfano, and A. Mercado. Advanced tsunami numerical simulations and energy considerations by use of 3D - 2D coupled models: The October 11, 1918, Mona Passage tsunami. *Pure Appl. Geophys.*, 172(6):1679–1698, 2015.

P. J. Lynett, J. C. Borrero, R. Weiss, S. Son, D. Greer, and W. Renteria. Observations and modeling of tsunami-induced currents in ports and harbors. *Earth and Planetary Science Letters*, 327:68–74, 2012.

P. J. Lynett, J. Borrero, S. Son, R. Wilson, and K. Miller. Assessment of the tsunami-induced current hazard. *Geophysical Research Letters*, 41(6):2048–2055, 2014.

S. Maretzki, S. Grilli, and C. D. P. Baxter. Probabilistic SMF tsunami hazard assessment for the upper east coast of the United States. In V. Lykousis, D. Sakellariou, and J. Locat, editors, *Submarine Mass Movements and Their Consequences*, pages 377–385. Springer Netherlands, 2007.

D. Masson, C. Habitz, R. Wynn, G. Pederson, and F. Lovholt. Submarine landslides: Processes, triggers and hazard protection. *Philos. Trans. R. Soc. A*, 364:2009–2039, 2006.

A. Pampell-Manis, J. Horrillo, Y. Shigihara, and L. Parambath. Probabilistic assessment of landslide tsunami hazard for the northern Gulf of Mexico. *J. Geophys. Res.-Oceans*, 2016. doi:10.1002/2015JC011261.

C. K. Paull, D. W. Caress, R. Gwiazda, J. Urrutia-Fucugauchi, M. Rebolledo-Vieyra, E. Lundsten, K. Anderson, and E. J. Sumner. Cretaceous–paleogene boundary exposed: Campeche escarpment, gulf of mexico. *Marine Geology*, 357:392–400, 2014.

U. S. ten Brink, H. J. Lee, E. L. Geist, and D. Twichell. Assessment of tsunami hazard to the U.S. East Coast using relationships between submarine landslides and earthquakes. *Mar. Geol.*, 264:65–73, 2009a.

U. S. ten Brink, D. Twichell, P. Lynett, E. Geist, J. Chaytor, H. Lee, B. Buczkowski, and C. Flores. Regional assessment of tsunami potential in the Gulf of Mexico. *U. S. Geol. Surv. Admin. Rep.*, 2009b.

R. Wilson, C. Davenport, and B. Jaffe. Sediment scour and deposition within harbors in california (usa), caused by the march 11, 2011 tohoku-oki tsunami. *Sedimentary Geology*, 282:228–240, 2012.

R. I. Wilson, A. R. Admire, J. C. Borrero, L. A. Dengler, M. R. Legg, P. Lynett, T. P. McCrink, K. M. Miller, A. Ritchie, K. Sterling, et al. Observations and impacts from the 2010 chilean and 2011 japanese tsunamis in california (usa). *Pure and Applied Geophysics*, 170(6-8):1127–1147, 2013.

Y. Yamazaki, Z. Kowalik, and K. F. Cheung. Depth-integrated, non-hydrostatic model for wave breaking and run-up. *Int. J. Numer. Meth. Fl.*, 61:473–497, 2008.